# GEOMETRIC AND MECHANICAL MODELLING OF THE HUMAN LOCOMOTOR SYSTEM

A DISSERTATION SUBMITTED TO THE
UNIVERSITY OF OXFORD




IN PARTIAL FULFILLMENT OF THE REQUIREMENTS
FOR THE DEGREE OF
DOCTOR OF PHILOSOPHY

BY
TUNG-WU LU

ST. PETER'S COLLEGE
OXFORD

TRINITY TERM 1997



# Abstract


## Geometric and Mechanical Modelling of the Human Locomotor System

Tung-Wu Lu
St. Peter's College

Doctor of Philosophy
Trinity Term 1997

A critical review of studies related to the modelling of the human locomotor system is given. Kinematic and dynamic modelling and analysis of the pelvis-leg apparatus as an ensemble of four rigid body segments are described.

Experiments were performed on two patients with custom-made instrumented massive proximal femoral prostheses implanted after tumour resection. Telemetered axial forces transmitted along the prostheses, together with kinematic, force plate and electromyographic data, were recorded synchronously during level walking, single and double leg stance, and isometric tests of the hip muscles.

A sagittal plane model of the locomotor system, with an anatomical model of the knee joint, was developed from an existing model and used for a comparative study of methods for the calculation of the internal forces. A three-dimensional computer graphics-based animated model of the locomotor system was developed, with the hip as a ball-and-socket joint, the knee as a parallel spatial mechanism and the ankle as a two-hinge complex. Thirty-four muscles or muscle groups were included. A method for the determination of the orientation of multi-joint systems from surface markers was developed to take account of measurement errors including skin movement artefacts. Both the 2D and 3D models of the locomotor system were evaluated and validated quantitatively with the telemetered femoral axial forces.

It is concluded that (a) a significant part of the bending moments along limbs are transmitted by a combination of tensile forces in muscles and compressive forces in bones so that moments transmitted by the bones are much less than the limb moments, (b) bi-articular muscles play a major role in modulating forces in bones, (c) appropriate simulation of muscle forces is important in experimental or theoretical studies of load transmission along bones, (d) computer graphics-based modelling and animation are important tools in bridging the gap between clinical users and biomechanists.

# Acknowledgements

I am most grateful to the people and government of the Republic of China in Taiwan for the national scholarship which made it possible for me to study in Oxford. Further financial assistance of The Committee of Vice-Chancellors and Principals of the University of the United Kingdom, via their Overseas Research Student Awards, is also gratefully acknowledged.

I would especially like to express my sincere gratitude to my supervisor, Professor John J. O'Connor, for his excellent guidance. I would also like to thank Gemma O'Connor for her warm hospitality during my time in Oxford.

I thank Professor Peter Walker and Mr Steve Taylor for the opportunity to access the instrumented subjects and for their help during the experiments. The collaboration of the two subjects is also greatly acknowledged.

I would like to thank Dr Amy Zavatsky who helped in many aspects of my research and gave me the opportunity to tutor undergraduate structural analysis at St. Hilda's College. My thanks are also given to Piaras Kelly, Richie Gill, David Wilson, Ahmed Imran, Danielle Toutoungi and Alberto Leardini.

I would like to thank my parents for their unwavering support and encouragement. I am also grateful for the support and help of both my family and my family-in-law.

My deepest thanks go to my wife, Shu-Ju, whose love, patience and support carried me through my Oxford Years.

Tung-Wu Lu
Oxford, April 1997

# Contents

**Abstract** ii

**Acknowledgements** iii

**1 Introduction** 1

1.1 Overview . . . . . 1

1.2 Anatomy of The Pelvis-Leg Apparatus . . . . . 4

1.2.1 Bones and Joints . . . . . 4

1.2.2 Ligaments, Muscles and Tendons . . . . . 7

1.3 Biomechanical Modelling . . . . . 9

1.3.1 Incorporation of Experimental and Theoretical Methods . 10

1.3.2 Direct Versus Inverse Dynamics . . . . . 10

1.3.3 Mechanical Modelling With The Inverse Dynamics Approach 12

1.4 Geometric Models . . . . . 13

1.4.1 Linkage Models . . . . . 14

1.4.2 Joint Models . . . . . 14

1.4.3 Geometry of Muscles and Their Tendons . . . . . 20

1.5 Structural Analysis . . . . . 22

1.5.1 Reduction Method . . . . . 23

1.5.2 Optimisation Method . . . . . 24

1.5.3 DDOSC Method . . . . . 26

1.5.4 Analytical Examination of Methods for Muscle Force Prediction . . . . . 27

1.5.5 Model Validation . . . . . 33

1.6 Aims and Scope of This Thesis . . . . . 34

**2 Kinematics and Dynamics of The Lower Limb as A Multibody System** **36**
2.1 The Rigid Body Assumption . . . . . 37
2.2 Coordinate Systems . . . . . 38
2.3 Attitude Representation: Cardan Angles . . . . . 40
2.4 Joint Coordinate System . . . . . 42
2.5 Dynamics of A Rigid Body . . . . . 44
2.6 Dynamics of The Lower Limb . . . . . 46
2.7 Anthropometric Parameters . . . . . 48

**3 Gait Analysis of Patients With Instrumented Prostheses: Experimental** [1] **52**
3.1 Introduction . . . . . 52
3.2 Subjects and Tests . . . . . 54
3.2.1 Patients With Instrumented Proximal Femoral Prostheses 54
3.2.2 Tests . . . . . 55
3.3 Apparatus and Procedures . . . . . 56
3.3.1 Motion Data Acquisition System . . . . . 57
3.3.2 Force Plates . . . . . 59
3.3.3 Electromyography System . . . . . 61
3.3.4 Equipment for the Isometric Tests . . . . . 62
3.3.5 Telemetry System for the Instrumented Prostheses . . . . 63
3.3.6 Subject Marker Systems . . . . . 64
3.4 Data Analysis . . . . . 64
3.4.1 Determination of Segment Orientation From Markers . . . 64
3.4.2 Determination of Segmental Velocities and Accelerations . 66
3.4.3 Force Magnification Ratio . . . . . 67
3.4.4 Moment Distribution in The Limb . . . . . 67
3.5 Results . . . . . 67
3.5.1 Isometric Hip Exercises . . . . . 68
3.5.2 Standing Postures . . . . . 70
3.5.3 Gait Trials . . . . . 70
3.6 Discussion . . . . . 71
3.6.1 Muscle-bone interaction . . . . . 71
3.6.2 Muscle recruitment . . . . . 73
3.6.3 Inter-subject comparison . . . . . 75

3.6.4 Relevance to Gait Analysis . . . . . 75
3.7 Summary . . . . . 76

**4 Modelling of The Knee Joint and Its Force-Bearing Structures 77**
4.1 Kinematics of The Knee Joint . . . . . 78
4.1.1 Unloaded Versus Loaded Movement . . . . . 78
4.1.2 Passive Motion: The Four-Bar Linkage Model . . . . . 79
4.2 Ligament Fibre Recruitment and Shape Changes During Motion [2] 82
4.2.1 Representation of Ligament Fibres . . . . . 84
4.2.2 Loaded Knee Joint Movement (Anterior/Posterior Tibial Displacement) . . . . . 88
4.2.3 Computer Visualisation . . . . . 89
4.2.4 Results . . . . . 89
4.2.5 Discussion . . . . . 95
4.2.6 Summary . . . . . 97
4.3 Lines of Action and Moment Arms of The Major Tension-Bearing Structures [3] . . . . . 98
4.3.1 Methods . . . . . 99
4.3.2 Results . . . . . 103
4.3.3 Discussion . . . . . 108
4.3.4 Conclusion . . . . . 111

**5 Two-Dimensional Modelling of The Lower Limb[4] 112**
5.1 Geometric Modelling . . . . . 112
5.1.1 Knee Joint Models . . . . . 113
5.1.2 Hip and Ankle Models . . . . . 114
5.1.3 Musculotendon Geometry . . . . . 115
5.2 Mechanical Analysis of Normal Level Walking . . . . . 116
5.2.1 Data Collection and Pre-analysis . . . . . 117
5.2.2 Problem Formulations . . . . . 117
5.2.3 Results . . . . . 122
5.2.4 Discussion . . . . . 129
5.3 Gait Analysis of Patients With Instrumented Prostheses: 2D Theoretical [5] . . . . . 131
5.3.1 Dynamic and Structural Analysis . . . . . 132
5.3.2 Isometric Tests . . . . . 133

5.3.3 Level Walking . . . . . 135
5.3.4 Discussion . . . . . 136
5.3.5 Summary . . . . . 139
5.4 Interactive Graphics-Based Window Interface . . . . . 140
5.4.1 Window Interface Structures . . . . . 140
5.5 Discussion . . . . . 144
5.5.1 Effects of Ligament Elasticity . . . . . 144
5.5.2 Ankle Modelling . . . . . 146

**6 Three-Dimensional Modelling of the Locomotor Apparatus [6] 147**
6.1 Knee Joint Model . . . . . 148
6.1.1 General Description . . . . . 148
6.1.2 Formulation of The Parallel Spatial Mechanism . . . . . 149
6.2 Hip Joint Model . . . . . 154
6.2.1 General Description . . . . . 154
6.2.2 Estimation of The Hip Joint Centre . . . . . 155
6.3 Model of The Ankle Joint Complex . . . . . 162
6.4 Force-Transmitting Structures . . . . . 163
6.4.1 Knee Joint . . . . . 163
6.4.2 Hip Joint . . . . . 166
6.4.3 Ankle Complex . . . . . 167
6.5 Geometry of The Muscles and Their Tendons . . . . . 167
6.5.1 Wrapping Around Bones . . . . . 169
6.5.2 Lines of Action of the Muscle Tendons . . . . . 169
6.5.3 The Knee Extensor Mechanism . . . . . 169
6.5.4 Anthropometric and Osteometric Scaling . . . . . 174
6.6 Three-Dimensional Computer Graphics Reconstruction and Animation . . . . . 174
6.6.1 Graphics Models . . . . . 175
6.6.2 The Computer Graphics-Based Animated Model . . . . . 177
6.7 Kinematics of Multi-Joint Skeletal Systems From Co-ordinates of Markers . . . . . 178
6.7.1 Introduction . . . . . 178
6.7.2 General Description of The Method . . . . . 180
6.7.3 Application to The Present Model . . . . . 182
6.7.4 Discussion . . . . . 184

**7 Three-Dimensional Analysis of Forces in The Locomotor System: Evaluation and Validation [7] 185**

7.1 Experimental Data and Tests . . . 186
7.1.1 Model Examination of the Quality of Kinematic Data . . . 186
7.1.2 Tests . . . 187
7.1.3 Isometric Tests . . . 187
7.1.4 Stance Postures . . . 187
7.1.5 Level Walking . . . 188
7.2 Mechanical Analysis . . . 188
7.2.1 Problem Formulations . . . 189
7.2.2 Calculation of Forces and Moments in Bones . . . 190
7.3 Results . . . 192
7.3.1 Isometric Tests . . . 192
7.3.2 Standing Postures . . . 197
7.3.3 Level Walking . . . 199
7.4 Discussion . . . 201
7.4.1 Validation of the Model . . . 201
7.4.2 Possible Source of Errors and Parameter Sensitivity . . . 201
7.4.3 The DDOSC method . . . 203
7.5 Clinical Relevance . . . 205
7.5.1 Implication for Hip Replacement . . . 206
7.5.2 Force Sharing Between the Knee Compartments . . . 207

**8 Conclusions, Suggestions and General Summary 210**

8.1 Conclusions . . . 211
8.1.1 Experimental Studies of The Instrumented Patients . . . 211
8.1.2 Two-Dimensional Modelling of the Knee Joint . . . 212
8.1.3 Two-Dimensional Modelling of the Locomotor System . . . 212
8.1.4 Three-Dimensional Modelling of the Locomotor System . . . 213
8.2 Suggestions for Further Studies . . . 215
8.2.1 Model Development . . . 215
8.2.2 Application of Computer Graphics-Based Models . . . 216
8.3 General Summary . . . 217

**A Anatomical Terminology 218**

**B Abbreviations 221**

C Computer Programs 223

Bibliography 224

# List of Tables


2.1 Definition of the bony landmarks used to define the body-embedded coordinate systems . . . . . 39
2.2 Anthropometric coefficients for segment mass and centre of mass . 49
2.3 Regression coefficients for the mass moment of inertia from Yeadon [274] . . . . . 50
2.4 Definition of parameters for moment of inertia models. Hip centre is defined as the geometric centre of the acetabulum. Knee centre is defined as the mid-point between the two epicondyles. Ankle centre is defined as the mid-point between the two malleoli. . . . . 51
3.1 Anatomical and tracking marker positions used on subjects. Definition of these markers, except MTHI, was given in Table 2.1. MTHI is a marker placed at the mid thigh. . . . . 65
3.2 Time-Averaged Force Magnification Ratio (FMR) During Activities . . . . . 68
3.3 Time-averaged isometric forces in the hip muscles . . . . . 70
6.1 Distance between the estimated and RSA determined HJCs in the pelvis co- ordinate system during flexion-abduction and circumduction exercises. The co-ordinates of the HJC measured with RSA is (-43, -90, 86). $\Delta$x, $\Delta$y and $\Delta$z are the three components of the distance, $\Delta$, along the three axes of the co-ordinate system. All the data are in millimetres. GT = greater trochanter; MT = mid thigh; LE = lateral epicondyle; FH = fibular head and LM = lateral malleolus. . . . . 159
6.2 Time-averaged segmental residual errors and hip joint position errors during flexion-abduction and circumduction exercises. In parentheses are standard deviations. . . . . 161

6.3 Muscle groups and ligaments considered in the three-dimensional lower limb model program. Also shown are the percentages of PCSAs of individual muscle units in their group. . . . . 164
6.4 Mean position of muscle origin and insertion relative to body-embedded co-ordinate system (BCS) compiled from White *et al.* [255]. . . . . 168
6.5 Landmarks for homogeneous scaling . . . . . 174
7.1 System unknowns considered in the present study. . . . . 190
7.2 Comparison of the time-averaged femoral axial forces: theory versus experiment. Forces are in Newtons. . . . . 193
7.3 Time-averaged forces transmitted in the force-bearing structures calculated by the model during DLS and SLS. . . . . 199
7.4 Resultant forces and moments transmitted at the mid shaft of the femur in the coronal plane under different loading conditions. Loading cases 1 to 3 were used by Carter *et al.* [43]. Loading condition 4 was from Huiskes [119]. Forces and moments calculated from the present model during SLS and gait are also listed for comparison. Two extreme loading conditions during walking were selected: Gait 1 corresponds to the first peak and Gait 2 the second, Figure 7.7. Conventions are according to Figure 7.8. For the present subject, $a = 15$ mm, $h = 43$ mm, and $L = 173$ mm. . 207

# List of Figures


1.1 The skeletal system of the lower extremities . . . . . 5
1.2 Envelope of contractile tensile force in terms of muscle length and contraction velocity . . . . . 8
1.3 A simple example showing different results obtained using reduction method, optimisation method with linear and non-linear criteria, and the DDOSC method. . . . . 27
2.1 Body-embedded coordinate systems . . . . . 37
2.2 Cardan angles defining the attitude of the BCS, $(\hat{x}_q, \hat{y}_q, \hat{z}_q)$, relative to the LCS, $(\hat{x}, \hat{y}, \hat{z})$ in $z \rightarrow y \rightarrow x$ sequence. First start from the BCS coincident with the LCS. Then rotate the BCS about $\hat{z}$ by an angle $\phi_3$ to have $\hat{x}$ rotate into $\hat{x}_1$ and $\hat{y}$ into $\hat{y}_1$ (a), then rotate about $\hat{y}_1$ by an angle $\phi_2$ (b) and then rotate about $\hat{x}_q$ by an angle $\phi_1$ to reach the final attitude of the BCS (c). $\phi_3$, $\phi_2$ and $\phi_1$ are the resulting Cardan angles. . . . . 41
2.3 Joint coordinate system . . . . . 43
2.4 Free body diagram of a general rigid body segment . . . . . 44
2.5 Free body diagram of the foot segment . . . . . 46
2.6 Free body diagram of the shank segment . . . . . 47
2.7 Free body diagram of the thigh segment . . . . . 48
2.8 Free body diagram of a cross section of the thigh segment . . . . . 49
2.9 Frustum used to model inertial properties of the distal part of a segment. . . . . 50
3.1 Modified prosthesis with inductive coupling in the case of subject IM (dimensions in mm). . . . . 54
3.2 Experimental arrangement of the isometric tests of the hip muscles: (a) flexors, (b) extensors, (c) adductors and (d) abductors. . . . . 56
3.3 The gait laboratory and the Vicon 370 motion data acquisition system . . . . . 58

3.4 The two AMTI force plates, showing the force plate ($S_1$ and $S_2$) and the laboratory ($S$) coordinate systems. . . . . 59
3.5 A typical set of simultaneous recordings from isometric hip exercises, captured from IM. (a) flexion, (b) extension, (c) abduction and (d) adduction. Solid lines are the measured telemetered force values, dashed lines the measured external loads. . . . . 69
3.6 Abductor test. Since the external force F is horizontal, the abductor muscle force T and axial compressive force C are equal and opposite. In this test, the Pauwels couple is dT and, together with the bending moment in the bone, $M_{bone}$, transmits the limb bending moment $M_{limb}$. The relative values of $dT$ and $M_{bone}$ are given in the text. . . . . 71
3.7 Force magnification and tensor fasciae latae activity during double (thin lines) and single (thick lines) leg stance: (a) measured ground reaction forces (dashed line) and telemetered axial forces (solid line) and (b) EMG envelope of the tensor fasciae latae. . . . . 72
3.8 Force magnifications during level walking. Thick line is measured axial force in prosthesis and thin line is measured ground reaction force. (HS = heelstrike; TO = toeoff). . . . . 73
3.9 Stick figures extracted from the Vicon system showing positions of the leg and the ground reaction forces during (a) double leg stance and (b) single leg stance. . . . . 74
4.1 Rotation about the longitudinal axis in the tibia: deviation experiment (Specimen M). From Wilson [259] . . . . . 79
4.2 Sagittal view of a human knee flexed to about 45° with most of the lateral femoral condyle removed. A possible four-bar cruciate linkage (ABCD) is superimposed. The instantaneous centre of the linkage is marked I. Note that in this view the attachment areas of the ligaments are obscured by the bones and by the ligaments themselves. . . . . 80
4.3 Diagrammatic representation of the four-bar linkage model used in the present study. The flexion angle is 70°. . . . . 81

4.4 The four-bar linkage model of the knee joint at (a) 0°, (b) 70° and (c) 140° flexion. Single thick lines are used to represent the two isometric fibres of the cruciate ligaments, $AB$ and $CD$. It is noted that the instant centre $I$ moves relative to each bones and that the tibiofemoral contact point moves posteriorly during flexion, from $X_1$ to $X_3$. The tibia is shown using line segments joining some particular bony landmarks. No attempt was made to reproduce the precise shape of the bone but the shape of the femoral condyle was calculated from the model. . . . . 83

4.5 Attachment areas of the ligaments were represented as straight thick lines and their shapes at the neutral position are displayed using five representative fibres: (a) ACL, (b) anterior half of PCL shown slack and posterior half straight, (c) MCL and (d) LCL. Slack fibres are shown buckled, taut fibres are shown straight. Detailed descriptions of the representation of the fibre shapes are given in Section 4.2.1.1 and 4.2.1.2 . . . . . 85

4.6 Fibres buckle when their attachments approach each other, as indicated by the posterior-most fibre. Here the anterior-most fibre represents an inextensible link which rotates about its distal attachment point, causing its proximal attachment point to move along a circle of radius $l_a$. It remains isometric during passive motion. . . . . 86

4.7 Right-handed co-ordinate system of a second mode buckled pin-ended fibre ($l < l_0$), with origin at its distal attachment point $\vec{d}_t$ and $x$ axis directed positively to its proximal attachment point $\vec{p}_t$. $\delta$ is the maximum transverse deflection in the direction of the $v$ axis. 87

4.8 Schematic representation of the fibre shape changes during anterior/posterior translation. An anterior-oriented fibre, as shown, is stretched with anterior translation and slackens with posterior translation. Anterior displacement increases the relative horizontal component of the force transmitted by the fibre. . . . . 88

4.9 Passive motion of the model ACL at 0°, 45° and 90° flexion: (a) in the first buckling mode ($n = 1$) and (b) in the second buckling mode ($n = 2$) . . . . . 90

4.10 Fibre recruitment patterns of the model ACL in response to anterior tibial translations of 4 and 8 mm at (a) 25° and (b) 90° flexion. . . . . 92
4.11 Model knee ligament at 0°, 45° and 90° of passive flexion. . . . . 93
4.12 Fibre recruitment patterns of the knee ligaments in response to anterior and posterior tibial translations of 4 and 8 mm at 25° flexion. . . . . 94
4.13 The geometric model of the knee joint at (a) 0°, (b) 70° and (c) 140° flexion. Single thick lines are used to represent the two isometric fibres of the cruciate ligaments. Straight dashed lines are also used to represent the quadriceps, hamstrings and gastrocnemius muscles except where they wrap around the bones. It is noted that the instant centre moves relative to each bones and, with the tibiofemoral contact point, moves posteriorly during flexion. The tibia is shown using line segments joining some particular bony landmarks. No attempt was made to reproduce the precise shapes of the bone but the shape of the femoral condyle was calculated from the model. (I = instant centre, A = ACL, P = PCL, C = tibiofemoral contact point, PT = patellar tendon, Q = quadriceps tendon, BB' = biceps, MM' = semimembranosus, TT' = semitendinosus and GG' = gastrocnemius). . . . . 100
4.14 The orientation of the line of action of a structure is defined by the angle $\theta$ between $-x$ and the vector directed from the insertion to the origin of the structure. Vectors oriented posteriorly for the extended position were given clockwise positive values (a); vectors oriented anteriorly for the extended position were given counterclockwise negative values (b). . . . . 102
4.15 Two possible representations of the line of action of the ACL: the isometric fibre (1) and the most posterior fibre (2). . . . . 103
4.16 Lines of action of the (a) two representations of the ACL: the isometric fibre (thick line) and the most posterior fibre (dashed line), (b) PCL, (c) LCL and (d) MCL as functions of knee joint angle. Lines with markers are experimental data from Herzog and Read [111]. . . . . 104

4.17 Lines of action of the (a) patellar tendon, (b) biceps, (c) semitendinosus and (d) semimembranosus as functions of knee joint angle. Lines with markers are experimental data from Herzog and Read [111]. . . . . 105
4.18 Moment arms of the (a) two representations of the ACL: the isometric fibre (thick line) and the most posterior fibre (dashed line) (b) PCL, (c) LCL and (d) MCL about the tibiofemoral contact point as functions of knee joint angle. Lines with markers are experimental data from Herzog and Read [111]. . . . . 106
4.19 Moment arms of the (a) patellar tendon, (b) biceps, (c) semitendinosus, (d) semimembranosus and (e) average of all hamstring muscles about the tibiofemoral contact point as functions of knee joint angle. Lines with markers are experimental data from Herzog and Read [111]. . . . . 107
4.20 Moment arms of the (a) patellar tendon and (b) average of all hamstring muscles about the centre of joint rotation (solid lines) and the tibiofemoral contact point (dashed lines) as functions of knee joint angle. . . . . 108
5.1 Two dimensional geometric model of the lower limb . . . . . 113
5.2 Computer model of the tibiofemoral and patellofemoral joints. . . 114
5.3 Joint angles (a-c) of the ankle, knee and hip during the walking cycle, obtained from an ensemble average from five subjects . . . 118
5.4 The two-dimensional model during walking based on data from the representative subject. . . . . 119
5.5 Joint angles (a-c) and resultant moments (d-f) of the ankle, knee and hip during the walking cycle . . . . . 123
5.6 Number of DDOSC solutions found at each data point over the walking cycle. (Minimum = 3, Maximum = 23, Mean = 9.16) . . 124
5.7 Temporal patterns of the DDOSC solutions over the walking cycle 125
5.8 Periods of muscle activity as indicated by EMG. From Collins [56]. 126

5.9 Temporal patterns of predicted muscle and ligament forces using optimisation method with (a) minimum sum of muscle forces (J1), (b) minimum sum of quadratic muscle forces (J2), (c) minimum sum of muscle stresses (J3), (d) minimum sum of ligament forces (J4), (e) minimum sum of joint contact forces (J5) and (f) minimum sum of cubic muscle stresses (J6). The EMG patterns of Figure 5.8 are plotted above the respective muscle patterns (bold lines). . . . . 127
5.10 Flexor test. Since the external force F is horizontal, the flexor muscle force T and axial compressive force C are equal and opposite. In this test, the Pauwels couple is $dT$ and, together with the bending moment in the bone, $M_{bone}$, transmits the limb bending moment $M_{limb}$. The relative values of $dT$ and $M_{bone}$ are given in the text. . . . . 133
5.11 Calculated (thick line) and measured (thin line) axial forces in the prosthesis during isometric hip flexion exercise from IM. Also shown are the external forces (dashed line). . . . . 134
5.12 Calculated (thick line) and measured (thin line) axial forces in the prosthesis during isometric hip flexion exercise from DG. Also shown are the external forces (dashed line). . . . . 135
5.13 Calculated (thick line) and measured (thin line) axial forces in the prosthesis during isometric hip extension exercise from IM. Also shown are the external forces (dashed line). . . . . 136
5.14 Calculated (thick line) and measured (thin line) axial forces in the prosthesis during isometric hip extension exercise from DG. Also shown are the external forces (dashed line). . . . . 137
5.15 Calculated (thick line) and measured (thin line) axial forces in the prosthesis during level walking from IM. (HS = heelstrike; TO = toeoff). . . . . 138
5.16 The interactive graphics-based window interface showing the animation of the passive motion of the knee joint . . . . . 141
5.17 Schematic block diagram demonstrating the interaction between the user, X window manager, window interface and modelling modules . . . . . 143

5.18 Geometry of the knee joints considering elastic ligaments with (a) anterior and (b) posterior translations of 4 and 8 mm at 25° of flexion. . . . . 145
6.1 Equivalent configuration of a ligament (From Wilson [259]) . . . . 151
6.2 Equivalent configuration of a articular contact point (From Wilson [259]) . . . . . 152
6.3 The parallel spatial mechanism model of the knee joint . . . . . 153
6.4 Co-ordinate system used for the evaluation of different methods for the estimation of the hip joint centre . . . . . 155
6.5 Errors associated with the rigid body assumption for the description of the motion of the pelvis-femur system. A: HJC errors; B: pelvis residual errors and C: femoral residual errors. . . . . 161
6.6 Axes of the ankle and subtalar joints: (a) sagittal view, (b) frontal view and (c) transverse view. Data compiled from Inman (1976) . 162
6.7 Two simple models for the description of muscles wrapping around the underlying bones: (a) a cylinder to simulate the shaft of a long bone such as the shaft of the femur and (b) a sphere to represent round bones such as the femoral head. $\vec{p}_{org}$ and $\vec{p}_{ins}$ are the position vecotrs of the origin and insertion of a muscle, respectively. The position vector of the wrapping point close to the origin of the muscle is represented by $\vec{p}_{wo}$ and the wrapping point close to the insertion of the muscle by $\vec{p}_{wi}$. The two wrapping points are determined by minimising the muscle length between the origin and insertion while subject to the constraint of the cylinder or the sphere. . . . . 170
6.8 Schematic representation of the geometry of the structures at the patellofemoral joint. The inset figure shows the force equilibrium of the three forces at the patellar force centre. . . . . 173
6.9 Stick figures of the three-dimensional model of the locomotor system during level walking in a series of positions. . . . . 175
6.10 Three stages of reconstruction of a femur: (A) data points on the surface of the bone, (B) wire frame reconstruction and (C) rendering and lighting. . . . . 176

6.11 Animation of the 3D model of the locomotor system as a series images using data obtained from a normal subject: (A) anterolateral and (B) posterolateral view. Ground reaction forces are shown as green lines. The length of a GRF vector of one body weight was scaled to the height of the ASIS so that the dynamic effect of the motion can be viewed by the length of the GRF. . . . . 179
7.1 Co-ordinate system at the level of prosthesis transducers used to represent the forces and moments transmitted by the prosthesis shaft. . . . . 191
7.2 Femoral axial forces during flexors test: theory (thick lines) and experiment (thin lines). . . . . 194
7.3 Femoral axial forces during extensors test: theory (thick lines) and experiment (thin lines). . . . . 195
7.4 Femoral axial forces during adductors test: theory (thick lines) and experiment (thin lines). . . . . 196
7.5 Femoral axial forces during abductors test: theory (thick lines) and experiment (thin lines). . . . . 197
7.6 Comparison of femoral axial forces during SLS and DLS: theory (thick lines) and experiment (thin lines). . . . . 198
7.7 Femoral axial forces during stance phase of gait: theory (thick lines) and experiment (thin lines). . . . . 200
7.8 Schematic representations of two typical proximal femoral models with the mid-shaft fixed and (a) subjected to a concentric force at the head of the femur or (b) additionally with simulated abductor muscle force. . . . . 205
A.1 The three reference body planes with a representative body in the standard anatomical position. . . . . 219
A.2 System for naming joint angles. . . . . 220

# Chapter 1

# Introduction

## 1.1 Overview

The human locomotor system is a highly complex leverage apparatus composed of bones, joints, muscles, ligaments and other soft tissues. While bones are held apart by articular surfaces at joints, ligaments hold them together, thus forming the skeletal link system. Controlled by the nervous system, muscles generate tensile forces between their origins and insertions on the bones and through relatively short lever arms apply moments at joints to provide static and dynamic stability of the skeleton in the presence of gravitational and other loads and to perform regularly precise control of limb movement. Human locomotion therefore involves a highly coordinated mechanical interaction between the muscles and other structural elements of the system. Any injury or lesion of any of the individual elements will change the mechanical environment and cause degradation, instability or disability of locomotion. On the other hand, proper modification, manipulation and control of the mechanical environment can help prevent injury, correct abnormality and speed healing and rehabilitation. Therefore, knowledge of the force transmission in the structural members of the locomotor system during activities provides a necessary basis for the design of prosthetic devices [97, 182, 216, 236, 250], the establishment and evaluation of rehabilitation programmes [48, 276], the study and treatment of bone fracture, the study of the aetiology and treatment of joint degeneration [206, 273], the prevention of injury and the improvement of athletic performance [104, 190]. However, direct measurement of internal forces in living subjects is possible only in exceptional circumstances such as through instrumented implants [4, 19, 35, 138, 214] and it

is highly unlikely that these procedures could be used routinely in human gait analysis. The estimation of the internal forces in the living body thus remains a great but attractive challenge for orthopaedic biomechanists.

One of the purposes of mathematical modelling is to allow calculation of the values of quantities which are difficult or impossible to measure from the values of quantities which can be measured. The human locomotor system represents a good example of the application. Many researchers have used mathematical modelling, in conjunction with noninvasive experimental measurements, to predict nonmeasurable internal forces in the locomotor system [56, 60, 100, 172, 193, 198, 209, 221, 222]. However, the results have not been completely satisfactory and the hope that mathematical modelling would provide all the necessary information for the above mentioned clinical applications still requires further research efforts. This situation can be attributed to the difficulties or inappropriate considerations in two primary aspects that stem from the mathematical modelling techniques which, in engineering terms, are *system identification* and *system analysis.*

System identification in the mechanical modelling of the locomotor system requires a comprehensive description of the geometry of the load-bearing structures both in static and moving states, here referred to as *kinematic geometry.* Unlike most engineering systems, the geometry and motion of which are clearly defined before analysis is performed, the locomotor system is more complicated and subject to a certain degree of biological uncertainty and variation [28, 255, 256], which makes system identification particularly difficult and prone to misrepresentation. As the body changes its shape during activity, the bones rotate and translate relative to each other, the muscle tendons and the ligaments rotate about their points of origin and insertion on the bones. Since they determine the lines of action of the forces transmitted by the articular surfaces of the joints and by the ligaments and muscles, the details of these movements are critical to an understanding of the way the structures of the body transmit their loads. Only when their lines of action have been defined can the calculation of internal force values, system analysis, be attempted. Accordingly, geometrical modelling of the locomotor system is a necessary and important preliminary to mechanical analysis. While it has been noted that joint kinematics determine the relative motion between body segments and thus the paths of the surrounding load-bearing structures, early studies devoted to the estimation of internal forces have mostly oversimplified the modelling of the joints. A common example is modelling the knee joint as a

simple hinge which ignores the rolling and axial rotational movements observed in natural knees [169, 252]. Using simple representations may easily overlook the contributions of the surrounding structures in the control of the kinematics of the joint and therefore introduce incomplete system identification. It seems that the improvement of the modelling of the kinematic geometry of the locomotor system relies strongly on more anatomical modelling [1] of the joints which will allow better representation of the lines of action of the load-bearing structures.

Determination of the forces transmitted by the load-bearing structures of the locomotor system under external loads is the main purpose of system analysis. The difficulty encountered in this stage results from the high mechanical redundancy of the locomotor system. According to Crowninshield and Brand [61], there are 47 muscles in each leg which could influence locomotion but the available equations of dynamic equilibrium are far too few to allow determination of all the forces simultaneously. Attempts to resolve this problem have been either to reduce the number of unknowns [172, 193, 203] based on certain mechanical or physiological principles or to introduce a certain selection principle which leads to the formulation of an optimisation problem [60, 100, 198, 209, 221, 222]. A different concept based on the search of mechanically and physiologically feasible dynamically determinate solutions was proposed by Collins [56] and Collins and O'Connor [58]. It is noted that, in most of the previous works, the only validation available was phasic electromyography (EMG) evidence, defining periods when each of several groups of muscles were on or off. A quantitative validation of a model which not only justifies the validity of the geometry of the locomotor system but also the mechanical interactions between its load-bearing structures is thus needed to fill the gap. Such a model would have immediate application to the design and testing of joint/bone prostheses and the evaluation of rehabilitation regimes of ligament deficient or reconstructed patients by studying the force interactions between muscles, bones and ligaments.

Another gap existing in the application of results from biomechanical studies to clinical problems has been the presentation and interpretation of the analytical data. Traditionally, analytical results are decomposed and presented at length in each anatomical plane in the form of graphs. While information in the anatomical

[1] Anatomical models are contrasted with phenomenological models. A phenomenological model is used to describe the response of the joint without considering its real structure whereas an anatomical model takes account of the behaviour of the various structural components forming the joint so anatomical modelling requires accurate geometric description of the real anatomy. Similar classification for knee joint models is found in [108]

plane of interest is helpful for clinical reference, a complete three dimensional data display provides more realistic support for clinical decision-making because the locomotor system itself and its responses to the internal and external forces are three dimensional in nature. In addition, it would not be an easy task for clinicians to reconstruct three-dimensional knowledge of a complex movement by themselves from individual components without any adequate technical support. In this regard, three dimensional solid modelling and image display could be a good tool for presentation of results and surgical simulation [49, 68, 137]. An interactive graphics-based window system may be useful in providing easy access to the analytical results by creating a 'look and feel' environment for the user to examine experimental data and interpret the analytical results with relatively few efforts.

In this chapter, some of the background information necessary for the study of the human locomotor system is presented, including an introduction to the anatomy of the human pelvis-leg musculoskeletal system. A review and discussion of the approaches utilised by other researchers is then presented. The role of geometric and mechanical modelling is emphasized. And finally the specific aims and scope of the current study are summarised.

## 1.2 Anatomy of The Pelvis-Leg Apparatus

Traditionally, knowledge of the anatomy of the human pelvis-leg apparatus has been established through visual inspection on dissected cadavers. Information acquired using this approach is usually qualitative or descriptive and limited to a single or small number of limb positions. Nonetheless, it can often give a good indication of the functions of individual structures. From the point of the current study, it can serve as a guideline for the development of a quantitative anatomical geometric model of the locomotor system which can be used to deduce the kinematic geometry of the system at any position and its use for further mechanical analysis.

### 1.2.1 Bones and Joints

The primary function of bones is to provide support and protection for the organs and soft tissues of the body. They form the main framework of the skeletal system. With muscles attached and articulating joints between them, bones form an

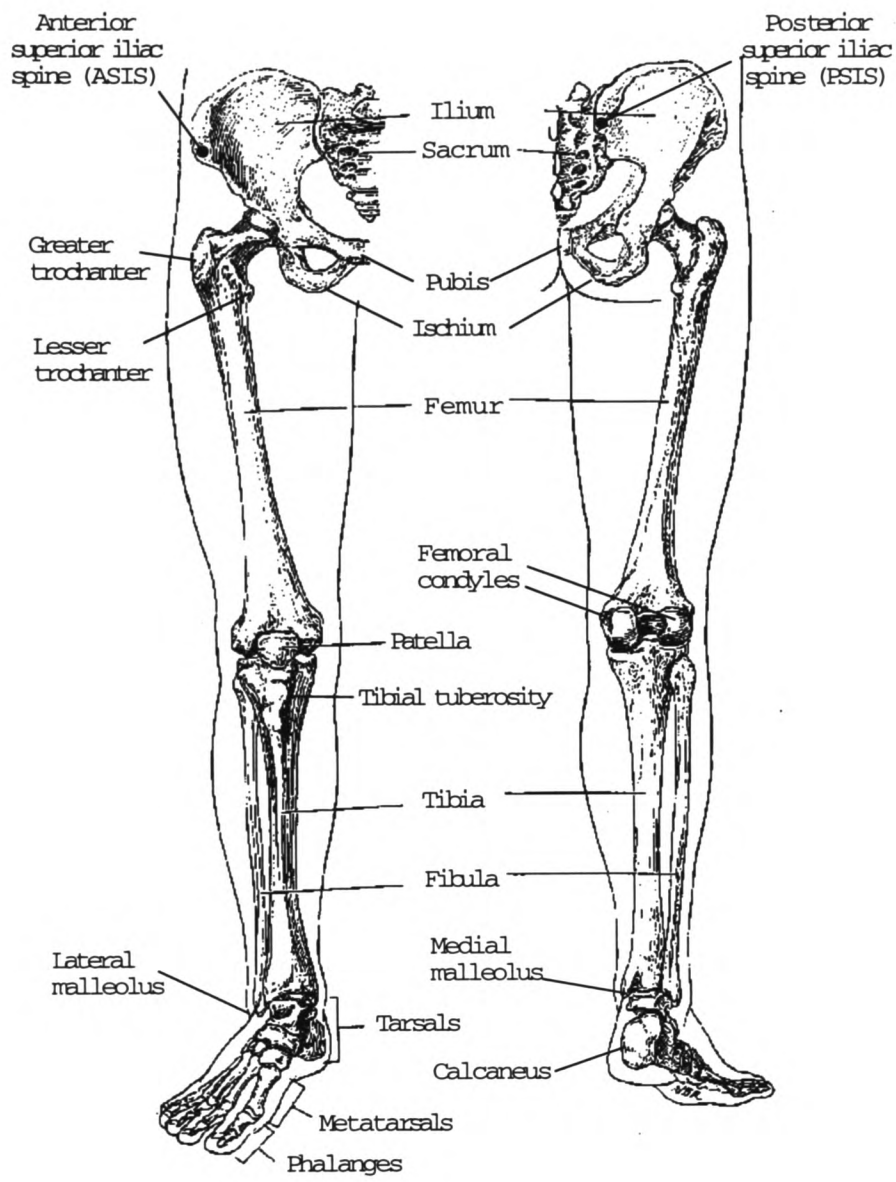



Figure 1.1: The skeletal system of the lower extremities

effective leverage system, which facilitates all kinds of human movements. Bones are living organs and through the activation of either *osteoblasts* (bone forming cells) or *osteoclasts* (bone absorbing cells) they can adapt their shapes or structural organisation to the surrounding mechanical environment, a process called *remodelling*. The relationship between bone remodelling and the surrounding mechanical environment is generally known as Wolff's Law [267]. Since bones adapt to mechanical stimuli, knowledge of the forces and thus stresses and strains experienced in the bones during activity is essential for a better understanding of their dynamic functions. Mechanical status of the bones can be affected by the forces applied by the muscles and ligaments and the forces between their articular surfaces and by any other changes of their shapes or mechanical properties such as those introduced by disease, injury or surgical procedures.

Joints are organs which function between two or more bones. The main joints

in the locomotor system are mostly *diarthrodial* joints, which permit basic free movement of one bone relative to another. The articular surfaces of the bones at the joint are covered by a thin layer of articular cartilage. The space between the articulating bones is called the *joint cavity.* Within the joint cavity, there is synovial fluid which acts as a lubricant for joint movement and serves as a nutritional source for articular cartilage. The final mobility of a diarthrodial joint is determined, in addition to its articular surfaces, by the connective tissue that makes up the organ, such as ligaments and joint capsule. Therefore, the function of a joint in controlling the relative motion of its articulating bones should be studied by considering the joint organ as a whole.

Figure 1.1 shows the skeletal system of the pelvis-leg apparatus. Bony structure of the lower limbs is connected with the torso by the *pelvis.* The pelvis consists of three components, namely the *ilium*, the *ischium* and the *pubis.* It provides a load path for the main bulk of the body weight to be supported by forces applied through the feet. The acetabulum is the socket which receives the head of the femur to form the hip joint. Normal hip joints are ball and socket joints which allow the pelvis and the femur to move relative to each other about a single point. The range of movement is constrained by the surrounding soft tissues, including muscles. Usually, the position and orientation of the pelvis can be determined by means of some palpable bony landmarks such as the anterior superior iliac spines (ASIS) and the posterior superior iliac spines (PSIS).

The *femur* is the longest bone in the body. The proximal end of the femur has a head, a neck and greater and lesser trochanters. The distal end of the femur is made up of two condyles. The greater trochanter is a large mass of bone which projects upwards at the base of the neck. It is the main insertion of the hip abductors such as gluteus medius and gluteus minimus and serves to lengthen their lever arms about the hip. The lesser trochanter is much smaller and is the elevation on the medial aspect of the upper end of the shaft. It is for the insertion of the iliopsoas muscle. The two femoral condyles form the upper articulating surface of the knee joint. The groove between them is the articulating surface with patella. The patella is a sesamoid bone, held in place by the quadriceps tendon and the patella tendon. It increases the lever arms of the two muscle tendons and acts in some senses as a pulley, allowing a change in direction of the pull of the muscles. A more detailed description and references of the knee joint and its structure will be given in Chapter 4. For the definition of the orientation of the femur, the greater trochanter and the two epicondyles on the distal femur

are usually used.

The lower articulating surface of the knee is formed by the condyles of the *tibia*, which is also known as the tibial plateau. The tibia, like the femur, is a long bone with a strong shaft and expanded proximal and distal ends. The proximal anterior tibia is a prominent *tibial tuberosity*, to which the patellar tendon is attached. On the under surface of the lateral condyle is the articulation of the tibia and the *fibula*. The fibula does not articulate with the femur. It provides an attachment for numerous muscles and forms the lateral part of the socket for the ankle joint by means of its lateral malleolus. The distal ends of the tibia and fibula and the upper surface and sides of the talus form the ankle joint or the tibiotarsal joint, which is mainly a hinge-like joint allowing plantar and dorsiflexion. Between the inferior surface of the talus and the superior surface of the calcaneus are the subtalar joints. Pronation and supination motion of the foot relative to the tibia is provided primarily by the subtalar joints. Bones of the foot are rather complex and are beyond the scope of this introductory section.

### 1.2.2 Ligaments, Muscles and Tendons

Ligaments are mainly bundles of fibrous connective tissue that are attached to the articulating bones at joints. They transmit tensile forces along the lines of their fibres and together with articular surfaces make up a joint. They guide and restrict the relative movement of the bones upon each other, maintain contact between the articulating surfaces of the bones and provide reinforcement in the joint capsule. Generally, they are considered to be passive structures that provide mainly structural stability for joints because the nervous system does not exert control over their actions. However, some investigations have suggested that the ligaments may have a proprioceptor role in addition to the well accepted mechanical function [14, 29, 129, 130].

Skeletal muscles are the prime force generators of the body, under the control of the nervous system. The smallest subunit of a muscle that can be controlled is called a *motor unit*, which consists of a motor neuron and all its target muscle fibres. The number of muscle fibres controlled by a motor unit depends on the fineness of the control required. It is generally accepted that the order of recruitment of motor units into activity is according to the *size principle*. That is, the smallest unit is recruited first and the largest last. When a muscle is activated, it produces tensile forces which are transferred to the skeletal system

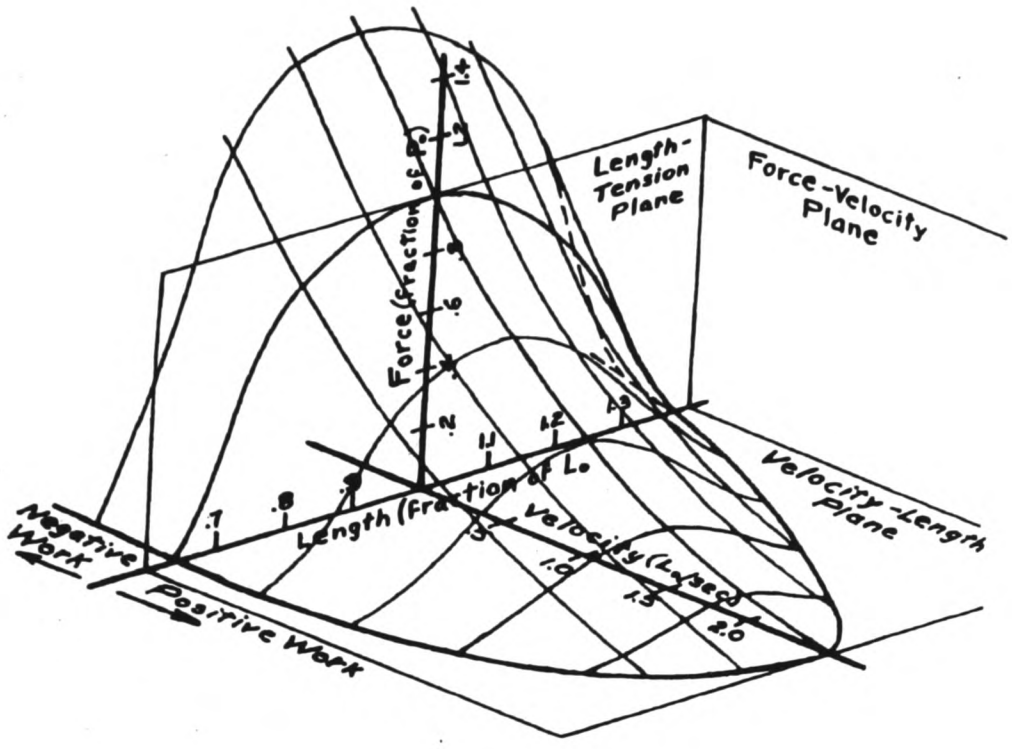



Figure 1.2: Envelope of contractile tensile force in terms of muscle length and contraction velocity

by the attaching tendons. The electrical indication of the contraction is the superposition of all action potentials of each motor unit involved. The resultant electrical signal associated the contraction is called an electromyogram (EMG). The study of muscle function through the inquiry of the electromyogram is known as electromyography [15].

Basically, skeletal muscles generate forces by through their contractile (active) elements, which are composed of two types of protein filaments, actin and myosin. The force development mechanism of the contractile elements has been explained by the crossbridge theory. The detail of this theory is discussed in McMahon [167]. Another element of the muscle is the connective (passive) element, which acts as an elastic spring. Figure 1.2 shows a three dimensional envelope of the tensile force generated by the fully activated contractile element in terms of muscle length and contraction velocity. At zero velocity, the contraction is called *isometric*, where muscle length remains constant. A contraction is referred to as *isokinetic* if the contraction velocity is constant. A muscle is said to be acting concentrically if it is allowed to shorten (contract with negative velocity) when it is activated. Otherwise, it is called eccentric contraction. The maximum tension a muscle can develop occurs at neutral muscle length (resting length). The force envelope shown in Figure 1.2 helps to understand the ability of a fully activated

muscle to generate force in a certain body position. However, the relationship between muscle force, length and contraction velocity when the muscle is not fully activated is not clear and still needs to be defined experimentally.

Usually, muscles are attached via tendons at two or more points to bones. For each muscle, the attachment points are distinguished as origin and insertion. For lower limb muscles, the origin is defined to be proximal and insertion to be distal. Accurate knowledge of the positions of muscle origins and insertions on the bones are important for the determination of muscle force orientation and moment arm with respect to joint rotation centres (or axes). A muscle crossing a joint can be further classified by the actions they produce in relation to a body movement. An *agonist* is the prime mover to resist the external moment at a joint. *Synergists* are muscles which work together with the agonist to prevent unwanted movements. *Antagonistic* muscles, on the other hand, are those opposing the action of the agonist.

Anatomy of the muscles and muscle groups that are responsible for the movement of the lower limbs are described in [171]. Their quantitative geometry will be described in Chapter 6.

## 1.3 Biomechanical Modelling

The scope and definition of *biomechanics* have not reached a consensus even among the research community of its own. Some authors held a broader view and defined biomechanics as mechanics applied to biology (e.g. [87]) while others tend to limit the scope to the investigation of the effect of internal and external forces on human and animal bodies in movement and rest [59, 148]. A precise definition is beyond the purpose of this thesis but from the point of view of mathematical modelling of the human locomotor system three categories of mechanical analysis can be applied: *kinematic, dynamic*, and *structural.* Kinematics is used to describe the change of the geometry over time of the elements of the body without reference to the forces that cause the change. Kinematic variables of interest include position, orientation, velocity, acceleration, and sometimes jerk. Dynamics deals with the kinematic responses of the system to internally and externally applied forces and therefore establishes the connection between the kinematic geometry and the forces applied. Using information from the previous two analyses, structural analysis determines forces transmitted among the members of the system and ultimately stress/strain distributions within each element. Depending

on the purposes of a study, the three analyses can be selectively performed.

### 1.3.1 Incorporation of Experimental and Theoretical Methods

The need for a combined experimental and theoretical modelling approach to the study of the human locomotor system has been discussed. Generally, experimental measurements are used to determine parameters of a system and to provide system inputs for the theoretical modelling analysis. Some experimentally determined quantities can serve as a means of validation of the theoretical modelling method. On the other hand, a theoretical model can be used to guide the design of experimental procedures which can be used for routine examinations in clinical practice. Moreover, using data from the experiments, it helps to estimate non-measurable quantities and to interpret experimental outcome. System parameters needed for theoretical analysis such as anthropometric data and anatomical information are mainly determined from experimental measurements [101, 112, 180]. Experimentally determined system inputs are usually kinematic and kinetic data associated with the movement investigated [56, 63, 100, 172, 221]. Experimental data that is not used for the above purposes is useful for the validation of the theory, such as EMG recordings.

### 1.3.2 Direct Versus Inverse Dynamics

Due to the fact that structural analysis of the locomotor system is difficult, there has been a large amount of research focusing on kinematic and dynamic analyses where the locomotor system was treated as a multi-link system without attempting to model the geometry of the structural elements, such as muscles and ligaments. They used measured kinematic and kinetic data to investigate human movement [106, 126, 135, 134] or partially to validate their simulation work [16, 41, 51, 186]. In utilising this data for theoretical analysis, two types of dynamics problems have been classified. A dynamics problem is called *Direct* when the forces applied to the system are said to be known and the objective is to determine the resulting motion of the system due to the applied forces. On the other hand, an *Inverse* dynamics problem is one which the motion of the system is known a priori and the applied forces are to be determined. This classification obviously comes from cause-effect considerations. However, it is important to

point out that from historical and practical points of view, the opposite is more appropriate.

Historically, Newton established his laws of motion by synthesizing the kinematic data of the moving planets and objects on the earth observed mainly by others including Kepler, Galileo and Descartes. His second law of motion which is the basis of dynamics states that the resultant force applied to a particle with a constant mass equals numerically the mass times the acceleration of the particle. In other words, kinematic data was used to calculate the resultant forces applied to the particle. If we recognise that Newton's approach as direct, which is most appropriate for the founder of dynamics, then the so-called direct dynamics becomes inverse. Moreover, practically, kinematic data is much easier to measure than forces which can only be deduced using the laws of mechanics. Most practical dynamic analyses therefore lie within the scope of the Newtonian dynamics. From these considerations, it seems that the present widely referred classification should be reexamined and Newton's approach deserves to be classified as direct. However, to avoid any confusion the current convention will be used in the presentation of the present study.

In the dynamic analysis of the human locomotor system as a multilink system, the force information of interest are resultant forces and moments at each joint. These are resultants of muscle forces and forces transmitted by the articular surfaces, ligaments and other soft tissues which are determined during structural analysis. If the inverse approach is used, a force distribution problem is formulated at each data frame and the dynamic indeterminacy of the system should be resolved, as mentioned previously.

In the case of the direct approach, optimal control theory is used to determine controls of the actuators of the dynamic system. Actuators considered can be joint moments or muscle forces. The experimentally measured kinematic data used varies with different problem formulations. However, a certain performance index is always needed. Chao and Rim [51] used an optimal control model to determine joint moments during gait by minimising the square differences between the measured states and those calculated from the system equations of motion. Although the authors proposed this method as an improvement of the differentiation process of measured displacement data commonly used in inverse dynamics approach, the formulation was actually direct dynamics. Others have used part of the measured displacement data as initial conditions for the optimal control problem and the rest as a means of validation [54, 53]. In the type

of problem formulation where joint moments were taken as actuators, a further structural analysis was needed to determine the forces transmitted in the muscles and other structural members of the system. On the other hand, in those formulations with muscles as actuators, the indeterminate problem was treated together with the dynamic problem. Various muscle models have been incorporated into dynamics models as actuators recruited by simulated optimal control strategies [11, 102, 190, 188].

Although optimal control of dynamic models with muscle actuators takes account of both muscle excitation-contraction and musculotendon dynamics, activities that fit into the framework of this approach are limited to those with a relatively clear performance criterion, such as maximum-height jump [190] and minimum time kicking [102]. It is difficult, if not impossible, to simulate pathological movement such as gait in children with cerebral palsy because working performance criteria for different groups of pathology are still unknown. In addition, the formulated problems involve non-linear skeletal and musculotendon dynamics, high dimensionality, unusual path constraints, and multiple controls so complete analytical solutions are not possible. Various numerical methods have been used to solve this problem but problems such as convergence to a global minimum, massive computational effort and model validation still remain unsolved [188]. Based on these considerations, the inverse dynamics approach was chosen for the present project to investigate the biomechanics of the human locomotor system during various activities.

### 1.3.3 Mechanical Modelling With The Inverse Dynamics Approach

The general procedure of the inverse dynamics approach is summarised as follows.

1. Model the pelvis-leg apparatus as an ensemble of rigid bodies connected by joints.

2. Embed a local coordinate system in each segment to define orientations of the links and their relative motion in space.

3. Collect position trajectories of surface markers placed on certain bony landmarks on each body segment, using stereophotogrammetry. Kinetic data using force plates, EMG data and other anthropometric measurements are also collected.

4. Smooth and differentiate the position trajectories to obtain velocity and acceleration information. Using this information along with kinetic data and anthropometric data, perform inverse dynamics analysis to yield inter-segmental forces and moments.

5. Establish geometric models of each segment and joint to describe the kinematic geometry of the structures of the lower limb, including muscles and ligaments, for the later determination of the forces transmitted by these structures.

6. Determine forces transmitted by each member of the system by solving the "force distribution problem".

7. Model validation.

8. Application of the model to various clinical problems.

Space kinematics and dynamics needed for items 1 to 4 will be discussed briefly in Chapter 2. Experimental apparatus and methods as well as associated data processing will be described in Chapter 3. Therefore, the review in the following sections is mainly on previous works in geometric modelling and on methodologies used to resolve indeterminate problems. Validation of these modelling works are discussed. Models used to study the influence of muscle activity on the forces in the bones and ligaments are also reviewed.

## 1.4 Geometric Models

Geometric modelling is central to the system identification of the locomotor system, which is a prerequisite of mechanical analysis. It contributes to the movement analysis in two aspects. One is the accurate description of joint motions so that kinematic information of the segmental system can be defined. The other is to give precise origins and insertions of muscles and ligaments, which allow the determination of orientations and moment arms of those force members during motion. With this information, only the magnitudes of the forces remain to be determined.

### 1.4.1 Linkage Models

Geometric models of the locomotor system can vary in complexity depending on the aims of the studies. A significant number of studies of human locomotion were done by treating the locomotor system as a multi-link system connected by idealised joints, hinge joints in two dimensional models [33, 16, 41, 51, 53, 186] and ball-and socket joints or a combination of the two in three dimensional models [9, 134, 139, 205]. No attempt was made to model the geometry of the joints and the surrounding structural elements, such as muscles and ligaments. These models were mainly used to get estimates of joint kinetics without attempting to determine forces transmitted in the internal structures. Similar mathematical link segment models have been adopted in current commercial motion analysis systems for the description of the joint kinematics and kinetics. Geometric and mechanical factors, such as lines of action, lever arms and forces of the muscles, that contribute to the observed kinematics and kinetics are unknown. Thus, it relies heavily on clinical experiences of the user to interpret the data and to judge the cause of the outcome. It is noted that since these models did not take account of actual motion of the joints, the results from these models can only be taken as approximations of true values. For the further study of internal forces, more detailed description of the joint kinematics and geometry of the load-bearing structures is needed. It seems that detailed analysis of the geometric and mechanical interaction between the muscles, ligaments and bones can provide more direct quantitative information for clinical decision making.

### 1.4.2 Joint Models

#### 1.4.2.1 Knee Joint

Perhaps because of the relatively complex structure and motion, and its essential role in locomotion, modelling of the knee joint has received extensive research effort [108]. Various types of knee models have been reported in the literature with different levels of complexity, from two-dimensional hinge joint to three-dimensional models with detailed descriptions of elastic articular surfaces and ligaments. However, only relatively simple models have been incorporated into lower limb models for the study of mechanics of the knee during activity. For example, the knee joint has been modelled either as simple hinge joints in two dimensional lower limb models [51, 66, 172, 209] or as ball-and-socket joints in

three dimensional works [9, 63, 222]. Its rolling and sliding movement pattern has been neglected, let alone the screw home mechanism in the three-dimensional motion of the knee.

In sagittal plane studies, only few considered the rolling and sliding motion of the femur on the tibia. The four-bar linkage model was the first that reproduced the rolling and sliding motion. It was proposed by Strasser [230] in 1917 and adopted subsequently by Barnett *et al.* [13], Kapandji [136], Huson [121], Menschik [168], Fuss [88] and O'Connor *et al.* [182, 184]. O'Connor *et al.* [184] used the model to explain the relationships between the geometry of the articular surfaces and the geometry of the ligaments and showed that the model reproduced accurately the rolling motion during flexion and extension of the femur on the tibia observed by Weber and Weber [252]. O'Connor *et al.* [180] added muscle tendons to the Strasser model and calculated their directions and moment-arms over the flexion range. The model was then incorporated into a lower limb model to study the muscle-ligament interactions at the knee during level walking by Collins and O'Connor [58] and Collins [57]. Delp *et al.* [68] incorporated an empirical model to take account of the rolling and sliding movement of the femur on the tibia but did not consider ligamentous actions.

Three dimensional models of the knee joint has largely been devoted to the study of joint stability and have become very complicated. Wismans *et al.* [266] developed a model with articular surfaces as rigid polynomial surfaces and 7 non-linear spring elements as the ligaments and joint capsule. For a given flexion angle, external forces and moments were assigned first and then the equilibrium position of the joint was calculated by solving 16 non-linear equations. Blankevoort *et al.* [25] extended Wisman's model to consider deformable articular surfaces and include more detailed representation of the ligaments. Essinger *et al.* [77] developed a model which included a rigid femoral articular surface and a deformable tibial surface. Ligaments were represented as extensible elements and a representation of the knee extensor mechanism was included. It is noted that these models were developed in such a way that equations of mechanical equilibrium together with constitutive equations and compatibility conditions were needed to determine the relative position of the femur and tibia and thus the associated structures. In other words, forces and moments should be known first in order to determine the geometry of the joint structures. This is a potential limitation and/or difficulty to its application to gait analysis because the geometry of the structure of the lower limb needs to be given as *a priori* before structural analysis can be performed.

Perhaps this is why the above mentioned models have not been incorporated into a lower limb model for the study of human movement.

Recently, Wilson and O'Connor [261, 259] proposed a three dimensional knee model based on a parallel spatial mechanism, which treated the knee joint in a different way. They suggested, based on studies using the geometry and mechanics of the four-bar linkage knee model [58, 57, 181, 277, 278, 279], that kinematics and mechanics of the knee can be dealt with separately and sequentially. Their model represents a three dimensional analogue to the four-bar linkage knee and is aimed at the description of the kinematic geometry of the knee joint. In the model, the anatomical structures constraining the knee (ACL, PCL and MCL) were modelled as higher kinematic pairs. The femoral and tibial condyles, contributing two other constraints to the motion of the knee, were considered to be spherical and flat, respectively and were also modelled as higher kinematic pairs. Given the parameters of the knee model which defined the geometry of the mechanism at the extended position, the geometry of the structures of the knee joint can be determined by a forward kinematic analysis without reference to any externally applied forces and moments. The main features of the knee motion, rolling and sliding and screw home motions, were successfully predicted by the model. Since the model defines the joint positions without needing to know the external forces and moments *a priori*, it is more suitable for incorporating into lower limb models for the study of the human motion.

#### 1.4.2.2 Patellofemoral Joint

The configuration of the patellofemoral joint facilitates the extension of the knee by increasing the lever arm of the extensor apparatus about the axis of flexion [85, 1]. The patella, sliding in the femoral trochlea, acts as a guide for the quadriceps tendon, bringing together the divergent inputs from the four heads of the quadriceps and transmitting these forces to the tibia through the patellar tendon. A proper representation of this mechanism is essential for the estimation of the forces transmitted at the knee.

In a review of knee joint models in 1988, Hefzy and Grood [108] pointed out that "even a 2-dimensional anatomical knee model which includes both patello-femoral and tibio-femoral joints does not exist". Indeed, the description of the knee extensor mechanism, compared with that of the tibiofemoral joint, has received less notice in the studies of internal forces in the lower limb during activity.

Seireg and Arvikar [221] simply joined straight lines between the origins of the quadriceps and the insertion of the patellar tendon at low flexion angles. At higher flexion angles, they assumed that the patellofemoral contact force is sharing the same line of action as the tibiofemoral joint contact force. In their studies of human gait [222], they distinguished the two joint contact forces but how the knee extensor mechanism was modelled was not described. Morrison [172], in his analysis of knee joint forces during gait, determined the changing direction of the patellar tendon from lateral x-ray taken at different positions. The calculated forces transmitted by the patellar tendon were taken as the quadriceps forces. In some studies [100, 209, 192], no description of the extensor mechanism was given whereas others [28, 196, 61] modelled the joint as a pulley in order to consider the effect of the patella in increasing the lever arm of the quadriceps muscles. In these studies, force transmission at the joint was not emphasised.

More anatomical models of the joint in the sagittal plane have been reported in the literature. van Eijden [243] developed a patellofemoral model using measured profiles of the articular surfaces of the femur and the patella as well as the patellar tendon length and patellar length as model parameters. The model was used to calculate the geometry of the joint structures, namely the patella, patellar tendon, quadriceps tendon and the patellofemoral contact force, in terms of knee flexion angle. Kinematics of the tibiofemoral joint were not incorporated and lever arms available to the two tendons were not studied. Yamaguchi and Zajac [272] reported a similar model to characterise the effective lever arms for the quadriceps muscles. The patella was modelled as a rectangle and the relative movement between the femur and tibia was prescribed based on experimental data of the instantaneous centre of joint rotation from the literature. O'Connor *et al.* [180] modelled the patellofemoral joint as a single point, the point at which the lines representing the quadriceps and patellar tendons and the patellofemoral contact force intersect, and incorporated into the four bar linkage tibiofemoral joint model to facilitate the kinematic interactions between the two joints. The combined knee joint model was then used to study the muscle-ligament interactions during activities [179, 178, 181, 58, 57]. For a better description of the orientation of the patella and the contact between the patella and the femoral condyles at high flexion angles, a bi-articulating patellofemoral joint model was recently proposed by Gill and O'Connor [93]. The model predicted the proximal rolling of the patella on the femur during flexion, as observed experimentally by Goodfellow *et al.* [96].

In 1991, Hirokawa [113] presented the first three-dimensional model of the patellofemoral joint with detailed mathematical description of the geometry of the articular surfaces based on experimental measurements. The patellar and quadriceps tendons were represented by elastic springs. The kinematics of the joint, the forces transmitted by the two tendons and the stresses in the articular surfaces were determined simultaneously using equations of equilibrium and constitutive and compatibility conditions. Recently, Heegaard *et al.* [107] developed a similar model based on finite element methods. The joint structures were modelled as non-linear elastic materials. The results were compared favourably with experimental measurements. Since the objectives of the above two studies were to describe the mechanics of the patellofemoral joint, the kinematics and mechanics of the tibiofemoral joint were not incorporated. Although these models contribute to the detailed description of the patellar kinematics and the stress analysis of the articular surfaces, their use in whole leg models to describe the knee extensor mechanism for the study of human movement is limited by the fact that force information was required to determine the geometry of the joint which is not suitable for the analysis using inverse dynamics. Moreover, these kind of models require extensive numerical calculations and seem computationally expensive for the purpose of gait analysis. It seems preferable that the kinematic geometry of the joint is first defined from pure geometrical arguments and then used for mechanical analysis.

#### 1.4.2.3 Hip Joint

The hip joint has been considered as a ball-and-socket joint, with three degrees of freedom, in three dimensional modelling works [9, 63, 61, 68, 82, 100, 103, 194, 196, 192, 209, 222] and as a simple hinge joint in two-dimensional models [51, 53, 56, 57, 66, 186, 189, 213, 247]. This agrees with the general understanding of the joint from a functional [136] and anatomical [171] point of view. Therefore, there exists no controversy in modelling the hip as a joint with a unique centre of rotation except in certain situations where significant joint deformities are involved and special considerations are needed to describe the kinematic geometry of the joint. The problem of the modelling of the hip joint thus reduces to the accurate and reliable estimation of the hip joint centre (HJC).

Various techniques have been utilised to locate the three-dimensional positions of the HJC. Radiographs were used by some investigators to locate precisely the

HJC [28, 63, 75] while others relied on their general knowledge of the location of the HJC in relation to external landmarks [193, 197, 65]. In general, invasive methods are not suitable for routine examination purposes in gait laboratories. For the estimation of the HJC on a subject specific basis, two less expensive but relatively accurate non-invasive methods have been proposed in the literature: the *prediction approach* and the *functional approach.* Prediction approaches [7, 8, 17, 237] are based on the establishment of a fixed relationship of the HJC and the selected aspects of the pelvis geometry (e.g. pelvic width) from anthropometric measurements on cadaveric pelves or on living subjects using x-ray. Using this relationship, the location of the HJC can be obtained from palpable bony landmarks. Since the relationship reported in the literature was established based on a limited number of specimens, its application to a wide range of subjects needs to be confirmed.

The functional approach, also known as the *rotational method*, was first proposed by Cappozzo [37]. This method is based on the assumption that the thigh is a rigid body and the HJC is the centre of a sphere described by the three-dimensional rotation of a point on that segment. In a comparative study using Roentgen Stereophotogrammetric measurements of the HJC as a reference, Cappozzo *et al.* [40] reported that the functional approach was more accurate than other prediction approaches, suggesting that the functional approach is more promising in routine gait analysis. However, in many clinical settings where the range of joint motion is limited, the application of this method may be difficult.

#### 1.4.2.4 Ankle and Subtalar Joints

In gait analysis, the gross motion of the foot relative to the shank has often been described using ball and socket joint models which allow three rotational degrees of freedom about a fixed joint centre [222, 63, 9, 100, 61]. Euler/Cardan angles [55, 269] are used to represent the joint motion in physiological terms, namely plantarflexion/dorsiflexion and inversion/eversion. Since the ankle joint axis is approximately mediolateral, Euler/Cardan angles along this axis can reasonably represent the plantarflexion/dorsiflexion motion of the talus relative to the tibia. This has been the basis of modelling the joint as a revolute joint in two-dimensional models [51, 53, 56, 57, 66, 186, 189, 213, 247]. However, the other two Euler/Cardan angles do not correspond directly to the inversion/eversion motion which is predominately accommodated at the subtalar joint.

In 1969, Isman and Inman [125] performed comprehensive anthropometric studies of the human foot and ankle and quantified the two principal joint systems at the ankle complex: the ankle (or talocrural) joint between the shank and the talus and the subtalar (or talocalcaneonavicular) joint between the talus and the foot. Two-revolute models of the ankle joint based on these findings were reported [68, 203]. Studies have been performed to decompose the relative motion of the foot relative to the tibia into rotations about the ankle and subtalar joint axes [71] and moments about these axes during gait were also reported [220]. Recently, van den Bogert *et al.* [240] used 3-D movement analysis to locate the positions and orientations of the joint axes. Parameters of their two-revolute model were fitted to the measured relative movements between the foot and shank using an optimisation method. The results were reported to be in good agreement with their previous *in vitro* studies and those in the literature.

It is noted that the models reviewed above are basically phenomenological models based on functional grounds. The ankle and subtalar joints were taken as simple hinge joints. A more anatomical model of the ankle joint complex which takes account of the geometry of the articular surfaces and ligamentous constraints has not been reported. More recent studies have shown that fixed axis of rotation may not be correct for both joints [227, 145]. An attempt to develop an anatomical kinematic model of the ankle joint considering articular and ligamentous constraints has been made by modelling the joint as a four bar linkage comprising the tibia/fibula, talus, calcaneofibular ligament and the tibiocalcaneal ligament [146]. The model predicted the moving pattern of the axis of rotation which was in good agreement with experimental measurements.

### 1.4.3 Geometry of Muscles and Their Tendons

In addition to the joint models used to describe the relative motion of the body segments, a comprehensive representation of the geometry of the musculotendon structures is needed for the structural analysis of the locomotor system. Two approaches have been suggested in the literature to describe the lines of action of the muscles and their tendons: the straight line approach and the centroid line approach [127, 128].

The straight line approach assumes that the force transmitted by the muscle acts along the straight line joining its points of origin and insertion while the centroid line approach is based on the assumption that the path of the force

transmitted by a skeletal muscle can be defined by the locus of the centroids of its transverse cross-sections. Since the centroid line approach requires the collection of a huge amount of data to represent even a single muscle in only one body position, its application to the modelling of the complex locomotor system during activity has been limited. Therefore, the straight line approach has been adopted in most of the modelling works [63, 70, 172, 193, 198, 209, 221, 222]. However, the representation of the line of action of a muscle by simply joining its origin and insertion can cause nonanatomical situations where the muscle line of action passes through the underlying bone [137]. Some authors have tried to avoid this problem by giving fictitious via points between the points of origin and insertion [28, 68] but these points are usually fixed relative to a bone segment so muscle penetration into the bones can not be totally avoided.

An improvement of the straight line approach may be through the modelling of the musculotendon wrapping around the underlying bone. Geometrical description of the bones is necessary for this approach. An attempt in two-dimensional modelling has been made by O'Connor *et al.* [180] in studying the geometry of the knee joint and its surrounding structures. In general, the use of the straight line approach requires the locations of origins and insertions be known as *a priori*. The determination of this information is thus necessary for the geometric modelling of the locomotor system.

While invasive methods are not applicable to living subjects, limitations (e.g. accuracy, cost, side-effects) on current non-invasive methods such as palpation and radiographs, have prevented them from being used for routine movement analysis. The most commonly used method is to establish a complete set of muscle data from cadaveric studies or from living subjects using non-invasive methods, and then map to individual subjects of varying stature following certain scaling procedures.

In cadaveric studies, methods used to measure locations of muscle origins and insertions include planar or biplanar radiography [172], direct digitisation [147] and serial cross-sectioning with photography and digitisation [6]. Computerised Tomography (CT) and Magnetic Resonance Imaging (MRI) may also be used to get data from living subjects [56, 212]. Limited databases of the three-dimensional co-ordinates of the attachments of the lower limb muscles have been reported in the literature. One commonly adopted data base is that of Brand *et al.* [28]. They defined co-ordinates of origin and insertion of 47 lower limb muscles from three cadaver specimens. Radiographically visible markers were used to mark muscle

origins and insertions, co-ordinates of which were then measured using biplanar X-ray images with digitisation. A homogeneous scaling scheme similar to the one proposed by Lew and Lewis [149], which was based on uniform deformation of bones along three orthogonal co-ordinate directions, was used to scale data from cadavers to individual subjects. They suggested that the scaling scheme would reduce substantially errors of muscle force predictions introduced by the use of single or average data.

Since the data base of Brand *at al.* required internal landmarks for scaling and fictitious attachments were used for bi-articular muscles, which are not suitable for movement analysis, White *et al.* [255] published another set of three-dimensional co-ordinates of 40 lower limb muscle units with respect to local co-ordinate systems defined by superficial landmarks. The same scaling scheme was used to map original data to living subjects but they based the scaling on co-ordinates of superficial landmarks rather than internal bony landmarks that could only be obtained using radiography or indirect estimation. In addition to errors caused by artefacts during measurements, both studies suggested that a main source of error in data mapping was due to anatomical variability not accounted for by homogeneous scaling. Lewis *et al.* [151] proposed a nonhomogeneous scaling method based on finite element theory to study anthropometric scaling between bones but no similar study in co-ordinates of lower limb muscles was reported. Since their method required at least 12 bony landmarks to define the scaling elements, it becomes a potential limitation in the application to the gait analysis.

## 1.5 Structural Analysis

Given resultant forces and moments at each joint, structural analysis is then applied to determine how these forces and moments are transmitted by the associate load-bearing structures. Since the geometry of the structure of the locomotor system and the resultant forces and moments are varying over time, the general approach is to perform structural analyses in a discrete manner. Only those time instants of interest are considered and these are usually instants where the movement data is collected. At each time instant, a "force distribution problem" is formulated according to force and moment equilibrium where the resultant forces and moments are distributed to the associate structural members. This gives a set of linear equations with force magnitudes of the structural members as unknowns which usually out-numbered the available equations. In other words, the

force distribution problems are mathematically indeterminate and the human locomotor system is an indeterminate system. Therefore, extra mechanical and/or physiological information is needed to resolve this problem. Two main approaches which have appeared in the literature are the *reduction method* and the *optimisation method.* The *dynamically determinate one-sided constrained (DDOSC)* method is a development of the reduction method. In this section, these methods are briefly reviewed. The strategies within these methods adopted to search for the final solution is also discussed via a simple example with three unknown variables and one equation.

### 1.5.1 Reduction Method

The first attempt known to the author, to distribute the joint resultants to individual muscles and articular surfaces, i.e. the structural analysis as defined in the present review, may be the works of Paul in 1965 and 1967 [193, 194]. He used the so-called reduction method to calculate forces transmitted by the muscles and articular surface at the human hip during level walking. In order to reduce the indeterminate problem to a determinate one, muscles spanning the hip joint were simplified to six functional groups and it was assumed that no more than three muscles were active at any instant. These assumptions were based on anatomical knowledge and physiological functions revealed by the phasic EMG activity. However, the possibility of antagonistic muscle activity was explicitly excluded from the analysis.

The same approach was then utilised by Morrison [172, 174] to investigate the mechanics of the knee joint. Three muscle groups, quadriceps, hamstrings and gastrocnemius, and four ligaments, the two cruciates and the two collaterals, were included in his knee model. The flexion axis of the knee was assumed to be fixed relative to the femur and the tibia. Thus, the movement between the femur and the tibia was pure sliding without rolling. The quadriceps was the only extensor to resist flexion moment, whereas extending moment was resisted by either hamstrings or gastrocnemius. By these simplifications, he was able to deduce a determinate system, which allowed the unique determination of member forces. Again, no antagonistic muscle activity was considered.

It is noted that the load sharing between co-operating individual muscles in each muscle group using the reduction method was not considered until the work of Procter and Paul [203]. Inverse dynamics was first performed to calculate

resultants at the human ankle joint for normal locomotion and then the reduction method allowed them to obtain unique solutions for the simplified muscle groups. Finally, the group muscle force was distributed to each member muscle according to their weighting factor, average tendon cross-sectional area as a proportion of the whole area for the group. The absence of antagonistic activity was also assumed.

The most important assumption of the reduction method is that muscles with consistent function and with similar anatomical orientations can be grouped into functionally equivalent units. However, this reduction process should be done with care since some muscles have not only a primary function (e.g. flexor) but also secondary function (e.g. rotator). It may be inappropriate to group muscles simply based on their primary function. In addition, in certain muscles with broad attachments, different parts of the muscle fibres may have different functions so sometimes it is necessary to separate it into functional parts rather than take it as a whole.

Another implicit assumption of the above studies, also in relation to reductionism, was that the total locomotor system could be analysed by a series studies of separate joints. This limited the explicit consideration of bi-articular muscles. Use of phasic EMG information to decide muscle sequencing prior to analytical calculation precluded the possibility of qualitative model validation.

### 1.5.2 Optimisation Method

In contrast to the reduction method, which reduces the number of unknowns, the optimisation method introduces an extra criterion, on which the search for the final unique solution over the feasible region is based. It is the selection of this extra criterion and therefore the optimisation method which has received mixed support and criticism.

From the engineers' point of view, it is always desirable to design a system with optimal performance while subjected to some physical constraints. In the field of biomechanics, an available example is Wolff's law [267] which states that the natural bone remodelling process adapts the structure and the microstructure of the bone to the loads borne by the skeleton with a minimum amount of material. In engineering terms, it is a minimum weight design. However, is it the actual minimisation objective that the body chooses? What is the minimisation objective our locomotor system follows in performing activities? Or, back to the

very beginning, does a global minimisation objective which applies in every instance exist? Experimental evidence is needed to answer these questions and to validate theoretical works that are based on certain minimisation assumptions.

The use of an optimisation method to evaluate quantitatively member forces in the redundant musculoskeletal system of the lower limb was introduced by Seireg and Arvikar [221]. They applied various criteria to their model at three static postures, standing, stooping and leaning, including minimum sum of muscle forces, minimum sum of muscle work, minimum sum of the vertical joint contact forces, minimum sum of joint moments carried by the ligaments, and their weighted combinations,. They suggested that the minimisation of the weighted sum of muscle forces and joint moments carried by the ligaments was most consistent with surface EMG signals. This criterion was then further used to study quasi-static walking, i.e. neglecting inertia forces of the segments [222]. The results were reported to be consistent with typical EMG patterns for level walking. Since the equilibrium equations and the proposed criteria were linear functions, the formulated problem was a standard linear programming problem. The simplex method was therefore used to solve it.

In 1978, Crowninshield [60] proposed another linear minimisation objective, minimum sum of muscle stress. Muscle stress is defined as force per unit muscle physiological cross-sectional area (PCSA). Crowninshield *et al.* [63] also used this criterion to study the mechanics of the hip during level walking, stair climbing and rising from a sitting position. In order to obtain a more physiologically reasonable solution and predict muscle synergism, extra constraints on maximum allowable tensile stress were imposed. In their model, ligamentous contributions and antagonistic muscle activity were neglected. Therefore, only equations of moment equilibrium at the three joints and equations of force equilibrium at the hip were used to define their feasible region. This implied that the solution domain was enlarged and muscles at the knee and ankle should transmit larger forces.

The concept of allowable muscle stress was also adopted by An *et al.* [5] to study the elbow joint. Instead of imposing different stress limits, they imposed a common upper bound on individual muscle stresses and calculated the optimum solution which minimised the common upper bound. In theory, this formulation is called a mini-max programming problem, which forced an even distribution among design variables, i.e. predicted muscle forces. Although results obtained was verified by EMG evidence, the physiological basis behind this formulation,

however, was not clearly explained.

Basically, the above formulated distribution problems were all in linear programming format. Therefore, the number of nonzero muscle forces could only be no greater than that of equations available, including design constraints. This theoretically expected result was also seen in Rohrle *et al.* [209] and noted by Hardt[100] and Pedotti *et al.* [198]. In light of this limitation and due to the challenges to the physiological basis of these minimisation objectives, more physiology based non-linear criteria were proposed. Crowninshield and Brand [61] proposed a criterion of maximum endurance of musculoskeletal function, which was related to the inversely non-linear relationship of muscle force and contraction duration, based on a number of experimental studies. An equivalent minimisation criterion, minimum of sum of cubic muscle stresses, was used to study human gait and substantial agreement between predicted activity pattern and EMG recordings was reported.

Dul *et al.* [73, 72] proposed a non-linear minimum fatigue criterion and suggested that load sharing between synergistic muscles should take account of muscle fibre type (i.e. fast and slow) as well as other mechanical parameters. Compared with other criteria, the proposed criterion was reported to have the best predicted results, verified by experimentally measured soleus and medial gastrocnemius force in the cat hindlimb during locomotion available in the literature.

### 1.5.3 DDOSC Method

Both reduction and optimisation methods aim to find an unique solution at the expense of either reducing the number of muscle investigated or choosing arbitrarily additional criterion, which has not been validated. Recent works by Collins [56] and Collins and O'Connor [58] suggested a different solution philosophy, called the Dynamically Determinate One-Sided Constrained (DDOSC) method. A set of mechanically admissible solutions was generated first by systematically eliminating redundant unknown variables and then one physiologically reasonable solution could be selected from this smaller solution set based on temporal EMG information. Detailed description of the method will be given in Chapter 5 as it is used for the mechanical analysis of the human locomotor system. In their studies, the aforementioned four bar linkage knee model [182, 183, 184, 180, 179], which allows the rolling and sliding movement between the femur and the tibia

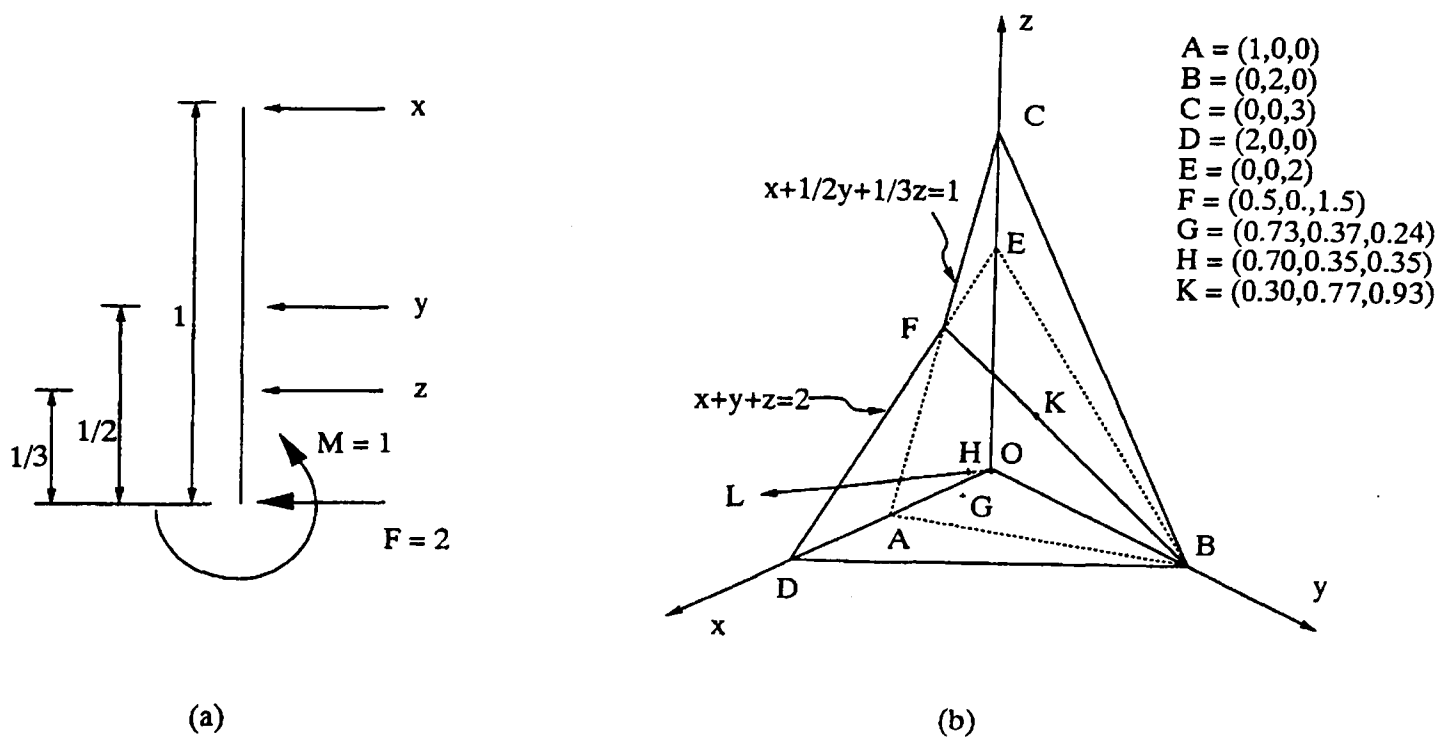



Figure 1.3: A simple example showing different results obtained using reduction method, optimisation method with linear and non-linear criteria, and the DDOSC method.

and so the determination of axis of joint rotation and orientations of two cruciates, articular contact force and associated muscles, was incorporated into their whole leg model. Due to this comprehensive geometrical joint modelling, they were able to include all equilibrium equations (not only moment equations as usually used in optimisation approaches) and consider fewer unknowns (orientations of ligaments and contact force were defined by the model). Antagonistic muscle activities were not precluded from this method. The calculated forces transmitted through the knee were in reasonable agreement with measurements on post-mortem specimens loaded in a number of simple static configurations.

### 1.5.4 Analytical Examination of Methods for Muscle Force Prediction

Although comparisons and validations of various optimisation criteria and formulations have been reported [46, 109, 196], a thorough examination of the strategies utilised by the reduction method, the optimisation method and the DDOSC method is still needed for a clear view of these methods. A simple example is devised to fulfil the discussion and to demonstrate the analysis procedures.

### 1.5.4.1 Problem Formulations

Consider a simple system as shown in Figure 1.3a. If, for simplicity, the joint contact force is assumed to have a known value, the resultant joint moment $M$ and force $F$ should be shared by three synergistic muscles, $x$, $y$ and $z$. Therefore, the equations of moment and force equilibrium can be expressed as follows:

$$x + \frac{1}{2}y + \frac{1}{3}z = 1 \quad \text{(moment equilibrium)} \tag{1.1}$$

$$x + y + z = 2 \quad \text{(force equilibrium)} \tag{1.2}$$

Requirements that muscle forces should be tensile give the following one-sided constraints:

$$x \geq 0 \tag{1.3}$$

$$y \geq 0 \tag{1.4}$$

$$z \geq 0 \tag{1.5}$$

If only the equation of moment equilibrium, Equation 1.1, and the one-sided constraints are considered, a case when orientations of ligaments and contact forces are not determined from geometric modelling, the force distribution problem for this system will have three unknown muscle forces and only one equation. This results in an infinite number of solutions, distributed throughout the feasible region $ABC$ as shown in Figure 1.3b. If the force equilibrium equation is further imposed, the feasible region is restricted to a line $BF$, Figure 1.3b. With the two different formulations, the problem of force distribution will be solved and discussed.

### 1.5.4.2 Optimisation Method

A general statement of a constrained optimisation problem is the following [10]: Find $\mathbf{x} = (x_1, \ldots, x_n)$, a design variable vector of dimension $n$, to minimise a cost function (or objective function) $f = f(\mathbf{x})$ subject to the equality constraints $h_i(\mathbf{x}) = 0$; $i = 1$ to $p$, the inequality constraints $g_i(\mathbf{x}) \leq 0$; $i = 1$ to $m$, and explicit bounds on design variables $x_{il} \leq x_i \leq x_{iu}$; $i = 1$ to $n$, where $x_{il}$ and $x_{iu}$ are the smallest and largest allowed values for the $i^{th}$ design variable $x_i$. The domain defined by the constraints and design bounds is called the *feasible region.* An optimisation problem is *linear* if all the constraints and the objective function are linear; otherwise, it is *non-linear.* While the optimum solution of a linear

problem lies at one of the vertices of the feasible region, that of a non-linear one could be anywhere within the feasible region.

An optimisation problem with only equality constraints can be solved using the Lagrange Multiplier Theorem [10]. For a mixed equality and inequality constrained problem, the Lagrange Multiplier Theorem is extended to give the Kuhn-Tucker (K-T) necessary conditions, which are stated as follows.

Let $\mathbf{x}^*$ be a regular point that is a local minimum for the problem. Define the Lagrange function for the problem as

$$L(\mathbf{x}, \mathbf{v}, \mathbf{u}) = f(\mathbf{x}) + \sum_{i=1}^{p} v_i h_i(\mathbf{x}) + \sum_{i=1}^{m} u_i g_i(\mathbf{x}) \tag{1.6}$$

Then there exist Lagrange multipliers $\mathbf{v}^*$ and $\mathbf{u}^*$ such that the Lagrangian is stationary with respect to $x_i$, $v_i$ and $u_i$, i.e.

$$\frac{\partial L}{\partial x_i} \equiv \frac{\partial f}{\partial x_i} + \sum_{j=1}^{p} v_j^* \frac{\partial h_j}{\partial x_i} + \sum_{j=1}^{m} u_j^* \frac{\partial g_j}{\partial x_i} = 0, \quad i = 1, \ldots, n \tag{1.7}$$

$$h_i(\mathbf{x}^*) = 0, \quad i = 1, \ldots, p \tag{1.8}$$

$$g_i(\mathbf{x}^*) \leq 0, \quad i = 1, \ldots, m \tag{1.9}$$

$$u_i^* g_i(\mathbf{x}^*) = 0, \quad i = 1, \ldots, m \tag{1.10}$$

$$u_i^* \geq 0, \quad i = 1, \ldots, m \tag{1.11}$$

The $m$ conditions in Equation 1.10 are known as the *switching conditions*. They can be satisfied by setting either $u_i = 0$ (in this case $g_i$ must be $\leq 0$ to satisfy feasibility) or, $g_i = 0$ (active inequality constraint). These conditions lead to several solution cases, in which candidate minimum points are obtained by solving the remaining necessary conditions. Equation 1.11 requires that Lagrange multipliers $u_i$ should be nonnegative, while $v_i$ are free in sign. To solve the present problem, two optimisation criteria are used: minimum sum of muscle forces (linear) and minimum sum of quadratic muscle forces (non-linear).

With the first formulation which defines the feasible region $ABC$(Figure 1.3b), the linear optimisation criterion gives a convex problem, in which the optimum point occurs at one of the vertices of the feasible region. It is obvious that point $A = (1, 0, 0)$ is optimum, which indicates that the muscle with maximum lever arm is recruited and no synergistic muscle is predicted, Figure 1.3b. And, evidently, the number of predicted muscle forces using a linear programming formulation is no greater than one. If the sum of quadratic muscle forces is minimised, the optimum solution is point $G = (\frac{36}{49}, \frac{18}{49}, \frac{12}{49})$, the intersection of

plane $ABC$ and a sphere centred at the origin and with a radius of 0.857 ( The equation of the sphere is $x^2 + y^2 + z^2 = (\frac{42}{49})^2$), Figure 1.3b. In this case, an even distribution of force is predicted among the synergistic muscles. Three muscles are all recruited. This shows that non-linear criteria predict that more muscles are active than linear ones, which was also pointed out by Pedersen *et al.* [196], based on their comparative study. The analysis procedure leading to the result is given in detail as follows.

The above non-linear optimisation problem can be stated mathematically in the standard non-linear programming format:

$$min. \quad f(x,y,z) = x^2 + y^2 + z^2 \tag{1.12}$$

$$s.t. \quad h \equiv x + \tfrac{1}{2}y + \tfrac{1}{3}z - 1 = 0 \tag{1.13}$$

$$g_1 \equiv -x \leq 0 \tag{1.14}$$

$$g_2 \equiv -y \leq 0 \tag{1.15}$$

$$g_3 \equiv -z \leq 0 \tag{1.16}$$

The Lagrangian for the problem is given as

$$L = x^2 + y^2 + z^2 + v(x + \frac{1}{2}y + \frac{1}{3}z - 1) + u_1(-x) + u_2(-y) + u_3(-z). \tag{1.17}$$

The K-T conditions give

$$\frac{\partial L}{\partial x} \equiv 2x + v - u_1 = 0 \tag{1.18}$$

$$\frac{\partial L}{\partial y} \equiv 2y + \frac{1}{2}v - u_2 = 0 \tag{1.19}$$

$$\frac{\partial L}{\partial z} \equiv 2z + \frac{1}{3}v - u_3 = 0 \tag{1.20}$$

$$\frac{\partial L}{\partial v} \equiv x + \frac{1}{2}y + \frac{1}{3}z - 1 = 0 \tag{1.21}$$

$$g_i \leq 0; \quad i = 1,2,3 \tag{1.22}$$

$$u_i g_i = 0; \quad i = 1,2,3 \tag{1.23}$$

$$u_i \geq 0; \quad i = 1,2,3 \tag{1.24}$$

The switching conditions in Equation 1.23 give eight cases for the solution of K-T conditions. Each case will be considered separately and solved.

**Case 1:** $u_1 = 0, g_2 = 0(y = 0), g_3 = 0(z = 0)$. For this case, Equations 1.18-21 give $x = 1, v = -2, u_2 = -1$ and $u_3 = -\frac{1}{3}$. This solution violates Equation (1.24) so it is not a candidate minimum point.

**Case 2:** $u_1 = 0, u_2 = 0, g_3 = 0 (z = 0)$. The solution obtained from Equations 1.18-21 is $(x, y, z) = (\frac{4}{5}, \frac{2}{5}, 0)$ with $v = -\frac{8}{5}$ and $u_3 = -\frac{8}{15}$. It is a feasible solution but not a candidate minimum point.

**Case 3:** $u_1 = 0, g_2 = 0 (y = 0), u_3 = 0$. For this case, the solution yielded is not a candidate minimum because $u_2 = -3$, which does not meet the requirement of Equation 1.24.

**Case 4:** $u_1 = 0, u_2 = 0, u_3 = 0$. With these conditions, Equations 1.18-21 yield a candidate minimum solution $(x, y, z) = (\frac{36}{49}, \frac{18}{49}, \frac{12}{49})$ with $f = (\frac{42}{49})^2$ and $v = -\frac{72}{49}$ (Point G in Figure 1.3b).

**Case 5:** $g_1 = 0 (x = 0), g_2 = 0 (y = 0), g_3 = 0 (z = 0)$. With these conditions, the inequality constraint is not satisfied so it is not a feasible solution.

**Case 6:** $g_1 = 0 (x = 0), u_2 = 0, g_3 = 0 (z = 0)$. For this case, Equations 1.18-21 give negative inequality Lagrange multipliers so the solution is not a candidate minimum point.

**Case 7:** $g_1 = 0 (x = 0), g_2 = 0 (y = 0), u_3 = 0$. Negative inequality Lagrange multipliers are also obtained in this case so the solution is not a candidate minimum point.

**Case 8:** $g_1 = 0 (x = 0), u_2 = 0, u_3 = 0$. The solution obtained is $(x, y, z) = (0, \frac{18}{13}, \frac{12}{13})$ with $u_1 = -\frac{72}{13}$. It is a feasible solution but not a candidate minimum point.

It should be noted that in general applications the K-T conditions lead to a set of non-linear equations that cannot be solved analytically. Numerical methods are thus needed to find the solutions.

With the second formulation, the feasible region, line $BF$, lies in an iso-cost plane of the linear criterion, i.e. $x + y + z = 2$ (Figure 1.3b). Therefore, we have multiple solutions that are all different from the previous solution, point A. Usually, either point $B$ or point $F$ is given by numerical solution if the Simplex Method is used. Applying K-T conditions, the solution predicted by the non-linear criterion is found to shift to point $K$, Figure 1.3b.

#### 1.5.4.3 Reduction Method

If the reduction method is used, weighting factors of each muscle for force sharing should be estimated first. Assume weightings for muscles $x$, $y$ and $z$ are $\frac{1}{2}$, $\frac{1}{4}$ and $\frac{1}{4}$, respectively, then solutions consistent with this assumption can be represented

by line $L$

$$(x, y, z) = (\frac{1}{2}, \frac{1}{4}, \frac{1}{4})t; \quad t \geq 0 \tag{1.25}$$

For the first formulation, an unique solution is obtained at point $H = (0.7, 0.35, 0.35)$, the interaction of plane $ABC$ and line $L$, Figure 1.3b. However, with the second formulation, a more accurate solution domain, it is noted that there is no intersection between lines $BF$ and $L$, which means that no feasible solution exists, Figure 1.3b. This suggests that the assumed weightings among the muscles are wrong. An adaptation of the weightings based on the second feasible region is needed to give a reasonable solution. These results suggest that grouping muscles with different lever arms to an unit may lead to erroneous result. Comprehensive geometric study is useful for more accurate estimation of muscle forces because it allows equations of force equilibrium to be incorporated into the formulation.

#### 1.5.4.4 DDOSC Method

Based on the first formulation, there are three limiting solutions to this problem: points $A = (1, 0, 0), B = (0, 2, 0)$ and $C = (0, 0, 3)$, Figure 1.3b. A unique solution can be further selected according to physiological information. Among these admissible limiting solutions, however, no synergistic muscles are predicted. According to Collins and O'Connor [58], the proposed limiting solutions approach was suggested for mechanical analysis of comprehensive geometrical models so that equations of force equilibrium could be used to further constrain the feasible region. Therefore, the second formulation is necessary for the use of the limiting solutions approach. With this formulation, two limiting solutions, $B$ and $F = (0.5, 0., 1.5)$, are predicted, one with single muscle $(B)$ and one with two synergistic muscles $(F)$, Figure 1.3b. These solutions demonstrate the possibility of compensating for systemic dysfunction. For example, if muscle $y$ is injured, then point $F$ could be a physiologically reasonable solution. Similarly, point $B$ is selected if the dysfunction occurs in muscle $x$ or $y$. A more detailed description of the DDOSC method is given in Chapter 5.

#### 1.5.4.5 Discussion

Based on the above simple calculations, it is noted that the two formulations give totally different solutions, no matter which method is used. This shows that force sharing is affected by the introduction of additional constraints. Failure to

incorporate force equations or any other physical constraints into the constraint set will lead to erroneous estimation of muscle forces. For this reason, the omission of force equations in [46, 109] is perhaps due to the lack of a comprehensive geometric model or because they simplified the formulation in order to obtain an analytical relationship between muscle forces using the Lagrange Multiplier Method. Therefore, a comprehensive geometric model of the system investigated is very important for further structural analyses. It has been suggested that improvement of muscle and joint force prediction is more crucially dependent on accurate determination of the joint axes of rotation and muscle orientation than on the particular optimisation criteria employed to solve the indeterminate problem [192].

Despite the problem of global convergence in most optimisation methods, an important feature of the optimisation method (also the reduction method) is that the final solution is fixed once the problem is formulated. In contrast, the DDOSC method provides many admissible solutions so interactions between load-bearing structures can be examined systematically. A further discussion of the optimisation method and the DDOSC method applied to the mechanical analysis of the human locomotor system during gait is given in Chapter 5.

### 1.5.5 Model Validation

#### 1.5.5.1 Qualitative Validation

Success of any theoretical model relies heavily on the validity of its assumptions. One way to test is through the validation of the predicted outcome. In most of the previous works, the results were usually qualitatively validated by phasic EMG evidence, mainly due to the difficulty of quantitative validation. However, despite the reliability and accuracy of EMG, the determination of EMG phases (i.e. active or inactive) is not straightforward. Signal processing techniques [15, 263] have been used to analyse EMG recordings but to distinguish noise from signal still remains as a subjective task. Moreover, although EMG patterns during gait are grossly repeatable, for more accurate comparison a temporal EMG recording is suggested. In validating their models, most researchers, except Pedersen *et al.* [196], did not use objective indices to describe the correlation between predicted results and EMG activity so it is not possible to evaluate the reported results in the form published.

### 1.5.5.2 Quantitative Validation

Only a limited number of quantitative validation of modelling works appeared in the literature. In 1991, Herzog and Leonard [109] measured time histories of force sharing among synergistic muscles at the ankle joint of an adult male cat during locomotion to validate the predictions of individual muscle forces obtained using optimisation models. They found that the predicted muscle forces did not agree well with the experimentally determined muscle forces.

Recently, Challis and Kerwin [46] compared theoretical muscle forces obtained by using an optimisation method with various criteria at the human elbow joint with those estimated using a validated muscle model and showed that they were in poor correspondence.

It is noted that both works of Herzog and Leonard [109] and Challis and Kerwin [46] considered single separated joints without taking account of the interaction between two adjacent joints in terms of the activity of bi-articular muscles. Ligamentous contributions were not included explicitly so only equations of moment equilibrium could be written. This allowed them to derive analytical expressions for muscle force sharing using the Lagrange Multiplier Method [105].

Recently, Brand *et al.* [30] reported a comparison between calculated hip joint contact forces and measurements from a patient with an instrumented hip implant. Their movement data and telemetered hip joint contact forces were not acquired simultaneously so variations between trials could not be eliminated. However, it is certain that simultaneously measured kinematic, kinetic and EMG data together with telemeterised forces in the instrumented prostheses will provide an excellent opportunity for the validation of mathematical models which will then be very useful in the study in normal subjects.

## 1.6 Aims and Scope of This Thesis

As revealed by the above review, there is considerable lack of knowledge and understanding of the kinematic and mechanical interaction between the structural elements of the human locomotor system. The principal aim of this thesis is therefore to contribute to fill in some of the gaps by developing and implementing mathematical models of the musculoskeletal system of the pelvis-leg apparatus for the study of the interaction between muscles, bones and ligaments in response to external loadings. Due to the general difficulty of direct measurement

of internal forces, geometric and mechanical modelling techniques in conjunction with noninvasive measurements on living subjects will be used. However, directly measured internal axial forces in the instrumented prostheses of two patients will be used to provide quantitative validation of the models.

In the following chapters, the kinematic and dynamic modelling and analysis of the pelvis-leg apparatus as a multibody system is presented first. It is followed by the experimental studies on patients with instrumented massive proximal femoral prostheses, with descriptions of the experimental apparatus and methods used. Two-dimensional geometric modelling of the knee joint and its surrounding structures is described and results compared with experimental measurements in the literature. The knee model was then incorporated into a two-dimensional model of the lower limb and a comparative study of the methods for the determination of the internal forces was performed using the 2D lower limb model. The two-dimensional models were then encapsulated into a prototype window system, which allow a unified approach to the geometric and mechanical modelling of the locomotor system with graphical animation and display. With the experience from the 2D modelling studies, a three dimensional model of the pelvis-leg apparatus was developed, with the hip as a ball-and-socket joint, the knee as a parallel spatial mechanism and the ankle as a two-hinge complex. Three-dimensional computer graphics techniques were used to reconstruct the musculoskeletal system of the locomotor system animated by movement data measured from the gait laboratory. Both the 2D and 3D models of the locomotor system were validated by the EMG and telemetered force data from the two instrumented patients. The influence of muscle activity on the forces in the femur was studied using the two validated models and further improvement is suggested of the current approach to the analysis of the stress/strain distributions in the femur by incorporating more physiological loading conditions and more realistic boundary conditions. Finally, discussion, conclusions and suggestions for further study conclude the thesis.

# Chapter 2

# Kinematics and Dynamics of The Lower Limb as A Multibody System

This chapter describes the kinematic and dynamic modelling and analysis of the locomotor system, a prerequisite for the estimation of forces transmitted by its structural members such as muscles, ligaments and bones. The human pelvis-leg apparatus was modelled as an ensemble of four rigid body segments. The kinematic variables of a segment (linear and angular position, velocity and acceleration) was described by a Body-embedded Coordinate System (BCS) relative to a fixed Laboratory Coordinate System (LCS). The BCSs of any two adjacent segments were then used to construct a Joint Coordinate System (JCS) in which relative attitude of the segments was defined. With kinematic variables and inertial parameters, dynamic free body analysis was applied iteratively to each segment, starting from the most distal segment, to obtain the intersegmental forces and moments, with a specified point common to each segment as origin of the force/moment system. The resultant forces and moments at a given cross-section of a segment can also be calculated in the same manner. Since there has been a need to represent results of biomechanical analysis in clinical terms, special attention was given to the definition of the relevant coordinate systems in which biomechanical variables are described. In the later chapters, the kinematic and dynamic model will be incorporated into geometric models of the locomotor musculoskeletal system to determine the contribution of each structural member in transmitting the intersegmental or cross-sectional forces and moments.

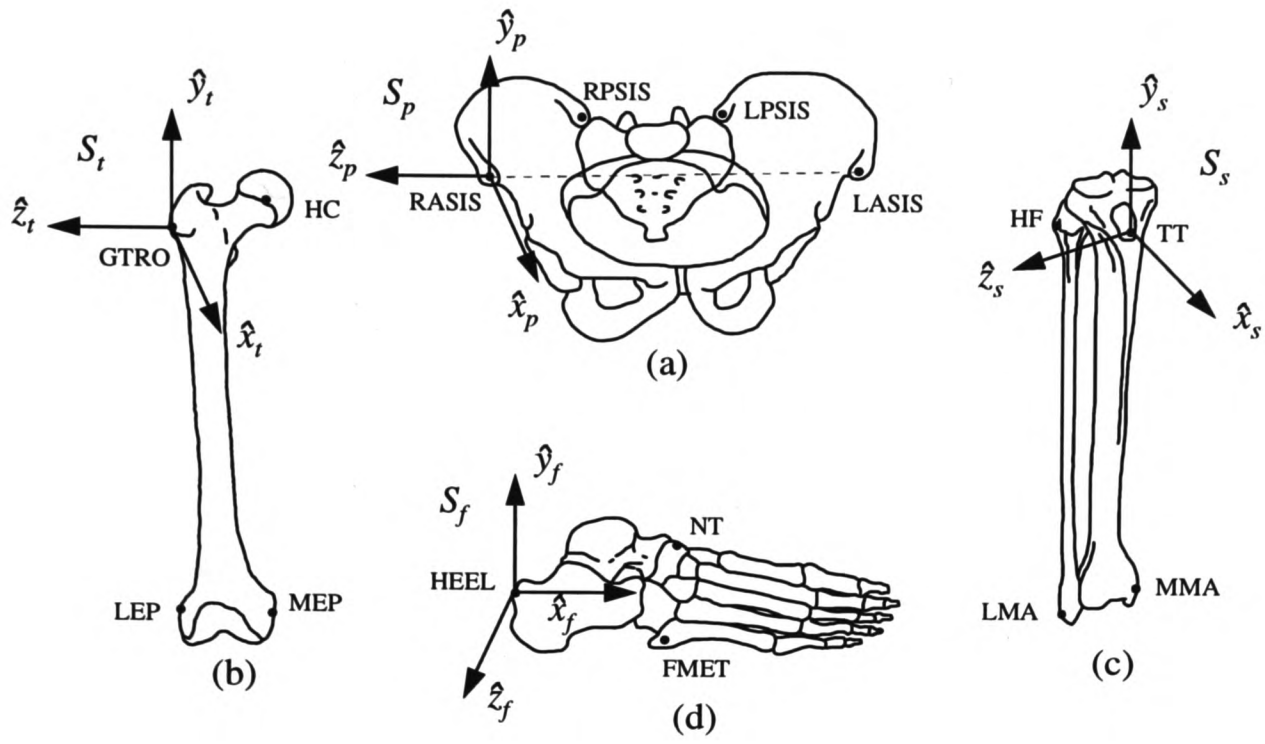



Figure 2.1: Body-embedded coordinate systems

## 2.1 The Rigid Body Assumption

The assumption of rigidity of body segments has been made since Elftman [74] did the first calculation of the internal forces in the human lower extremities and has been adopted widely in later studies of human movements (e.g. [33, 221]). The same assumption was also made in the present study. The rationale behind it and its appropriateness and limits are discussed.

A rigid body is a collection of matter that does not deform. In other words, the distance between any two particles in it remains constant. Therefore, a rigid body has fixed inertial properties, such as mass, centre of mass and moment of inertia. This characteristic largely simplifies the analysis of its dynamic behaviour as opposed to the dynamic analysis of deformable bodies whose inertial properties are coupled with the mechanical properties and the forces applied. Although there is no perfect rigid body in the world, within an acceptable range the assumption of rigidity can significantly simplify the analysis process without compromising the understanding of the dynamic behaviour of interest. This is especially useful when the system under investigation is very complicated such as the human locomotor system.

## 2.2 Coordinate Systems

In order to define the position and attitude of a rigid body in space, a Cartesian coordinate system is embedded. This is achieved by considering at least three known points on the body. Generally, the selection of body-embedded coordinate systems for the study of body kinematics and dynamics should consider the following requirements [38]:

1. The determination of the coordinate systems from experimental data should be repeatable both inter- and intra-individually.

2. In view of the quantitative description of the relevant joint kinematics, they should possibly incorporate or permit the determination of suitable axes with respect to which both rotations and translations of the joint may be defined (joint axes).

3. Since the analysis of the limb will be dynamic, it should permit an easy implementation of the estimation techniques aimed at the location of the body segment centre of mass and principal axes of inertia. In addition, sufficient information must be available to locate the reference coordinate system with respect to which the intersegmental forces and moments are calculated.

4. Requirements associated with the description of muscle and ligament line of action and the location and orientation of the articulation surfaces must also be taken into careful consideration.

With these considerations in mind, the BCSs of the segments of the lower limb were defined using coordinates of at least three bony landmarks with respect to the LCS, $S = (\hat{x}, \hat{y}, \hat{z})$. Definitions of the bony landmarks used to define body embedded coordinate systems are given in Table 2.1. In principle, the $x$ axis is directed anteriorly, $y$ axis superiorly and $z$ axis laterally, following the ISB suggestions [271]. As shown in Fig.2.1, the pelvic coordinate system, $S_p = (\hat{x}_p, \hat{y}_p, \hat{z}_p)$, was defined using the right anterior superior iliac spine (RASIS), left anterior superior iliac spine (LASIS) and right posterior superior iliac spine (RPSIS). The origin was fixed at the RASIS. Given coordinates of these bony landmarks in $S$, unit vectors along the axes of $S_p$ can be obtained as follows.

$$\hat{z}_p = \frac{\vec{p}_{RASIS} - \vec{p}_{LASIS}}{|\vec{p}_{RASIS} - \vec{p}_{LASIS}|} \tag{2.1}$$

| Name | Description |
|---|---|
| LASIS | Most anterior projection of the left anterior superior iliac spine |
| RASIS | Most anterior projection of the right anterior superior iliac spine |
| RPSIS | Most posterior projection of the right posterior superior iliac spine |
| GTRO | Most lateral projection of the greater trochanter |
| MEP | Most medial projection of the medial femoral epicondyle |
| LEP | Most lateral projection of the lateral femoral epicondyle |
| TT | Prominence of the tibial tuberosity |
| HF | The head of fibula |
| MMA | Most medial projection of the medial malleolus |
| LMA | Most lateral projection of the lateral malleolus |
| HEEL | Posterior projection where the Achilles tendon insert on the calcaneus |
| NT | Prominence of the navicular tubercle |
| FMET | Most proximal lateral aspect of the fifth metatarsal |

Table 2.1: Definition of the bony landmarks used to define the body-embedded coordinate systems

$$\hat{y}_p = \frac{(\vec{p}_{RPSIS} - \vec{p}_{RASIS}) \times \hat{z}_p}{|(\vec{p}_{RPSIS} - \vec{p}_{RASIS}) \times \hat{z}_p|} \tag{2.2}$$

$$\hat{x}_p = \hat{y}_p \times \hat{z}_p \tag{2.3}$$

where $\vec{p}_B$ is the position vector of bony landmark B in $S$ and $|\vec{a}|$ is the magnitude of $\vec{a}$.

Similarly, the local coordinate system of the thigh segment, $S_t = (\hat{x}_t, \hat{y}_t, \hat{z}_t)$, was defined by the greater trochanter (GTRO), the lateral femoral epicondyle (LEP) and the medial femoral epicondyle (MEP), with origin fixed at the GTRO. The unit vectors of the system were calculated according to the following equations, Fig.2.1.

$$\hat{z}_t = \frac{\vec{p}_{LEP} - \vec{p}_{MEP}}{|\vec{p}_{LEP} - \vec{p}_{MEP}|} \tag{2.4}$$

$$\hat{x}_t = \frac{(\vec{p}_{GTRO} - \vec{p}_{LEP}) \times \hat{z}_t}{|(\vec{p}_{GTRO} - \vec{p}_{LEP}) \times \hat{z}_t|} \tag{2.5}$$

$$\hat{y}_t = \hat{z}_t \times \hat{x}_t \tag{2.6}$$

The origin of the shank coordinate system, $S_s = (\hat{x}_s, \hat{y}_s, \hat{z}_s)$, was located at the tibial tuberosity (TT) and the axes were established using the medial malleolus

(MMA), the lateral malleolus (LMA) and the head of the fibula (HF), Fig.2.1. The $x$ axis, $x_s$, is orthogonal to a quasi-frontal plane defined by the MMA, LMA and HF and is calculated by

$$\hat{x}_s = \frac{(\vec{p}_{HF} - \vec{p}_{MMA}) \times (\vec{p}_{LMA} - \vec{p}_{MMA})}{|(\vec{p}_{HF} - \vec{p}_{MMA}) \times (\vec{p}_{LMA} - \vec{p}_{MMA})|} \tag{2.7}$$

A quasi-sagittal plane, orthogonal to the quasi-frontal plane, is defined by the midpoint between the malleoli and TT. The $y$ axis is defined by the intersection between the above two planes. The z axis is orthogonal to the xy plane such that

$$\hat{z}_s = \frac{\hat{x}_s \times [\vec{p}_{TT} - (\vec{p}_{MMA} + \vec{p}_{LMA})/2]}{|\hat{x}_s \times [\vec{p}_{TT} - (\vec{p}_{MMA} + \vec{p}_{LMA})/2]|} \tag{2.8}$$

$$\hat{y}_s = \hat{z}_s \times \hat{x}_s \tag{2.9}$$

For the foot system, $S_f = (\hat{x}_f, \hat{y}_f, \hat{z}_f)$, the most posterior projection of the calcaneus (HEEL), the navicular tuberosity (NT) and the fifth metatarsal (FMET) were used. The origin was defined at HEEL. The $x$ axis is defined by HEEL and the midpoint between NT and FMET with its positive direction anterior. The $y$ axis is orthogonal to the plane defined by NT, HEEL and the midpoint between NT and FMET. The $z$ axis is then defined according to the right handed rule.

$$\hat{x}_f = \frac{(\vec{p}_{NT} + \vec{p}_{FMET})/2 - \vec{p}_{HEEL}}{|(\vec{p}_{NT} + \vec{p}_{FMET})/2 - \vec{p}_{HEEL}|} \tag{2.10}$$

$$\hat{y}_f = \frac{\hat{x}_f \times (\vec{p}_{NT} - \vec{p}_{HEEL})}{|\hat{x}_f \times (\vec{p}_{NT} - \vec{p}_{HEEL})|} \tag{2.11}$$

$$\hat{z}_f = \hat{x}_f \times \hat{y}_f \tag{2.12}$$

## 2.3 Attitude Representation: Cardan Angles

For the angular motion of a segment, its attitude is defined relative to the LCS, $S$. Basically, the attitude of a segment $q$ is defined by a 3×3 rotation matrix $R_q$, composed of nine directional cosines of angles between axes of the BCS and LCS. For a point $p$ in space, its position vector with respect to the BCS, $S_q$, is denoted as $\vec{p}_q$ and its position vector with respect to $S$ as $\vec{p}$. They are related by the following transformation

$$\vec{p} = R_q \vec{p}_q + \vec{o}_q \tag{2.13}$$

$$R_q = \begin{bmatrix} \hat{x}_q & \hat{y}_q & \hat{z}_q \end{bmatrix} \tag{2.14}$$

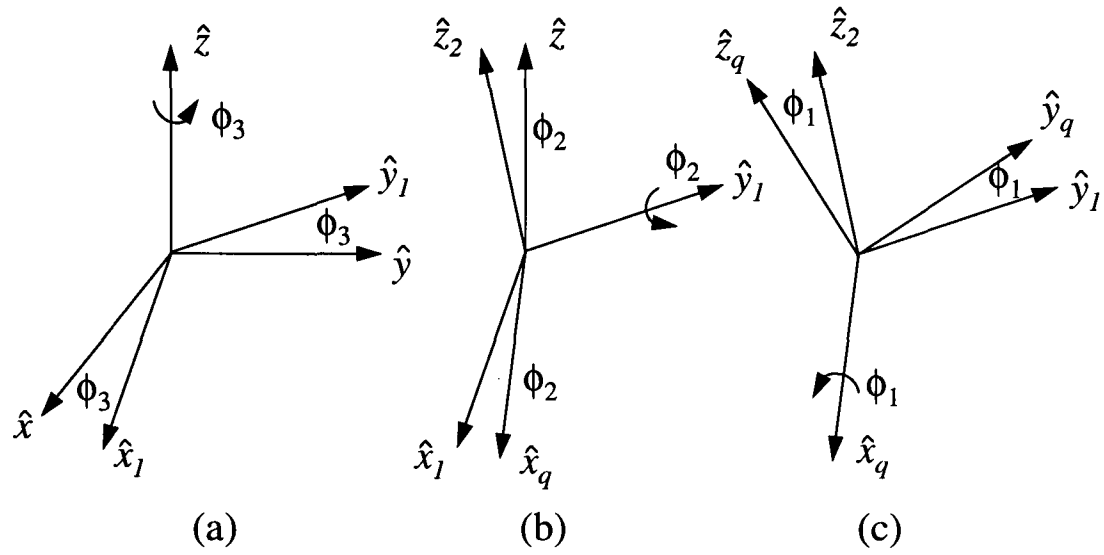



Figure 2.2: Cardan angles defining the attitude of the BCS, $(\hat{x}_q, \hat{y}_q, \hat{z}_q)$, relative to the LCS, $(\hat{x}, \hat{y}, \hat{z})$ in $z \rightarrow y \rightarrow x$ sequence. First start from the BCS coincident with the LCS. Then rotate the BCS about $\hat{z}$ by an angle $\phi_3$ to have $\hat{x}$ rotate into $\hat{x}_1$ and $\hat{y}$ into $\hat{y}_1$ (a), then rotate about $\hat{y}_1$ by an angle $\phi_2$ (b) and then rotate about $\hat{x}_q$ by an angle $\phi_1$ to reach the final attitude of the BCS (c). $\phi_3$, $\phi_2$ and $\phi_1$ are the resulting Cardan angles.

where $\vec{o}_q$ is the position vector of the origin of $S_q$ with respect to $S$.

However, these directional cosines are not independent. In theory, they can be represented using three independent parameters. One commonly used method is to parameterize the rotation matrix in terms of three sequential rotational components, called either Euler or Cardan angles. This parameterisation is generally achieved by an ordered sequence of rotations $(\phi_i, \phi_j, \phi_k)$ about the axes of the BCS, starting with a position coincident with the LCS, $R = R_i(\phi_i)R_j(\phi_j)R_k(\phi_k)$, to obtain the attitude of the BCS. If $i$, $j$, and $k$ are all different, the three rotational parameters, $\phi_i, \phi_j$, and $\phi_k$, are called Cardan angles. When $i$=$k$, the term Euler angles is used [269]. Since there exists a singularity called gimbal-lock [98] in the neutral joint attitude, i.e. $R$=$I$, using Euler angles representation, Cardan angles, for which gimbal-lock occurs only if $\phi_j = \pi/2 + n\pi$, n = 0, $\pm$1, $\pm$2, ..., will be used. As shown in Fig.2.2, two coordinate systems $(\hat{x}, \hat{y}, \hat{z})$ and $(\hat{x}_q, \hat{y}_q, \hat{z}_q)$ are the LCS and BCS, respectively. The rotational sequence of the global coordinate system is $z \rightarrow y \rightarrow x$ and the resulting Cardan angles are $\phi_3$, $\phi_2$, and $\phi_1$, Fig.2.2. With known unit vectors along the coordinate axes of both systems, the three Cardan angles can be calculated as the following:

$$\phi_2 = \arcsin\left[-(\hat{z} \cdot \hat{x}_q)\right] \tag{2.15}$$

$$\phi_1 = \arcsin\left[(\hat{z} \cdot \hat{y}_q)/cos(\phi_2)\right] \tag{2.16}$$

$$\phi_3 \quad = \quad \arcsin\left[(\hat{y} \cdot \hat{x}_q)/cos(\phi_2)\right] \tag{2.17}$$

It is noted again that there exists a critical case (gimbal lock), when $\phi_2 = \pi/2 + n\pi$, $n = 0, \pm1, \pm2, ...$, in which $\phi_1$ and $\phi_3$ can not be uniquely determined. However, this problem will not be encountered in lower limb modelling because axial rotations of the lower limb segments are generally less than 90°.

## 2.4 Joint Coordinate System

While the kinematics of each segment of the multibody system relative to the LCS are sufficient for the purpose of dynamic analyses, a direct perception of the motion of the whole system is reinforced by the description of the relative motion of adjacent segments. This is achieved by quantifying the rotational motion of a joint. Descriptions of joint motion are made generally by the attitude of the distal segment relative to the proximal segment. If the rotation matrix of the proximal segment (m) relative to $S$ is $R_m$ and that of the distal segment (n) is $R_n$, the description of the relative attitude of the two segments is defined by the joint attitude matrix $R_{n/m}$ :

$$R_{n/m} = R_m^T R_n \tag{2.18}$$

where $R^T$ is the transpose of $R$. Three-dimensional joint orientation is interpretated as a set of three rotations about the axes of a Joint Coordinate System, JCS, Figure2.3. The JCS used in the present study is the one proposed by Grood and Suntay [99] and Cole *et al.* [55]. The axis of the BCS that is oriented predominantly in the medio-lateral direction is chosen as the flexion-extension axis, denoted as F-axis. The longitudinal axis, L-axis, is chosen as the axis of the BCS that is oriented predominately lengthwise along the segment. The F-axis and L-axis are described by the unit vectors $\hat{f}$ and $\hat{l}$, respectively. The third axis, T-axis, is determined as the cross-product of the L-axis and the F-axis. Its unit vector is defined as:

$$\hat{t} = \hat{l} \times \hat{f} \tag{2.19}$$

As shown in Fig.2.3, the unit vectors of the axes of the JCS is defined as follows:

$$\hat{e}_1 \quad = \quad \hat{f}_m \tag{2.20}$$

$$\hat{e}_3 \quad = \quad \hat{l}_n \tag{2.21}$$

$$\hat{e}_2 \quad = \quad A \cdot \left( \frac{\hat{e}_3 \times \hat{e}_1}{|\hat{e}_3 \times \hat{e}_1|} \right) \tag{2.22}$$

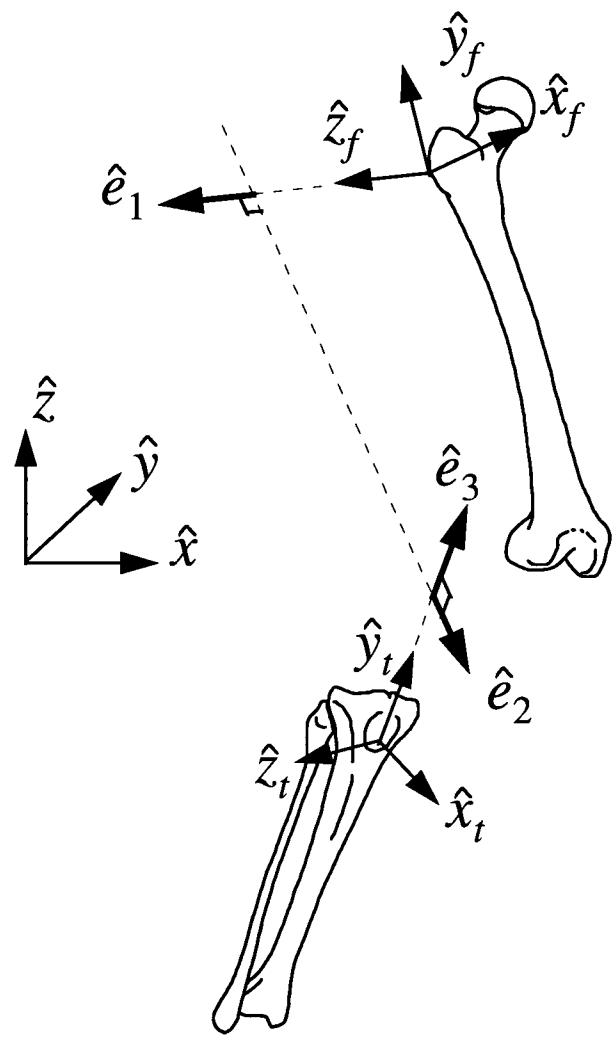



Figure 2.3: Joint coordinate system

where $A = -1$, if $(\hat{e}_3 \times \hat{e}_1) \cdot \hat{t}_n < 0$ and $((\hat{e}_3 \times \hat{e}_1) \times \hat{e}_3) \cdot \hat{f}_n > 0$, otherwise $A = +1$. $\hat{e}_2$ moves relative to each bone. The three angles that represent the three-dimensional orientation of the target segment,$n$, with respect to the reference segment, $m$, relative to a neutral position are calculated as follows:

For the angle of rotation about the axis for flexion-extension:

$$\phi_1 = \cos^{-1}(\hat{e}_2 \cdot \hat{t}_m) \cdot sign(\hat{e}_2 \cdot \hat{l}_m) \tag{2.23}$$

where $sign(x) = 1$ if $x \geq 0$, $sign(x) = -1$ if $x < 0$.

For the angle of rotation about the axis for adduction-abduction:

$$\phi_2 = \cos^{-1}(\hat{r} \cdot \hat{l}_n) \cdot sign(\hat{e}_1 \cdot \hat{e}_3) \tag{2.24}$$

where

$$\hat{r} = \frac{\hat{e}_1 \times \hat{e}_2}{|\hat{e}_1 \times \hat{e}_2|}$$

For the angle of rotation about the axis for axial rotation:

$$\phi_3 = \cos^{-1}(\hat{e}_2 \cdot \hat{t}_n) \cdot sign(\hat{e}_2 \cdot \hat{f}_n) \tag{2.25}$$

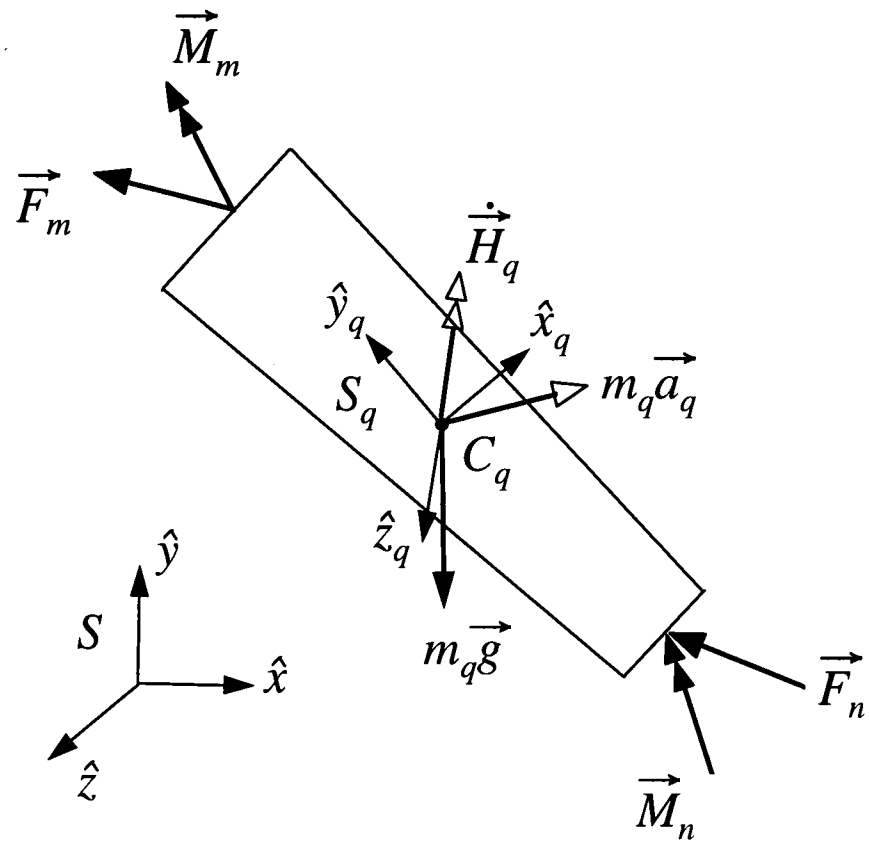



Figure 2.4: Free body diagram of a general rigid body segment

Counter-clockwise rotation relative to the neutral position has been defined as positive. The scalar $A$ is used to ensure that each of the three angles are continuous in the range, $-\pi \leq \phi \leq \pi$, and the unit vector $r$ has been added to ensure that counter-clockwise rotations about the axis $e_2$ are always positive regardless of which axes are chosen for $\hat{e}_1$ and $\hat{e}_3$.

## 2.5 Dynamics of A Rigid Body

Dynamic analysis of a multibody system can be accomplished by considering iteratively the free body of each segment, Figure 2.4. For a segment $q$, the projected components of segmental angular velocity onto the local coordinate axes can be expressed in terms of Cardan angles defined by Equation (2.15-2.17):

$$\begin{bmatrix} \omega_x \\ \omega_y \\ \omega_z \end{bmatrix}_q = \begin{bmatrix} 1 & 0 & -\sin\phi_2 \\ 0 & \cos\phi_1 & \sin\phi_1\cos\phi_2 \\ 0 & -\sin\phi_1 & \cos\phi_1\cos\phi_2 \end{bmatrix} \begin{bmatrix} \dot{\phi}_1 \\ \dot{\phi}_2 \\ \dot{\phi}_3 \end{bmatrix}_q \tag{2.26}$$

By further differentiating with respect to time, the above angular velocity

components yield the corresponding components of segmental angular acceleration:

$$\begin{bmatrix} \dot{\omega}_x \\ \dot{\omega}_y \\ \dot{\omega}_z \end{bmatrix}_q = \begin{bmatrix} 1 & 0 & -\sin\phi_2 \\ 0 & \cos\phi_1 & \sin\phi_1\cos\phi_2 \\ 0 & -\sin\phi_1 & \cos\phi_1\cos\phi_2 \end{bmatrix} \begin{bmatrix} \ddot{\phi}_1 \\ \ddot{\phi}_2 \\ \ddot{\phi}_3 \end{bmatrix}_q +$$

$$\begin{bmatrix} 0 & 0 & -\dot{\phi}_2\cos\phi_2 \\ 0 & -\dot{\phi}_1\sin\phi_1 & \dot{\phi}_1\cos\phi_1\cos\phi_2 - \dot{\phi}_2\sin\phi_1\sin\phi_2 \\ 0 & -\dot{\phi}_1\cos\phi_1 & -\dot{\phi}_1\sin\phi_1\cos\phi_2 - \dot{\phi}_2\cos\phi_1\cos\phi_2 \end{bmatrix} \begin{bmatrix} \dot{\phi}_1 \\ \dot{\phi}_2 \\ \dot{\phi}_3 \end{bmatrix}_q \tag{2.27}$$

Since angular accelerations are obtained based on a body embedded local coordinate system, the time derivative of the angular momentum of the segment with respect to its centre of mass ($C_q$) is calculated in $S_q$ as follows:

$$\dot{\vec{H}}_q = J_q \cdot \dot{\vec{\omega}}_q + \vec{\omega}_q \times (J_q \cdot \vec{\omega}_q) \tag{2.28}$$

where the inertia tensor $J_q$ of the segment contains the mass moment of inertia ($I_{xx}, I_{yy}, I_{zz}$) and the mass products of inertia ($I_{xy}, I_{yz}, I_{zx}$) and is of the following form

$$J_q = \begin{bmatrix} I_{xx} & -I_{xy} & -I_{xz} \\ -I_{yx} & I_{yy} & -I_{yz} \\ -I_{zx} & -I_{zy} & I_{zz} \end{bmatrix} \tag{2.29}$$

If the axes of the embedded coordinate system are aligned with the principal axes of the segment, the products of inertia vanish and the above equation becomes

$$\begin{bmatrix} \dot{H}_x \\ \dot{H}_y \\ \dot{H}_z \end{bmatrix}_q = \begin{bmatrix} I_{xx}\dot{\omega}_x + (I_{zz} - I_{yy})\omega_y\omega_z \\ I_{yy}\dot{\omega}_y + (I_{xx} - I_{zz})\omega_z\omega_x \\ I_{zz}\dot{\omega}_z + (I_{yy} - I_{xx})\omega_x\omega_y \end{bmatrix}_q \tag{2.30}$$

By applying the Eulerian laws of angular motion, the equations of moment equilibrium in $S$ can be written about $C_q$:

$$\sum \vec{M}_q = R_q \, \dot{\vec{H}}_q \tag{2.31}$$

where $\sum \vec{M}_q$ is the vector sum of all external moments about $C_q$ and $R_q$ is the rotation matrix of the segment. The equations of force equilibrium for the free body are given by applying Newton's laws of linear motion:

$$\sum \vec{F}_q = m_q \vec{a}_q \tag{2.32}$$

where $\sum \vec{F}_q$ is the vector sum of all the external forces applied on the segment and $\vec{a}_q$ is the linear acceleration of $C_q$.

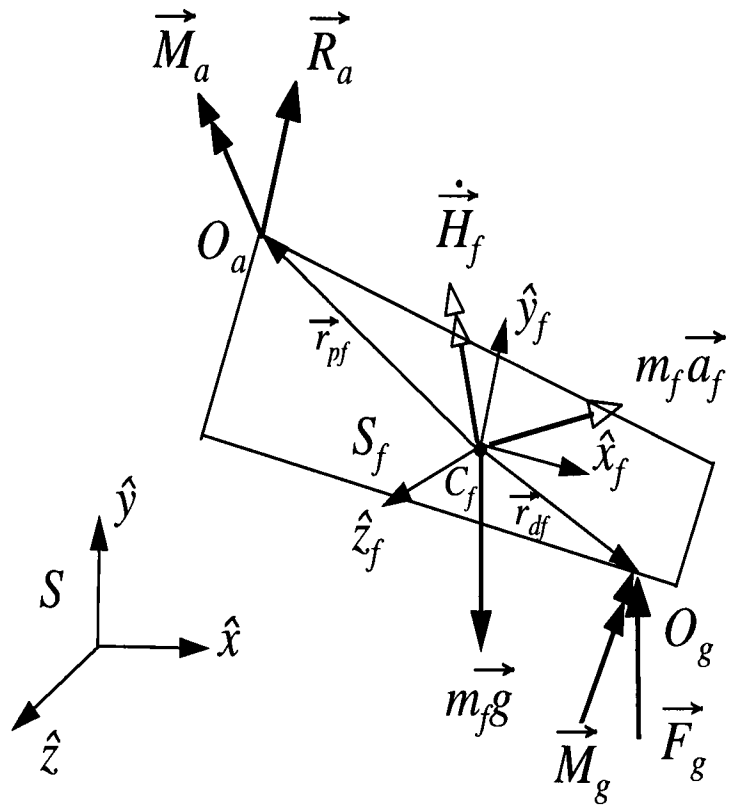



Figure 2.5: Free body diagram of the foot segment

## 2.6 Dynamics of The Lower Limb

In the dynamic analysis of human movement, the above analysis procedure usually begins from the most distal segment, namely the foot, and continues proximally until the analysis of the whole system is complete. Since external forces and moments applied to the system can vary significantly depending on the activity involved, the following analysis of the lower limb is performed on the basis of tests considered in the present study and made as general as possible.

For the calculation of the resultant forces and moments at the centre of the ankle ($O_a$), Equations 2.31 and 2.32 are applied to the free body of the foot segment, Fig. 2.5 which gives

$$\vec{R}_a = m_f\vec{a}_f - m_f\vec{g} - \vec{F}_g \tag{2.33}$$

$$\vec{M}_a = R_f\,\dot{\vec{H}}_f - \vec{r}_{df} \times \vec{F}_g - \vec{r}_{pf} \times \vec{R}_a - \vec{M}_g \tag{2.34}$$

where $\vec{R}_a$ and $\vec{M}_a$ are the resultant force and moment vectors at the centre of the ankle respectively, $\vec{g}$ is the constant of gravity, $\vec{r}_{pf}$ is the distance vector from $C_f$ to $O_a$, and $\vec{r}_{df}$ is the distance vector from $C_f$ to the application point of the ground reaction force (GRF), $\vec{F}_g$ and the free moment, $\vec{M}_g$.

For the shank segment, a general external force $\vec{F}_e$ representing external loadings during isometric tests considered in the present study is applied. Considering

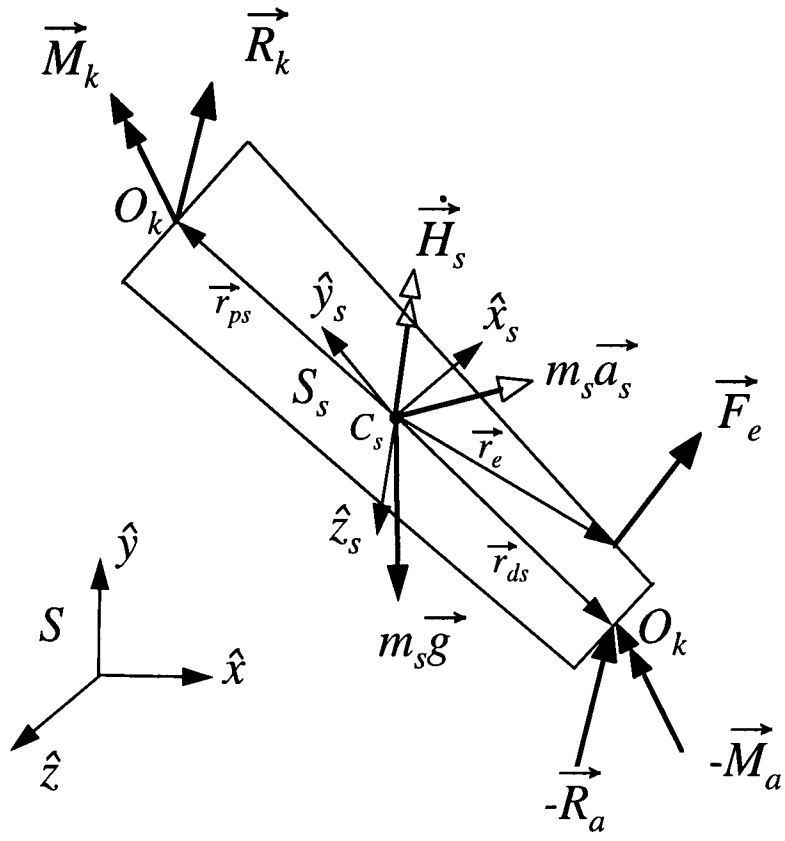



Figure 2.6: Free body diagram of the shank segment

the free body of the shank segment, Fig. 2.6, the resultant force vector $\vec{R}_k$ and resultant moment vector $\vec{M}_k$ at the centre of the knee joint ($O_k$) can be obtained as follows:

$$\vec{R}_k = \vec{R}_a + m_s\vec{a}_s - m_s\vec{g} - \vec{F}_e \tag{2.35}$$

$$\vec{M}_k = R_s\,\dot{\vec{H}}_s + \vec{r}_{ds} \times \vec{R}_a - \vec{r}_{ps} \times \vec{R}_k - \vec{r}_e \times \vec{F}_e + \vec{M}_a \tag{2.36}$$

where $\vec{r}_{ps}$ is the distance vector from $C_s$ to $O_k$, $\vec{r}_{ds}$ is the distance vector from $C_f$ to $O_a$ and $\vec{r}_e$ is the distance vector from $C_s$ to the application point of $\vec{F}_e$.

Similar procedure applied to the free body of the thigh segment, 2.7, gives the resultant force vector $\vec{R}_h$ and resultant moment vector $\vec{M}_h$ at the centre of the hip joint:

$$\vec{R}_h = \vec{R}_k + m_t\vec{a}_t - m_t\vec{g} \tag{2.37}$$

$$\vec{M}_h = R_t\,\dot{\vec{H}}_t + \vec{r}_{dt} \times \vec{R}_k - \vec{r}_{pt} \times \vec{R}_h + \vec{M}_k \tag{2.38}$$

where $\vec{r}_{pt}$ is the distance vector from $C_t$ to $O_h$ and $\vec{r}_{dt}$ is the distance vector from $C_t$ to $O_k$.

Using the technique of free body analysis, it is also possible to calculate the resultant force vector $\vec{R}_c$ and resultant moment vector $\vec{M}_c$ at any cross-section of a segment. As shown in Fig. 2.8, a cross-section is taken at the thigh and

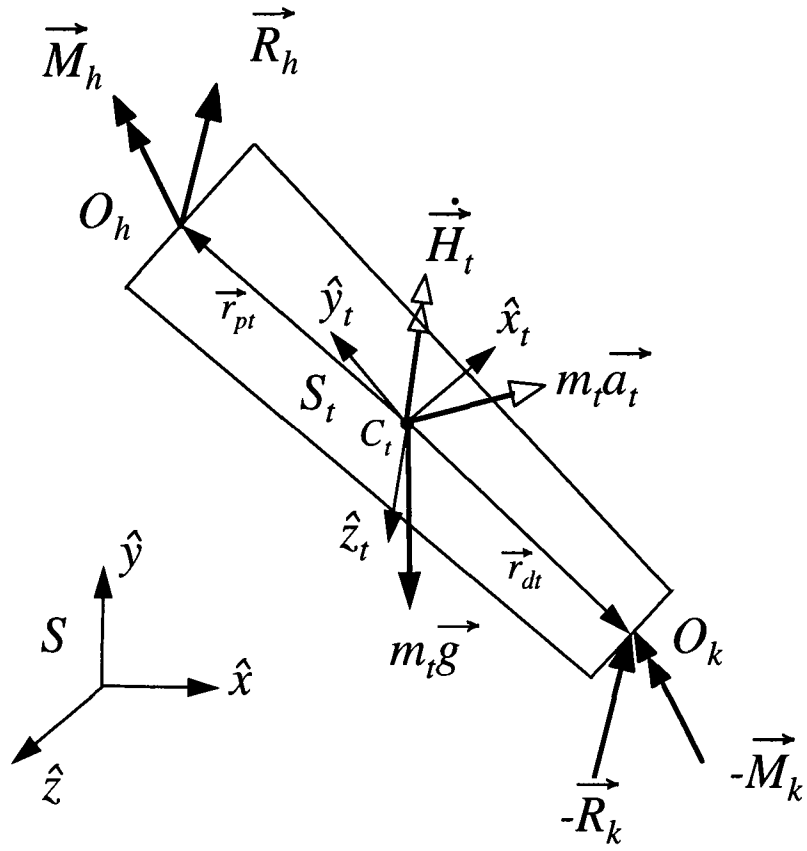



Figure 2.7: Free body diagram of the thigh segment

the distal part of the thigh segment ($c$) is considered as a free body. Therefore, expressions for $R_c$ and $M_c$ are given as

$$\vec{R}_c = \vec{R}_c + m_c\vec{a}_c - m_c\vec{g} \tag{2.39}$$

$$\vec{M}_c = R_c\,\dot{\vec{H}}_c + \vec{r}_{dc} \times \vec{R}_k - \vec{r}_{pc} \times \vec{R}_c + \vec{M}_k \tag{2.40}$$

where $\vec{r}_{pc}$ is the distance vector from $C_c$ to the centroid of the cross-section $O_c$ and $\vec{r}_{dc}$ is the distance vector from $C_c$ to $O_k$. Since free body $c$ is a part of the thigh segment, its attitude, angular velocity and angular acceleration are the same as those of the thigh segment. Therefore,

$$R_c = R_t \tag{2.41}$$

$$\vec{\omega}_c = \vec{\omega}_t \tag{2.42}$$

$$\dot{\vec{\omega}}_c = \dot{\vec{\omega}}_t \tag{2.43}$$

## 2.7 Anthropometric Parameters

Anthropometric parameters of each segment needed for the above dynamic analysis includes length, mass, centre of mass and mass moment of inertia.

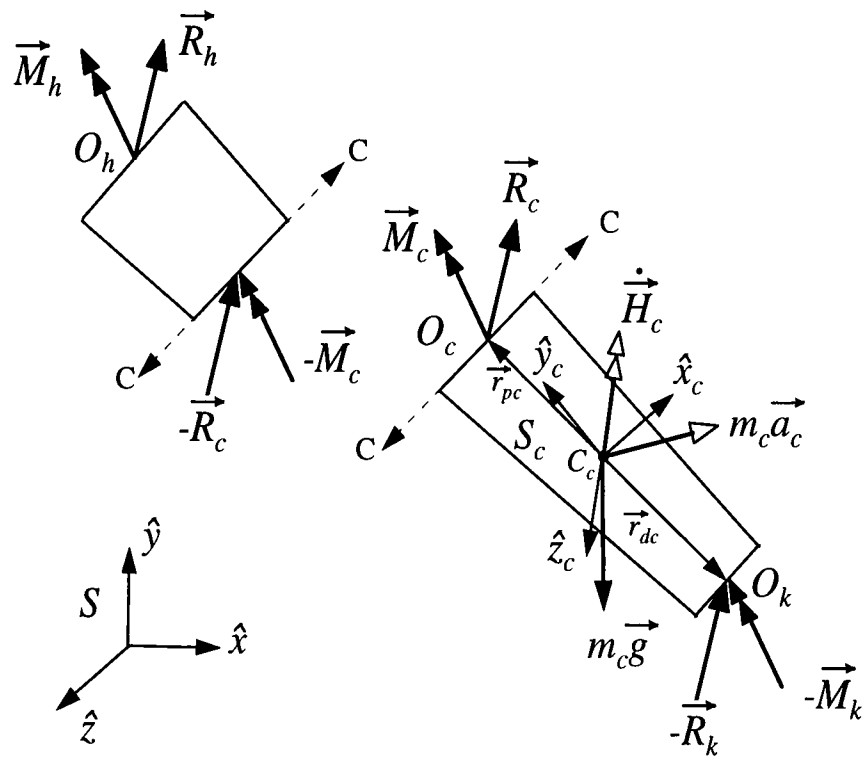



Figure 2.8: Free body diagram of a cross section of the thigh segment

| Segment | Definition | $K_m$ | $K_c$ |
|---|---|---|---|
| Foot | Lateral malleolus/head metatarsal II | 0.0145 | 0.500 |
| Shank | Femoral condyles/medial malleolus | 0.0465 | 0.433 |
| Thigh | Greater trochanter/femoral condyles | 0.1000 | 0.433 |

Table 2.2: Anthropometric coefficients for segment mass and centre of mass

Among these parameters, the length of a segment ($l_q$) and the total body mass ($m_b$)can be easily measured from the tested subject. Measurement of other parameters, however, requires more specific instrumentation. For the purpose of movement analysis, inertial properties are generally estimated from anthropometric studies in the literature. In the current study, segment mass $m_q$ is expressed as a proportion of $m_b$

$$m_q = K_m \cdot m_b \tag{2.44}$$

and the location of the centre of mass $\vec{C}_q$ is given as a percentage of the segment length from the proximal end point $\vec{O}_p$

$$\vec{C}_q = \vec{O}_p + K_c \cdot (\vec{O}_d - \vec{O}_p) \tag{2.45}$$

where $\vec{O}_d$ is the position vector of the distal end point and the two coefficients $K_m$ and $K_c$ are obtained from the literature and summarised in Table 2.2.

| Segment | $k_1$ | $k_2$ |
|---|---|---|
| Foot | 1.001 | 3.72 |
| Shank | 0.853 | 5.73 |
| Thigh | 1.593 | 8.12 |

Table 2.3: Regression coefficients for the mass moment of inertia from Yeadon [274]

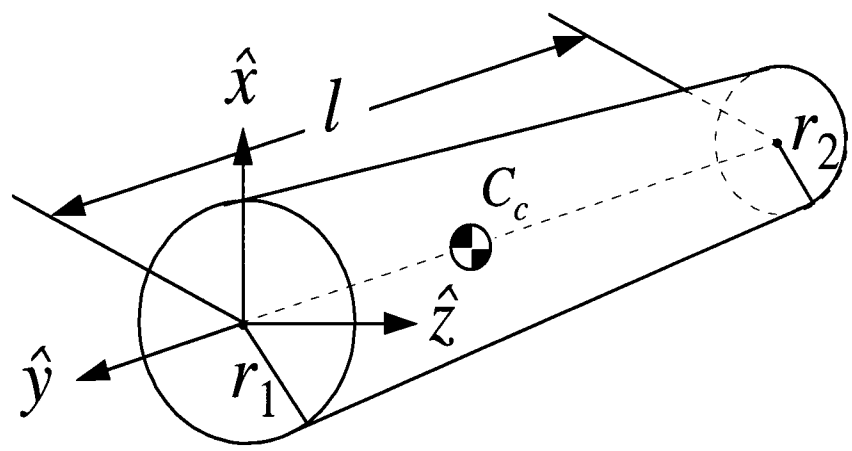



Figure 2.9: Frustum used to model inertial properties of the distal part of a segment.

Mass moment of inertia is obtained using the regression equations suggested by Yeadon and Morlock [274]. It is assumed that $I_{xx} = I_{zz} = I_t$. $I_{yy}$and $I_t$ are of the following form

$$I_{yy} = k_1 p^4 l_q \tag{2.46}$$

$$I_t = \frac{1}{2} I_{yy} + k_2 p^2 l_q^3 \tag{2.47}$$

where $k_1$ and $k_2$ are regression constants, Table 2.3, and $p$ is the mean perimeter calculated as

$$p = (p_1 + 2p_2 + p_3)/4 \tag{2.48}$$

with $p_1$, $p_2$, $p_3$ and $l_q$ measured directly from the subject, Table 2.4.

For a distal part of a segment, for the purpose of estimating resultant force and moment at a cross-section, its inertial properties are estimated by modelling the part as a rigid frustum as shown in Fig. 2.9. Its mass $m_c$ is estimated by the volume ratio

$$m_c = \frac{V_c}{V_q} \cdot m_q \tag{2.49}$$

| Segment | Parameter | Definition |
|---|---|---|
| Foot | $l_q$ | Length: heel to toe |
| | $p_1$ | Perimeter: minimum near ankle |
| | $p_2$ | Perimeter: arch |
| | $p_3$ | Perimeter: ball |
| Shank | $l_q$ | Length: knee centre to ankle centre |
| | $p_1$ | Perimeter: knee |
| | $p_2$ | Perimeter: maximum |
| | $p_3$ | Perimeter: minimum near ankle |
| Thigh | $l_q$ | Length: hip centre to knee centre |
| | $p_1$ | Perimeter: below gluteal furrow |
| | $p_2$ | Perimeter: mid-thigh |
| | $p_3$ | Perimeter: knee |

Table 2.4: Definition of parameters for moment of inertia models. Hip centre is defined as the geometric centre of the acetabulum. Knee centre is defined as the mid-point between the two epicondyles. Ankle centre is defined as the mid-point between the two malleoli.

where $V_q$ is the segment volume, $V_c$ the volume of its distal part and $m_q$ is the segment mass. The centre of mass of the segment part $\vec{C}_c = (C_{cx}, C_{cy}, C_{cz})$, density $\rho$ and its mass moment of inertia are given as follows:

$$\rho = \frac{3m_c}{\pi l \cdot (r_1^2 + r_1 r_2 + r_2^2)} \tag{2.50}$$

$$C_{cy} = -\frac{l}{4} \cdot \left( \frac{r_1^2 + 2r_1 r_2 + 3r_2^2}{\alpha} \right) \tag{2.51}$$

$$C_{cx} = C_{cz} = 0 \tag{2.52}$$

$$I_{yy} = \frac{\rho \pi l}{10} \cdot \beta \tag{2.53}$$

$$I_{xx} = \frac{\rho \pi l}{20} \cdot \left[ \beta + \frac{l^2}{4} \cdot \frac{(r_1 + r_2)^4 + 4r_1^2 r_2^2}{\alpha} \right] \tag{2.54}$$

$$I_{zz} = I_{xx} \tag{2.55}$$

where

$$\alpha = r_1^2 + r_1 r_2 + r_2^2$$

$$\beta = r_1^4 + r_1^3 r_2 + r_1^2 r_2^2 + r_1 r_2^3 + r_2^4$$

and $r_1$ and $r_2$ are the proximal and distal radii of the circumferences respectively.

# Chapter 3

# Gait Analysis of Patients With Instrumented Prostheses: Experimental [1]

## 3.1 Introduction

Knowledge of the forces and moments transmitted by the bones is essential for the design and fixation of implants and their pre-clinical testing. There is a similar need to understand the effects of mechanical environment on fracture repair and limb lengthening procedures. The values of forces in bones are controversial and there are continuing studies using experimental methods and theoretical modelling techniques. Instrumented hip prostheses have given important data on forces transmitted at the joints [19, 20, 21, 34, 67, 76, 140, 214] but little data exists for the level of force transmitted along the shafts of the bones [219]. Instrumented massive prostheses provide an excellent opportunity to estimate such forces *in vivo* [232, 233, 234].

One major mechanical function of muscles is to provide static and dynamic stability of the musculoskeletal system by balancing external moments not only at joints but also along limbs. Pauwels [195] suggested that bending moments are transmitted along limbs by a combination of tensile forces in the muscles and compressive forces in bones. As a result, the bending moments transmitted by

[1] Part of the material in this chapter was presented by the author at the British Orthopaedic Research Society Meeting, March 1995 [158]. Part of the report has been accepted for publication in *J Biomechanics* [159]. Co-authors: S.J.G. Taylor, J.J. O'Connor, P.S. Walker

the bones should be much less than the net limb moments and the maximum stresses in the bones should be correspondingly smaller. He also suggested that bi-articular muscles are particularly effective. Since lever arms available to the external loads can be longer than those of the muscles, muscle forces can be much larger than the external loads. As a result, the forces transmitted by the joints and the bones will be even larger. A full appreciation of the forces transmitted in the bones cannot be achieved without considering the interaction of forces transmitted in muscles and bones in response to external loads. Although Pauwels performed two-dimensional photoelasticity experiments and simple calculations to support his hypotheses, direct evidence from living subjects has not been found.

Instrumented hip endoprostheses have been used to monitor joint contact forces *in vivo* in various activities [19, 20, 21, 34, 67, 76, 140, 214]. These results provide useful loading information for further strain/stress analyses in *in vitro* and finite element models. Force data in the shaft of the femur provides more direct information about the problem of prosthesis fixation [234]. With simultaneous measurement of kinematic, kinetic and EMG data, it is possible to gain insight into the force interaction of muscles and bones and, with further analysis, the strain/stress distribution in the femur.

In this chapter, telemeterised axial forces along the instrumented massive proximal femoral prostheses from two subjects during several activities is presented with simultaneously measured kinematic, kinetic and EMG data. In order to study the muscle-bone interaction in response to external loads, these activities were selected to vary lever arms available to the external loads. The following hypotheses, suggested by Pauwels' work, were considered:

1. axial force in the shaft of the femur is larger than the external load because of muscle activity;

2. bi-articular muscles are major modulators of the forces in the bones and

3. bending moments along limbs are transmitted mainly by a combination of tensile forces in muscles and compressive forces in bones so that moments transmitted by the bones are much less than the limb moments.

Access to the two instrumented patients was through collaboration with the Biomedical Engineering Division of the University College London at Stanmore. The experimental apparatus and methods used are described. They also form the general protocol for the collection of data on normal subjects and have been

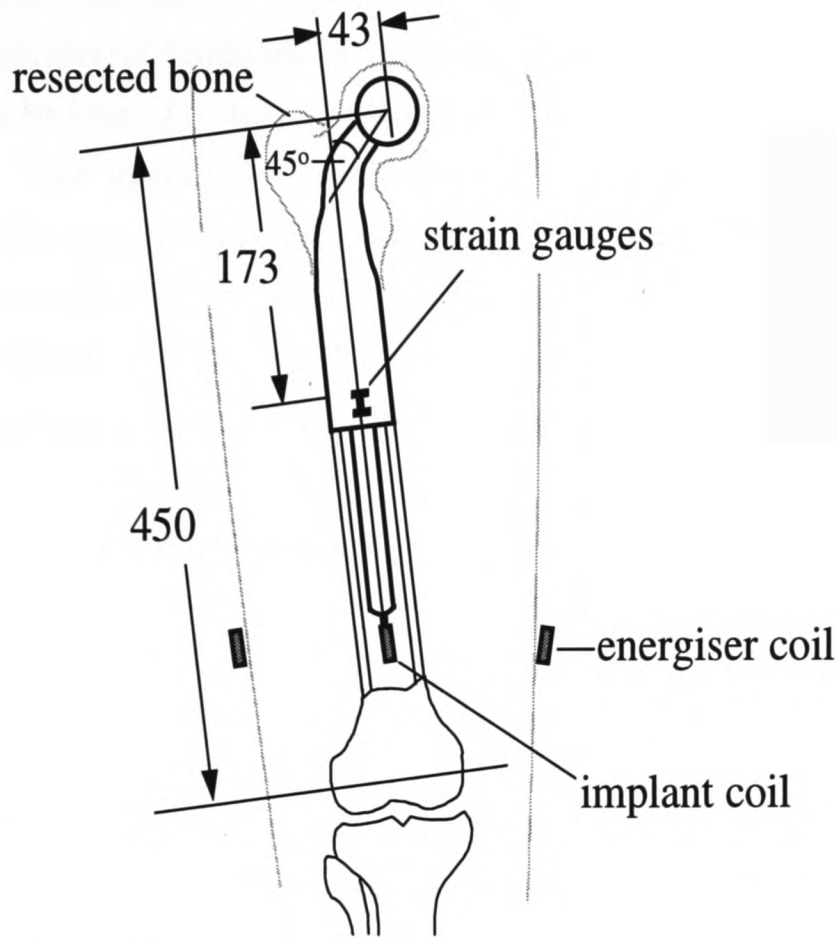



Figure 3.1: Modified prosthesis with inductive coupling in the case of subject IM (dimensions in mm).

adopted by other research students at the Oxford Orthopaedic Engineering Centre. For an insight into the influence of muscle activity on force levels in bones, mathematical models were used to provide a comparison with and further interpretation of the measurements and the results will be described in Chapters 5 and 7.

## 3.2 Subjects and Tests

### 3.2.1 Patients With Instrumented Proximal Femoral Prostheses

Two male subjects implanted with custom-made massive proximal femoral prostheses participated in the study. The first subject (IM; age: 48; body mass: 86.5 kg; height: 176.5 cm; leg length: 96 cm) suffered from a large clear cell chondrosarcoma in the right proximal femur; the second subject (DG; age: 47; body mass: 73 kg; height: 173 cm; leg length: 88 cm) from a giant cell tumour in the

proximal third of the left femur [234]. The operation on the subjects required removal, immobilisation or transfer of muscles arising from or inserting into the proximal femur, including the vastus lateralis, the psoas tendon and part of the gluteus maximus. The abductors, including the gluteus medius and minimus, were sutured over the tensor fasciae latae (in the case of IM) and to the fasciae latae itself (in the case of DG). Small rotators of the hip were removed. Axial forces transmitted along the prostheses were detected by transducers inside the shafts of the prostheses (173 mm distal to the centre of the head of the prosthesis in IM, and 107 mm in DG) and captured using telemetry, Fig. 3.1. A brief description of the instrumented prostheses and the telemetry system will be given in Section 3.3.5.

### 3.2.2 Tests

The subjects performed the following tests: level walking, single and double leg stance, and isometric exercises of hip flexors, extensors, abductors and adductors. These activities were selected to vary the lever arms available to the external loads: minimum for double leg stance and maximum for hip isometric exercises. This range of exercises involved the use of different sets of muscles, with consequent effect on the measured axial force.

#### 3.2.2.1 Standing Posture

In the double leg stance trials, the patients stood in the anatomical position with the instrumented leg placed on the force plate. Data were captured for three trials, each lasting 4 seconds. Similarly, data were acquired for single leg stance with the tested leg placed on the force plate.

#### 3.2.2.2 Isometric Tests of The Hip Muscles

During the isometric tests, the instrumented leg was constrained by a wire with a cuff around the ankle, Figure 3.2. The other end of the wire was fixed to the wall. The patients were asked to pull against the wire as much as possible, with knee extended, using corresponding hip flexors, extensors, adductors or abductors. A load-cell was connected in series with the wire to measure the forces transmitted. The line of action of the force in the wire was identified by two retroreflective markers, which allowed the calculation of the moments at the hip and at the level

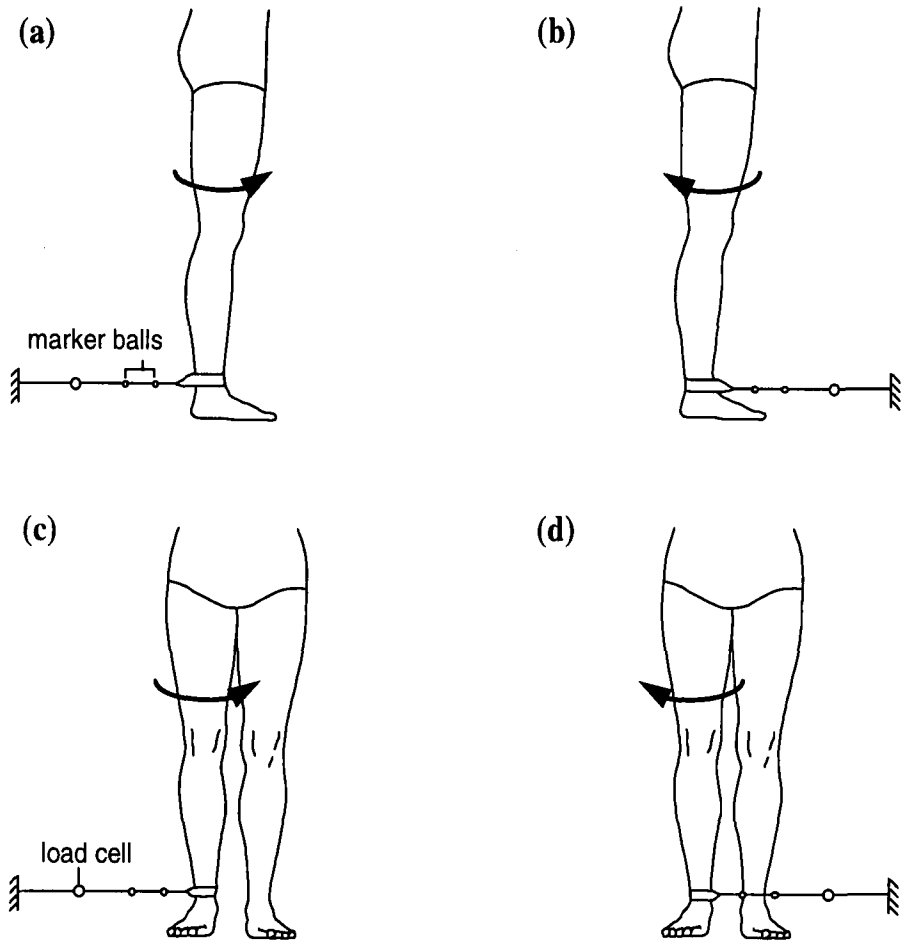



Figure 3.2: Experimental arrangement of the isometric tests of the hip muscles: (a) flexors, (b) extensors, (c) adductors and (d) abductors.

of the prosthesis transducers.

#### 3.2.2.3 Level Walking

For level walking, subjects were asked to walk along the walkway several times until natural walking patterns were acquired, judged by the repeatability of data from successive walks. Data were then collected for a complete gait cycle at the subject's natural pace.

## 3.3 Apparatus and Procedures

The experimental work for the present investigations was carried out in the Gait Laboratory of the Oxford Orthopaedic Engineering Centre (O.O.E.C.), Nuffield Orthopaedic Centre. The O.O.E.C. is a research unit of the University of Oxford, which was established jointly in 1975 by the Department of Engineering Science

and the Nuffield Department of Orthopaedic Surgery. In this section, the equipment and procedures used to collect kinematic, kinetic, EMG and telemetered force data are described.

### 3.3.1 Motion Data Acquisition System

Close-range photogrammetry has been used extensively in the measurement of the kinematics of human movement since the work of Marey [161], Muybridge [176] and Braune and Fischer [32]. For the present studies, a video camera based motion data acquisition system, Vicon 370 (Oxford Metrics Ltd, Oxford, England), was used to record motion patterns of the body segments. As discussed in Section 2.2, at least three points on a body segment are needed to give a full three-dimensional description of its orientation. Low inertia infrared retroreflective markers, perspex balls with a diameter of 2.5 cm and covered with reflective tape, were used for this purpose.

The system consisted of seven video cameras (V494; 50Hz, Oxford Metrics Ltd, England) placed equidistant from the centre of an eight metre gait analysis walkway as shown in Figure 3.3. The cameras were connected through a Datastation to a dedicated PC (IBM compatible), running the Vicon 370 system software under Microsoft Windows$^{TM}$. Each camera was fitted with an infrared strobe close to the camera lens, operating at 50Hz synchronously with the video camera. Without distracting the subjects, they were used to illuminate the passive retroreflective markers attached to the body segments, which show up as bright spots on the video image. The Datastation synchronised the video cameras and digitised in real time the images of the passive retroreflective markers for subsequent use in three-dimensional reconstructions.

For the reconstruction of three-dimensional coordinates of the markers from two-dimensional video images, the Vicon 370 system was calibrated using four ceiling mounted calibration rods, each with five markers mounted at known positions. The calibration was performed with the system which used the Direct Linear Transformation (DLT) method [163] to establish a direct linear relationship between the two-dimensional coordinates of the video image and the corresponding known calibration marker coordinates in the laboratory coordinate system. In order to reconstruct the three-dimensional coordinates, a marker must be seen simultaneously by at least two cameras. Therefore, seven cameras were used to ensure that each marker were seen by at least two cameras. Marker configuration

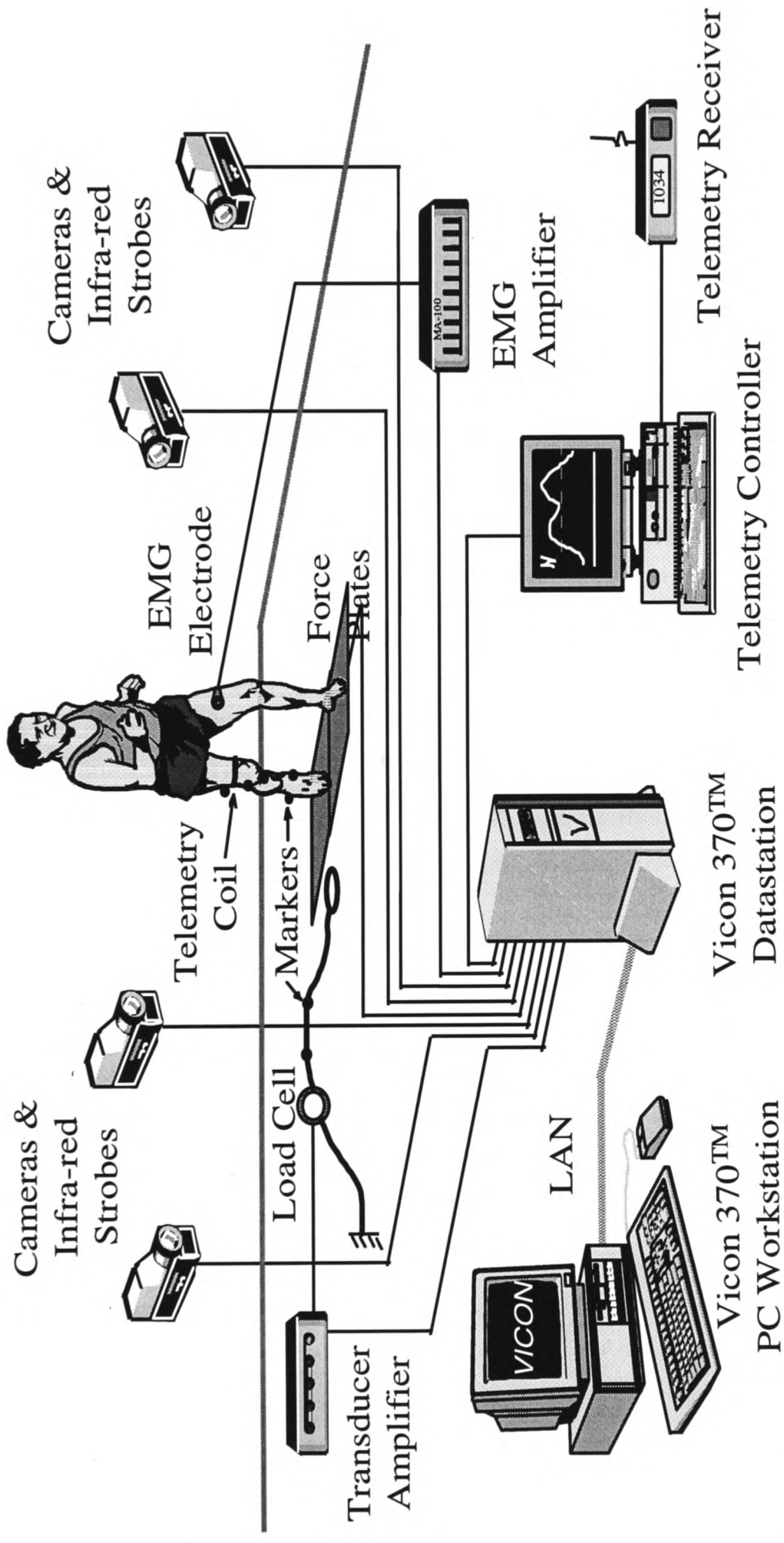



Figure 3.3: The gait laboratory and the Vicon 370 motion data acquisition system

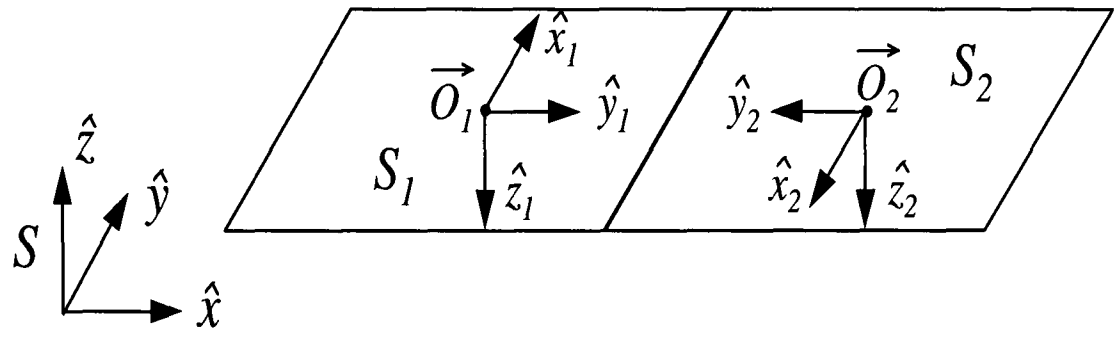



Figure 3.4: The two AMTI force plates, showing the force plate ($S_1$ and $S_2$) and the laboratory ($S$) coordinate systems.

is also crucial to the outcome of the experiment. It must be selected so that the images of each marker can be easily distinguished. The marker system used in the present studies will be described in Section 3.3.6.

For the simultaneous measurement of kinematic and other analog data, an analog to digital (A/D) converter with 32 analog channels was connected to the Datastation. This allowed the Vicon 370 system to be synchronised with other measuring devices such as force plates and EMG system. After all the measuring systems were connected to the Vicon 370 system, the measurement of relevant movement data can then be controlled through the Vicon 370 system software.

### 3.3.2 Force Plates

In addition to kinematic data, it is necessary to know the forces applied to the body during locomotion so that a complete dynamic analysis can be performed to obtain intersegmental forces and moments using models such as the one described in Chapter 2. The ground reaction force (GRF) and spin moment applied by the ground to the foot, together with gravity, are the most common force directly acting on the body during locomotion. In the present studies, two strain-gauged force plates (OR6-6-1000, AMTI, Newton, MA, U.S.A.) were used to measure the resultant GRF.

The configuration of the two force plates, numbered 1 and 2, in the O.O.E.C. gait laboratory is shown in Figure 3.4. They were embedded in the walkway and were flush with the floor. The force plate coordinate systems were defined by the manufacturers and their origins were located at the geometric centres of the plates and at a distance $Z_i, i = 1, 2$ below the top surfaces, which were determined

during calibration. The outputs were connected to the Vicon Datastation for synchronising data collection as described in the previous section. The GRF vector was detected by the force plates and recorded as three components along the local axes, $(F_{xi}, F_{yi}, F_{zi})$. The moments about these axes, $(M_{xi}, M_{yi}, M_{zi})$, were also outputs from the force plates. Since the contact between the foot and the force plate was not a point but rather a varying area and the pressure and traction over which was not even distributed, the GRF vector is therefore the resultant of the pressure over this area. Using the force plates, the mechanical contact between the foot and ground was represented by a resultant GRF vector and a spinning moment along the vertical axis, $M_{zi}$. Paths of the location of the centre of pressure $\vec{A}_i = (A_{xi}, A_{yi}, A_{zi})$ was then calculated by taking moments at the origins as follows

$$\vec{A}_i = (A_{xi}, A_{yi}, A_{zi}) = (-\frac{M_{yi} - Z_i F_{xi}}{F_{zi}}, \frac{M_{xi} + Z_i F_{yi}}{F_{zi}}, -Z_i), \qquad i = 1, 2 \quad (3.1)$$

In order to align the measured GRF vector and spinning moment with body segments for mechanical analysis, the local force, moment and position vectors were transformed to the LCS according to the following equations:

$$\begin{aligned} \vec{F} &= R_i \vec{F}_i, \qquad i = 1, 2 \\ \vec{M} &= R_i \vec{M}_i, \qquad i = 1, 2 \\ \vec{A} &= Ri\vec{A}_i + \vec{O}_i, \qquad i = 1, 2 \end{aligned}$$

where

$$R_1 = \begin{bmatrix} 0 & 1 & 0 \\ 1 & 0 & 0 \\ 0 & 0 & -1 \end{bmatrix}, R_2 = \begin{bmatrix} 0 & -1 & 0 \\ -1 & 0 & 0 \\ 0 & 0 & -1 \end{bmatrix}$$

and $\vec{O}_i$ are position vectors of the origins of the force plates in the LCS.

The accurate determination of the GRF vector and the centre of pressure is essential for the calculation of joint moments. In the assessment of the error introduced in the joint moment calculation, Cappozzo *et al.* [41] suggested that the alignment of the GRF vector with the lower limb was a major source of error. In a recent study, McCaw and DeVita [164] reported that shifts of $\pm 1.0$ cm in the location of the centre of pressure caused 14% changes in maximum joint moment values. A proper calibration of the force plates helps to reduce errors arising from

the determination of the GRF vector and the centre of pressure. The calibration and accuracy tests of the force plates were performed with Dr H.S. Gill following the procedure described in Gill and O'Connor [94]. The mean error between the calibration and measured force values was less than 2.8% for the vertically applied loads ($F_z$). Mean cross-talk between horizontal and vertical force channels was within 0.3% for $F_x$ and 0.4% for $F_y$. The mean error for the position of the centre of pressure was less than 2.5 mm for the $x$ component and 0.9 mm for the $y$ component.

### 3.3.3 Electromyography System

The study of the electrical signals associated with muscle activity is known as eletromyography (EMG), Section 1.2.2. Generally, the amplitude of EMG of a muscle increases with the tension developed by that muscle. This presents a potential use of EMG for the *in vivo* measurement of muscle forces. However, early attempts to correlate the EMG signal of a muscle quantitatively to the force developed in that muscle have come to rather diverse results. Controversy exists even for isometric contraction [15, 200]. Some authors found linear force-EMG relationships [115, 152] while others reported varying degrees of nonlinearity in the muscles tested [144, 281]. During dynamic contractions, there are many factors that can influence the tension generated in the muscle such as contraction length, velocity, and fatigue. Thus, the correlation between EMG and force becomes more difficult to quantify [15, 185, 246]. There are continuing studies trying to assess the force-EMG relationships of skeletal muscles of animals using simultaneously measured force and EMG data [224, 110]. Nonetheless, this approach is not appropriate for humans. Therefore, in the present studies, EMG was only used to indicate the active/inactive phasic patterns for individual muscles and muscle groups. No attempt was made to relate the EMG signal to the values of muscle forces.

The EMG signal of a contracting muscle can be detected by attaching appropriate electrodes to the muscle. Several types of electrodes have been used but generally they fall within three major categories: surface electrodes, needle electrodes and wire electrodes. The choice of electrodes depends on the purpose of the usage. Needle and wire electrodes can be used to detect activity of deep muscles and individual motor units but they are invasive and need special training to use. Surface electrodes, on the other hand, are useful for the detection

of gross EMG of surface muscles which reflect activity of several muscle fibres. They are relatively easy to apply. Since the use of EMG in the present studies was to determine muscle phasic activity, surface electrodes were selected.

Bipolar surface electrodes (Motion Lab Systems, Inc., U.S.A.) were prepared and applied to seven major thigh muscles (rectus femoris, biceps femoris, semitendinosus, adductor magnus, tensor fasciae latae and gluteus maximus) according to Basmajian and De Luca (1989). The position of the electrode placement was following Winter and Yack [265]. Muscle function testing was used to confirm the placement of the surface electrodes. EMG signals were amplified and band-pass filtered (20-200 Hz) with an electromyographic system (Motion Lab Systems, Inc., U.S.A.) which was connected to the Datastation of the Vicon 370 system. EMG data were sampled along with other analog channels at 500Hz. The recorded digital signals were subsequently rectified and smoothed using a bilateral second order Butterworth low pass digital filter with a cut-off frequency of 4 Hz, implemented using MATLAB language. The resulting linear envelopes of the EMG data were used to indicate muscle on/off status.

### 3.3.4 Equipment for the Isometric Tests

While a motion data acquisition system with force plates and EMG systems was sufficient for the data collection of activities such as level walking and stance, an extra device was needed for the isometric tests. During the tests, a wire was used to restrain the tested leg. A load-cell was connected in series with the wire to measure the magnitude of the restraining force in the wire while two retroreflective markers visible to the Vicon 370 system were attached to the wire to determine the line of action of the force. Signals from the load-cell were amplified using a transducer amplifier (Electronic Laboratories Ltd., England) before being passed to the Datastation of the Vicon 370 system.

The load-cell was synchronised and calibrated with the Vicon 370 system using standard weights between 0 kg to 51 kg with an interval of 5 Kg. This corresponds to force values between 0 to 500 N. The calibration loads were applied in ascending and descending order. During calibration, output levels from the transducer channel were collected through the Vicon 370 system and recorded in volts. These output levels were then used to give a linear regression equation, which relates the applied load to the amplified output voltage. There was a highly significant linear relationship ($p < 0.0001$) between the actual and calculated

force. The slope of the relationship between actual and calculated load was not significantly different from 1.0 ($p < 0.0001$). The correlation between the actual and calculated load was 0.9999. The error in force magnitude was expressed as a percent of full scale. The average error was $0.14 \pm 0.02\%$.

### 3.3.5 Telemetry System for the Instrumented Prostheses

The instrumented prostheses and the telemetry system for the measurement of the axial forces in the prostheses were developed at the Biomedical Engineering Division, University College London at Stanmore and have been described in Taylor *et al.* [232, 233]. A brief description will be given here.

The instrumented prosthesis for each subject was custom-made. The main shaft and the intramedullary stem of the prosthesis were machined from solid Titanium-6A1-4V (Ti-6-4) rod, with a large cavity in the distal part of the main shaft, Figure 3.1. This cavity was used to house the electronics and the strain gauges were bonded to the internal surfaces of the cavity for the measurement of the strains of the wall which were then calibrated to give axial forces. Calibration details are given in Taylor *et al.* [234], together with an estimation of the likely measurement errors. A portable battery-powered energiser was used to induce power for the electronics in the prosthesis by electromagnetic coupling between an internal coil in the cavity and an external coil strapped around the thigh of the subject (Figure 3.1). The same two coils were also used for the purpose of data telemetry. The data from the prosthesis was transmitted from the subject over to a 418mhz UHF radio link to a receiver linked to a portable PC, where the telemetered signals are demodulated and converted into digital signals for quantitative analysis.

For simultaneous measurements of the axial forces and the kinematic and kinetic data of the subjects, the telemetry system was connected to the Datastation of the Vicon 370 system. The synchronisation between the two systems was tested. The frequency of the telemetry system output was 100Hz so the sampling rate for the analogue channels in the Vicon 370 system which was set to be 500Hz (> Nyquest frequency) would be enough to avoid any aliasing during the data collection.

### 3.3.6 Subject Marker Systems

Two types of retroreflective markers were used for the measurement of movement and definition of the bony landmarks during motion: *tracking markers* and *anatomical markers*. Tracking markers were used to optimise camera visibility and to minimise the relative motion between the soft tissue and the underlying bone. They defined a Technical Coordinate System (TCS) embedded in each body segment to allow the measurement of segmental movement during activity. Anatomical markers were used to indicate bony landmarks and to define the Body-embedded Coordinate Systems (BCS) to which anatomical geometry is referenced. Both marker sets were placed on the segments of the subject and a *subject calibration* trial was performed. The purpose of the subject calibration was to determine the relative position of the BCS's and TCS's or the transformation matrices between the two systems so that both segmental movement and anatomical geometry can be determined solely by tracking the technical markers. After subject calibration, anatomical markers were removed, leaving only tracking markers for the later trials. To reduce the number of markers used, some markers were common to both marker sets. The two sets of markers are summarised in Table 3.1.

Palpation of the bony landmarks was performed according to the guidelines suggested by the CAMARC committee [18].

## 3.4 Data Analysis

### 3.4.1 Determination of Segment Orientation From Markers

In the study of human locomotion using stereophotogrammetry, due to soft tissue movement relative to the underlying bone and measuring inaccuracies, relative positions of the markers are not fixed. An orthogonal co-ordinate system can be obtained by translating and rotating a reference rigid marker frame, usually defined during static subject calibration, to match the displaced position so that marker positions obtained through this transformation are closest to the measured marker positions in a least squares sense. The resulting kinematic variables, namely rotation matrix and translational vector, are then used for the description of the orientation of the body segment. This optimisation process is referred to

| Name | Anatomical | Tracking |
|---|---|---|
| LASIS | √ | √ |
| RASIS | √ | √ |
| LPSIS | √ | |
| RPSIS | √ | √ |
| GTRO | √ | √ |
| MTHI | | √ |
| MEP | √ | |
| LEP | √ | √ |
| TT | √ | √ |
| MMA | √ | |
| LMA | √ | √ |
| HEEL | √ | √ |
| NT | √ | √ |

Table 3.1: Anatomical and tracking marker positions used on subjects. Definition of these markers, except MTHI, was given in Table 2.1. MTHI is a marker placed at the mid thigh.

as *segment level optimisation* in this thesis and a *system level optimisation* for the determination of the orientation of a multi-joint system will be described in Chapter 6.

A segment level optimisation procedure can be described mathematically as a movement from position 1 to position 2 as follows. The movement of a rigid body from one position (co-ordinate system $\Sigma_1$) to another (co-ordinate system $\Sigma_2$) can be characterised by a translational vector $\vec{v}$ and a rotation matrix $R$,

$$\vec{q_i} = R\vec{a_i} + \vec{v}, \qquad for \quad i = 1, 2, ..., n. \tag{3.2}$$

where $\vec{a_i}$ are the position vectors of $n$ ($n \geq 3$) noncollinear points in $\Sigma_1$, $\vec{q_i}$ are position vectors of these points in $\Sigma_2$ and $R$ should satisfy orthogonality

$$R^T R = I \tag{3.3}$$

$R$ and $\vec{v}$ are unknown and must be determined from the measured position vectors $\vec{p_1}, \vec{p_2}, ..., \vec{p_n}$ in $\Sigma_2$. However, the measured position vectors $\vec{p_i}$ are generally different from the exact vectors $\vec{q_i}$. An overall measure for this difference is given by the error function $e$ of $\vec{v}$ and $R$, defined by

$$e(v, R) = \frac{1}{n}\sum_{i=1}^{n}(R\vec{a_i} + \vec{v} - \vec{p_i})^T(R\vec{a_i} + \vec{v} - \vec{p_i}) \tag{3.4}$$

By minimising the above error function, $R$ and $\vec{v}$ can be estimated.

Several methods have been developed for this purpose [45, 52, 229, 249]. The method by Spoor and Veldpaus [229], the singular variable decomposition (SVD) method proposed by Challis [45] and the method by Veldpaus *et al.* [249] were implemented and tested using simulated data, including two coincident coordinate systems. However, the first two methods failed to give correct answer for the case of coincident systems. Therefore, the algorithm proposed by Veldpaus *et al.* [249] was used in the present study for segment level optimisation. The minimum value of the error function is referred to as *segmental residual error* in this thesis.

### 3.4.2 Determination of Segmental Velocities and Accelerations

An important step in the inverse dynamics analysis with stereophotogrammetry is the determination of the necessary kinematic variables, namely velocities and accelerations of the limb segments, from measured position data. This generally involves a differentiation process. Finite difference methods could be applied directly to the measured position data to obtain first and second derivatives but this can result in big errors as there is usually noise introduced in the measured data. To avoid direct differentiation of the position data, Chao and Rim [51] proposed an optimisation method to obtain joint forces and moments. Their method can be regarded as a curve-fitting process. Winter *et al.* [264] used a digital low-pass filter to reduce the noise in the measured data and then calculated time derivatives using finite difference method. This approach was supported by Pezzack *at al.* [201] who evaluated three methods of smoothing and differentiating: finite difference method, Chebyshev least squares polynomials and digital filtering followed by finite difference techniques. Cappozzo *et al.* [41] used a Fourier series expansion approach to smooth displacement data and calculate its derivatives. The use of spline curve fitting has been suggested by several authors [166, 270, 248]. Cubic spline was shown to be superior than finite difference and polynomial curve fitting methods [166]. Wood and Jennings [270], using data extracted from Pezzack *et al.* [201], demonstrated that quintic splines provided an excellent fit to their raw position data and that the derived second derivatives closely matched their analogue acceleration curves. They also showed that quintic splines did not suffer from the third derivative discontinuities and end-point problems of cubic splines. In a comparative study, Vaughan [248] showed that

quintic splines were superior to cubic spline and digital filtering techniques.

In the light of the advantages and disadvantages of the various techniques, quintic splines were used to smooth and differentiate measured position data and the associated velocities and accelerations. A widely used package for spline smoothing and differentiation among the biomechanics community was developed by Woltring [268]. A C version of this programme was obtained through the ISB WWW site and incorporated into the modelling software developed in the present study.

### 3.4.3 Force Magnification Ratio

In order to quantify the axial force in the prosthesis as a result of muscle response to the external loads, a parameter called the force magnification ratio (FMR) was used. It was defined as the ratio of the telemetered axial force to the external force. External forces were those in the wire during isometric exercises and the component of the measured ground reaction force along the prostheses during ground-contact tests. FMRs were calculated at each data frame for each trial. The average of the FMRs over time was then calculated for each exercise, where appropriate. Means and standard deviations of the time-averaged FMRs were determined.

### 3.4.4 Moment Distribution in The Limb

The tests were chosen to demonstrate the wide range of possible FMRs, depending on the lever arm of the external load. For each test, the value of the external moment transmitted by the test limb ("the limb moment") was calculated by multiplying the magnitude of the external force by the perpendicular distance of its line of action from the axis of the prosthesis at the level of the transducer. The position of the prosthesis in the femur relative to the greater trochanter and epicondyles was determined from x-ray films. The position of the transducer relative to the markers was then deduced.

## 3.5 Results

Table 3.2 shows a summary of time-averaged FMR mean values and corresponding standard deviations during all the static tests for both subjects.

| Activity | Mean (Std. Dev) | | | |
|---|---|---|---|---|
| | DG | | IM | |
| Hip Flexion | 17.4 | (0.24) | 19.5 | (0.41) |
| | 17.8 | (0.16) | 20.5 | (0.52) |
| | - | (-) | 20.8 | (0.69) |
| Hip Extension | 8.5 | (0.39) | 16.2 | (0.36) |
| | 8.8 | (0.59) | 16.3 | (0.38) |
| | - | (-) | 14.8 | (0.24) |
| Hip Adduction | 8.7 | (0.45) | 22.9 | (0.51) |
| | 8.7 | (0.41) | 17.4 | (0.39) |
| | - | (-) | 17.2 | (0.35) |
| Hip Abduction | 20.5 | (0.32) | 29.8 | (2.15) |
| | 22.7 | (0.52) | 25.0 | (0.74) |
| | - | (-) | 26.2 | (1.64) |
| Double Leg Stance | 1.3 | (0.01) | 1.9 | (0.06) |
| | 1.4 | (0.01) | 2.0 | (0.02) |
| | - | (-) | 2.0 | (0.02) |
| Single Leg Stance | 3.0 | (0.09) | 3.2 | (0.11) |
| | - | (-) | 3.0 | (0.14) |
| | - | (-) | 3.2 | (0.12) |

Table 3.2: Time-Averaged Force Magnification Ratio (FMR) During Activities

### 3.5.1 Isometric Hip Exercises

During the isometric tests, the FMR ranged from 8.5 to 22.7 for DG and from 14.8 to 29.8 for IM, Table 3.2. A general trend of bigger FMRs was found in IM. Figure 3.5 shows a typical set of simultaneous recordings from the isometric hip exercises, captured from IM. The internal forces were much larger than the external loads. Linear envelope EMGs showed that applied external loads were mainly balanced by the appropriate agonist muscles: rectus femoris during flexion, hamstrings during extension, tensor fasciae latae and gluteus maximus acting through the iliotibial tract during isometric abduction, and adductor magnus during adduction.

Since external forces were applied perpendicular to the limb in these experiments, there was no resultant force component along the prosthesis, apart from the forces required to balance the weight of the limb. The prosthesis force therefore gives a direct measure of muscle force at the level of the transducer (Figure

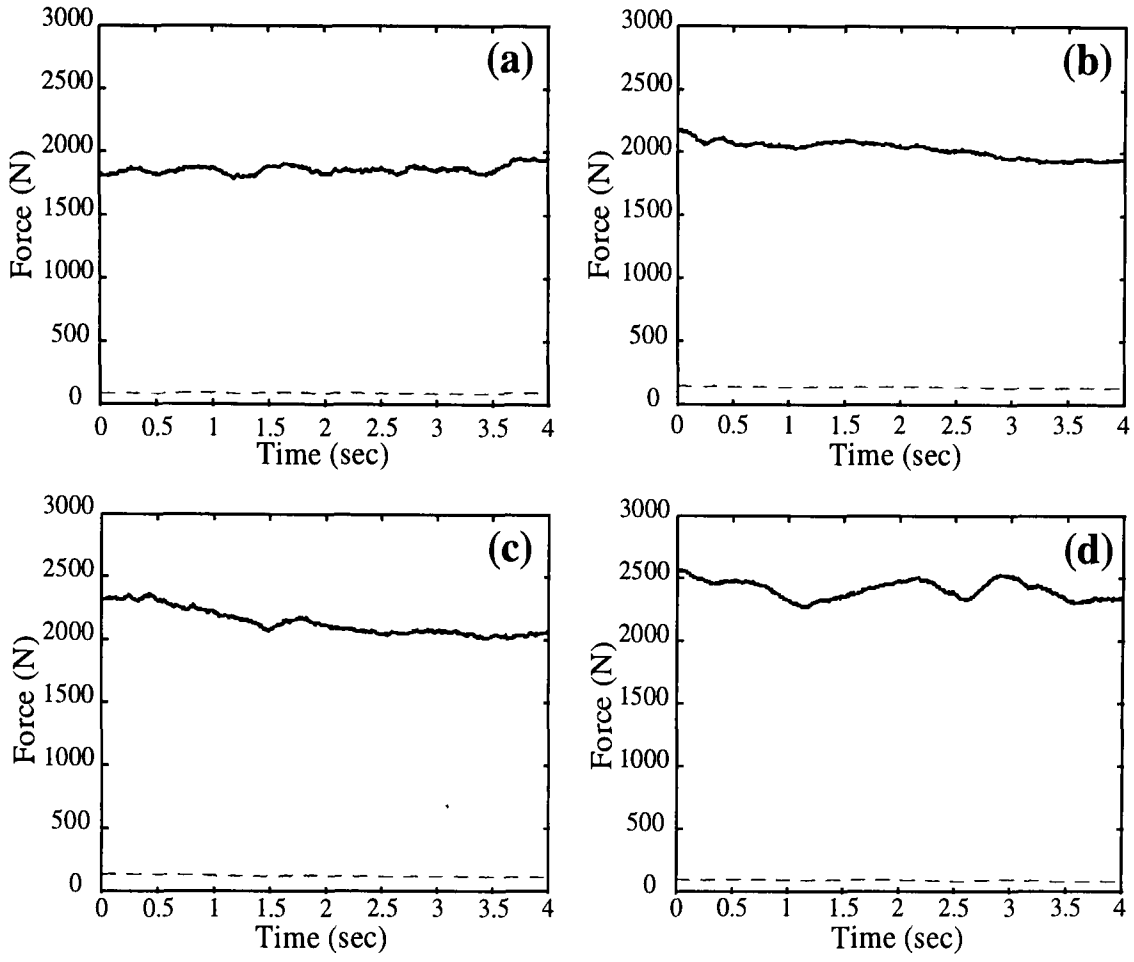



Figure 3.5: A typical set of simultaneous recordings from isometric hip exercises, captured from IM. (a) flexion, (b) extension, (c) abduction and (d) adduction. Solid lines are the measured telemetered force values, dashed lines the measured external loads.

3.6). The measured isometric forces of the hip muscles for both subjects are summarised in Table 3.3. The moments at this level, carried by force couples of the telemetered axial compressive forces and the equal tensile forces transmitted by the appropriate muscle (the Pauwels couple, Figure 3.6), were calculated for muscle lever arms varying from 2.5 to 4.0 cm. This should embrace the normal anatomical range for the muscles [127]. One can examine the contribution of muscle forces and that of the residual bending moment in the bone in transmitting net limb moment. The estimated proportion of the external moment transmitted by the Pauwels couple ranged from 54% to 94% during hip extension depending on the assumed value of the lever arms. The corresponding figures were 71% and 100% (2.5 - 3.3 cm$^2$)for flexion; 63% and 100% (2.5 - 3.1 cm) adduction and 91% and 100% (2.5 - 2.7 cm) abduction. Less than 30% of the external moment was found to be transmitted directly as bending moment in the bone in most tests.

[2]Calculations were not taken beyond that value of the lever-arm which gave the Pauwels

| Activity | Mean (Std. Dev), N | | | |
|---|---|---|---|---|
| | DG | | IM | |
| Hip Flexion | 2030.5 | (135.4) | 2050.1 | (29.9) |
| | 1838.5 | (120.9) | 1788.6 | (30.1) |
| | - | (-) | 1851.6 | (25.2) |
| Hip Extension | 793.1 | (110.3) | 2007.3 | (101.7) |
| | 1389.9 | (130.8) | 2255.2 | (105.1) |
| | - | (-) | 2078.0 | (29.5) |
| Hip Adduction | 1188.9 | (49.5) | 2405.4 | (54.1) |
| | 1227.8 | (64.2) | 2373.9 | (57.1) |
| | - | (-) | 2219.6 | (82.5) |
| Hip Abduction | 1683.8 | (46.8) | 1639.7 | (39.9) |
| | 1935.2 | (115.0) | 2390.8 | (77.1) |
| | - | (-) | 2411.6 | (73.4) |

Table 3.3: Time-averaged isometric forces in the hip muscles

### 3.5.2 Standing Postures

The FMRs were about 1.3 in DG and 2.0 in IM during double leg stance, Table 3.2. The absolute values of the axial forces were 382 N and 866 N. The corresponding figures for single leg stance were 3.0 and 3.2. The corresponding absolute values of the axial forces were 2143 N and 2715 N. Since subject DG had difficulty in maintaining balance, only one successful single leg stance trial was achieved. IM was able to perform three trials but had to lean his trunk forward to keep balance. Activity of the tensor fasciae latae in both postures was indicated by the EMG recordings as shown in Figure 3.7.

### 3.5.3 Gait Trials

Both subjects walked normally, judging from visual inspection and the measured gait patterns, except for IM having a stiff knee during stance phase. Axial force histories and simultaneously measured ground reaction force components along the prosthesis from subject IM are shown in Figure 3.8. It is noted that the telemetered forces during level walking started to build up before heelstrike and achieved a maximum FMR of 3.5. The telemetered forces remained significant

---

couple equal value to the net limb moment ($M_{limb}$) since the sign of the bending moment in the bone would then be opposite to that of $M_{limb}$.

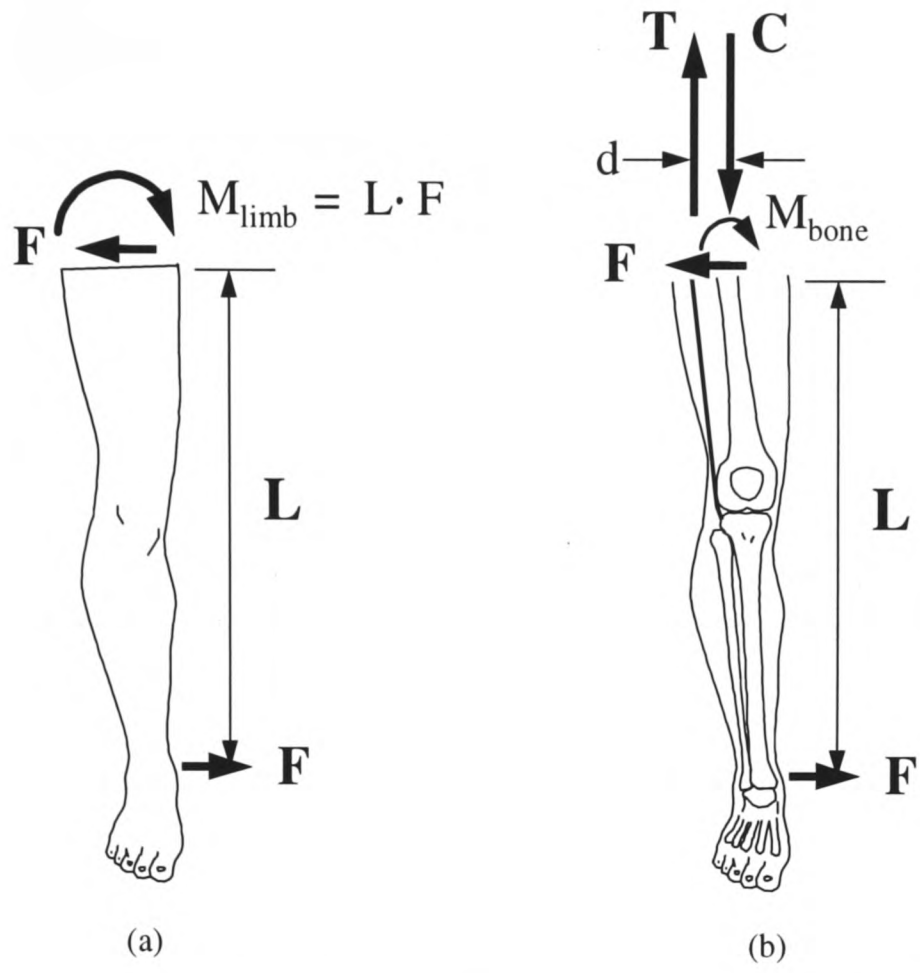



Figure 3.6: Abductor test. Since the external force F is horizontal, the abductor muscle force T and axial compressive force C are equal and opposite. In this test, the Pauwels couple is dT and, together with the bending moment in the bone, $M_{bone}$, transmits the limb bending moment $M_{limb}$. The relative values of $dT$ and $M_{bone}$ are given in the text.

even after toeoff. Subject DG exhibited a similar axial force/GRF pattern and also had a maximum FMR of 3.5.

## 3.6 Discussion

### 3.6.1 Muscle-bone interaction

As shown in Table 3.2, FMRs varied in different activities, depending on the lever arms available to the external loads and the counteracting muscles. Among the activities tested, external lever arms were minimum during double leg stance, Figure 3.9, while the isometric exercises were designed to maximise the external lever arms. These were reflected by the increase of FMRs from double leg stance to isometric exercises, with intermediate values for single leg stance and level walking. The very large values of the FMRs during the isometric exercises are explained

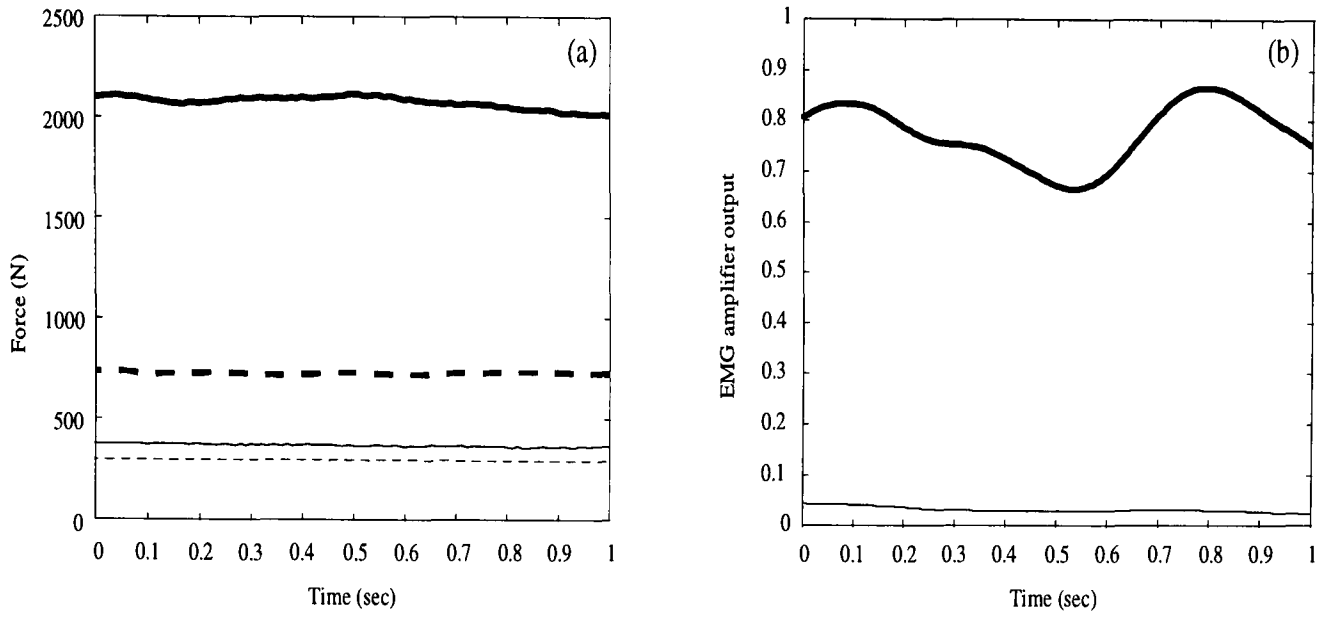



Figure 3.7: Force magnification and tensor fasciae latae activity during double (thin lines) and single (thick lines) leg stance: (a) measured ground reaction forces (dashed line) and telemetered axial forces (solid line) and (b) EMG envelope of the tensor fasciae latae.

in Figure 3.6, showing how the bending moment in the limb is transmitted by the Pauwels couple. The large FMRs for the abduction exercise emphasise the relatively shorter lever arm available to the iliotibial tract and the consequently large value of the iliotibial tract force. It might be supposed that the difference between the FMRs of the two subjects during isometric tests could be due to muscular pathology caused by the implantation surgery but it will be shown that it is explained by anatomical variations between subjects [157], Section 5.3. It is also possible that the relative strengths and lines of action of individual muscles of a functional group were different in the two subjects following surgery. In general, the big values of FMRs indicate significant muscular effects on the forces in the bones.

The co-operative nature of muscle/bone interaction is further revealed by the moment sharing between the muscle/bone force couple and bending moment in the bone during isometric tests. In response to external loads, muscles apply tensile forces along the bones and thus increase the compressive axial force levels in the bone shaft, with the resulting muscle/bone force couple usually transmitting more than 70% of the limb moment, confirming Pauwels' suggestion that muscles act to protect bones from being subjected to excessive bending moment.

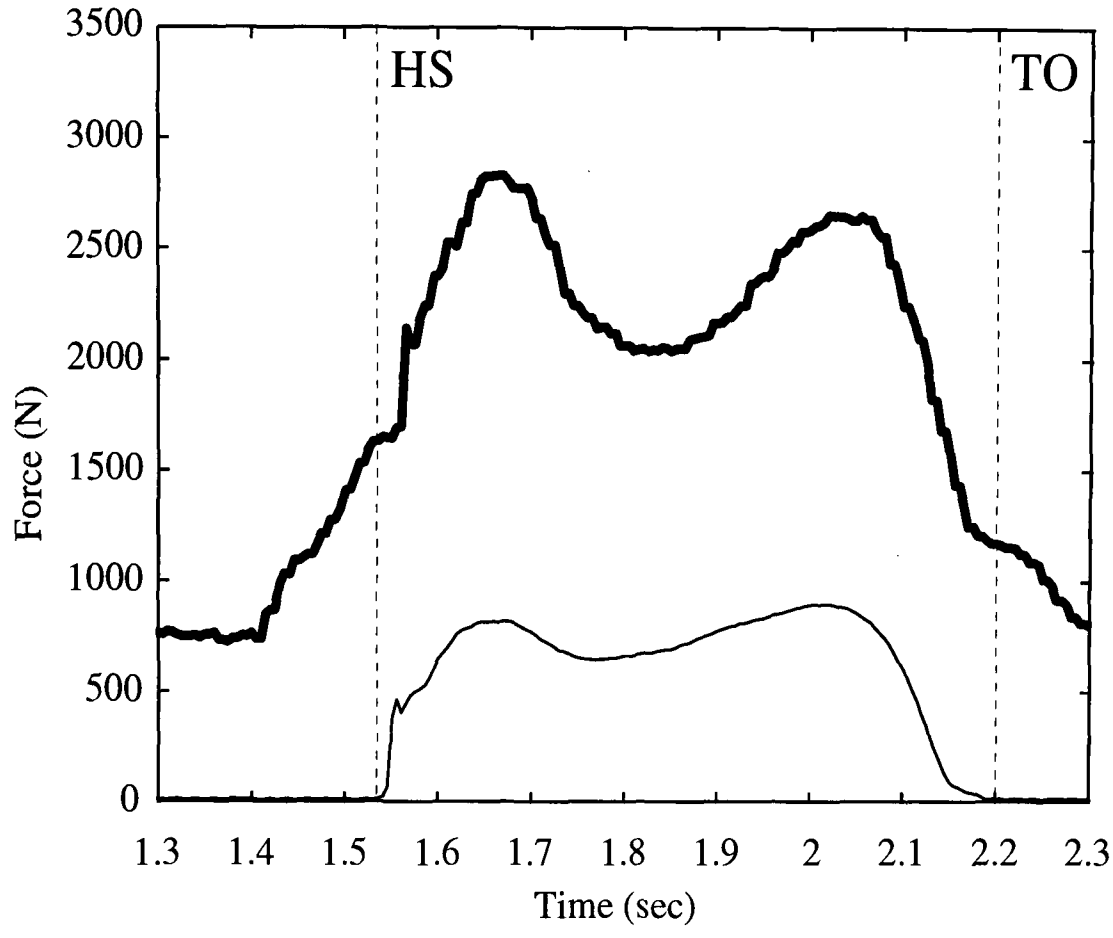



Figure 3.8: Force magnifications during level walking. Thick line is measured axial force in prosthesis and thin line is measured ground reaction force. (HS = heelstrike; TO = toeoff).

### 3.6.2 Muscle recruitment

Although there are redundant muscles in the musculoskeletal system, in many activities only the minimum number of muscles that are necessary for the dynamic equilibrium of the system are recruited, as indicated by EMG studies [199]. In the present study, only flexors were active during isometric hip flexion while extensors, abductors and adductors were recruited, in co-operation with compressive forces in bones, mainly to counteract the corresponding external forces and their resulting moments. Antagonistic muscle activity at the hip was not found during these exercises. Therefore, using isometric tests, it is relatively easy to examine the strength of a functional group and its influence on the forces in the bones, Table 3.3.

It is noted that bi-articular muscles were always recruited during the tests. EMG shows them to be active in the stance phase of normal level walking [199]

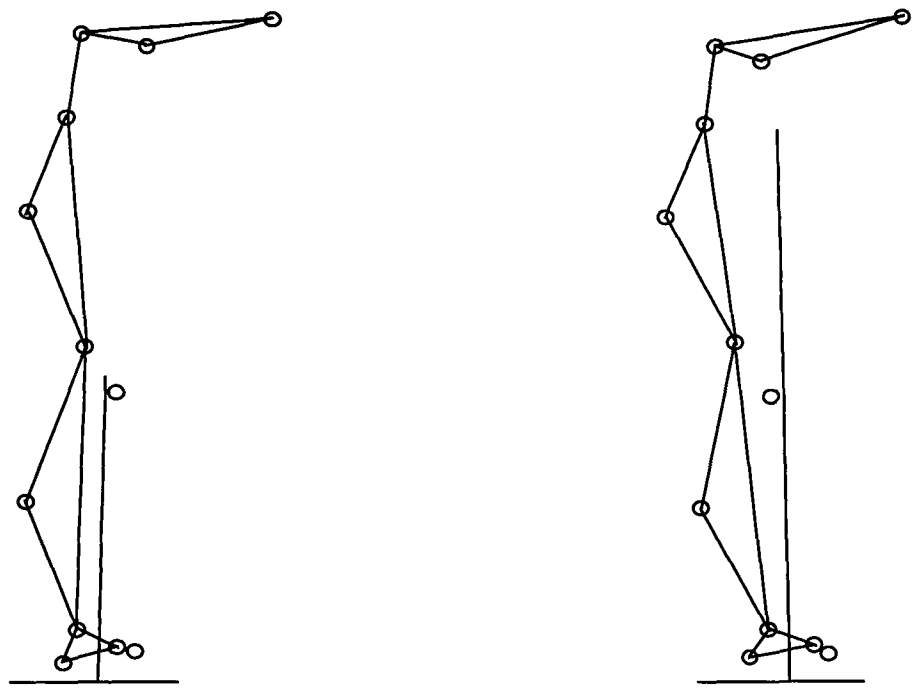



Figure 3.9: Stick figures extracted from the Vicon system showing positions of the leg and the ground reaction forces during (a) double leg stance and (b) single leg stance.

and during isometric and isokinetic tests [187]. Although it may not be appropriate at this point to suggest that bi-articular muscles are preferable to mono-articular muscles during activity, the contribution of bi-articular muscles to the transmission of moment along a limb cannot be overlooked. Bi-articular muscles provide them with the ability to balance external moments not only at the joints but also along the lengths of bones, modulating the distribution of bending moment in bones. This conclusion justifies Pauwels' hypothesis that bi-articular muscles are major modulators of stress/strain distributions in bone but further quantitative analyses are required to determine the relative contributions of synergistic mono- and bi-articular muscles.

During double leg stance, only small muscle activity was needed. Transferring from double leg stance to single leg stance yielded a substantial increase of muscle activity mainly from the abductors and muscles inserted into the iliotibial tract, as indicated by the FMR values (Table 3.2) and EMG recordings (Figure 3.7). The peak FMRs during stance phase of gait were 3.5 (equivalent to prosthesis forces of 3.3 times body weight), similar to those measured by Kotzar *et al.* [140] and Bergmann *et al.* [19] who reported peak hip joint contact forces during walking with medium speed ranging from 2.8 to 4.8 times body weight. Although

comparable FMR values were found during single leg stance and the stance phase of gait, it is noted that muscles recruited for these activities are not the same. Recruited muscles at the hip during the mid-stance phase of gait were similar to those for single leg stance, mainly abductors but during the first and last one-thirds of the stance phase where peak hip moments and peak ground reaction forces occurred, significant flexor and extensor activity was also found in the present study and in the studies of Kadaba *et al.* [135]. It indicates that axial forces in the bones during stance phase are sensitive to flexor and extensor as well as abductor actions.

### 3.6.3 Inter-subject comparison

The general characteristics of the forces in bones as a result of muscular response to external loads were shown with the data measured from the two subjects. Further acquisition of data from a larger population of instrumented subjects is needed for statistical analysis and comparisons between subjects and for the establishment of quantitative regression profiles of the FMR values for general use. Since muscles dissected in the subjects were mainly those inserting and arising on the proximal femur, the results may over-emphasise the contribution of the bi-articular muscles. Direct application of the results to normal subjects should be made cautiously although both subjects showed no difficulty in stair climbing and were almost normal during level walking, except for IM having a stiff knee during the stance phase of gait. One possible alternative may be through the development of a mathematical model which can reasonably estimate the force interactions within the musculoskeletal system of the lower limb, taking account of the anatomy and anthropometry of the subject under test. Such a model should be able to predict the difference of the FMRs during isometric tests between the two subjects and allow quantitative analysis of these activities. A lower limb model in the sagittal plane was developed towards this purpose and to provide a comparison with and further interpretation of the measurements [157], Chapter 5.

### 3.6.4 Relevance to Gait Analysis

The dramatic effects of loads applied perpendicular to the limb on FMRs emphasises the importance of accurate calibration of the horizontal components of force measured by force plates in gait laboratories. Attention so far has concentrated

on the calibration of the vertical component [26, 94] which, although larger in magnitude, has a shorter lever-arm about the knee and the hip.

## 3.7 Summary

Simultaneous *in vivo* measurements of external loads and the telemetered axial compressive forces along the femur provided an opportunity to examine the effects of muscle activity on the forces in the femoral prostheses. It has been found that

1. flexors/extensors contribute a significant part in the forces in the femur;
2. bi-articular muscles may have a major role in the modulation of forces in the bones; and
3. muscles balance external bending moments by applying axial compressive forces along the bones and thus increase the axial compressive force level in the bone shaft.

The big variation of the FMRs during isometric tests between the two subjects suggests that quantitative analysis of these activities are needed to estimate the forces transmitted within the musculoskeletal system. Modelling work is required to enhance further applications to daily clinical practice and this will be dealt with in the following chapters.

# Chapter 4

# Modelling of The Knee Joint and Its Force-Bearing Structures

The need for mathematical models in the study of the forces transmitted in the locomotor system has been briefly described in Chapter 1 and further shown in Chapter 3. It was suggested that modelling of the joints is essential in the development of models of the locomotor system. Because of its complexity and the high incidence of disease and injury, it was decided to start the model development from the knee joint. In this chapter, the modelling of the knee joint and its surrounding force-bearing structures in the sagittal plane is presented. It will begin with a brief discussion of the kinematic geometry of the knee joint followed by a description of a computer graphics-based model of the knee ligaments, built upon the four-bar linkage model developed by O'Connor *et al.* [182, 184] for the study of the shape changes and fibre recruitment of the ligaments during motion. The ligament model is a development of the model of Zavatsky and O'Connor [277, 278]. This chapter will conclude with a section on the geometry of the tension-bearing structures of the knee joint in terms of their lines of action and lever arms and the comparison of the model outputs with the experimental measurements reported by Herzog and Read [110].

# 4.1 Kinematics of The Knee Joint

## 4.1.1 Unloaded Versus Loaded Movement

The knee is a relatively incongruent joint so articular surfaces alone cannot control its motion. The mobility and stability of the joint therefore must involve a complex interaction between the articular surfaces and the surrounding connective tissues including ligaments and muscles. Due to the variable external loads and muscle forces involved, the variance of the motion pattern of the knee joint during activity can be significant [47, 143, 225, 235]. This makes it difficult to study the contribution of each individual joint structure in controlling the observed joint motion. When the variables involving the external loads and muscle forces are removed, the inherent characteristics of the motion of the joint as a consequence of the kinematic interaction of only the passive structures can be obtained. This unloaded motion is called *passive motion* [23]. The description of passive motion is useful for *in vitro* studies because an unloaded situation is much easier to simulate in laboratories and results from different sources can be compared.

In his *in vitro* experiments, Wilson [259] showed that the knee follows a unique path of movement in passive motion and external forces are needed to deviate the joint from this path. Figure 4.1 shows results from one of his deviation experiments in which, at three arbitrary positions during passive motion, the knee was stopped and an external moment was applied to the femur about the longitudinal axis of the fixed tibia and then released to allow the femur to spring back to a resting position before passive motion was continued. It can be seen that the rotation paths of the femur relative to the tibia were almost the same for movements from extension to flexion and from flexion to extension and that the femur always sprang back to the same position that it occupied in passive motion. These findings were recently further confirmed by Wilson *et al.* [260]. This characteristic justifies the modelling of the joint as a single degree of freedom mechanism, or a linkage in two dimensions, and elicits the basic idea that the kinematic modelling and mechanical analysis of the knee can be done separately and sequentially, as proposed by Wilson and O'Connor [262].

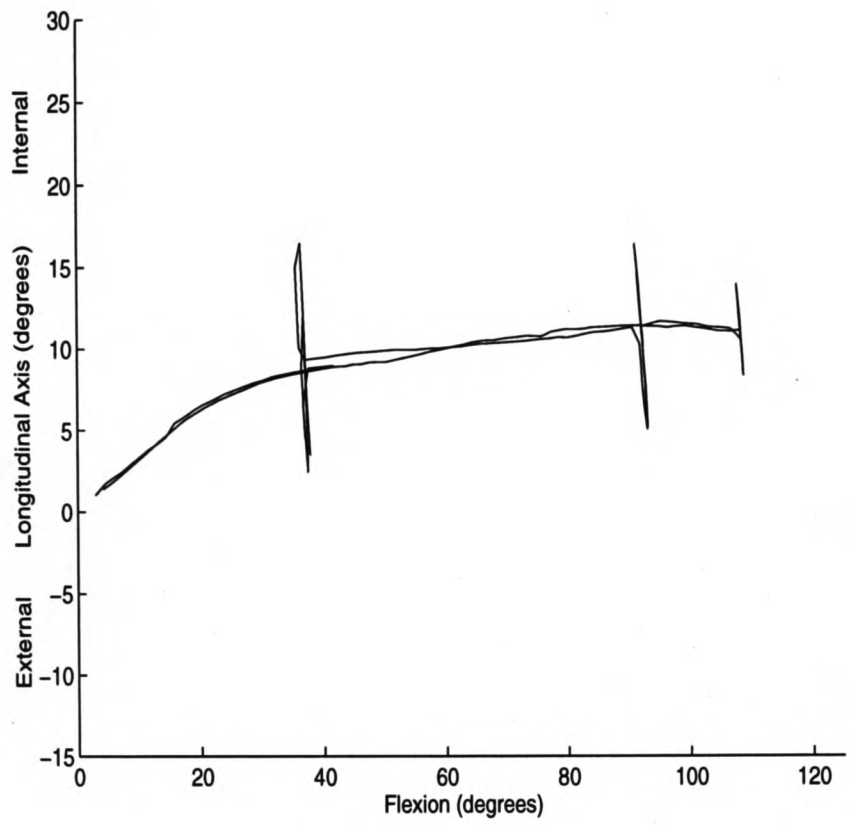



Figure 4.1: Rotation about the longitudinal axis in the tibia: deviation experiment (Specimen M). From Wilson [259]

### 4.1.2 Passive Motion: The Four-Bar Linkage Model

In order to derive changes in the geometry of the major structures of the knee joint during movement, the relative motion of the femur and tibia should be defined first. As discussed above, this can be done by considering separately and sequentially the unloaded and loaded situations. To determine the unresisted neutral (passive) movement of the femur relative to the tibia in the sagittal plane, the four-bar linkage knee model [182, 184] was used. Unresisted displacement of a linkage from one position to another can occur without deformation of its links or the need to apply external forces and the linkage, as such, is a good model of the passive motion of the knee. As shown in Figure 4.2, the linkage is formed by inextensible line segments representing the isometric fibres of the cruciate ligaments (AB and CD) and by similar line segments which join their attachments on the tibia and femur and are rigidly fixed in the bones.

Figure 4.3 shows a diagrammatic representation of the four-bar linkage. Body-fixed coordinate systems were embedded in the femur and tibia. The origin of the tibial system is the tibial attachment of the isometric fibre of the ACL. The $x$ axis is directed posteriorly and is parallel to the flat tibial plateau ($EF$), which is an approximation of the convex lateral and concave medial tibial plateaux. The

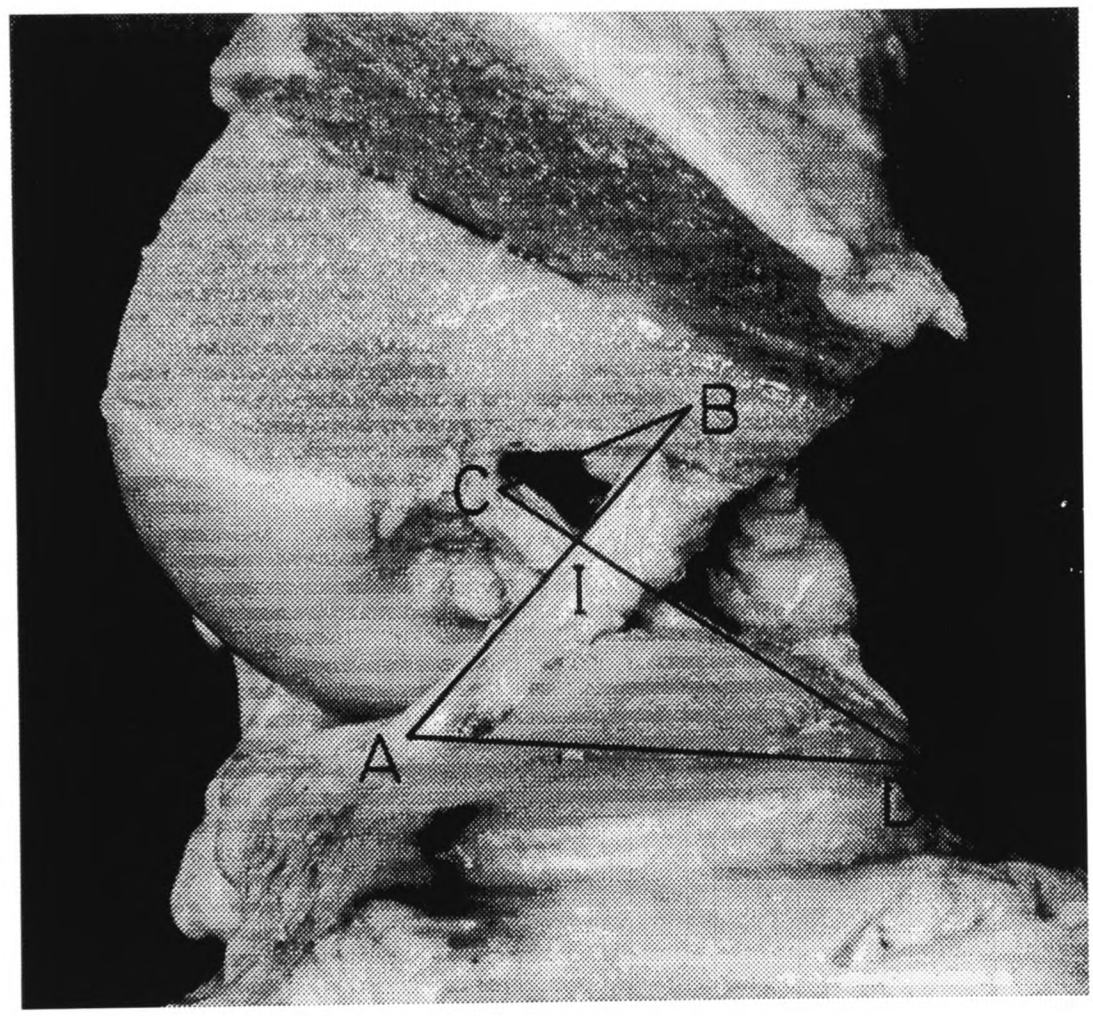



Figure 4.2: Sagittal view of a human knee flexed to about 45° with most of the lateral femoral condyle removed. A possible four-bar cruciate linkage (ABCD) is superimposed. The instantaneous centre of the linkage is marked I. Note that in this view the attachment areas of the ligaments are obscured by the bones and by the ligaments themselves.

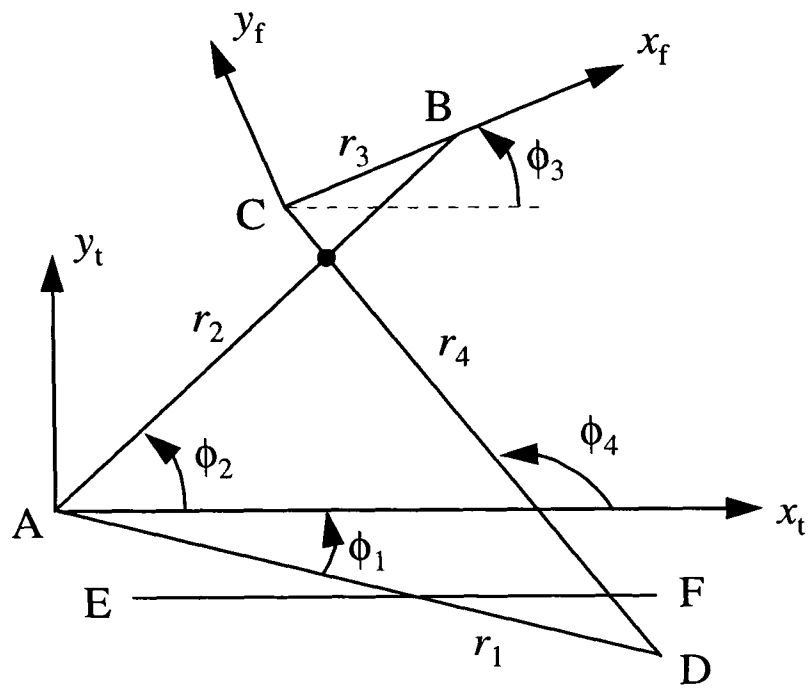



Figure 4.3: Diagrammatic representation of the four-bar linkage model used in the present study. The flexion angle is 70°.

origin of the femoral system is the femoral attachment of the isometric fibre of the PCL. The $x$ axis lies along the femoral link of the four-bar linkage and is directed posteriorly at full extension. The movement of a point with position vector $\vec{p}_f$ in the femoral co-ordinate system relative to the tibial co-ordinate system can be described as the following transformation relationship

$$\vec{p}_t = \vec{v}(\theta) + R(\theta)\vec{p}_f \tag{4.1}$$

The translational vector $\vec{v}(\theta)$ and the rotational matrix $R(\theta)$ of the transformation are obtained from the analysis of the linkage and represented as functions of the knee flexion angle $\theta$. Formulae and model parameters describing the geometry of the linkage system were given in O'Connor *et al.* [182] and Zavatsky and O'Connor[277].

During passive knee flexion/extension, the cruciate ligaments rotate isometrically about their points of attachment on the bones. The instant centre of zero velocity of the femur relative to the tibia, known as the instant centre of rotation, is the point at which the cruciates intersect, an important property of a four-bar linkage, Figure 4.4. It is the point at which the flexion axis intersects the sagittal plane so we shall refer to it as the flexion axis in the present study. The flexion axis moves relative to each bone. To avoid interpenetration or separation of the bones, the common normal to the articular surfaces at their point of contact

must pass through the flexion axis [184]. Since the flexion axis moves posteriorly relative to the femur during flexion, the point of contact must move posteriorly on the tibia, Figure 4.4, explaining why the natural femur rolls posteriorly on the tibia during flexion and anteriorly during extension [252]. Since the articular surfaces are virtually frictionless [204], the contact force transmitted between the surfaces is normal to both and its line of action must therefore pass through the flexion axis [184].

The tibial plateau was approximated as a flat surface, a compromise between the concave medial condyle and the convex lateral condyle. The shape of the compatible femoral condyle was then deduced from the common normal theorem. It was found to be polycentric and polyradial but closely approximated by a circular arc [184].

The lines of action of the model ligament and contact forces are determined from the four-bar linkage. Since the ACL and PCL and the contact force pass through the flexion axis, the lengths of their moment arm about the flexion axis are thus zero, so that they cannot transmit moments about the flexion axis. All external flexing and extending moments about the flexion axis have to be balanced by muscle action.

## 4.2 Ligament Fibre Recruitment and Shape Changes During Motion [1]

As discussed above, the ligaments of the knee and their interactions with the articular surfaces and muscles control the mobility and stability of the joint. Knowledge and understanding of those interactions are essential in the design and implantation of knee prostheses and ligament replacements in diseased or injured knees. Direct measurement of ligament forces in vivo is difficult [12, 150, 4]. A combined theoretical and experimental approach is a powerful means of estimating such quantities [24].

Although theoretical studies representing the ligaments as single lines based on gross anatomy have provided estimates of the ligament forces during activity [174, 58], a full appreciation of the functional and structural behaviour of the ligaments requires more detailed modelling at the architectural level. For example, single

[1] The work in this section has been published in *Proc Inst Mech Eng, Part H, J Engng Med*, 210: 71-79 [154]. Co-author: J.J. O'Connor.

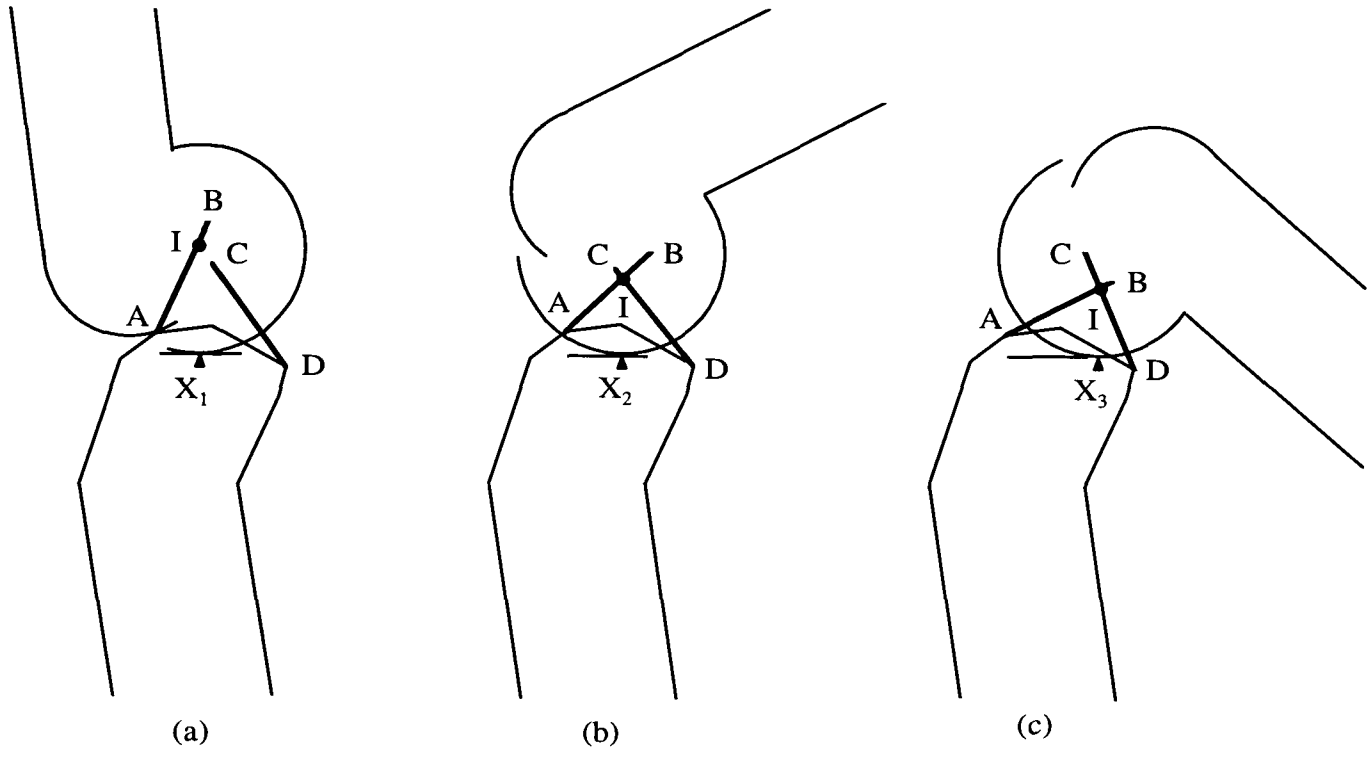



Figure 4.4: The four-bar linkage model of the knee joint at (a) 0°, (b) 70° and (c) 140° flexion. Single thick lines are used to represent the two isometric fibres of the cruciate ligaments, $AB$ and $CD$. It is noted that the instant centre $I$ moves relative to each bones and that the tibiofemoral contact point moves posteriorly during flexion, from $X_1$ to $X_3$. The tibia is shown using line segments joining some particular bony landmarks. No attempt was made to reproduce the precise shape of the bone but the shape of the femoral condyle was calculated from the model.

line representation of ligaments cannot account for the mechanism of partial tear of the ACL, an injury occurring frequently in sports and other strenuous activities [114]. In fact, experimental studies have shown that the ligaments are subjected to inhomogenous strain over their cross-sectional areas during knee motion [84, 231, 215, 2]. Thus, information on the stress and strain distributions in the ligaments at any position of the joint is important for a better design of ligament replacements.

The phenomenon of non-uniform strain/stress distribution in the knee ligaments was confirmed theoretically by Zavatsky and O'Connor [277, 278]. In their study, ligaments were represented in the sagittal plane as bands connecting the femur and the tibia. The shape of the ligament band in different positions of the joint was determined by the relative orientations of the attachment areas (line segments in the sagittal plane) and an ordered arrays of straight-line

fibres, mapped proportionally from the femoral to tibial attachments. The resulting shape changes of ligaments were represented by the different positions of the areas formed by the attachment line segments and lines connecting their end points. This method had been adopted by van Dijk *et al.* [242, 241] in presenting experimental data. Slack fibres were shown as straight lines; however, numerous anatomical studies [84, 95] have shown that ligament fibres can buckle, presumably when they are slack.

With the appearance of high performance computers, there has been an increasing application of computer graphics in the visualisation and simulation of musculoskeletal systems. Introducing interactive computer graphics was suggested by Boysen *et al.* [27] in 1977. Delp *et al.* [68] emphasised further the capability of computer graphics in the study of orthopaedic surgical procedures. Chao *et al.* [49] discussed the simulation and animation of musculoskeletal joint system using computer graphics. Recently, for the geometric and mechanical analysis of the locomotor system, Lu *et al.* [153] developed an interactive graphics-based window interface, which unifies solution procedures and provides an user-friendly environment for clinical users. This section describes a development of the Zavatsky-O'Connor work [277, 278] which accounts for buckling of slack fibres during passive flexion and anterior/posterior tibial translation. The interactive graphics-based interface of Lu *et al.* [153], to be described in Chapter 5, was used for the simulation, visualisation and animation of the model output.

### 4.2.1 Representation of Ligament Fibres

Four major knee ligaments, the anterior cruciate ligament (ACL), posterior cruciate ligament (PCL), medial collateral ligament (MCL), and lateral collateral ligament (LCL), were incorporated in the present model. They were considered as ordered arrays of fibres mapped from the femur to tibia through straight-line segments on the bones, Figure 4.5, as suggested in [277]. The ligaments were assumed to be composed of a continuous ordered array of fibres, but, for visualisation purpose, only a number of selected fibres are used for model animation. The attachment length of a fibre is taken to be the straight-line distance between its points of origin and insertion on the bones. If a fibre attached to the femur at $\vec{p}_f$ and to the tibia at $\vec{d}_t$, its attachment length $l$ can be calculated using the following equation

$$l = \left| \vec{p}_f - \vec{d}_t \right| \tag{4.2}$$

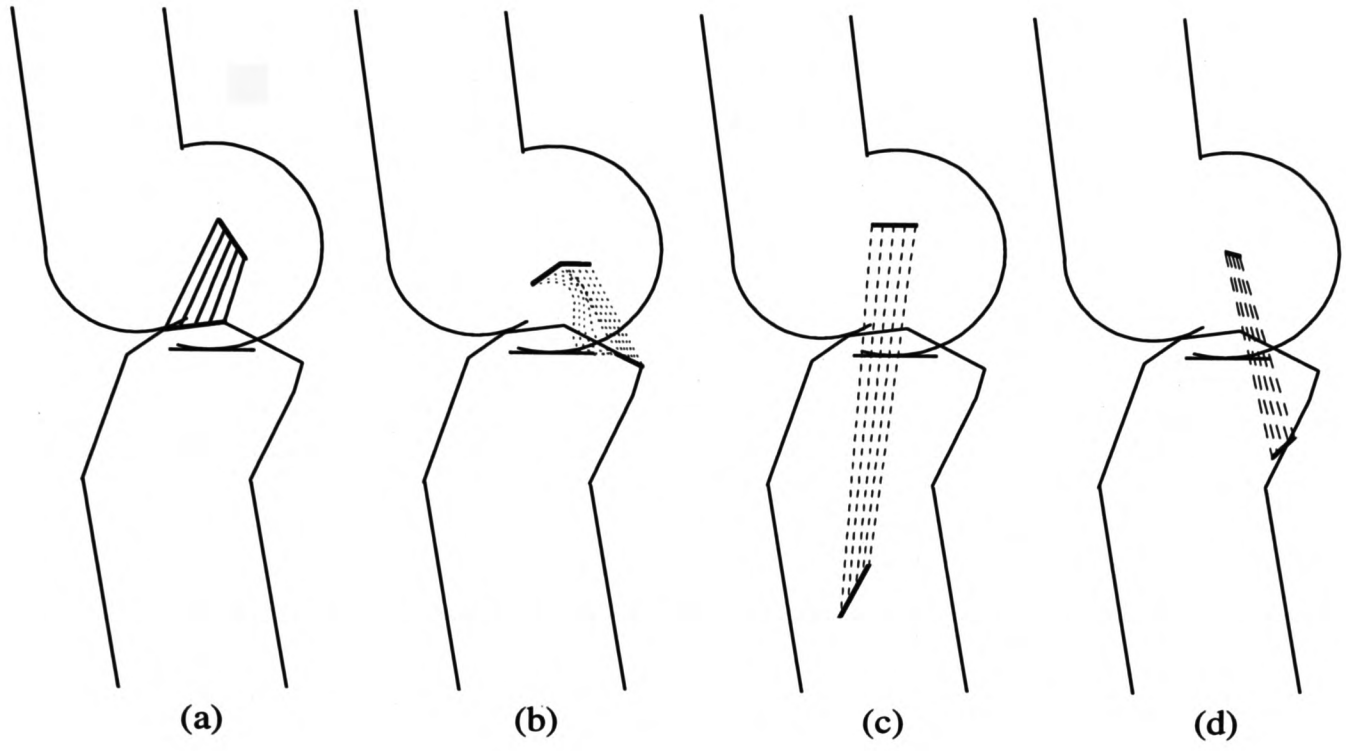



Figure 4.5: Attachment areas of the ligaments were represented as straight thick lines and their shapes at the neutral position are displayed using five representative fibres: (a) ACL, (b) anterior half of PCL shown slack and posterior half straight, (c) MCL and (d) LCL. Slack fibres are shown buckled, taut fibres are shown straight. Detailed descriptions of the representation of the fibre shapes are given in Section 4.2.1.1 and 4.2.1.2

as well as Equation (4.1). If the attachment length is greater than the reference length $l_0$, the fibre is tight; on the contrary, slack. The reference length $l_0$ of each fibre was calculated at the reference position where the fibre is just tight and without tension. This definition has been useful since it allowed Zavatsky and O'Connor [277, 278] make direct comparison between their calculations and measurements such as those of Sapega *et al.* [215], Amis *et al.* [2] and van Dijk *et al.* [242, 241]. Both theory and experiment showed that all but the isometric fibres of the ACL and PCL are slack during passive motion. It is thus noted that, in the unloaded joint, no fibre can be longer than its reference length so that the ligaments offer no resistance to passive motion; the attachment lengths of the isometric fibres (AB and CD in Figure 4.2) always remain constant. The shapes of other fibres then require additional structural and functional considerations.

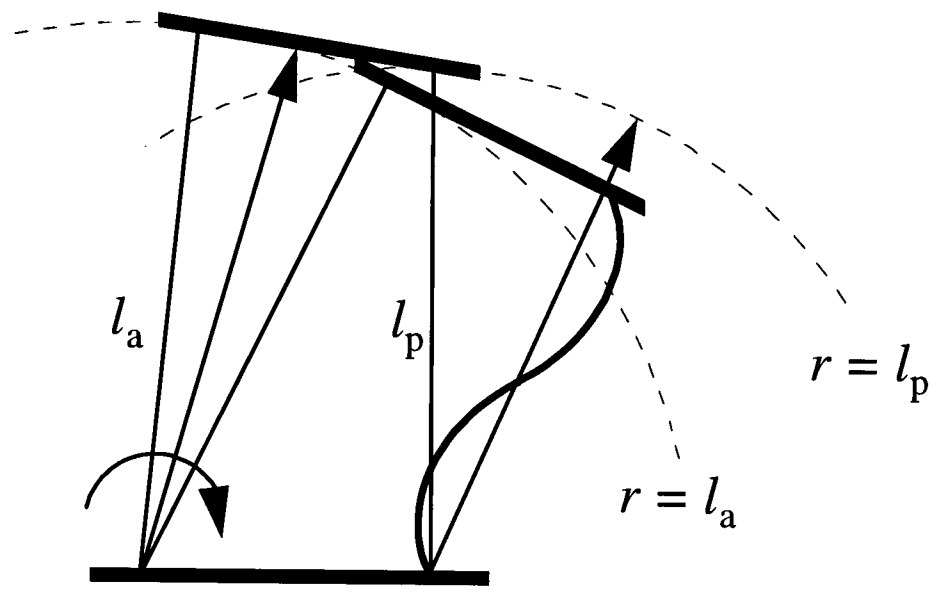



Figure 4.6: Fibres buckle when their attachments approach each other, as indicated by the posterior-most fibre. Here the anterior-most fibre represents an inextensible link which rotates about its distal attachment point, causing its proximal attachment point to move along a circle of radius $l_a$. It remains isometric during passive motion.

#### 4.2.1.1 Tight Fibres ($l \geq l_0$)

If the attachment length of a fibre is longer than its reference length, it is stretched and is able to transmit tensile forces. If the fibre does not wrap around a bone etc., it can be modelled as a straight line, which can be represented mathematically as the following equation in the tibial co-ordinate system.

$$\vec{m}_t = \vec{d}_t + \frac{s}{l}(\vec{p}_t - \vec{d}_t) \tag{4.3}$$

where $0 \leq s \leq 1$ and $\vec{m}_t$ is the position vector of any point on the fibre.

#### 4.2.1.2 Slack Fibres ($l < l_0$)

A fibre is slack if its attachment length is shorter than its reference length. Since a ligament fibre cannot resist compression, it buckles even with the very small load caused by the relative approach of its attachments, as shown in Figure 4.6. We shall assume that each slack fibre adopts the shape of a buckled pin-ended strut according to Euler buckling theory [91] which can be represented mathematically as follows.

$$v = \delta \sin(\frac{n\pi x}{l}) \tag{4.4}$$

where $n = 1, 2, ...$ and $v$ is the deflection of the fibre transverse to the long axis joining the two attachment points at a point distance $x$ from the tibial

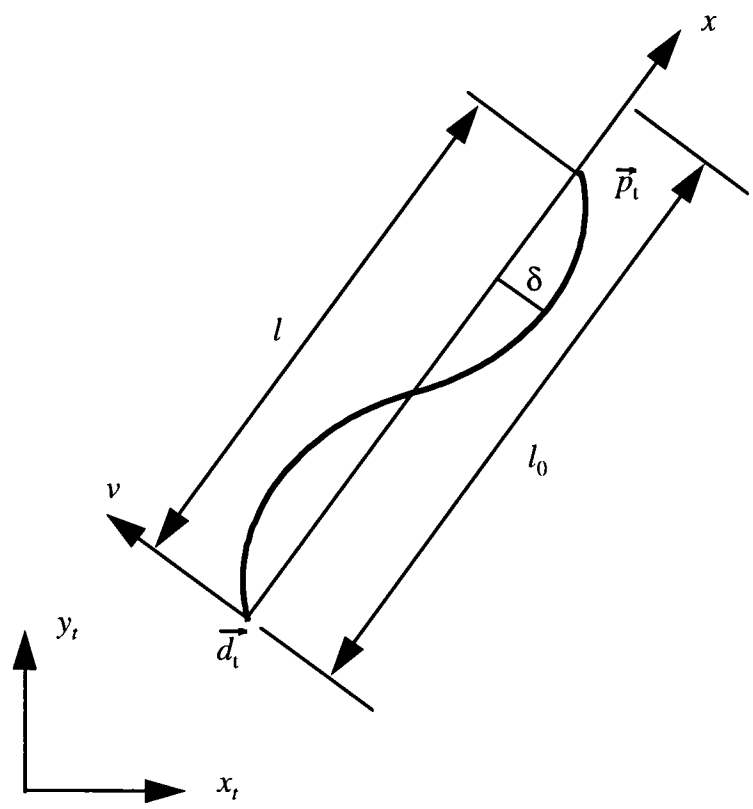



Figure 4.7: Right-handed co-ordinate system of a second mode buckled pin-ended fibre ($l < l_0$), with origin at its distal attachment point $\vec{d}_t$ and $x$ axis directed positively to its proximal attachment point $\vec{p}_t$. $\delta$ is the maximum transverse deflection in the direction of the $v$ axis.

attachment, and $n$ is the buckling mode, as shown in Figure 4.7. The symbol $\delta$ represents the maximum transverse deflection and can be determined by applying another geometrical constraint that the length of the fibre remains the same as its reference length. The constraint is

$$l_0 = \int_0^l \sqrt{(v'^2 + 1)} dx \tag{4.5}$$

where $v' = dv/dx$. Equation (4.4) and (4.5) are mathematical representation of the buckled fibre shape in the fibre local co-ordinate system. To express the shape of a slack fibre in the tibial co-ordinate system, a co-ordinate transformation from the fibre system to the tibial system is required. Later in Section 4.2.4.1, modelling using mode 1 and 2 ($n = 1$ or 2) will be discussed in the light of experimental observations.

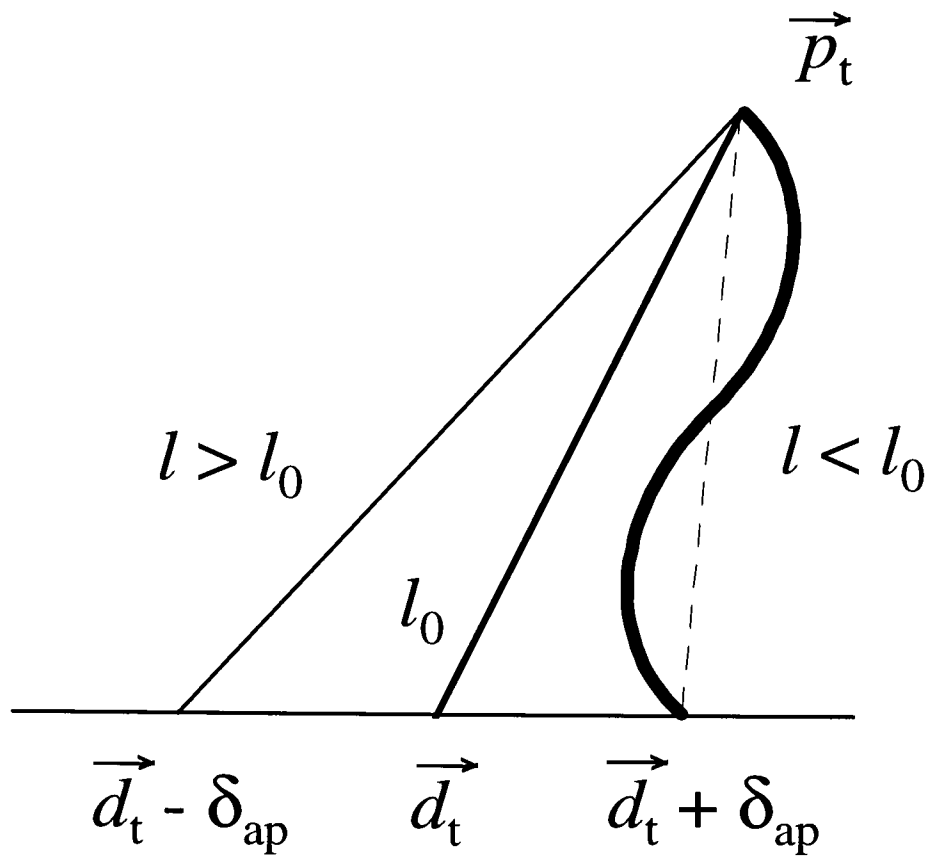



Figure 4.8: Schematic representation of the fibre shape changes during anterior/posterior translation. An anterior-oriented fibre, as shown, is stretched with anterior translation and slackens with posterior translation. Anterior displacement increases the relative horizontal component of the force transmitted by the fibre.

### 4.2.2 Loaded Knee Joint Movement (Anterior/Posterior Tibial Displacement)

When external loads and muscle forces are applied, the shear components of force parallel to the tibial plateau are transmitted by the ligaments. An anteriorly directed shear force stretches fibres in the ACL and slackens fibres in the PCL; a posteriorly directed force stretches PCL fibres and slackens ACL fibres. The quantity $\vec{d_t}$ in Equation (4.2) is modified as

$$\vec{d_t} = \vec{d_t} + \delta_{ap}\vec{i_t} \tag{4.6}$$

where $\vec{i_t}$ is the unit vector along the x axis of the tibial co-ordinate system and $\delta_{ap}$ is the amount of anterior/posterior translation, the positive sign taken with posterior translation, as shown in Figure 4.8. Therefore, the attachment length $l$ increases as the fibre is recruited to bear load.

### 4.2.3 Computer Visualisation

To allow interactive visualisation and animation of the model, the modelling procedure was implemented using C language and incorporated into the interactive graphics-based window interface [153] under the X-window environment on SUN workstations. With the aid of colour display and the user friendly interface, users are able to use the model to visualise the shape changes of the ligaments during animation through the full range of passive motion. Users are also allowed to apply anterior/posterior translation of the tibia at any flexion angle to see the pattern of the fibre recruitment of the ligaments.

### 4.2.4 Results

Since the present model was developed and implemented using a graphics approach to allow interactive animation and visualisation, results reported here were produced basically by taking snapshots of the animated model. For simplicity of presentation and for the general interest of the clinical orthopaedics community, the ACL is used as an example to demonstrate ligament shape changes and fibre recruitment during passive motion and anterior/posterior tibial translation.

#### 4.2.4.1 Shape Changes During Passive Movement

Figure 4.9(a) shows the animated model ACL drawn in the first buckling mode as a series of snapshots at 0°, 45°, and 90° of passive knee flexion. The same motion with second buckling mode is given in Figure 4.9(b). The configuration of the four-bar linkage is also shown in dashed lines. It is noted that the anterior-most fibre, which serves as a link of the four-bar mechanism, remains isometric, while other fibres slacken as soon as the knee starts to flex and their attachment points approach each other. The appearance of the ligament is thus formed by the gradual shape changes of individual fibres. As shown in these figures, the model ACL is a sheet-like band with all the fibres just tight at full extension. With flexion, fibres slacken and change their orientations. At large flexion angles, the ACL fibres become crossed when the attachment areas rotate through more than 90° approximately relative to each other. Examination of the buckled fibres reveals that the first buckling mode predicts much bigger lateral displacement than the second mode. Since real ligaments are collagenous structures with connective cross-links between longitudinal elements [257], it is unlikely that fibres buckle

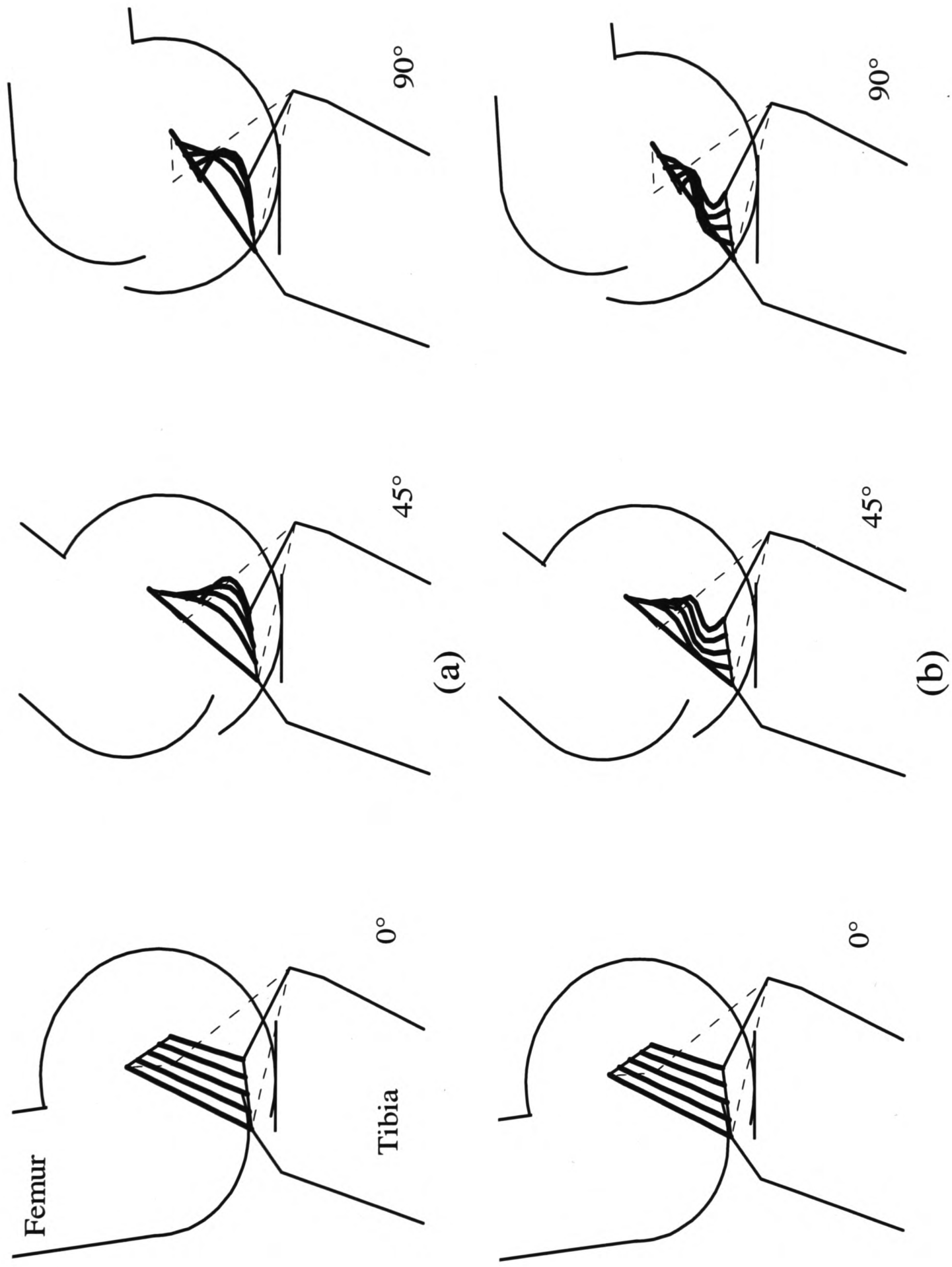



Figure 4.9: Passive motion of the model ACL at 0°, 45° and 90° flexion: (a) in the first buckling mode ($n = 1$) and (b) in the second buckling mode ($n = 2$)

with as large a lateral displacement as predicted by the first mode, which implies a significant separation between fibres. Thus, the second buckling mode is used throughout the rest of the presentations.

#### 4.2.4.2 Fibre Recruitment During Anterior/Posterior Tibial Translation

When the tibia is displaced from its neutral position, some ligament fibres must be stretched to resist the applied external force. The fibre recruitment process is illustrated for the knee at 25°, Figure 4.10(a), and at 90°, Figure 4.10(b). These are the angles at which the Lachman and drawer tests are performed, respectively. In both figures, the tibia is pulled anteriorly 4 mm and 8 mm. At 25°, all but the anterior-most fibre are slack, as a result of passive motion. With increasing anterior translation, the anterior fibre stretches as do an increasing number of its neighbours as more and more fibres are recruited. It takes 8 mm translation to recruit about 80% of fibres.

Most fibres are slacker at 90° of passive flexion than at 25°, except the anterior-most fibre which remains just tight, Figure 4.10(b). As anterior translation increases, fibres are successively recruited. In contrast to 25°, at 8 mm translation only 60% of the fibres are recruited. From both figures, it should be noted that strain distributions in the tight portion of the ligament are non-uniform.

#### 4.2.4.3 Animation of The Model

To give an impression of the shape changes of all the ligaments during passive motion, the full extent of the animation of the model, again at a series of flexion angles, is shown in Figure 4.11. The most anterior fibre of the model PCL lengthens with flexion, while the most posterior fibre slackens and then tightens again. During the motion, the central fibre is nearly isometric. All LCL fibres slacken with increasing flexion, while the anterior fibre of the model MCL stretches slightly and then slackens with flexion. Fibre recruitment patterns of the knee ligaments in response to anterior and posterior tibial translations are shown in Figure 4.12. It is noted that fibres of the ACL and MCL are recruited to resist anterior translation whereas fibres of the PCL and LCL act together to resist posterior translation.

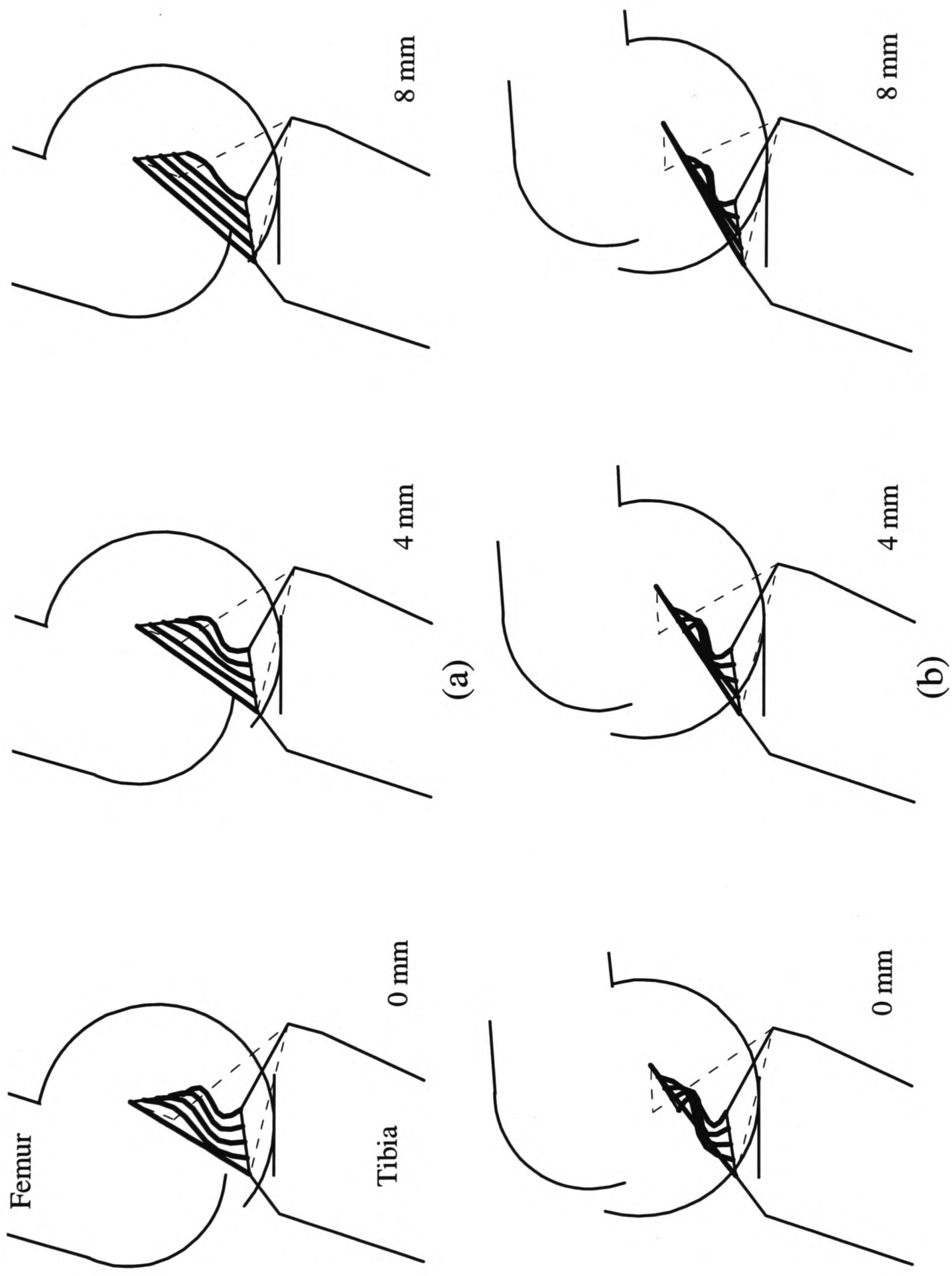



Figure 4.10: Fibre recruitment patterns of the model ACL in response to anterior tibial translations of 4 and 8 mm at (a) 25° and (b) 90° flexion.

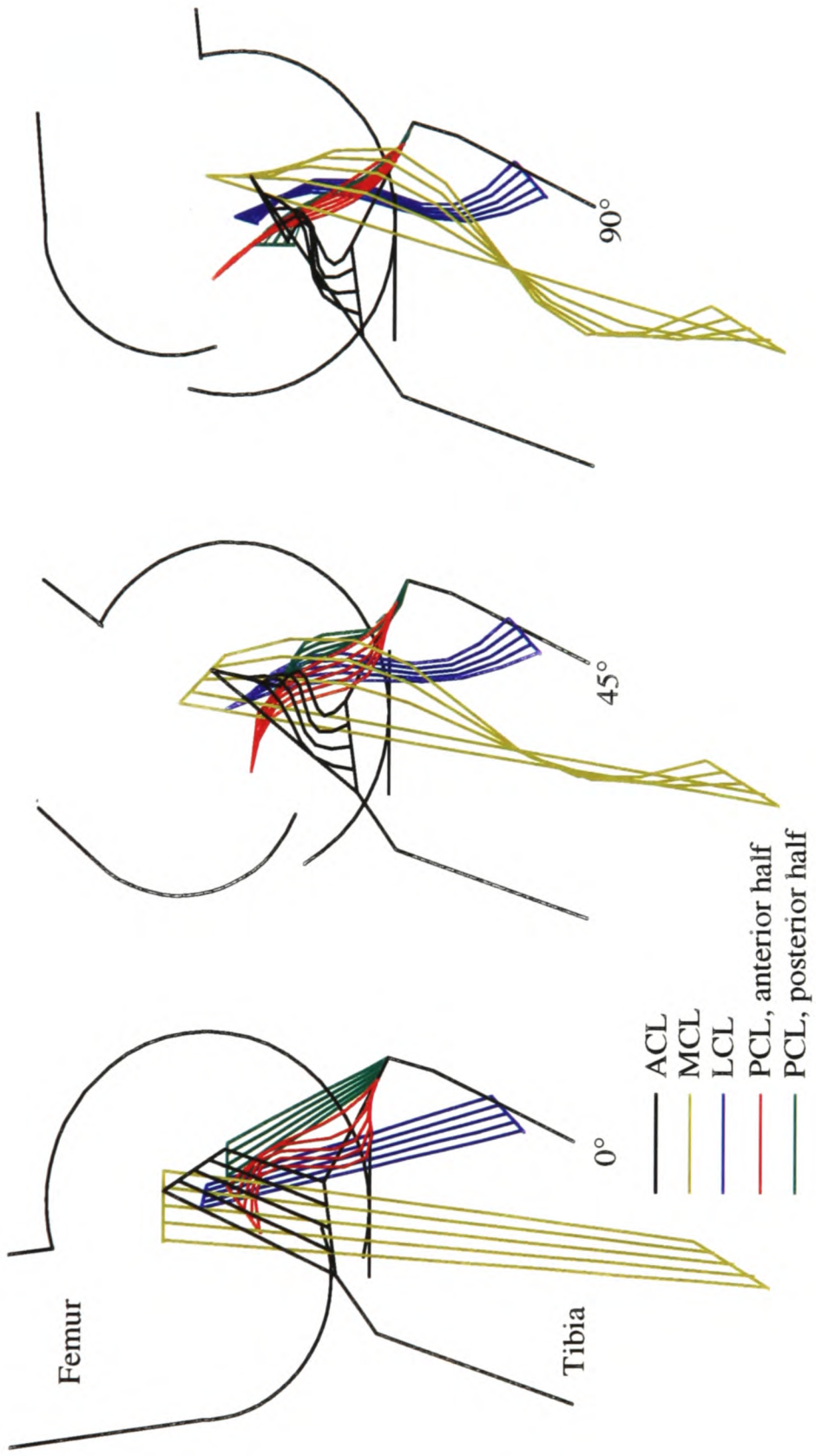



Figure 4.11: Model knee ligament at 0°, 45° and 90° of passive flexion.

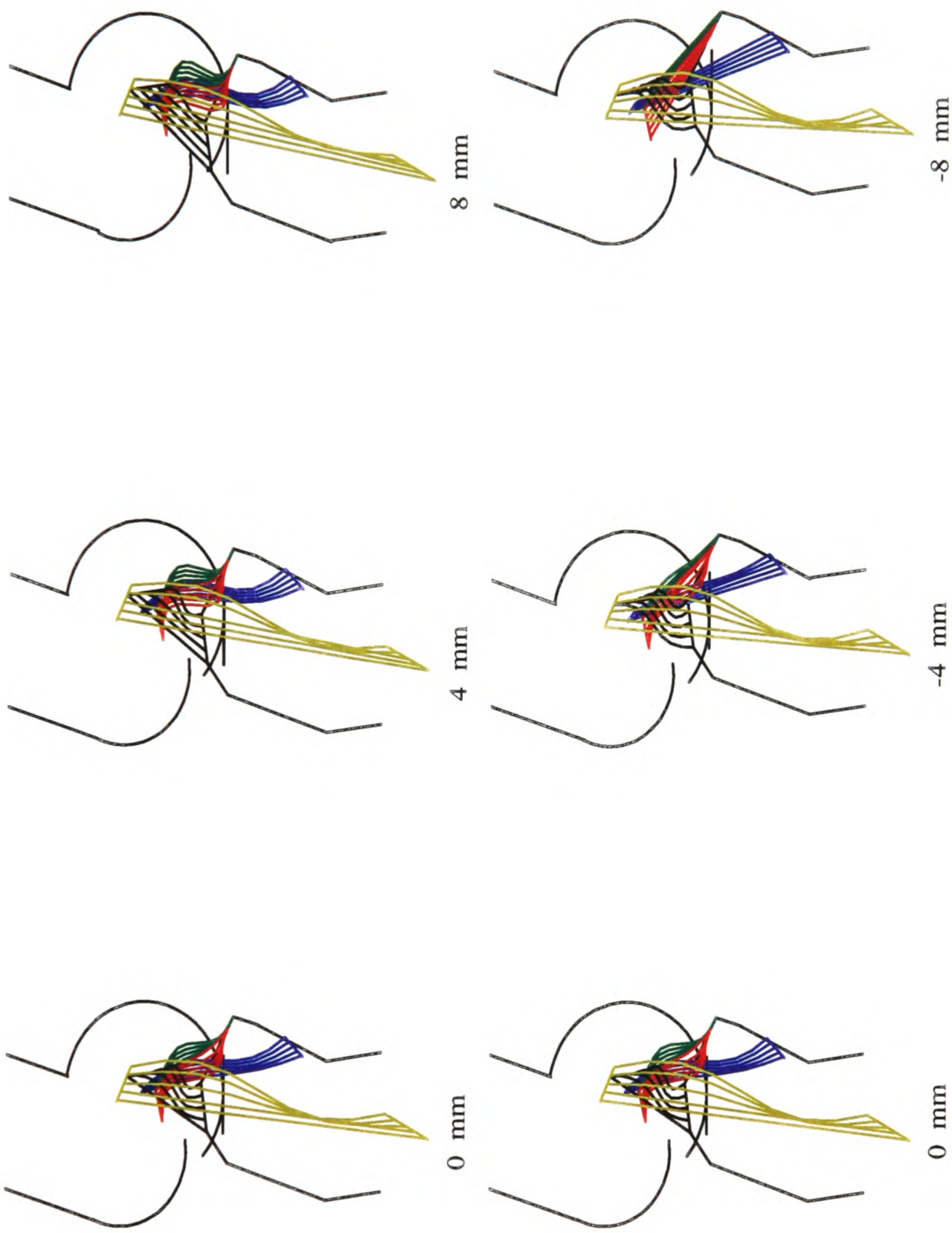



Figure 4.12: Fibre recruitment patterns of the knee ligaments in response to anterior and posterior tibial translations of 4 and 8 mm at 25° flexion.

## 4.2.5 Discussion

### 4.2.5.1 Comparison With Experimental Studies

The effects illustrated in this section have been deduced from purely geometric arguments, without appeal to the mechanical properties of the tissues or the laws of mechanics.

**Ligament Shape Changes** Ligaments change their shapes as a result of knee movement. By considering the relative position of the femur and tibia, and the geometrical relationship of the attachments of the ligaments, the graphics-based model was able to simulate the changes as a combination of stretched and buckled fibres. While representing tight fibres as straight lines is straight forward, one of the major features of the model is the simulation of the buckled fibres. As shown in Equation (4.4), different mode shapes can be obtained by assigning different values of $n$. However, the second mode shape is suggested because it is easy to implement, allows clear graphical animation, and most importantly produces results consistent with experimental observations. For instance, Friederich *et al.* [84] and Girgis *et al.* [95] drew comparable diagrams from their observations of the human ACL. Brantigan and Voshell [31] reported similar patterns for the PCL.

**Fibre Recruitment During Loaded Knee Movement** While passive movement of the knee joint is an ideal condition where no external force is allowed, in the real situation, deformation of structural members is needed to resist external loads which tend to deviate the joint from its ideal neutral configuration. This is mainly achieved by the sequential recruitment of the ligament fibres. Therefore, modelling of fibre recruitment is a prerequisite for an estimation of the strain/stress distribution and accordingly the force in the ligament. Since the loaded condition is easier to achieve than passive motion, there have been many experimental studies aimed at measuring the anterior/posterior force-displacement response of the knee at various flexion positions. Although it was not the intention of the current study, being two-dimensional, to estimate force levels in the ligaments, qualitative comparison with the experimental studies in the literature can be made by examining the fibre recruitment pattern of the ligament. As shown in Figures 4.10(a) and (b), the fibre recruitment pattern is different at different flexion angles, which implies that with the same external

force, the resulting displacements vary with flexion angle. This agrees qualitatively with the finding of Markolf *et al.* [162]. The results shown in Figures 4.10(a) and (b) also indicate that the anterior fibres of the ACL are always recruited while the knee is subjected to anterior forces. Blankevoort *et al.* [24] came to the same conclusion from their study of cadaveric knee specimens. This may explain the phenomenon of partial tears of the ACL. The model suggests that not all of the fibres of the ligaments experience the same history of stress/strain during motion. The model throws light on the concept of isometry which is possible for an individual fibre only during ideal unloaded passive movement. Any loads present will lead to some fibre stretching and it would then be most unlikely that any individual fibre could remain isometric over the entire flexion range.

**Limitations of The Model** As discussed in the above sections, the model predicts the ligament fibre recruitment pattern and shape changes which are in general consistent with experimental observations; however, as a two dimensional model, it suffers some obvious limitations. For example, the model cannot be used to show the shape changes in the coronal plane. The model also cannot demonstrate the twisting of fibres around each other, although it did suggest the phenomenon as the fibres cross in the sagittal plane. Deformation of the tibio-femoral cartilage layers, as moderated by the menisci, has not been taken into account. Blankevoort *et al.* [24] suggests that the effects of such deformation would be quite small at moderate loads. Another limitation is that cross- links between fibres were not explicitly incorporated in the model. This effect was significant as shown in Figure 4.9(a), where the first mode shape was used to model buckled fibres. Lateral displacements were reduced by considering the second buckling mode, Figure 4.9(b). Nonetheless, using a second mode representation of a buckled fibre is merely phenomenological. A more detailed study of cross-linking is required. Tightening of the anterior fibres of the model MCL during passive flexion indicates the need to take account of coupled axial rotations. It is hoped that the present calculations can be repeated with a three-dimensional model of the knee [259] and then to calculate ligament forces and joint laxity.

#### 4.2.5.2 Computer Aided Simulation And Visualisation

Although ligament shape changes and fibre recruitment have been shown in the literature by presenting the length changes of the fibres on a graph, as did Sapega *et al.* [215], Amis *et al.* [2], van Dijk *et al.* [242, 241], Hollis *et al.* [116]

etc., or by shading the tight part of the ligament as in Zavatsky and O'Connor [278], a graphical simulation considering realistic shapes of individual fibres seems to provide a more direct means of illustration and an easy way of acquiring insight into ligament behaviour at the architectural level. With the aid of an interactive, user friendly interface, the computer graphics-based model presented in this paper suggests a promising way of studying the ligament fibre recruitment process and the corresponding ligament shape changes during knee movement. The use of computer aided simulation and visualisation will be more important for three dimensional modelling, because the shape changes of the ligaments in space involve translation, rotation, and twisting of fibres with different orientations [280], which makes it difficult to describe them clearly using traditional methods.

#### 4.2.5.3 Clinical Relevance

The model, by demonstrating the inhomogeneous stress/strain distribution in the ligaments, provides a possible account for the mechanism of partial tear or full rupture of ligaments, and accordingly, suggests that the improvement or design of ligament replacements should be made by taking their architectural behaviour into account. The present study also suggests an interactive way for clinical users to visualise the fibre recruitment process, which may be helpful in the diagnosis of ligament injuries using laxity tests.

### 4.2.6 Summary

A computer graphics-based model of knee ligaments at the architectural level was developed to study the shape changes and fibre recruitment of the ligaments during knee movement, under unloaded and loaded conditions. The study began with the simulation of ligament shape changes during unloaded passive movement, and then demonstrated that deviation from the unloaded configuration of the knee joint, resulting in sequential fibre recruitment, is needed to resist the external forces and stabilise the joint. The simulated results agree well with experimental studies in the literature, apart from inherent limitations of a two-dimensional model. The study suggests that computer graphics-based models provide a more direct and efficient way to visualise the results of the simulation. This may help to get insight into the possible mechanism of ligament injuries, to improve replacement design and to assist clinical diagnosis.

## 4.3 Lines of Action and Moment Arms of The Major Tension-Bearing Structures [2]

Knowledge of the normal functions of the knee joint and its surrounding structures provides a necessary basis for the design and implantation of knee prostheses and ligament replacements in diseased or injured knees. During motion, the articular surfaces of the knee roll and slide upon each other while the ligaments and muscle tendons rotate about their origins and insertions on the bones. The positions and directions of the lines of action of the forces transmitted by these structures and their moment arm lengths relative to the axis of rotation of the joint therefore vary systematically over the range of motion. As a consequence, the relationships between muscle, ligament and contact forces also vary. For example, force in the patellar tendon pulls the tibia forward relative to the femur near extension and backwards in the highly flexed joint so that the anterior cruciate ligament (ACL) is loaded by an active quadriceps mechanism near extension and the posterior cruciate ligament (PCL) is loaded in flexion. Determination of the lines of action of the muscle, ligament and contact forces and their moment arms is therefore a necessary preliminary to mechanical analysis.

There have been many studies of the orientations of the structures of the knee. Both experimental and theoretical methods or a combination of both have been used. Morrison [172] determined the changing direction of the patellar tendon from lateral x-ray taken at different positions. He calculated the directions of the ligaments and of the hamstrings tendons by modelling the knee as a simple hinge and determining the relative motion of the origins and insertions of these structures. He estimated the moment arm lengths of the muscle tendons as their perpendicular distances from the contact point of the femur and the tibia, as seen in lateral x-ray. Van Dijk [242] inserted small tantalum balls around the origins and insertions of the cruciate ligaments and determined the orientations and changing shapes of the ligaments over the flexion range from successive x-rays. Maquet [160] and Bishop and Denham [22] used x-ray methods to study the lines of action of the patellar and quadriceps tendons, deducing the relationships between the patellofemoral contact force and the forces in the two tendons. Spoor and van Leeuwen [228] established moment arm lengths of all major muscles at the knee joint using MRI and tendon travel methods; however, corresponding

[2] Part of the work described in this section has been published in *J Anatomy*, 189: 575-585 [155]. Co-author: J.J. O'Connor.

information from ligaments or data on lines of action of the muscles were not determined. Recently, Herzog and Read [111] reported data on lines of action and moment arms of the major load-bearing structures measured from five cadavers using a mechanical digitiser. These data were represented as functions of knee joint angle and expressed as polynomial regression equations. Corresponding information for the gastrocnemius muscles was not given. In order to establish a complete relationship between the measured data and knee flexion angle, the experimental measurement approach requires intensive measurements through the whole range of knee flexion and hence relies heavily on a high standard of measurement skills. It is also difficult for this method to examine possible changes to the mobility and stability of the joint due to any alteration of the geometric configuration of the load-bearing structures introduced by injury or surgery.

Another approach is to develop an anatomy-based mathematical model, which requires minimum measurements from cadavers or living subjects to establish model parameters. Lines of action and moment arm lengths over the range of flexion can then be deduced from the model. The four-bar linkage model, being confined to the sagittal plane, has obvious limitations but the data of Herzog and Read [111] provide the opportunity to compare an extensive body of experimental results with the predictions of the model. This section presents the comparison and discusses methods of defining moment arms.

## 4.3.1 Methods

The anatomy-based geometric model of the knee joint described in the previous sections was further developed to include the surrounding muscles and their tendons. It was then used to calculate lines of action and moment arms of the major tension-bearing structures, namely the quadriceps, hamstrings, the two cruciate ligaments, lateral collateral ligament (LCL) and medial collateral ligament (MCL). A brief description of the model is given below.

### 4.3.1.1 Geometry of muscle tendons and ligaments

The knee ligaments were modelled as bands of fibres. Their attachment areas on the bones were represented in the sagittal plane as straight lines, as shown in Figure 4.5, Section 4.2. The ligament attachment areas rotate relative to each other during flexion and extension so that all but the isometric fibres of the cruciate ligaments slacken and elongate during passive movement. The insertions of the

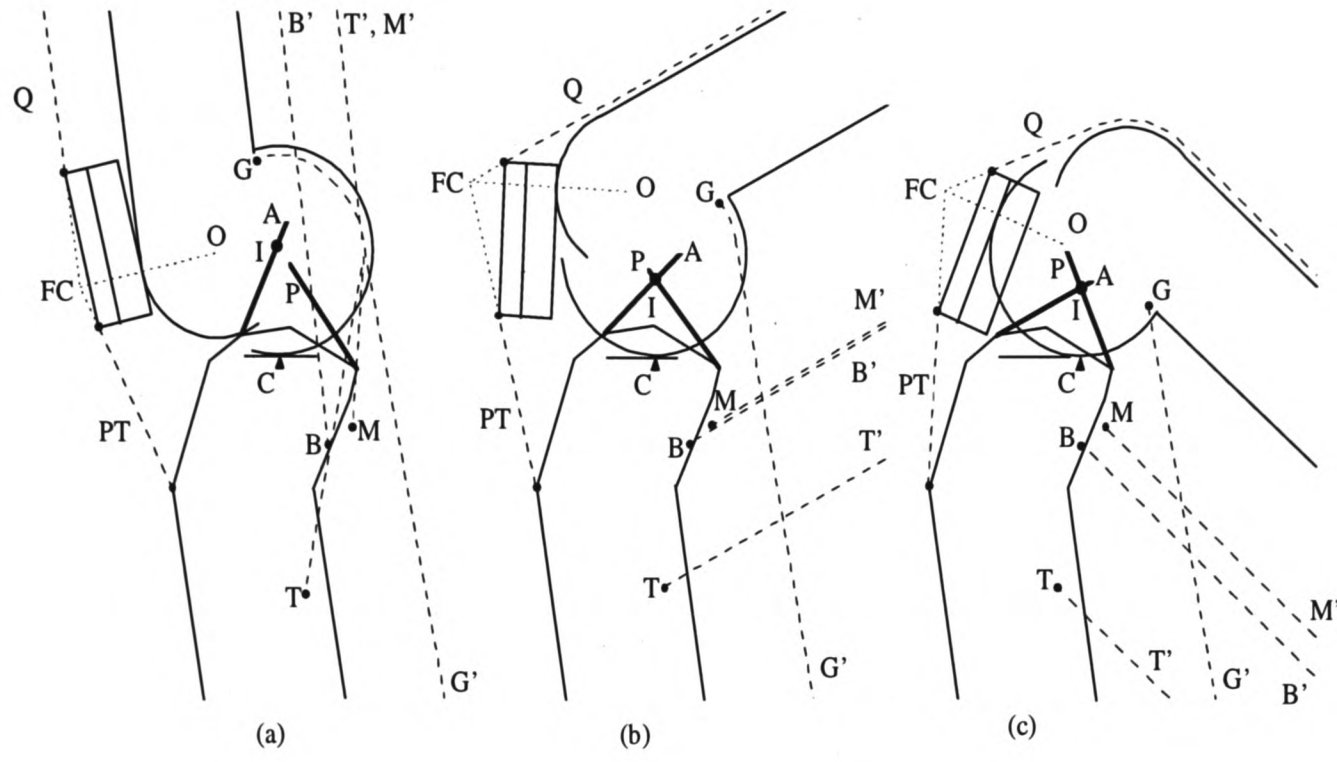



Figure 4.13: The geometric model of the knee joint at (a) 0°, (b) 70° and (c) 140° flexion. Single thick lines are used to represent the two isometric fibres of the cruciate ligaments. Straight dashed lines are also used to represent the quadriceps, hamstrings and gastrocnemius muscles except where they wrap around the bones. It is noted that the instant centre moves relative to each bones and, with the tibiofemoral contact point, moves posteriorly during flexion. The tibia is shown using line segments joining some particular bony landmarks. No attempt was made to reproduce the precise shapes of the bone but the shape of the femoral condyle was calculated from the model. (I = instant centre, A = ACL, P = PCL, C = tibiofemoral contact point, PT = patellar tendon, Q = quadriceps tendon, BB' = biceps, MM' = semimembranosus, TT' = semitendinosus and GG' = gastrocnemius).

muscles were approximated by single points, Figure 4.13. The gastrocnemius tendon was modelled as a single line connecting its origin at the back of the femoral condyle to the insertion of the Achilles tendon into the heel. The tendons of the hamstrings, semimembranosus, semitendinosus and biceps femoris, were represented as single lines inserting into the model tibia and taken to lie parallel to the long axis of the femur over the range of flexion. However, near extension, the gastrocnemius, semitendinosus and semimembranosus tendons wrap around the distal end of the femur so combinations of line segments and circular arcs were used, Figure 4.13. The wrapped tendons are shown as circular arcs in Figure 4.13 and lie within the outline of the model femoral condyle to take account of their positions between the condyles of the natural knee.

#### 4.3.1.2 Knee extensor mechanism

Unlike other structures whose lines of action are simply defined by their origins and insertions, the quadriceps tendon transmits forces to the tibia through the patellar tendon so it is necessary to model the geometric relationship of the quadriceps tendon and the patellar tendon. In the present study, a bi-articulating patellofemoral joint model developed recently by Gill and O'Connor [93] was used to characterise the knee extensor mechanism. It was built on the four-bar linkage model described above. As shown in Figure 4.13, the patella was modelled as a rectangle with two articulating surfaces. The more posterior articulating surface, making contact with the trochlear groove, represents the median ridge of the patella while the more anterior articulating surface is an idealised representation of the medial and lateral edges of the patella, contacting the femoral condyles at large flexion angles. The model assumes an inextensible patellar tendon and a single contact point between the patellofemoral articulating surfaces. The quadriceps tendon was assumed to be parallel to the long axis of the femur and taken as a single line, wrapping around the femoral trochlear groove at high flexion angles. To satisfy mechanical equilibrium, the three forces acting on the patella, namely the quadriceps tendon force, the patella tendon force and the patellofemoral contact force, should be co-planar and concurrent. As a consequence, the patella rolls proximally on the femur during flexion, as described by Goodfellow *et al.* [96]. The model determines the lines of action and force ratios of the tendon and contact forces over the range of knee flexion.

#### 4.3.1.3 Calculation of lines of action and moment arms

In order to make comparisons with the published experimental results, the conventions used in describing the orientation of the lines of action of the ligaments and muscles were made consistent with those used by Herzog and Read [111], Figure 4.14. Since ligaments were modelled as bands of fibres, lines of action of each fibre can be calculated. This allows one to estimate total ligament forces under external loads, taking account of contributions from individual tight fibres [278]. However, as the measurements were performed under unloaded condition, isometric fibres in the ACL and PCL were used to determine their lines of actions while the fibres joining the midpoints of the attachment areas on the femur and tibia were used for the MCL and LCL (Herzog and Read used the most anterior fibre for the ACL and the fibre joining the midpoints of the insertion area on the

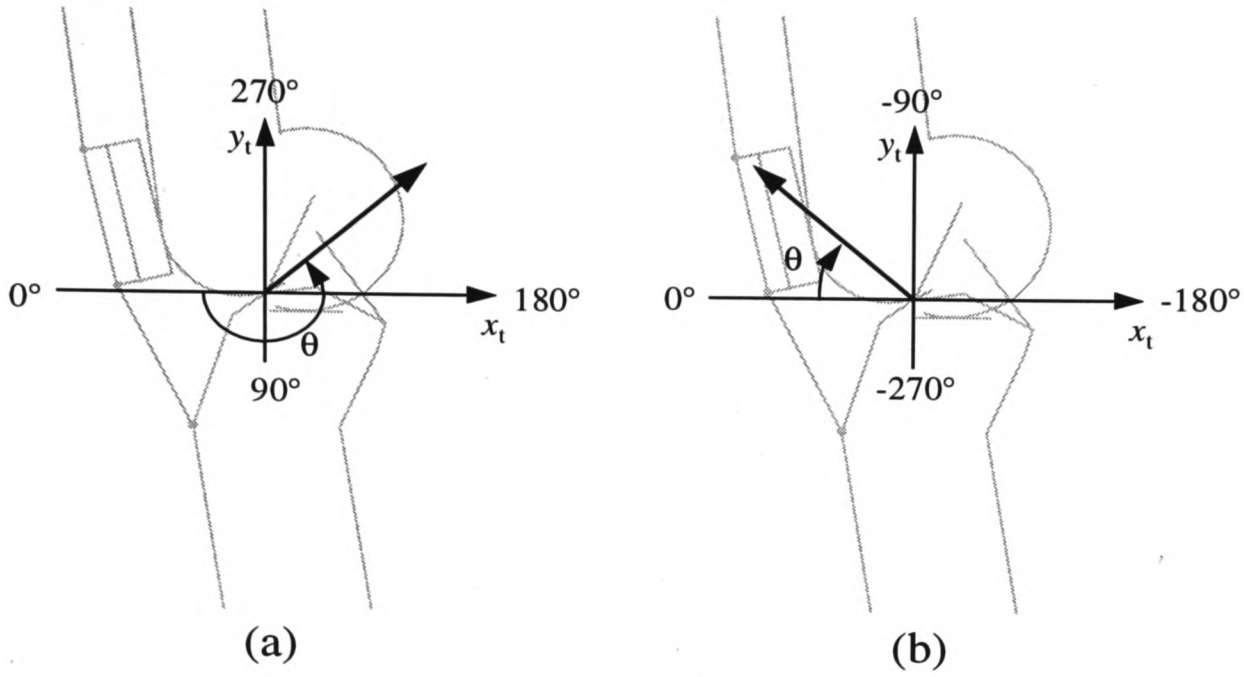



Figure 4.14: The orientation of the line of action of a structure is defined by the angle $\theta$ between $-x$ and the vector directed from the insertion to the origin of the structure. Vectors oriented posteriorly for the extended position were given clockwise positive values (a); vectors oriented anteriorly for the extended position were given counter-clockwise negative values (b).

tibia and femur for the PCL. These definitions were approximately the same as the isometric fibres used in the current model). To evaluate possible discrepancies due to various definitions of lines of action of ligaments and to demonstrate the differences of the orientations between fibres during motion, the most posterior fibre of the ACL was chosen as an alternative definition for its line of action, Figure 4.15.

Moment arms of each structure were initially obtained by calculating the perpendicular distance from the line of action of the structure to the contact point of tibia and femur as did Herzog and Read [111]. As discussed above, the flexion axis of the model knee joint is the point where the two isometric fibres of the cruciate ligaments cross. Cruciate ligament forces cannot contribute directly to resisting flexion or extension of the joint. Moment arms of the patellar tendon and the hamstring muscles were further calculated about the flexion axis for comparison.

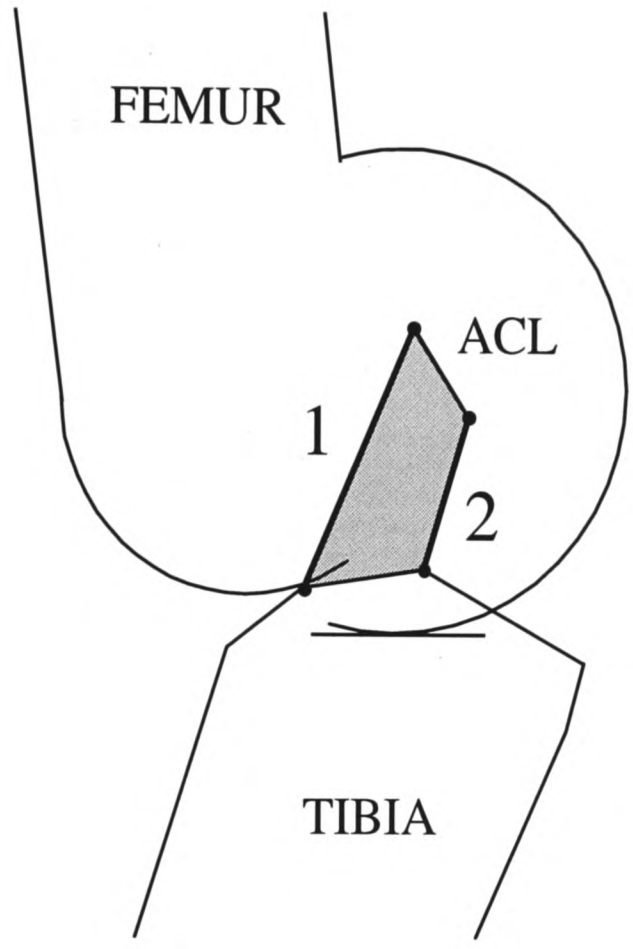



Figure 4.15: Two possible representations of the line of action of the ACL: the isometric fibre (1) and the most posterior fibre (2).

## 4.3.2 Results

### 4.3.2.1 Lines of action

The calculated lines of action of the four ligaments over the range of knee flexion are shown in Figure 4.16 with experimental results from Herzog and Read [111] imposed. Calculated and experimental results for the patellar tendon and the hamstring muscles are presented in Figure 4.17.

### 4.3.2.2 Moment arms

Figure 4.18 shows simultaneously the calculated and experimental results for the moment arms of the ligaments over the range of knee flexion. Results for the patellar tendon and the hamstring muscles are shown in Figure 4.19. Comparisons of the moment arms for the patellar tendon and the hamstrings about the tibiofemoral contact point and the flexion axis are shown in Figure 4.20.

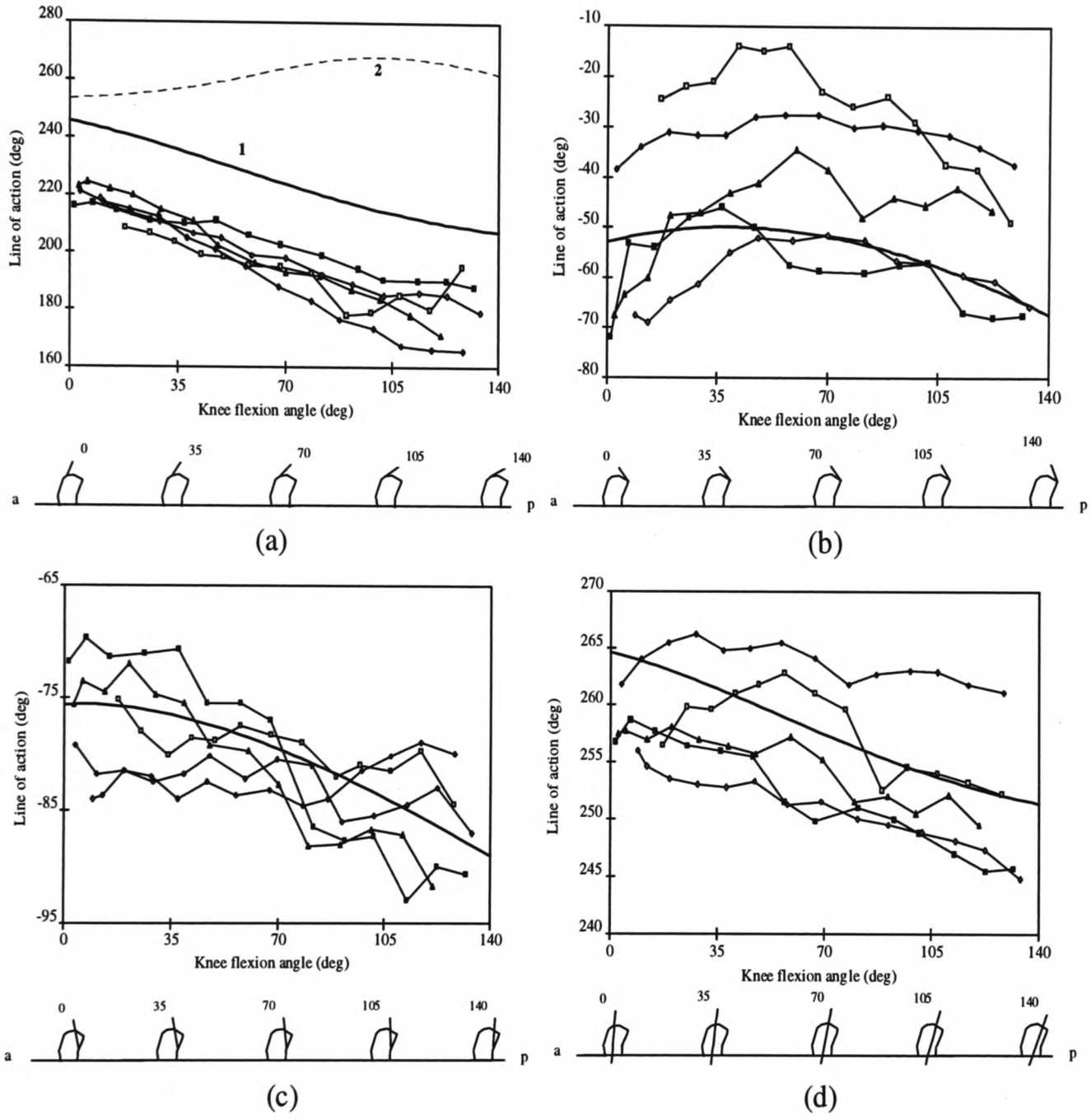



Figure 4.16: Lines of action of the (a) two representations of the ACL: the isometric fibre (thick line) and the most posterior fibre (dashed line), (b) PCL, (c) LCL and (d) MCL as functions of knee joint angle. Lines with markers are experimental data from Herzog and Read [111].

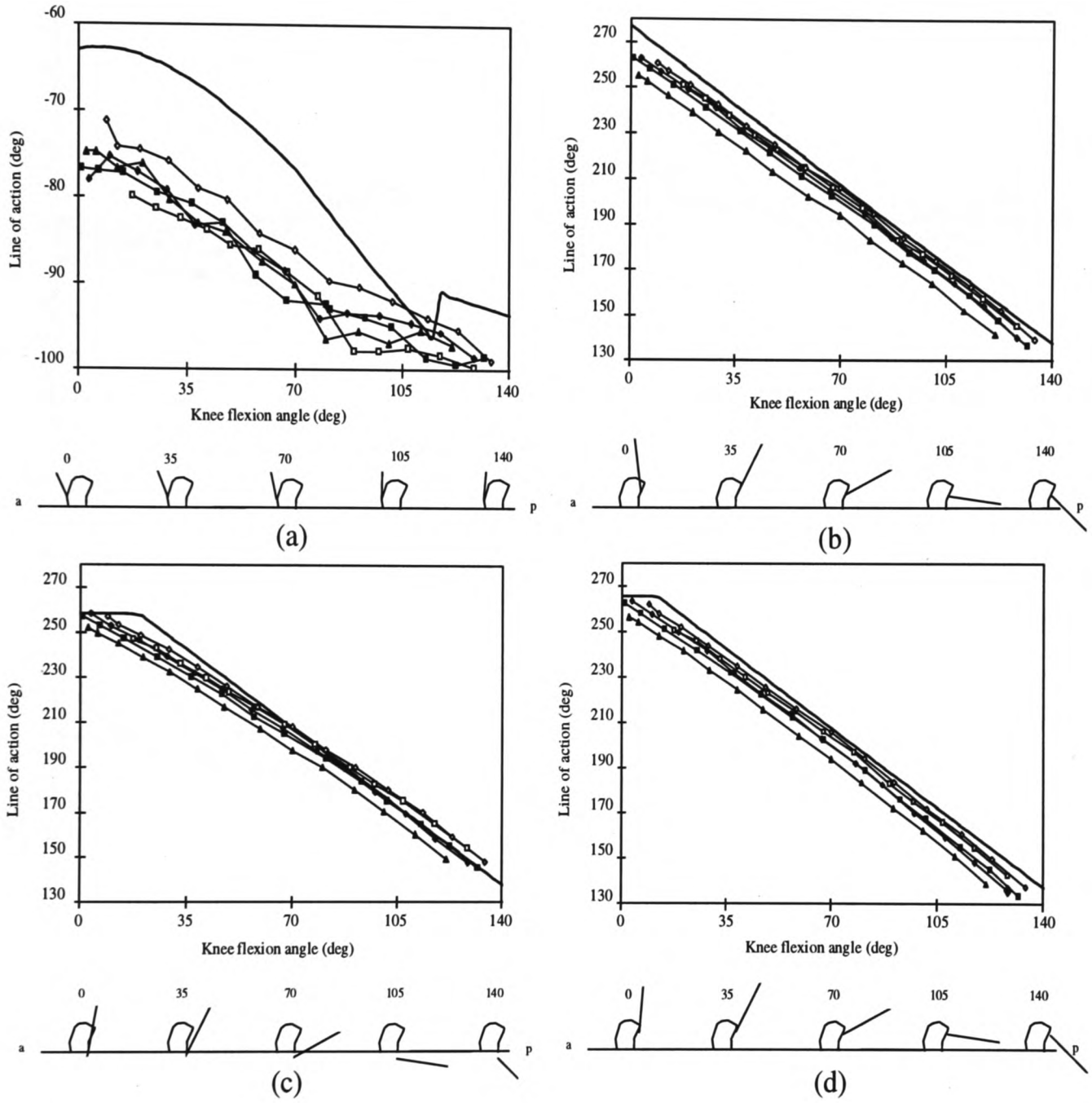
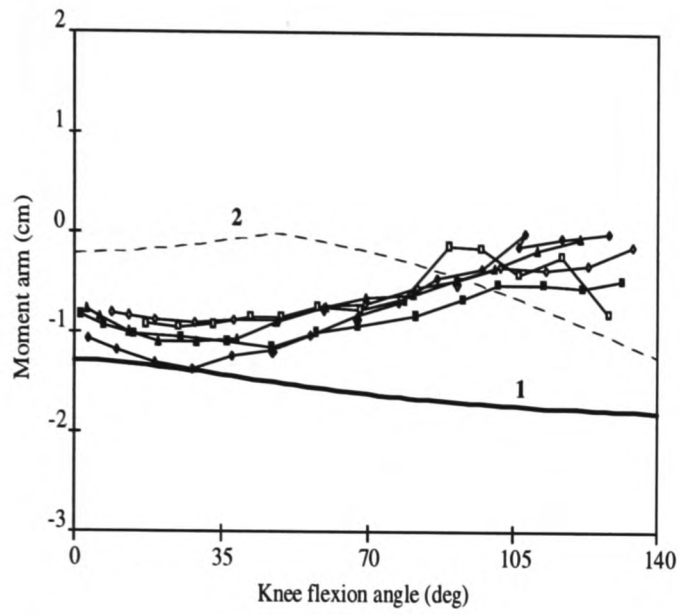
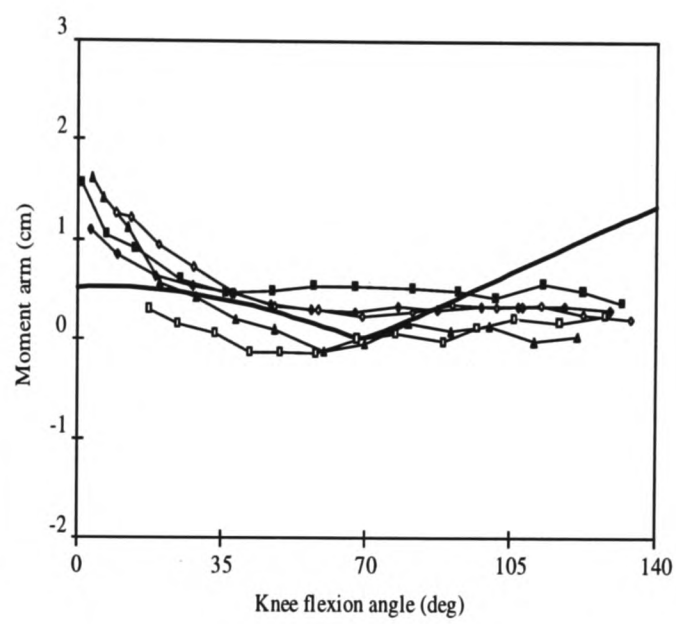


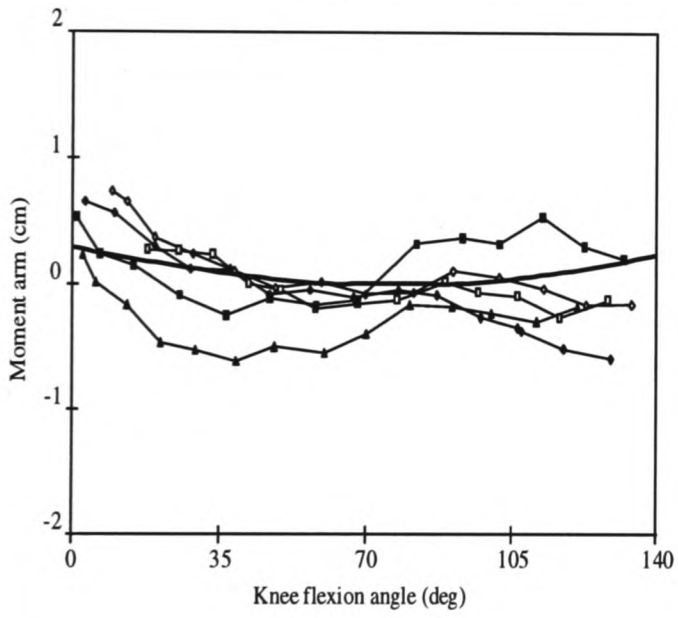

Figure 4.17: Lines of action of the (a) patellar tendon, (b) biceps, (c) semitendinosus and (d) semimembranosus as functions of knee joint angle. Lines with markers are experimental data from Herzog and Read [111].



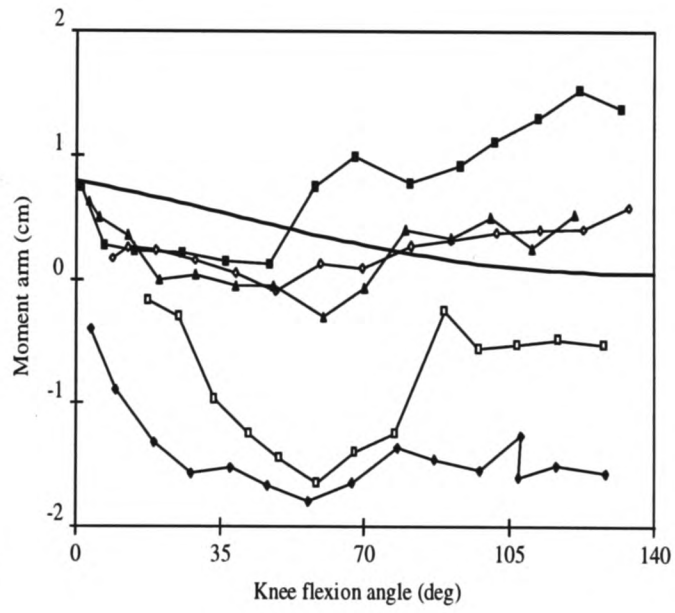

(a)




(b)




(c)

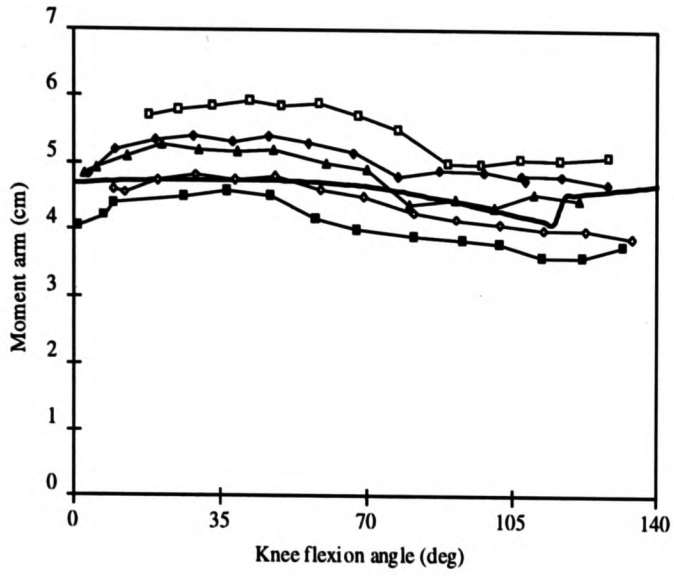



(d)

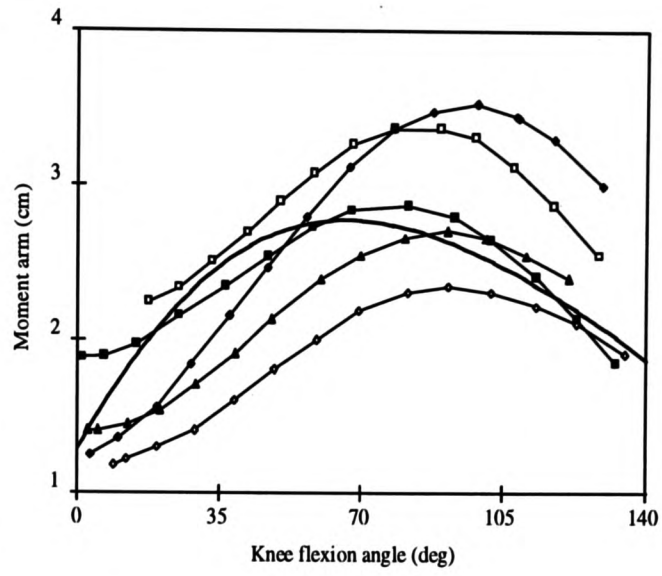
Figure 4.18: Moment arms of the (a) two representations of the ACL: the isometric fibre (thick line) and the most posterior fibre (dashed line) (b) PCL, (c) LCL and (d) MCL about the tibiofemoral contact point as functions of knee joint angle. Lines with markers are experimental data from Herzog and Read [111].

Knee flexion angle (deg)

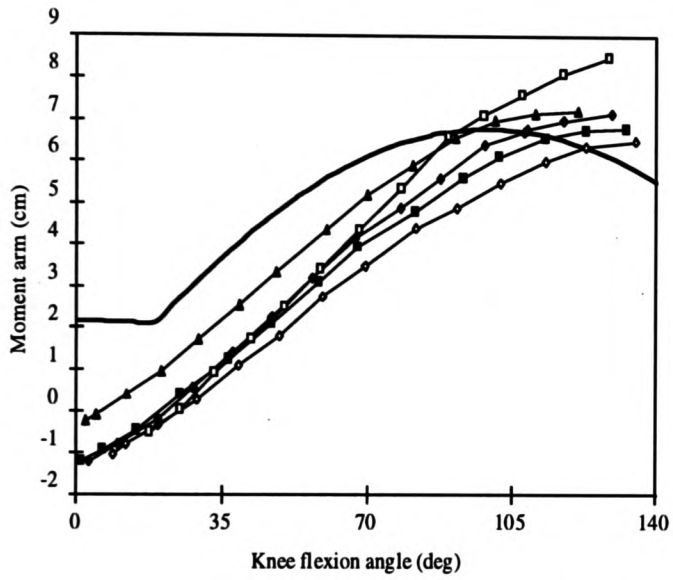
(e)



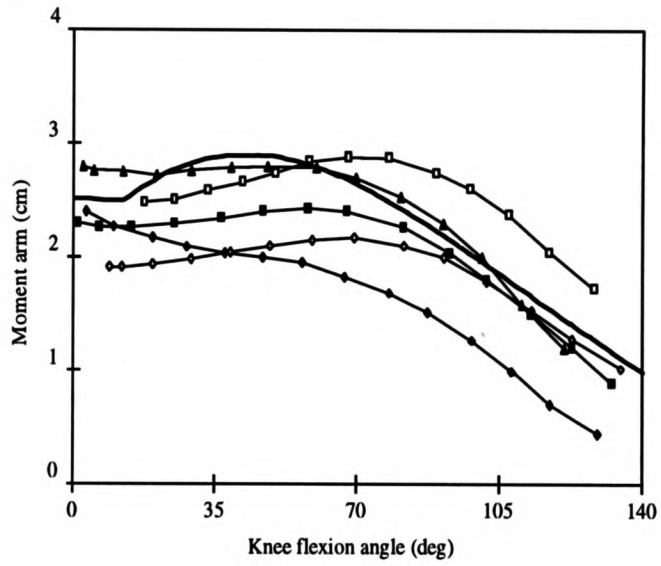

(a)



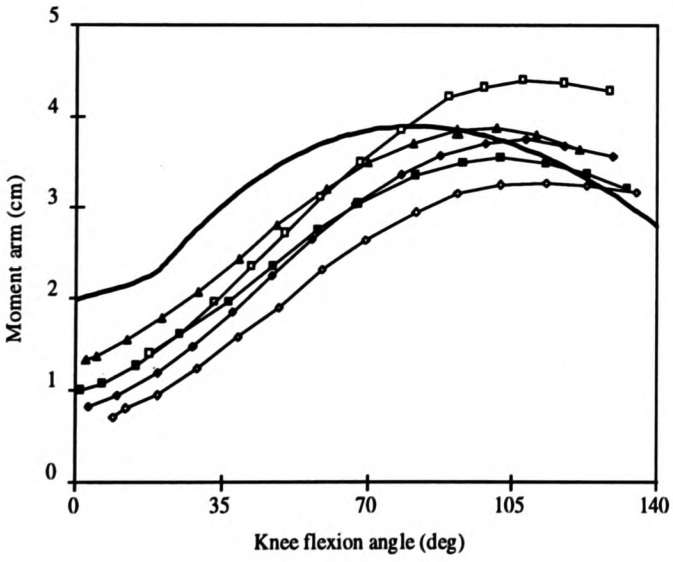

(b)




(c)




(d)




(e)

Figure 4.19: Moment arms of the (a) patellar tendon, (b) biceps, (c) semitendinosus, (d) semimembranosus and (e) average of all hamstring muscles about the tibiofemoral contact point as functions of knee joint angle. Lines with markers are experimental data from Herzog and Read [111].

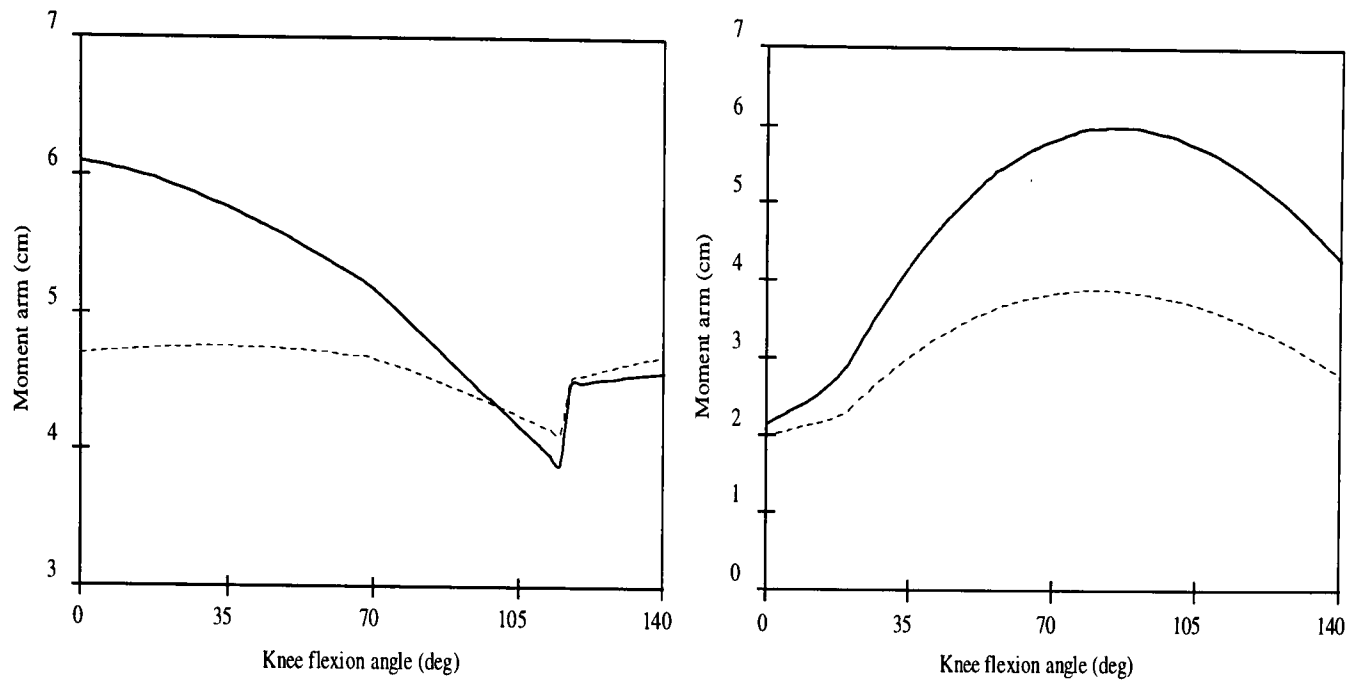



Figure 4.20: Moment arms of the (a) patellar tendon and (b) average of all hamstring muscles about the centre of joint rotation (solid lines) and the tibiofemoral contact point (dashed lines) as functions of knee joint angle.

## 4.3.3 Discussion

### 4.3.3.1 Lines of action

Good agreement between the calculated and experimental results for the lines of action of the major tension-bearing structures are seen in Figures 4.16 and 4.17. All the calculated curves lie within the range of measurement envelopes, except that of the ACL and the patellar tendon. As shown in Figure 4.16(a), the isometric fibre of the model ACL experienced about the same amount of rotation about its tibial insertion as experimental specimens when the knee flexion angle increased. The constant difference between the lines of action of the specimens may be due to anatomical variances of specimens used to determine model parameters. The model ACL has a more vertical orientation than any of the Herzog and Read specimens. Both the experimental data and the model calculations show that the ACL rotates about its tibial attachment point through approximately 30° while the femur flexes relative to the tibia from full extension to 140°. This suggests that there is 110° of relative rotation between the ACL and the femur rather than 140° as assumed by Amis and Zavras [3]. Appropriate rotation of a prototype ligament prosthesis about each of its attachment areas

should be reproduced accurately in laboratory tests if its fatigue life is to be assessed reliably.

Figure 4.5 demonstrates that rotation of the attachment areas of a ligament during flexion and extension determines the patterns of fibre shortening and tightening within the ligament. In effect, the attachment areas pivot relative to each other about the points of attachment of the isometric fibres so that the lengths of those fibres remain constant during flexion and extension while all other fibres must either slacken or tighten. Correct placement of a ligament graft or prosthesis on its attachment areas is necessary if natural patterns of slackening and tightening are to be reproduced and excessive tightening avoided.

Also shown in Fig. 4.16(a) is the curve derived from the second definition of the line of action of the ACL. The wide separation of the two curves suggests that any fibre posterior to the isometric fibre can have quite different orientations during flexion and that measurements should be carefully performed to secure the same definition throughout the whole range of movement. During knee flexion, the model patellar tendon rotated about the tibial tuberosity from 26°( anterior to the tibial longitudinal axis to 6°( posterior, passing through the vertical at 100° of knee flexion, Figure 4.17(a), slightly different from the experimental data (19° anterior, 10° posterior and 60° – 90° knee flexion) but similar to the results reported by Nisell *et al.* [177] (30° anterior, 10° posterior and 100° knee flexion). As indicated in Figures 4.17(c) and (d), the lines of action of the model semitendinosus and semimembranosus tendons remain constant during the initial 20° and 10° knee flexion respectively because of the wrapping around the posterior aspect of the medial femoral condyle. The wrapping effect was not considered by Herzog and Read [111].

#### 4.3.3.2 Moment arms

Moment arms of the ligaments calculated by the model agree well with experimental measurements except that the model ACL showed a 1 cm difference beyond 60° of knee flexion, Figure 4.18(a). The experimental data exhibited almost zero moment arms at high flexion angles, which indicated that the line of action of the ACL passes through the tibiofemoral contact point, inconsistent with observations by others [95]. Different definitions of the lines of action of the ACL again demonstrated significant differences in the calculations of the moment arms, Figure 4.18(a). Calculated moment arms for the patellar tendon and the hamstring

muscles also agree with the experimental data, Figure 4.19. It is worth mentioning that the model semitendinosus has a constant flexor moment arm for the first 20° of flexion due to its wrapping around the femoral condyle while the experimental data showed extensor moment arms instead (negative values in Figure 4.19(c). Herzog and Read [111] suggested that the experimental results might be associated with their assumption of representing the muscle as a single line. The model calculations support these arguments. Because of the wrapping effect of the semitendinosus, the average moment arms of the hamstring muscles ranged from 2 cm near extension to a maximum of 4 cm, with a 1 cm difference from the experimental data near extension but similar to the results reported by Spoor and van Leeuwen [228] who calculated moment arms about the flexion axis, Figure 4.20.

#### 4.3.3.3 Effects of the definition of joint centre

In theory, for the purpose of mechanical analysis, one can calculate moment arms of the structures with respect to any point in space as long as one always uses the same point for the calculation of moments exerted by external loads. However, arbitrary selections of the reference point may produce very different values of the moment arms, as shown in Figure 4.20 and in Herzog and Read [111]. Although the choice of reference point makes no difference to the estimation of forces transmitted by the structures if one always refers the calculations to the same reference point, an inappropriate choice might give a false impression of the ability of the muscles to generate moment or to induce joint motion. Since the model cruciate ligament forces and the joint contact force all intersect at the flexion axis and have zero moment about that axis, the distance of a muscle tendon from the flexion axis gives the most direct measure of the capacity of the muscle to balance external moment and to induce motion. This definition is also of particular importance in the estimation of muscle power (moment times angular velocity about the flexion axis), which has been suggested for the evaluation of muscle function [263].

#### 4.3.3.4 Power and limitations of the model

The general purpose of a mathematical model is to allow calculation of the values of quantities which are difficult or impossible to measure from the values of quantities which can be measured. The current model, being limited to the sagittal

plane and to the use of a specific set of model parameters, has demonstrated its ability in achieving this purpose, as shown by the comparison of calculated results with the published experimental data. However, it is important to note that there is significant anatomical variation between different subjects, as indicated by the wide distribution of the experimental data (ligaments in particular). Changing the geometry of the structures can alter the force distributions among them [258] so account should be taken of anatomical variation in order to obtain accurate results of mechanical analysis. Since measurements required to establish the model parameters are no more difficult but much less extensive than the measurements performed by Herzog and Read [111], it seems reasonable to concentrate effort on the measurement of subject-specific model parameters which then allows the calculation of a wide range of variables, such as ligament directions and tendon moment arms.

The model described in this section was developed from purely geometric arguments, without appeal to the mechanical properties of the tissues or the laws of mechanics. The results were deduced assuming passive movement throughout the range of flexion, a condition where no external force is present. The data of Herzog and Read [111], acquired in the same condition, thus provides a consistent basis for the comparison of theory and experiment. External loads tend to deviate the joint from its neutral (unloaded) configuration because of the consequent deformation of the structures of the joint. Development of the model to consider deformation and recruitment of the fibres of the cruciate ligaments in resisting anterior/posterior forces during drawer tests has been described by Zavatsky and O'Connor [278, 279], showing good agreement with experiments performed in similar loading conditions.

### 4.3.4 Conclusion

With relatively simple and less extensive measurements, the anatomy-based mathematical model predicted results that are comparable to those experimentally measured. It is suggested that, in order to take account of anatomical variations, efforts should be concentrated on the measurement of subject-specific model parameters. Since moment arms represent the ability of a load-bearing structure in generating or resisting angulation of the joint about its flexion axis, it seems more appropriate to express the moment arms about the moving flexion axis.

# Chapter 5

# Two-Dimensional Modelling of The Lower Limb[1]

In this chapter the geometric and mechanical modelling of the human locomotor system in the sagittal plane is presented. A geometric model of the human lower extremity, similar to the model described in Collins [56], was developed and used as the basis for a comparative study of the Dynamically Determinate One-Sided Constrained (DDOSC) method [56, 58] and various optimisation methods [51, 63, 60, 61, 221, 222] which have been proposed in the literature for the prediction of muscle forces during normal level walking. The lower limb model was used to provide comparison with and further interpretation of some of the tests of the two instrumented patients described in Chapter 3, namely isometric tests of the hip flexors and extensors and level walking. Muscle-bone interaction during activity is discussed based on the validated model calculations. An interactive graphics-based window interface was developed to provide a unified user-friendly environment for the modelling and graphical animation of the models of the locomotor system.

## 5.1 Geometric Modelling

Basically, the human pelvis-leg apparatus was modelled in the sagittal plane as four rigid body segments, namely the pelvis, thigh, shank and foot (Figure 5.1).

[1]Part of the material in this chapter was presented by the author at the 2nd International Symposium on Computer Methods in Biomechanics and Biomedical Engineering, Swansea, 1994 [153]. Co-authors: H.S. Gill and J.J. O'Connor.

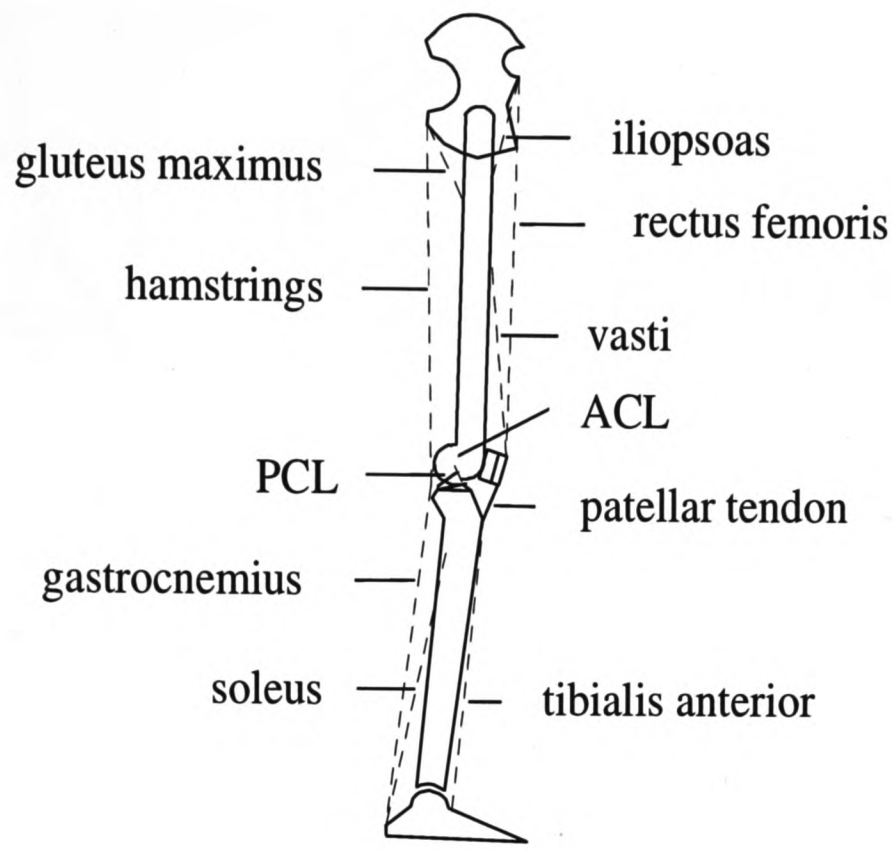



Figure 5.1: Two dimensional geometric model of the lower limb

The hip and ankle were modelled as simple hinge joints. The knee was modelled as an incongruent joint, allowing rolling and sliding movements of the femur on the tibia, controlled by the ligaments. The principal muscles of the lower limb and the cruciate ligaments of the knee were represented by straight lines, wrapping around the bones when necessary. A total of eight muscles or muscle groups, iliopsoas, rectus femoris, vasti, hamstrings, gluteus maximus, gastrocnemius, soleus and tibialis anterior, were included. Muscles with small physiological cross sectional areas (PCSA) and/or short intrinsic muscle tendon lever-arms were neglected [173]. A further description of the models of the joints and muscles is given below.

### 5.1.1 Knee Joint Models

The knee model described in Chapter 4 was incorporated into the lower limb model. However, as a starting point for subsequent force analysis, a simplification was made. The two cruciate ligaments were first considered as inextensible links, represented by their isometric fibres. The MCL and LCL were neglected. The contribution of the MCL in resisting anterior tibial translation was taken by the ACL and the contribution of the LCL in resisting posterior tibial translation

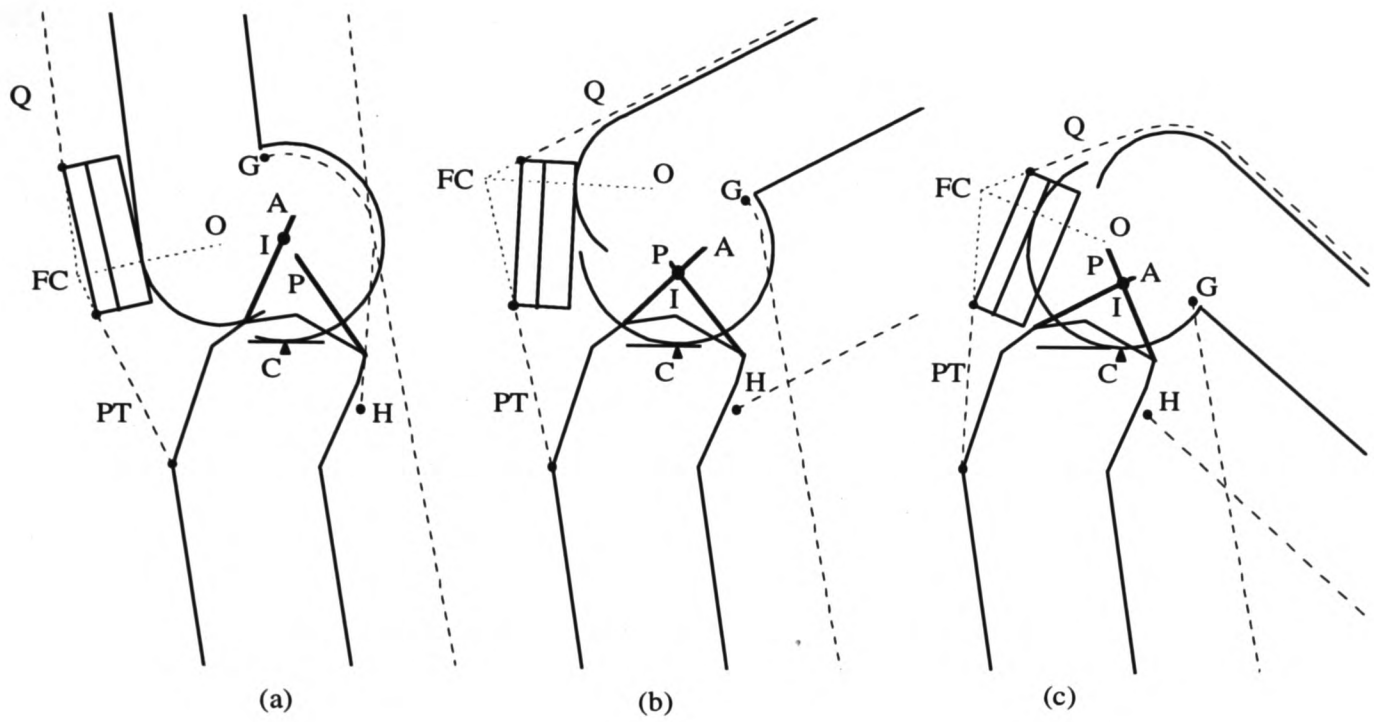



Figure 5.2: Computer model of the tibiofemoral and patellofemoral joints.

was taken by the PCL. Extending the inelastic assumption to consider fibre recruitment will be discussed later in this chapter. The simplified configuration of the knee joint model is shown in Figure 5.2.

In the lower limb model of Collins [56], the knee extensor mechanism was described by the patellofemoral joint model proposed by O'Connor *et al.* [183, 180], in which the patella was approximated as a single point, called *patellar force centre*. At this point, the lines representing the quadriceps and patellar tendon and the line of action of the patellofemoral contact force intersect, due to the requirement of force equilibrium of the patella. This was an important feature of the model because the articulation was not represented as a simple, frictionless pulley which would lead to the same force in the quadriceps and patellar tendon. In order to provide a more anatomical representation of the patellofemoral joint while keeping the above feature, the model developed by Gill and O'Connor [92] was used in the present study. The patella was represented as a rectangle with two articulating surfaces, Figure 5.2. A more detailed description of the model in characterising the knee extensor mechanism has been given in Section 4.3.1.2.

### 5.1.2 Hip and Ankle Models

The ankle and hip were modelled as simple hinge joints with congruent surfaces, allowing rotation only in the sagittal plane. For the present study, the superior

surface of the talus and the femoral head were modelled as circular arcs, and the distal end of the tibia and the acetabulum were represented as reciprocally shaped circular cavities, respectively. Thus, the geometry and mechanics of the model hip and ankle were defined by the geometry of the articulating bones. The positions of the model ankle and hip centres of rotation were the geometric centres of the trochlea and femoral head, respectively. As with the knee joint, the articular surfaces were assumed to be frictionless and therefore the contact forces were pure compressive and passed through the respective centres of joint rotation. The talo-tibial contact force and the femoro-pelvic contact force should remain within the embraces of the distal end of the tibia and the acetabulum, respectively. The ligamentous contributions of the ankle and the hip were not included in the model at this stage.

### 5.1.3 Musculotendon Geometry

In addition to the joint models, it is necessary to develop a representation of musculotendon geometry. Eight muscles or muscle groups, namely iliopsoas, rectus femoris, vasti, hamstrings, gluteus maximus, gastrocnemius, soleus and tibialis anterior, were incorporated into the lower limb model, Figure 5.1. The biceps, semitendinosus and semimembranosus were grouped and the average geometry was used to represent the hamstrings muscle group.

The origins and insertions of the muscles were approximated by single points. For muscles with broad attachments, these points were chosen at the centroids of the attachment areas. Each of these eight muscles were then represented by a single line. However, the geometric models of bi-articular muscles, namely gastrocnemius, hamstrings and quadriceps, would wrap around the distal end of the femur at certain positions so combinations of line segments and circular arcs would be used, Figure 5.2. A set of musculotendon sites of attachment obtained from measurements using MRI [56] was used as reference parameters of the lower limb model. These were then customised to individual subjects using homogeneous scaling techniques suggested by Brand *et al.* [28] and White *et al.* [255] based on the distances between the greater trochanter and lateral epicondyle, between the ASIS and PSIS and between the tibial tuberosity and lateral malleolus. This procedure can reduce significantly the inter-specimen variability [28, 255].

## 5.2 Mechanical Analysis of Normal Level Walking

Walking is the most basic form of locomotion in daily living and has been the subject of extensive study. Gait analysis has become an important tool for the routine examination of patients, contributing to the detailed diagnosis of pathology and to the planning and assessment of treatment. However, due to the difficulty of the estimation of internal forces, data derived from gait analysis are still limited to intersegmental kinematics and kinetics information. As reviewed in Chapter 1, several optimisation criteria have been proposed for the selection of a unique solution from the indeterminate problem arising from the locomotor system during walking [63, 61, 198, 209, 222]. Usually, optimisation can be regarded as a decision-making process. Each criterion reflects the preference of the decision maker. Since the preference of the locomotor system is not known, the proposed criteria only represent some of the possibilities. Other possibilities are still unavailable. To avoid any subjective or artificial criterion, the DDOSC method [58, 57] produces all the possible dynamically determinate solutions, each representing an extreme of the solution domain and thus an optimum of a certain criterion. Therefore, more potential criteria can be systematically examined. It is not the purpose of the present study to find the unique preference of the locomotor system, if there is any, but to find a better approach which can be used to perform more accurate force analysis. Therefore, a comparative study is needed.

An evaluation of some of the most widely used criteria proposed in the literature based on DDOSC solutions has been reported in Collins[57]. He first calculated a set of DDOSC solutions among which a unique solution was selected using different criteria. He showed that none of the tested criteria predicted satisfactory results in terms of EMG consistency. Since optimisation methods were not used directly to solve his problem, it seems necessary for a direct comparison to confirm his conclusions. It is also noted that the criteria tested were either linear or quadratic. The performance of a nonlinear (higher than quadratic) criterion was not evaluated.

In this section, a comparative study between the DDOSC method and various optimisation methods is presented. A widely used nonlinear criterion proposed by Crowninshield and Brand [61] was included in addition to the criteria tested in Collins[57]. Non-linear programming was used to solve optimisation problems. The geometric model was used as a basis for these methods so the comparison

between predicted muscle recruitment patterns with reference to EMG evidence was sufficient for qualitative evaluation. Quantitative validation of the model as well as the selected solution method using data from the two instrumented patients will be presented in Section 5.3.

### 5.2.1 Data Collection and Pre-analysis

Five adult male subjects (body mass: 62.5-86.7 kg, mean 68.8 kg; height: 168-184 cm, mean 174 cm) participated in the present study. Following the experimental protocol described in Chapter 3, four trials of each subject walking with their natural pace were collected. The intersegmental resultant forces and moments at each joint were calculated, using inverse dynamics as described in Chapter 2. The associated indeterminate problems were then formulated to distribute these forces and moments to individual structural members.

The average angular motion of a walking cycle with an envelope of one standard deviation from the subjects is shown in Figure 5.3. However, for a direct comparison of the various methods for muscle force prediction, a set of gait data from a male subject with a body mass of 68kg and a height of 175 cm was used as a representative. It was chosen because the subject was anthropometrically similar to the subject from whom the reference musculotendon data was obtained [56]. Figure 5.4 shows the two-dimensional model during walking based on data from the representative subject.

### 5.2.2 Problem Formulations

#### 5.2.2.1 Number of Model Unknowns and Equations for Structural Analysis

Since lines of action of muscles, ligaments and the tibiofemoral contact force were determined from the geometric model, only force magnitudes were considered as system unknowns except for the hip and ankle where the joint contact forces were each defined by two parameters: force magnitude and direction. Therefore, there were fifteen unknowns to be determined for the thirteen structural members. At the ankle, five unknowns for four structural members were considered: G = gastrocnemius, S = soleus, T = tibialis anterior, C = magnitude of the talo-tibial contact force, and D = direction of C. Seven unknowns for seven structural members were considered at the knee: R = rectus femoris, V = vasti, H =

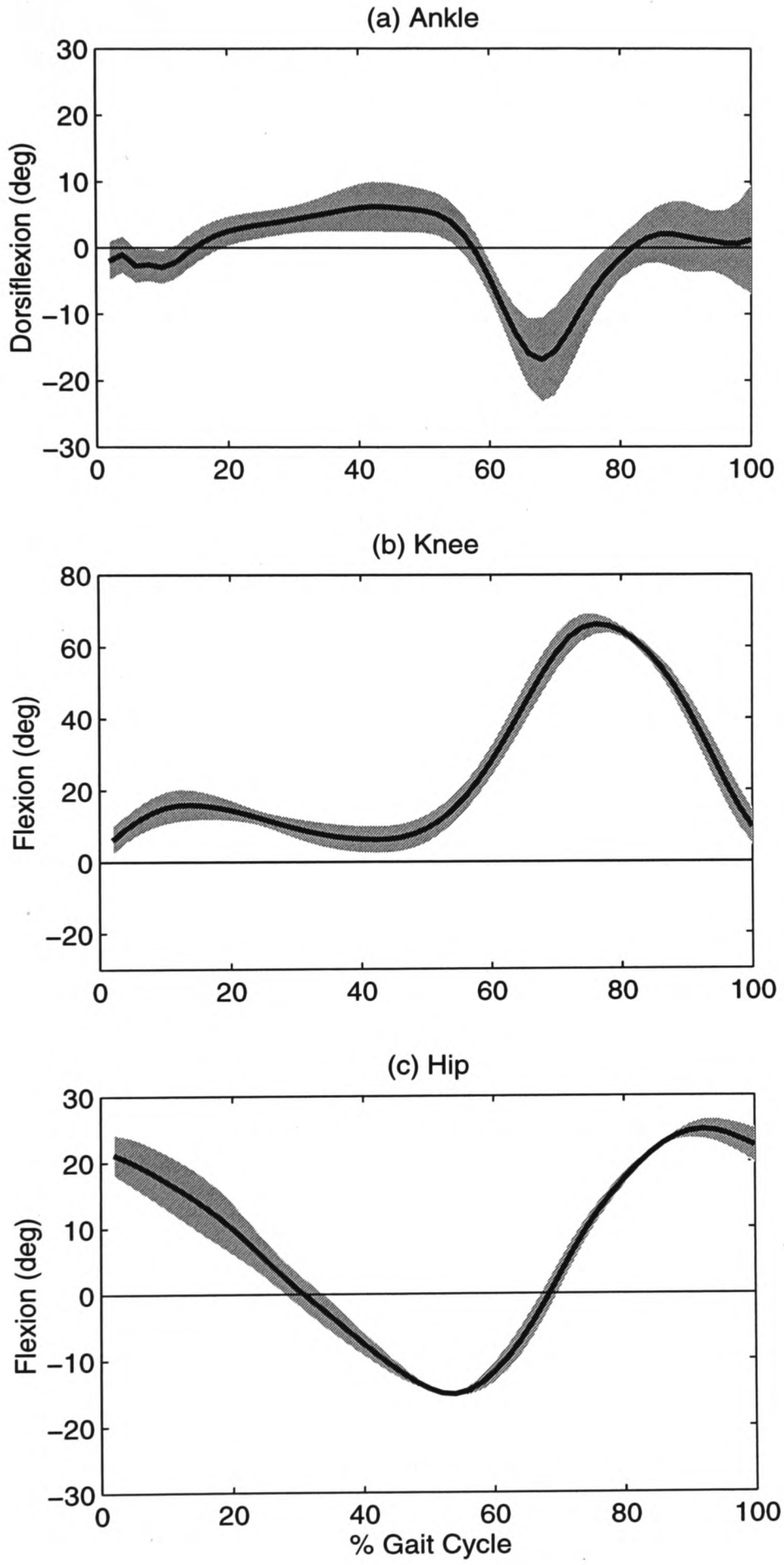



Figure 5.3: Joint angles (a-c) of the ankle, knee and hip during the walking cycle, obtained from an ensemble average from five subjects

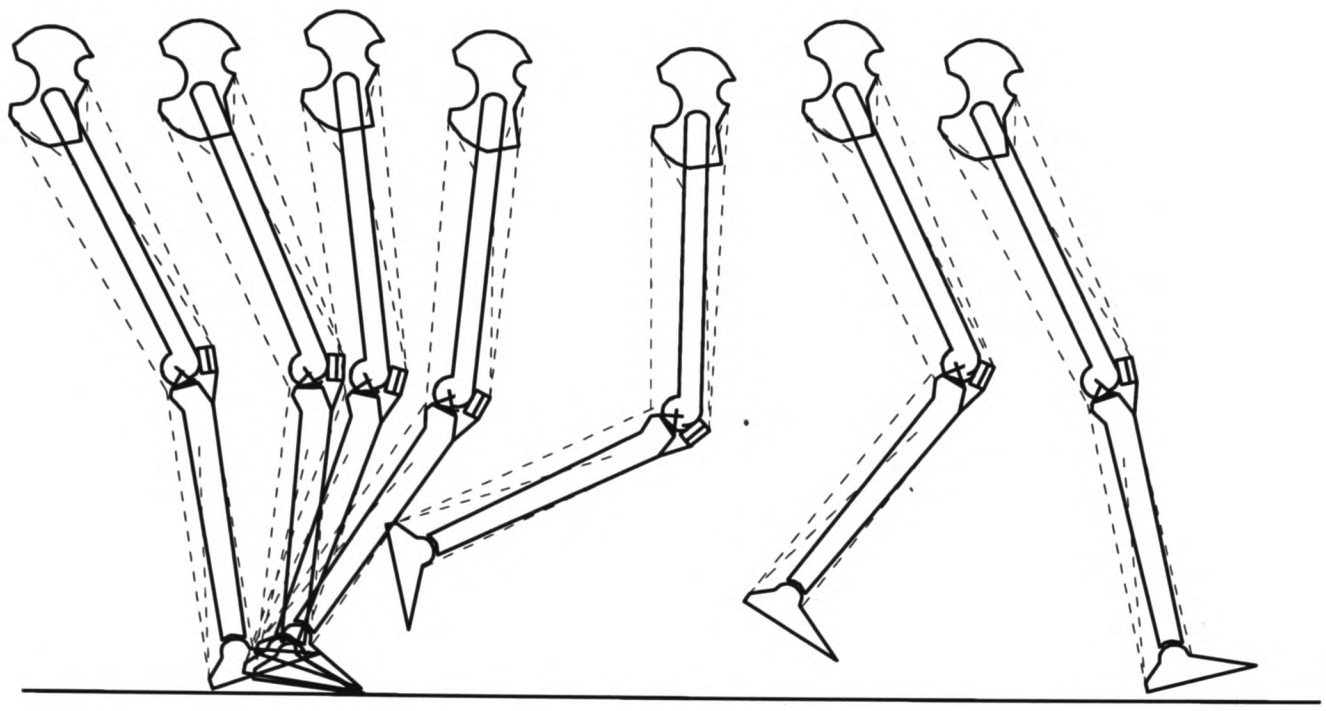


Figure 5.4: The two-dimensional model during walking based on data from the representative subject.

hamstrings, G = gastrocnemius, A = ACL, P = PCL, and C = magnitude of the tibio-femoral contact force. Finally, six unknowns for five structural members were considered at the hip: I = iliopsoas, R = rectus femoris, H = hamstrings, L = gluteus maximus, C = magnitude of the femoro-pelvic contact force, and, as with the ankle model, D = direction of C.

Since the intersegmental forces and moments calculated must be provided by the corresponding force-bearing structures, they represent a force/moment system that is statically equivalent to (or equipollent with) the system formed by the actual force-bearing structures, such as muscles, ligaments and bones. Therefore, considering force and moment equipollence at each joint, a total of nine equations were formulated in terms of the fifteen model unknowns. Therefore, the description of the mechanics of the lower limb involved an indeterminate set of equations which had an infinite number of solutions. The DDOSC method and the optimisation method were used to resolve the indeterminate problem. Solution procedures and results obtained are described in the following sections. To simplify the calculations, it was assumed that the tension was the same throughout the length of a muscle. To facilitate a comparison with the study of Collins [57], the rectus femoris and vasti forces were grouped and represented by the quadriceps force (Q). Further separation of the two muscles was considered later for quantitative validation, to be described in Section 5.3.

#### 5.2.2.2 Dynamically Determinate One-Sided Constrained (DDOSC) Method

The Dynamically Determinate One-Sided Constrained (DDOSC) method decomposes the original indeterminate problem into a series of dynamically determinate (DD) sub-problems established by considering at any one time only the number of unknowns (9) that makes the original problem determinate, setting the values of other forces to zero or choosing specified directions for hip and/or ankle forces. The specified direction at the ankle was along the long axis of the tibia and at the hip was along the long axis of the femur, based on experimental observations and theoretical calculations reported in the literature [56]. Solutions corresponding to the DD sub-problems are referred to as DD solutions (limiting solutions in Collins and O'Connor [58] and Collins [57]). Since muscles and ligaments transmit only tensile forces and joint articular surfaces resist only compression, DD solutions that violate these one-sided constraints are rejected. The remaining DD solutions are referred to as DDOSC solutions. Of these DDOSC solutions, an EMG consistent solution is then selected.

A total of 498 DD sub-problems were considered in the present study. Each DDOSC solution was expressed as a set of three ordered triads representing unknowns at the ankle, knee and hip, respectively. For example, a DDOSC solution with, at the ankle, tibialis anterior (T) and the magnitude (C) and direction (D) of the contact force, at the knee, quadriceps (Q), PCL (P) and the magnitude (C) of the contact force and, at the hip, iliopsoas (I) and the magnitude (C) and direction (D) of the contact force, is denoted by TCD-QPC-ICD. Since bi-articular muscles spanned two joints, a DDOSC solution such as GCD-QPC-HCD would actually mean GCD-GQHPC-QHCD, with antagonistic muscle action at both knee and hip.

Generally, a DD problem can be expressed as the following linear system:

$$F_1 \cos\phi_{1_j} + F_2 \cos\phi_{2_j} + \cdots + F_9 \cos\phi_{9_j} = F_{jx} \tag{5.1}$$

$$F_1 \sin\phi_{1_j} + F_2 \sin\phi_{2_j} + \cdots + F_9 \sin\phi_{9_j} = F_{jz} \tag{5.2}$$

$$d_{1_j} F_1 + d_{2_j} F_2 + \cdots + d_{9_j} F_9 = M_j \tag{5.3}$$

where $d_{i_j}$ is the lever-arm magnitude and $\phi_{i_j}$ is the direction of the $i^{th}$ structural member at the $j^{th}$ joint, and $F_{jx}$, $F_{jz}$ and $M_j$ are resultant forces and moment at $j^{th}$ joint. A LU decomposition combined forward and backward substitution to the coefficient matrix can then be used to solve this system.

#### 5.2.2.3 Optimisation Method

The most essential consideration in the application of optimisation techniques is the problem formulation, including the definition of the feasible region and the selection of a proper objective function. Trying to resolve the indeterminacy problem encountered in the prediction of muscle force sharing, optimisation techniques have received extensive research effort [5, 63, 60, 198, 221, 222]. Usually, forces of structural members to be predicted, including muscle forces, ligament forces and articular forces, are chosen as design variables. Equations of force and moment equipollence are the main equality constraints. Design bounds include the requirements that muscle and ligament forces should be tensile and contact forces compressive. Sometimes, physiological limits on muscle forces are also imposed as upper bounds. One example of an inequality constraint is the restriction on individual muscle stress. As discussed earlier in Chapter 1, there are not only various definitions of the design feasible region but also different proposals of objective functions reported in the literature. Therefore, a comparative study of optimisation methods with various objective functions and the DDOSC method should be based on the same musculoskeletal model and the same problem formulation.

In the present studies, six objective functions commonly used in the literature were studied based on the lower limb model described above. These objective functions were

- sum of muscle forces ($J_1$),
- sum of quadratic muscle forces ($J_2$),
- sum of muscle stresses ($J_3$),
- sum of knee ligament forces ($J_4$),
- sum of joint contact forces ($J_5$),
- sum of cubic muscle stresses ($J_6$).

$J_6$ is related to maximum muscle endurance [61]. They were minimised over an identical feasible region, defined by equations of force and moment equipollence and by requirements that muscle and ligament forces should be tensile and joint contact forces compressive. A Quasi-Newton optimisation method, Sequential Quadratic Programming (SQP) method [10], was used to solve the formulated optimisation problems.

### 5.2.3 Results

Figure 5.5(a-c) shows the patterns of the ankle, knee and hip joint flexion/extension angles of the representative subject during a gait cycle. Corresponding resultant joint moments, which were needed to balance the moments of external loads about the centre of joint rotation, are presented in Figure 5.5(d-f).

#### 5.2.3.1 DDOSC Method

There were 498 DD subproblems at each sampling point. However, the number of DDOSC solutions, which were sufficient to satisfy the equations of equipollence and the inequality constraints was reduced to a minimum of 3, a maximum of 23 and a mean of 9.16, Figure 5.6. Temporal patterns of the admissible DDOSC solutions are presented in Figure 5.7. They represent possibilities which the human body can adopt to achieve the movement pattern. To demonstrate the capability of the model to predict physiologically feasible solutions, these DDOSC solutions are examined by comparing with EMG evidence. Temporal EMG patterns [56] are shown in Figure 5.8.

*Early Stance (0-20%):* During the period of 0-5% of the walking cycle, a dorsiflexing moment was needed at the ankle, a flexing moment at the knee and an extending moment at the hip (Figure 5.5(d-f)). After that, the external loads tended to flex the knee and extend the hip. From 0 to 10 percent of the walking cycle, EMG indicated four active muscles (Figure 5.8): tibialis anterior, hamstrings, gluteus maximus and quadriceps. During this interval, the model found the DDOSC solution TCD-QAC-HLC (tibialis anterior, the direction and magnitude of the contact force at the ankle, quadriceps, anterior cruciate ligament, contact force at the knee, hamstrings, gluteus maximus and contact force at the hip), which was wholly consistent with EMG (Figure 5.7). For a brief period after 10% of the walking cycle, three lower limb muscles were active (as indicated by EMG, Figure 5.8): tibialis anterior, gluteus maximus and quadriceps. The model found TCD-QAC-LCD to be consistent with EMG. At the end of the early stance phase, the DDOSC solution TSC-QAC-LCD, which was also consistent with EMG was obtained for two data frames. In summary, solutions consistent with EMG were found over 90-95% of the early stance phase.

*Mid-Stance (20-50%):* During the first one third of the mid-stance phase, the external loads were tending to dorsiflex the ankle, flex the knee and extend the hip. For the rest of the phase, a flexing moment at the knee was needed

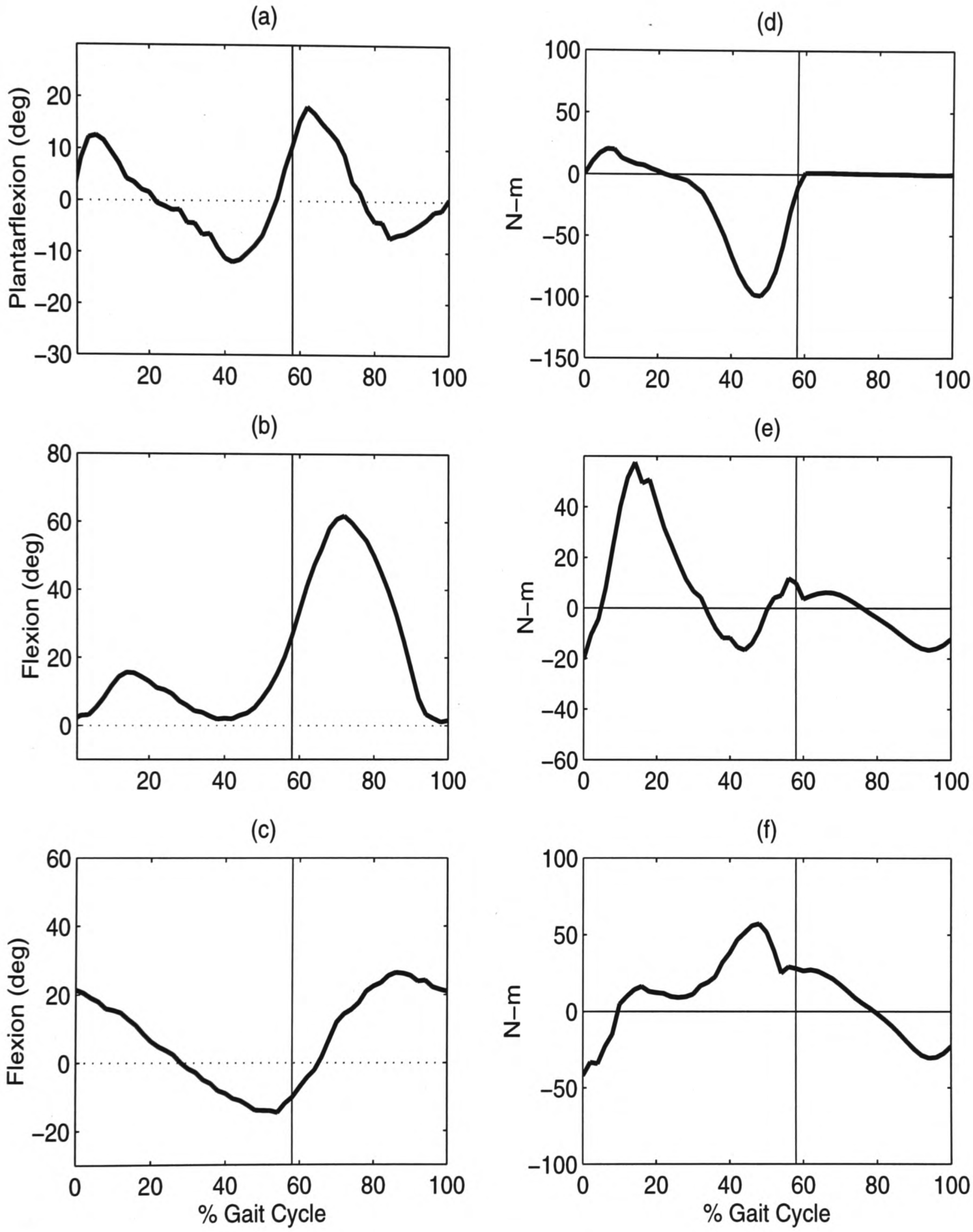



Figure 5.5: Joint angles (a-c) and resultant moments (d-f) of the ankle, knee and hip during the walking cycle

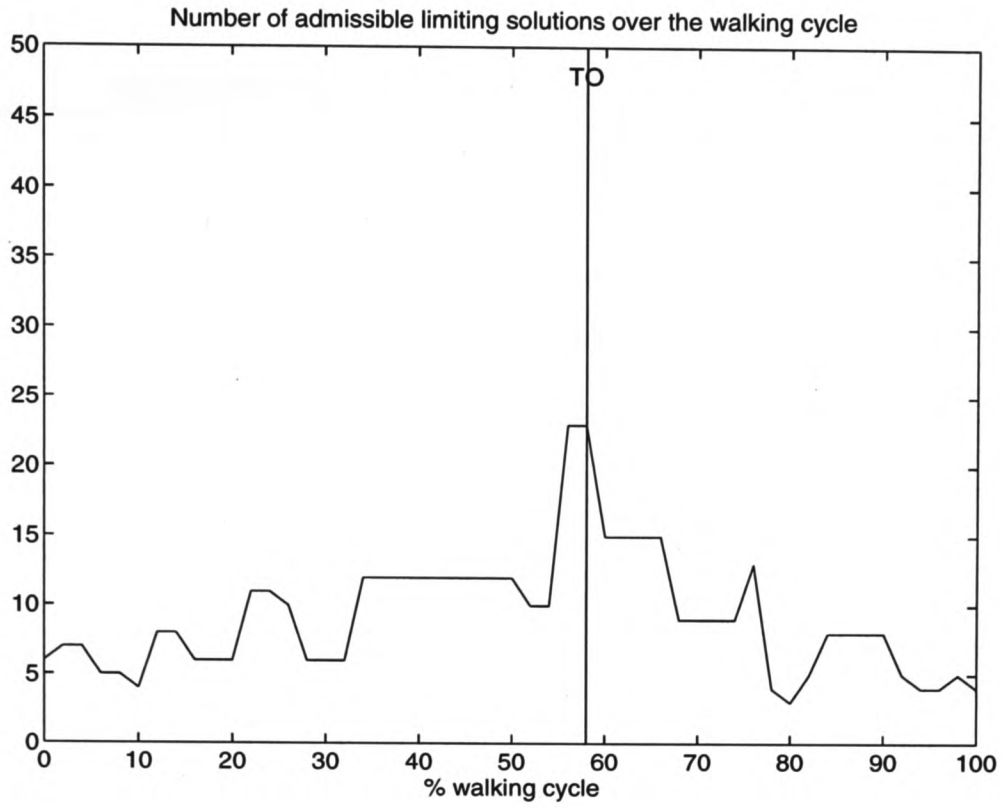



Figure 5.6: Number of DDOSC solutions found at each data point over the walking cycle. (Minimum = 3, Maximum = 23, Mean = 9.16)

(Figure 5.5(e-f)). Throughout most of the mid-stance, gastrocnemius, soleus and iliopsoas were active simultaneously, as indicated by EMG in Figure 5.8. The model found the DDOSC solution SCD-GPC-ICD to be consistent with EMG during 30-50% walking cycle, which meant that nearly 70% consistency of the theoretical prediction with EMG evidence was obtained in the mid-stance phase.

*Late Stance (50 - 58%):* At the beginning of the first one third of late stance, EMG indicated activity in three muscles: gastrocnemius, soleus and iliopsoas. The DDOSC solution SCD-GAC-ICD was found by the model. Shortly after, the external loads were tending to dorsiflex the ankle, flex the knee and extend the hip. Quadriceps was recruited during this interval. The EMG consistent DDOSC solution SCD-GAC-QIC was obtained. During the second one third of the interval, gastrocnemius was inactive (Figure 5.8) and the solution SCD-QPC-ICD was found. Throughout the last one third of late stance, active muscles as indicated by EMG were tibialis anterior, iliopsoas and quadriceps. The EMG consistent DDOSC solution was TCD-QAC-ICD. In general, the model found solutions consistent with EMG over 98-100% of the late stance phase.

*Early Swing (58 - 72%):* A small dorsiflexing moment was needed at the ankle, an extending moment at the knee and a flexing moment at the hip. Throughout this interval, activity in three muscles was indicated by EMG: tibialis anterior,

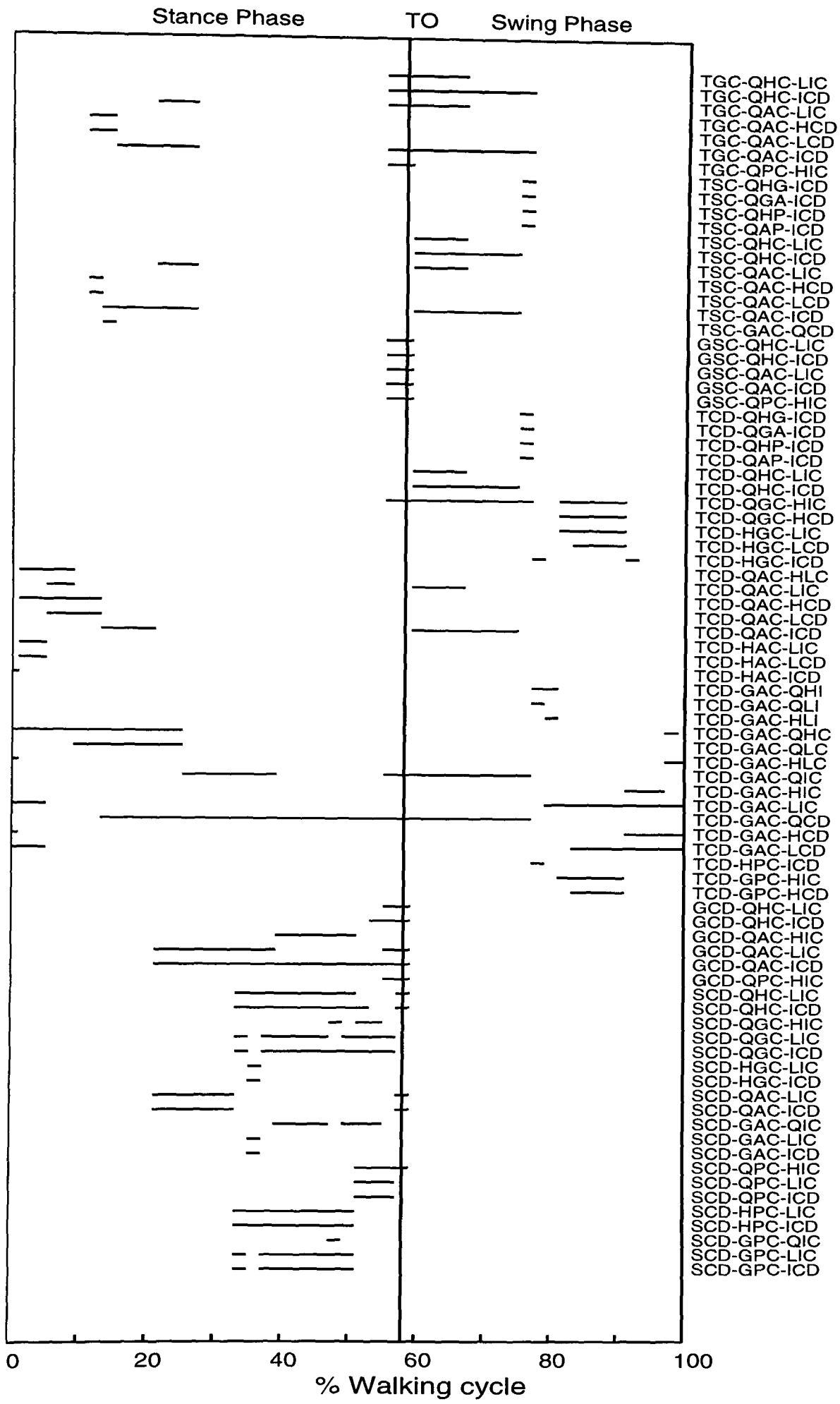



Figure 5.7: Temporal patterns of the DDOSC solutions over the walking cycle

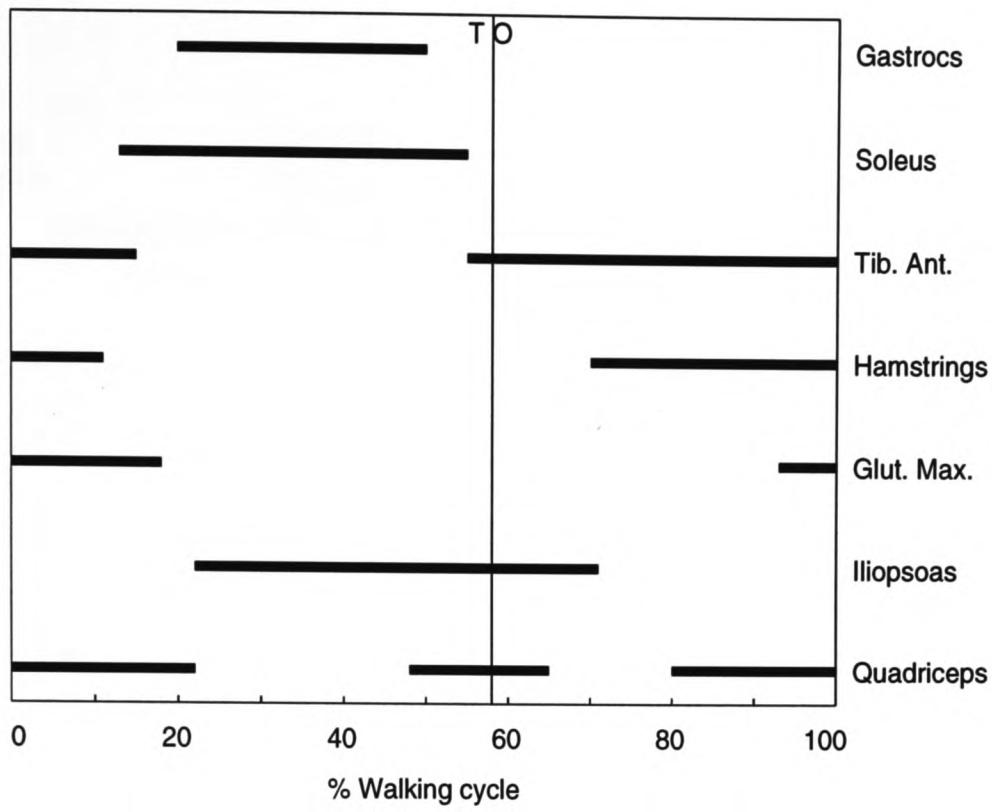



Figure 5.8: Periods of muscle activity as indicated by EMG. From Collins [56].

iliopsoas and quadriceps. The DDOSC solution TCD-QAC-ICD was found by the model. The consistency of the predicted muscle activity with EMG was obtained over 70-80% of early swing.

*Mid-Swing (72 - 86%):* Throughout the first half of mid-swing, the external loads were tending to plantarflex the ankle, extend the knee and hip. During the second half mid-swing, an extending moment were needed at the hip. For a brief period at the beginning of mid-swing, three muscles were active: tibialis anterior, hamstrings and iliopsoas (Figure 5.8). The DDOSC solution TCD-HPC-ICD was found by the model.

*Late-Swing (86 - 100%):* During late swing, a small dorsiflexing moment was needed at the ankle, a flexing moment at the knee and an extending moment at the hip. EMG indicated three active muscles throughout this interval: tibialis anterior, hamstrings and quadriceps. Gluteus maximus was also active immediately before heelstrike, Figure 5.8. However, only partially consistent DDOSC solutions, i.e. TCD-GAC-QHC and TCD-GAC-HLC were found by the model.

In brief, solutions consistent with EMG were found over 70-75% of the walking cycle. Similar results were also obtained by Collins [56].

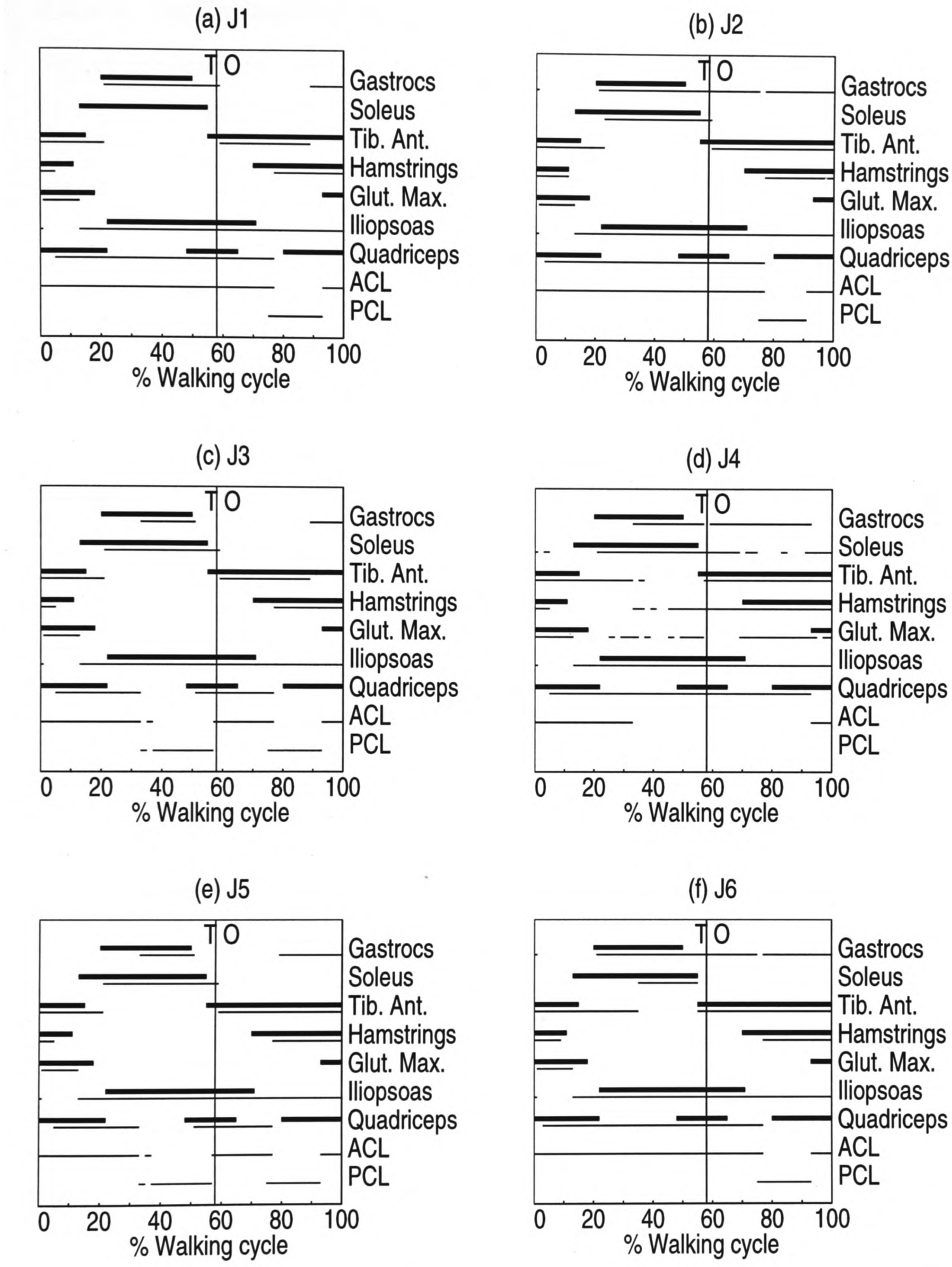



Figure 5.9: Temporal patterns of predicted muscle and ligament forces using optimisation method with (a) minimum sum of muscle forces (J1), (b) minimum sum of quadratic muscle forces (J2), (c) minimum sum of muscle stresses (J3), (d) minimum sum of ligament forces (J4), (e) minimum sum of joint contact forces (J5) and (f) minimum sum of cubic muscle stresses (J6). The EMG patterns of Figure 5.8 are plotted above the respective muscle patterns (bold lines).

### 5.2.3.2 Optimisation Method

Figure 5.9 shows the temporal patterns of muscle and ligament forces predicted by using the optimisation method with six different minimum objectives. The EMG patterns of Figure 5.8 are also plotted above the respective muscle patterns for comparison.

*a. Minimum Sum of Muscle Forces (J1):* This criterion preferred muscles with large lever arm among synergistic muscles. During mid-stance, a plantarflexing moment was needed at the ankle and a flexing moment at the knee. Therefore, the bi-articular muscle gastrocnemius was recruited to meet this requirement and the soleus muscle was left silent during this period. However, this was not consistent with EMG, Figure 5.9(a). Gastrocnemius activity was also predicted during late swing whereas EMG did not demonstrate such activity. The temporal pattern of activity of hamstrings was in excellent agreement with EMG evidence but those for other muscles were not as good. While the antagonistic activities of hamstrings and quadriceps around heelstrike were indicated by EMG, quadriceps was not selected by this criterion. When the predicted solutions were compared frame by frame with EMG, it was found that they were consistent only for 10% of the gait cycle.

*b. Minimum Sum of Quadratic Muscle Forces (J2):* This criterion minimised the sum of the squares of the muscle forces and penalised large individual muscle forces. This led to a more even force distribution among gastrocnemius and soleus, as shown in Figure 5.9(b). While the theoretical results for hamstrings, gluteus maximus, iliopsoas and quadriceps were similar to those for $J1$, the activity of tibialis anterior was in good agreement with EMG for this criterion. Nonetheless, it was estimated that the predicted solutions were consistent with EMG indications only for 15% of the gait cycle.

*c. Minimum Sum of Muscle Stresses (J3):* Theoretically, this criterion was equivalent to the minimisation of the sum of muscle forces but penalised individual muscle forces with small PCSA's. The predicted patterns of muscle activities were in good agreement with EMG during stance phase and early swing, except a brief period after heelstrike, Figure 5.9. During mid-swing and late swing, the theoretical results were similar to those for $J1$ and $J2$. No antagonistic activities of quadriceps and hamstrings were predicted around heelstrike. The predicted solutions were found to be consistent with EMG activities for only about 30-35% of the gait cycle.

*d. Minimum Sum of Ligament Forces (J4):* This criterion minimised the ligamentous contributions at the knee joint so muscles surrounded were expected to carry larger forces. Numerically, since the ligament forces occurred only in two of the nine equilibrium equations, the sensitivity of the objective function to other unknown variables was small. Therefore, the formulated problem was not well behaved. There were three frames during mid-stance, where the formulated optimisation problems could not converge to a stable solution. As shown in Figure 5.9(d), predicted solutions were in poorest agreement with EMG patterns. Discontinuous muscle activities were frequently found in soleus, tibialis anterior, hamstrings and gluteus maximus, which were evidently not the way muscles act. It was noted that during mid-stance, late stance, early swing and mid-swing, hamstrings and quadriceps were recruited to compensate the inability of ACL and PCL.

*e. Minimum Sum of Joint Contact Forces (J5):* This criterion minimised the sum of joint contact forces and thus was equivalent to the minimisation of sum of muscle forces. How the resultant forces were distributed among the muscles seemed dependent upon muscle orientations. The criterion predicted patterns of muscle activity quite similar to those for $J3$ but with better consistency of tibialis anterior with EMG.

*f. Minimum Sum of Cubic Muscle Stresses (J6):* Basically, this criterion is equivalent to the minimisation of sum of muscle forces but with different penalties to each muscle forces based on muscle force magnitudes and muscle PCSA's. Generally, the theoretical results during early stance and late stance, except immediately after heelstrike, were in good agreement with EMG evidence. Temporal patterns of activity of hamstrings were also in excellent agreement with EMG. Solutions patterns during swing phase were almost identical to those for $J2$. The predicted solutions were consistent with EMG for only about 15-20% of the gait cycle.

### 5.2.4 Discussion

Six minimisation objectives were evaluated based on the same lower limb model. It should be pointed out that these criteria, except $J4$, were basically co-operative goals, which tended to minimise the sum of muscle forces. The differences between them were the penalties assigned to the individual muscle forces. Based on frame by frame comparison of the predicted solutions with EMG, it was found that the

best results were obtained by criteria $J3$, minimum sum of muscle stresses, and $J5$, minimum sum of joint contact forces. However, even in these best predictions, only 30-35% of the muscle patterns were consistent with EMG. In the worst case, no EMG consistent solution was found for minimum sum of ligament forces (J4), which to some extent implied that ligamentous contributions to stabilising the knee joint could not be neglected, an important factor which has been largely ignored in gait studies. From these results, it is hard to suggest any of the tested criteria as an appropriate analogy to the way in which the locomotor apparatus actually functions.

In the work of Pedersen *et al.* [196], two indices were established to quantify the agreement between predicted results and EMG signals: active and inactive concurrence. The active concurrence represents the percentage of active EMG time that both force predictions and EMG are active, while the inactive concurrence determines the percent of time of EMG inactivity that predicted forces are also inactive. Among the seven tested criteria, the maximum averaged active concurrence is 40, which means that for an individual muscle only 40% of the active predictions are consistent with EMG. It is likely that if a frame by frame check was performed, the percentage of consistency between predicted solutions and EMG signals would be much less than 40%. This agrees with the present study.

In contrast to the optimisation method, the DDOSC solutions approach seems more successful. Although the approach itself can not be used to find an unique solution, it reduces an infinite set of solutions to a small group of mechanically admissible ones among which a final solution can be selected in the light of temporal physiological considerations, e.g. EMG activity. In the present study, the number of solutions was reduced to a minimum of 3, a maximum of 23 and a mean of 9.16. Solutions consistent with EMG were found over 70-75% of the gait cycle. It was noted that EMG consistent DDOSC solutions were mostly identified during stance phase and early swing. This suggests that the human locomotor system functions in a dynamically determinate manner during this period. Although EMG consistent solutions were not well identified during mid-swing and late swing; and around heelstrike,theoretical results during stance phase were considered to be sufficient for clinical applications because peak structural member forces occurred during this period. An advantage of the DDOSC solutions approach over the optimisation method is that all mechanically admissible solutions are identified. These alternatives, as indicated in Figure 5.9, demonstrate a

possible solution to the problem of compensating for systemic dysfunction, such as ligament disruption and isolated muscle injury, because each of them can be utilised at an instant to produce the co-ordinated, time-varying segmental movements of normal gait.

In summary, the present study suggests that it is unlikely that the human locomotor system performs a complex and varying skilled task, such as walking, following a single optimality criterion. Instead, the final learned gait pattern may be the result of a compromise of multiple objectives. For example, it may be that during stance phase muscles are mainly used to provide (maximum) stability while maintaining (maximum) mobility. Compromise between the two conflicting objectives results in the dynamically determinate movement pattern, as shown by the results obtained using the DDOSC method. During mid-swing, stability of the body is provided by muscles of the other leg so it seems that mobility dominates other objectives for the swing leg. Thus, the number of muscles involved reaches a minimum of two, as indicated by EMG evidence (Figure 5.8). Around heelstrike, antagonistic quadriceps and hamstrings activity is found in EMG, Figure 5.8. It may be proposed that another objective, precise position and velocity control, which may require more mechanical effort, dominates during this period, to ensure accurate placement of the foot on the ground. Before a full understanding of the compromise of possible objectives is established, it is inadequate to approach the force distribution problem using a single objective optimisation method. For the purpose of clinical applications, however, the DDOSC method represents a more reasonable and flexible way to examine the force interactions between structural members of the human locomotor system.

## 5.3 Gait Analysis of Patients With Instrumented Prostheses: 2D Theoretical [2]

In this section, the validation of the two-dimensional model using simultaneously measured *in vivo* axial forces along the instrumented massive proximal femoral prostheses in two patients is presented. Influence of hip flexors and extensors on the forces in the femur as revealed by the validated model calculations is discussed. It was hoped to show if

[2]The material in this section has been accepted for publication in *J Biomechanics* 1997 [157]. Co-authors: J.J. O'Connor, S.J.G. Taylor, P.S. Walker

1. a sagittal plane model with good representations of the anatomy and anthropometry of the tested subject can predict accurately forces in the bones under in-plane loadings and will underestimate forces in the bones under out-of-plane loadings;

2. during the activities examined, the minimum *number* of forces necessary to achieve dynamic equilibrium are deployed and

3. bi-articular muscles play a major role in modulating forces and moments in the bones.

Since the model was basically developed for analysis in the sagittal plane, only the isometric tests of the hip flexors and extensors and level walking were considered in the present study.

### 5.3.1 Dynamic and Structural Analysis

Activities were analysed using inverse dynamics as described in Chapter 2, giving intersegmental resultant forces and moments at each joint. The associated indeterminate problem was then formulated to distribute these forces and moments to individual structural members, using the DDOSC method. The quadriceps were further separated into rectus femoris and vasti and a total of 1179 DD subproblems were considered.

To examine the interaction between muscles and bones in response to external loads, the cross-section of the lower limb at the level of prosthesis transducers (173 mm distal to the centre of the head of the prosthesis in IM, Fig. 3.4, and 107 mm in DG) was selected. The net limb moment due to the external loads and inertial effects, $M_{limb}$, should be balanced by the Pauwels couple, $M_{pauwels}$, formed by the axial compressive force in the prosthesis and the tensile force transmitted by the appropriate muscle, as defined in Chapter 3, together with the residual bending moment in the prosthesis, $M_{bone}$ (Figure 5.10). That is,

$$M_{limb} = M_{pauwels} + M_{bone} \tag{5.4}$$

The proportion of the net limb moment transmitted by the Pauwels couple at this level, $M_{pauwels}/M_{limb}$, was calculated once an EMG consistent DDOSC solution was obtained.

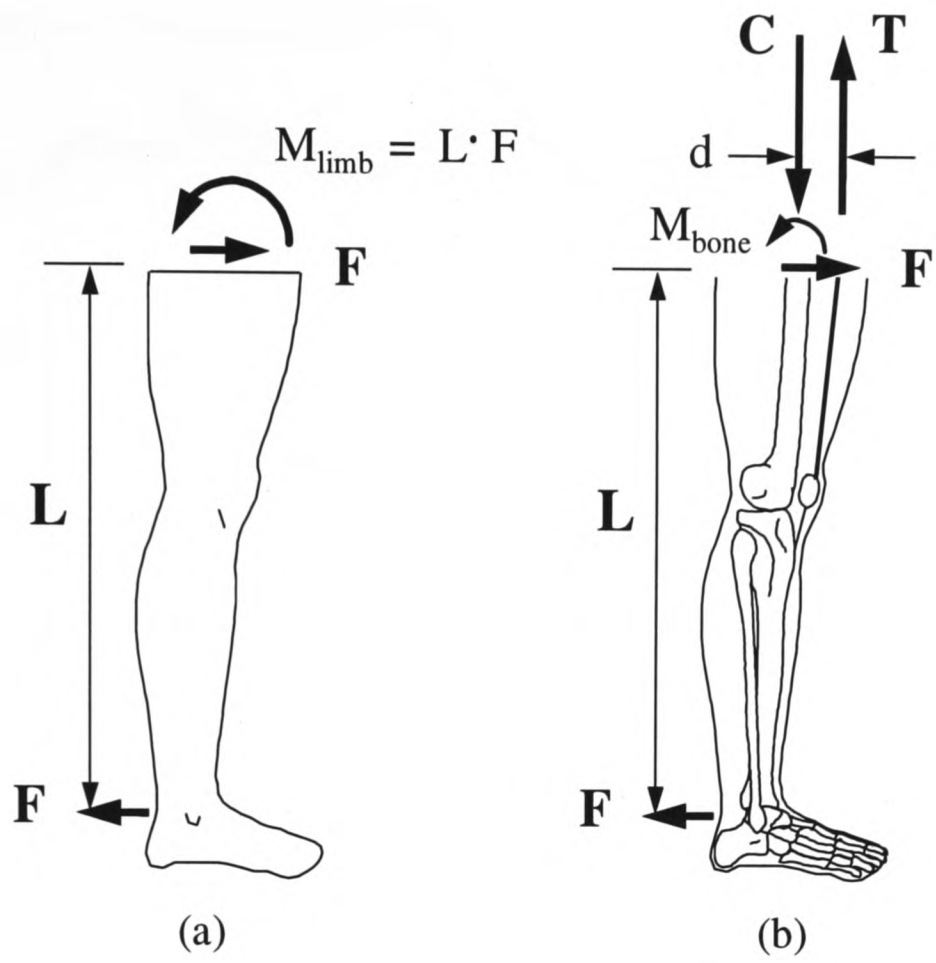



Figure 5.10: Flexor test. Since the external force F is horizontal, the flexor muscle force T and axial compressive force C are equal and opposite. In this test, the Pauwels couple is $dT$ and, together with the bending moment in the bone, $M_{bone}$, transmits the limb bending moment $M_{limb}$. The relative values of $dT$ and $M_{bone}$ are given in the text.

## 5.3.2 Isometric Tests

### 5.3.2.1 Isometric Hip Flexion

Analysis of the hip flexion exercises using the model yielded only seven DDOSC solutions for both subjects. Since iliopsoas tendons of the subjects had been removed or immobilised during operation, DDOSC solutions involving iliopsoas were not feasible, leaving only one of the seven DDOSC solutions, namely TCD-GAC-RCD. This was consistent with the EMG. Axial forces calculated in this combination, telemetered forces and the external forces are shown in Figure 5.11 for IM and Figure 5.12 for DG. The average $M_{pauwels}/M_{limb}$ ratios at this level were 98% for IM and 92% for DG, leaving less than 10% transmitted by the bone itself. If the iliopsoas tendon had not been removed, the DDOSC solution TCD-GAC-RIC would provide a measure of its contribution in transmitting forces and moments at the hip. Axial forces calculated in this combination were about 10%

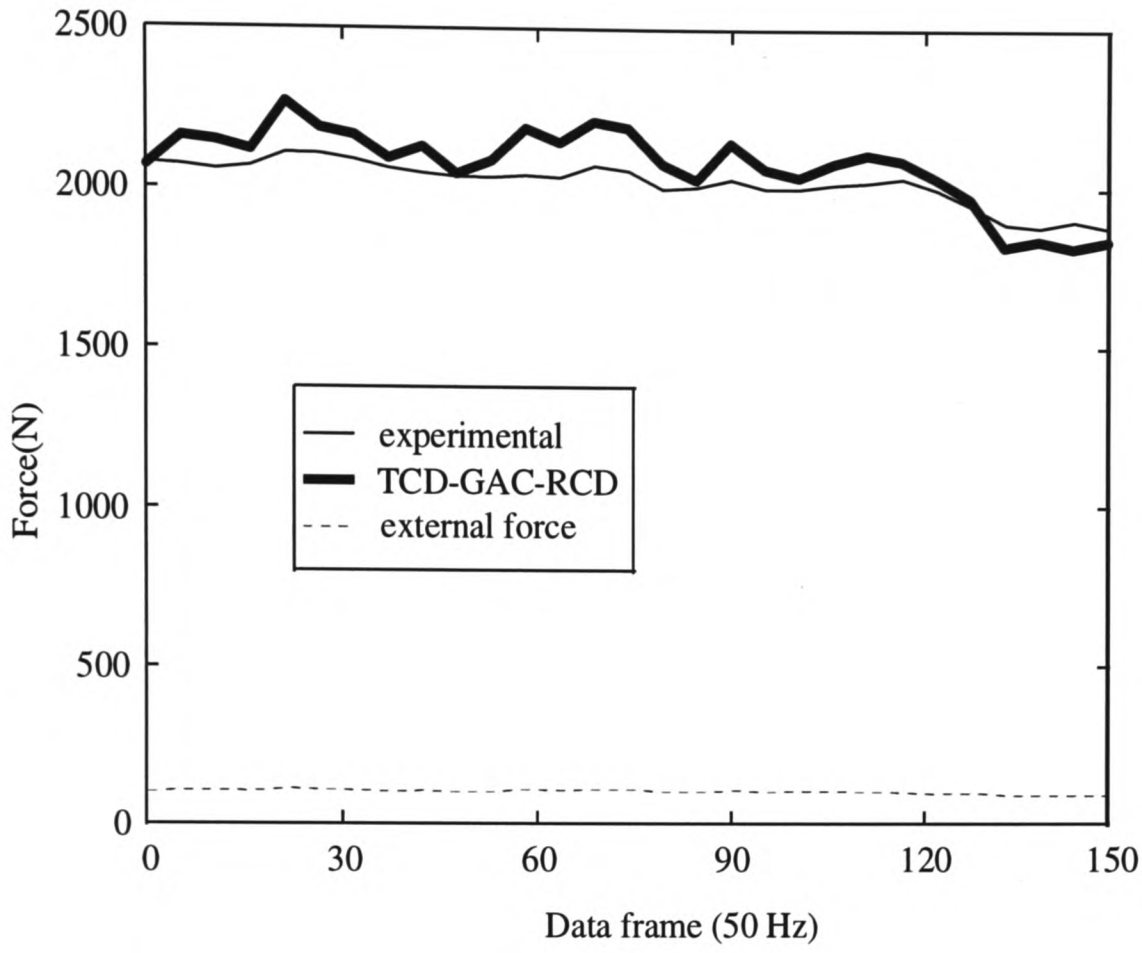



Figure 5.11: Calculated (thick line) and measured (thin line) axial forces in the prosthesis during isometric hip flexion exercise from IM. Also shown are the external forces (dashed line).

higher than those measured. Rectus femoris forces were about 2.5 times higher than forces in the iliopsoas tendon.

#### 5.3.2.2 Isometric Hip Extension

For isometric extension exercises, the model predicted sixteen DDOSC solutions for both subjects. After considering muscular pathology, only one EMG consistent DDOSC solution remained (TCD-GPC-HCD). Comparisons of theoretical calculations and telemetered values of the axial forces for IM and DG are shown in Figure 5.13 and Figure 5.14, respectively. The average $M_{pauwels}/M_{limb}$ ratios at the level of prosthesis transducers were 98.6% for IM and 73.8% for DG, leaving less than 30% transmitted by the bone itself. In order to simulate the effects of an intact gluteus maximus as a mono-articular hip extensor on the forces in the femur, the DDOSC solution TCD-GPC-HLC was examined. In this combination, the calculated hamstrings forces were about eight times higher than the gluteus maximum forces. Axial forces calculated were about 3% higher than

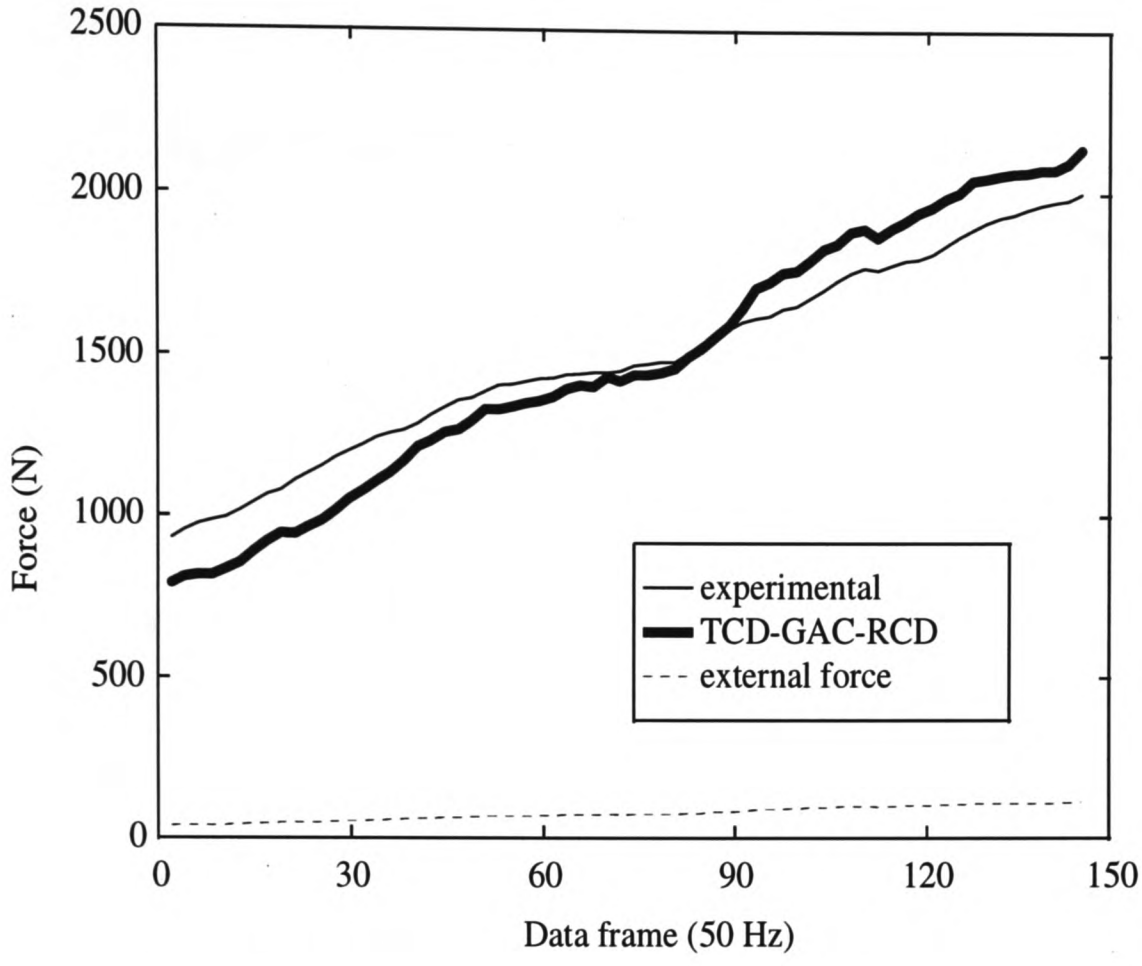



Figure 5.12: Calculated (thick line) and measured (thin line) axial forces in the prosthesis during isometric hip flexion exercise from DG. Also shown are the external forces (dashed line).

those measured.

### 5.3.3 Level Walking

During level walking, the number of predicted DDOSC solutions ranged from 4 to 24. Due to the number of EMG channels allowed at the time of the experiment, only the EMGs of the major thigh muscles were monitored. They were used to reduce the predicted DDOSC solutions to a unique solution. For certain data frames during the mid-stance phase, however, more than one DDOSC solution involving different calf muscles remained. Activity of these muscles was then obtained from the literature [56, 123, 239] to select a unique solution. Following the above procedure, the most EMG-consistent DDOSC solution was selected at each data point in the gait cycle and the corresponding axial forces calculated, as shown with those measured in Figure 5.15. During stance phase, where maximum axial forces occurred, the ratio of the calculated values to the measured ones

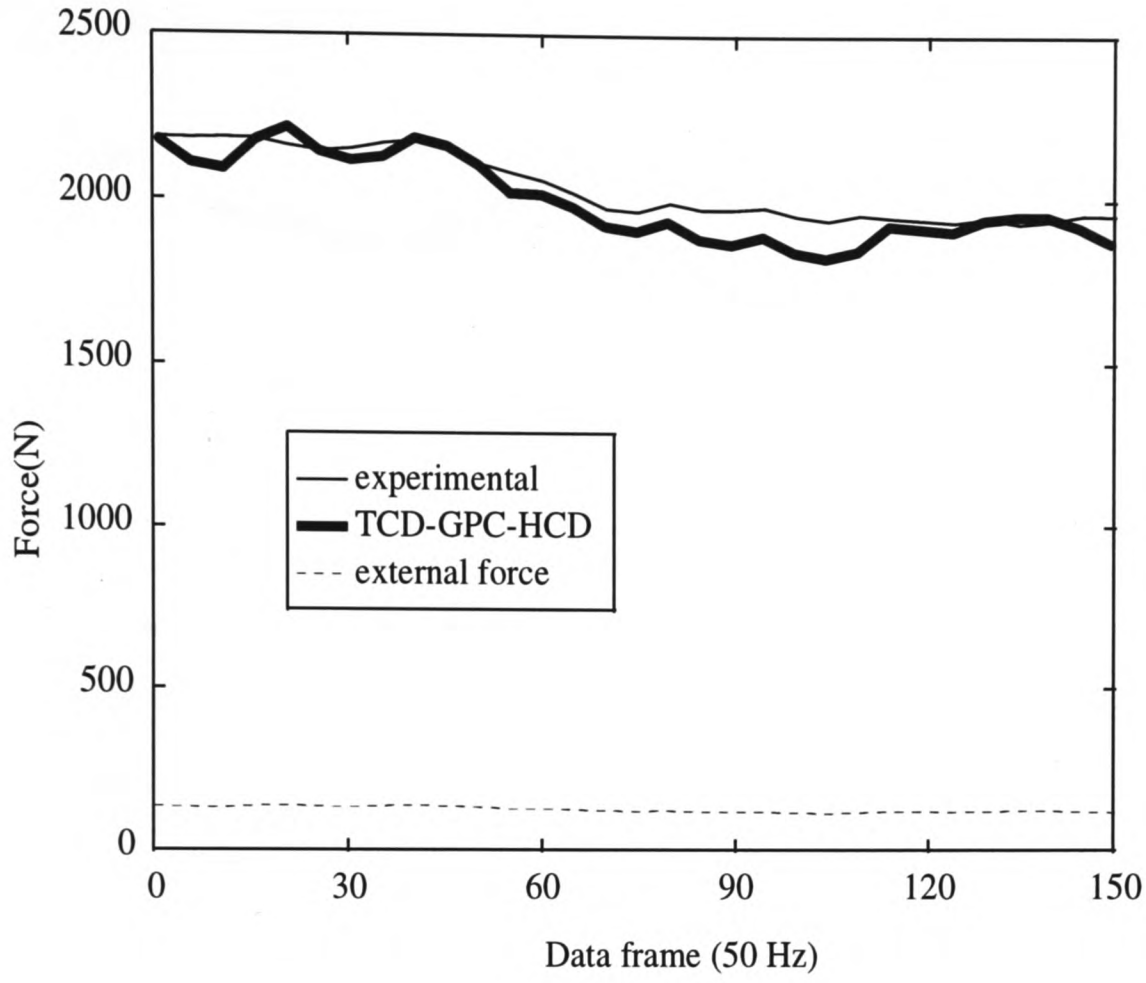



Figure 5.13: Calculated (thick line) and measured (thin line) axial forces in the prosthesis during isometric hip extension exercise from IM. Also shown are the external forces (dashed line).

ranged from 50% to 100% with a mean of 70% in both subjects.

## 5.3.4 Discussion

### 5.3.4.1 Validation of The Model

Simultaneously measured movement data and *in vivo* forces from instrumented prostheses allowed direct comparisons between model calculations and measurements. By using parameters measured from each subject, the model accommodated inter- and intra-subject variations and produced outputs reflecting these differences. Values of the forces transmitted along the prostheses estimated by the model during isometric flexor/extensor tests were in good agreement with telemetered values (Figures 5.11-5.14). The model also followed very well the time-dependent variations of the forces as the effort used by each subject varied. Inter-subject differences in internal forces noted in Chapter 3 are largely explained by parameter differences. A model which does not account for the leg abductors

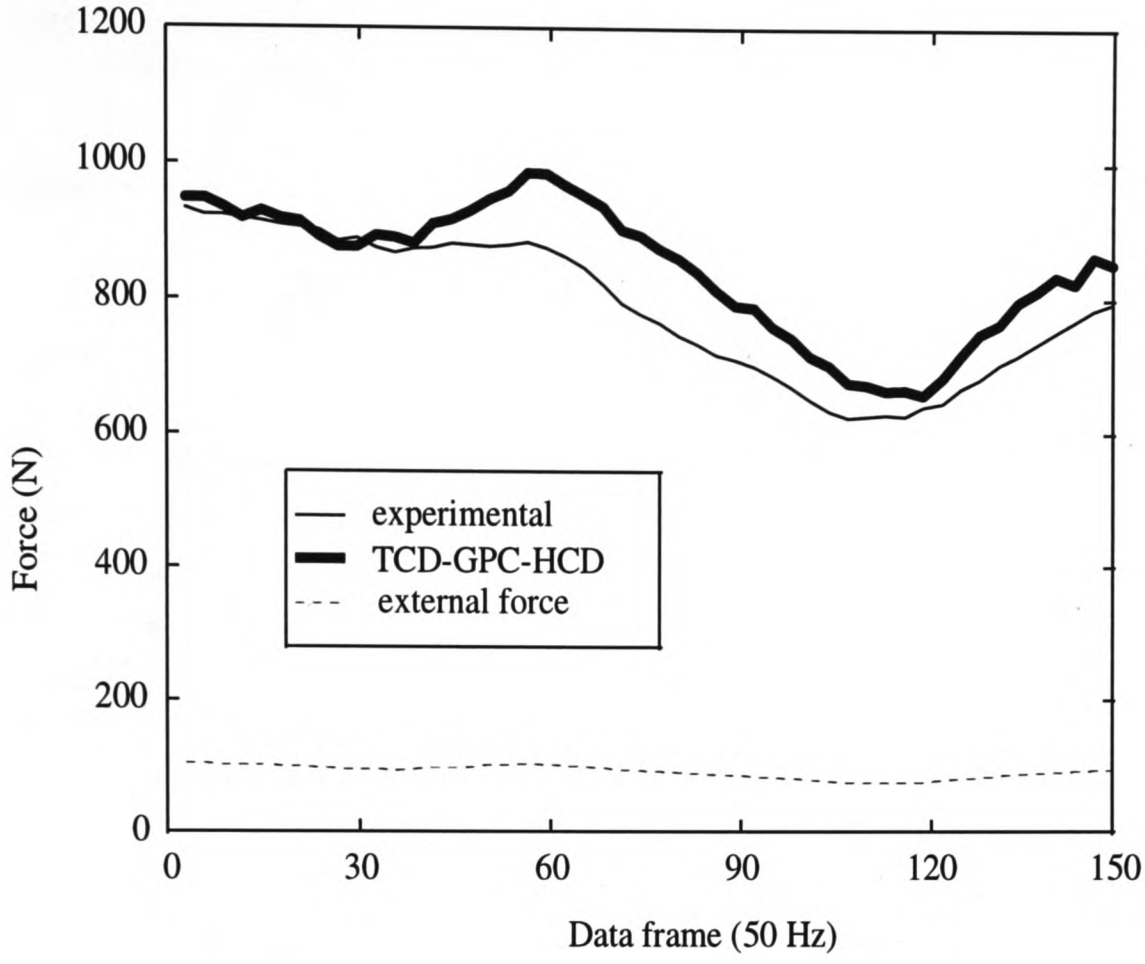



Figure 5.14: Calculated (thick line) and measured (thin line) axial forces in the prosthesis during isometric hip extension exercise from DG. Also shown are the external forces (dashed line).

should underestimate the value of the axial force during single leg stance in gait although flexor and extensor activity during stance phase can account for much of the measured axial force during stance phase of walking and 70% of the maximum axial force. These conclusions were reinforced by 3D calculations to be reported in Chapter 7. By applying the equations of dynamic equipollence and one-sided constraints, the DDOSC method yielded only a small number of admissible solutions out of a possible 1179. One solution was selected based on EMG recordings and/or actual anatomy of the tested subject. The selected solution agrees quite well with measured data. Although the method does not yield a unique solution directly, it provides an opportunity for a close examination of possible muscle recruitment strategies. It also provides an explanation for the muscle compensation mechanisms of the human locomotor system, as demonstrated in the analysis of isometric tests. Instead of trying to find a globally validated muscle recruitment principle, the DDOSC method starts by considering dynamically determinate solutions. This is based on the EMG findings which show that, during most

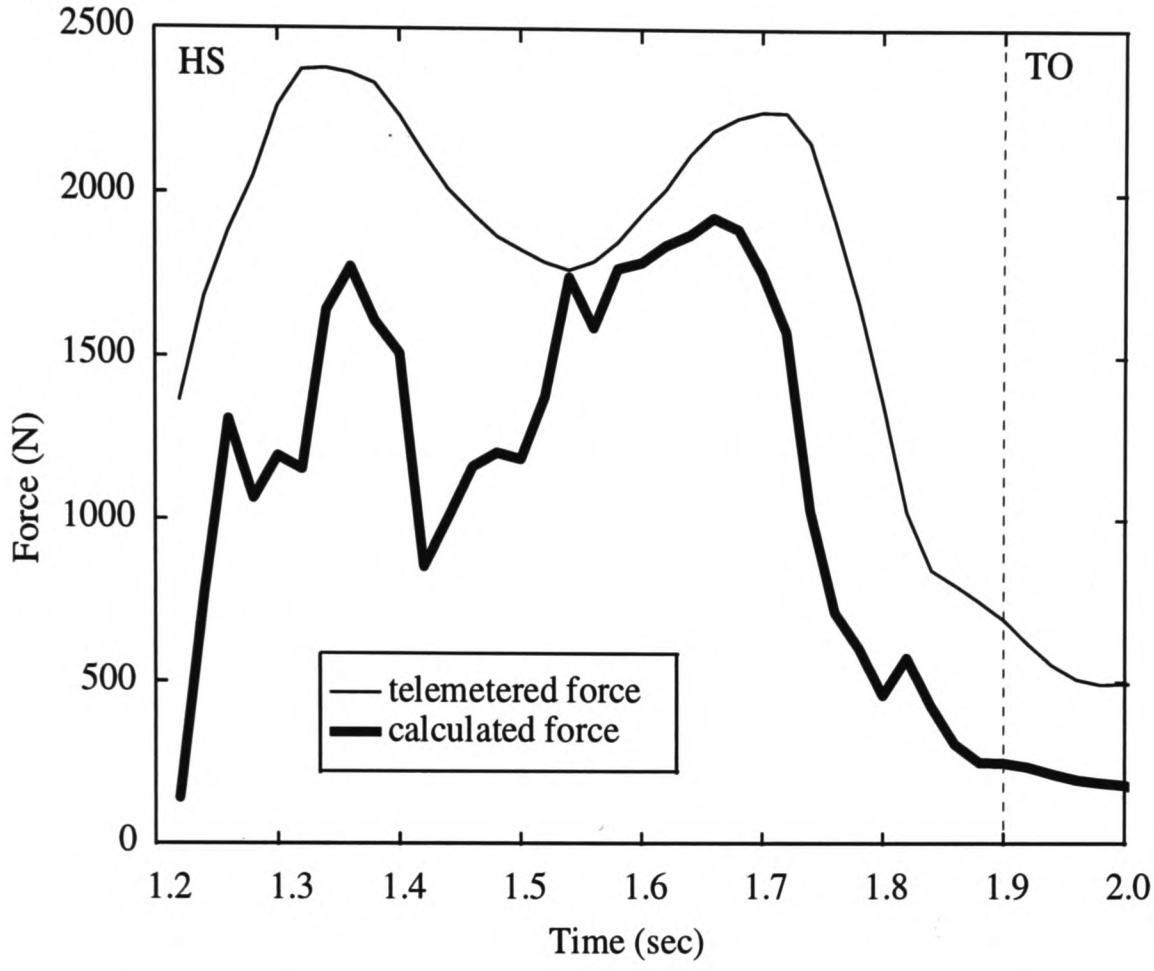



Figure 5.15: Calculated (thick line) and measured (thin line) axial forces in the prosthesis during level walking from IM. (HS = heelstrike; TO = toeoff).

activities, only a small number of muscles are active. The works of Collins and O'Connor [58] and Collins [57] and the present study suggest that during many activities the locomotor system performs movements in a dynamically determinate manner, deploying the minimum *number* of forces. It should be noted that consideration of dynamically determinate solutions includes antagonistic muscle activity which was not predicted by most linear optimisation methods [196] and not so far considered by the reduction method [172, 193]. Generally, predicted DDOSC solutions involving antagonistic hip flexor/extensor activity yielded large compressive axial forces in the bone while the DDOSC solution selected according to EMG and actual muscular conditions predicted values very close to those measured.

Since the force distribution problem is formulated as a set of simultaneous linear equations with two groups of one-sided linear constraints, it defines a linear convex solution domain on which DDOSC solutions represent the vertices. Because of the linear and convex property of the problem, any feasible solution can be represented as a linear combination of the DDOSC solutions. In other words,

any muscle recruitment pattern can always be decomposed to a weighted sum of DDOSC solutions. Therefore, DDOSC solutions serve as a basis of possible muscle recruitment strategies and define bounds on force values of the structural members.

#### 5.3.4.2 Bi-articular Muscles

The role of bi-articular muscles has been studied from the point of view of mechanical efficiency [69], anatomical configuration [211] and motor control [244, 245, 247, 275]. Its contribution to the modulation of stress/strain distribution was suggested by Pauwels in 1950 and supported by the experimental results reported in Chapter 3 [159]. Model calculations performed in the current study provide further quantitative evidence in favour of Pauwels' hypothesis. They show that bi-articular muscles take a major share of the synergistic muscle forces (2.5 times mono-articular muscle forces in flexion and 8 times in extension) and, acting with the axial compressive force in the bone, balance most of the net limb moment, reducing bending moments transmitted directly by the bone shaft. It seems that mono-articular muscles have effects mainly around the joints while bi-articular muscles act to balance the external moments not only at the joints but also along the whole lengths of the bones. Therefore, bi-articular muscles may be thought of as more efficient in protecting the bones from excessive bending strains.

In this section, the influence of hip flexors and extensors on the forces and moments in the femur was studied using the 2D lower limb model. For the study of abductors and adductors, a three-dimensional model was used to analyse transverse and coronal planes effects.

### 5.3.5 Summary

The development of a geometric model of the human pelvis-leg apparatus in the sagittal plane was presented. The model was used to study the influence of activity of hip flexors and extensors on the forces in the femur, using data from two subjects with instrumented massive proximal femoral prostheses during isometric hip flexion/extension exercises and level walking. The problem of system redundancy was resolved using the DDOSC method. Quantitative validation of the multi-joint model of the human lower limb was performed for the first time using simultaneously telemetered in vivo axial forces along the prostheses. Axial

forces calculated by the model during isometric exercises were in good agreement with telemetered forces. During gait, the model calculations suggest that about 70% of the maximum axial force in the femur is a result of action of the flexors or extensors. It was also shown that bi-articular muscles are major force modulators for the bones. It is suggested that appropriate simulation of muscle force is necessary in *in vitro* laboratory experiments and in theoretical studies of stress distributions in bone.

## 5.4 Interactive Graphics-Based Window Interface

In order to simplify the analysis of the human lower limb during activity, an interactive graphics-based window interface, which unified the separate models described in Chapter 4 and this chapter was developed, Figure 5.16. This interface was established in the X-window environment, a standard in UNIX, and all the models were implemented in C so the portability of the resulting system was enhanced. Through buttons, dialogue boxes and 'pull-down' menus and with graphical display windows, geometric and dynamic analyses of the lower limb can be performed in a 'look and feel' manner. It is hoped that this would bring the results of biomechanical studies to clinical users.

### 5.4.1 Window Interface Structures

Main features of the window interface are summarised as follows:

- Unification of separate models: Mathematical models integrated are treated as separate modules, communicating with each other under the coordination of the top level window while responding to users' command events individually. Therefore, sequence dependence in performing analysis is minimised.
- Control of modelling modules: Modelling modules are controlled by 'pull-down' menus, activated by clicking dedicated buttons using a mouse pointer. Each menu contains a group of function buttons or submenus, which should be selected to perform such functions as changing model parameters, graphing and model animation.

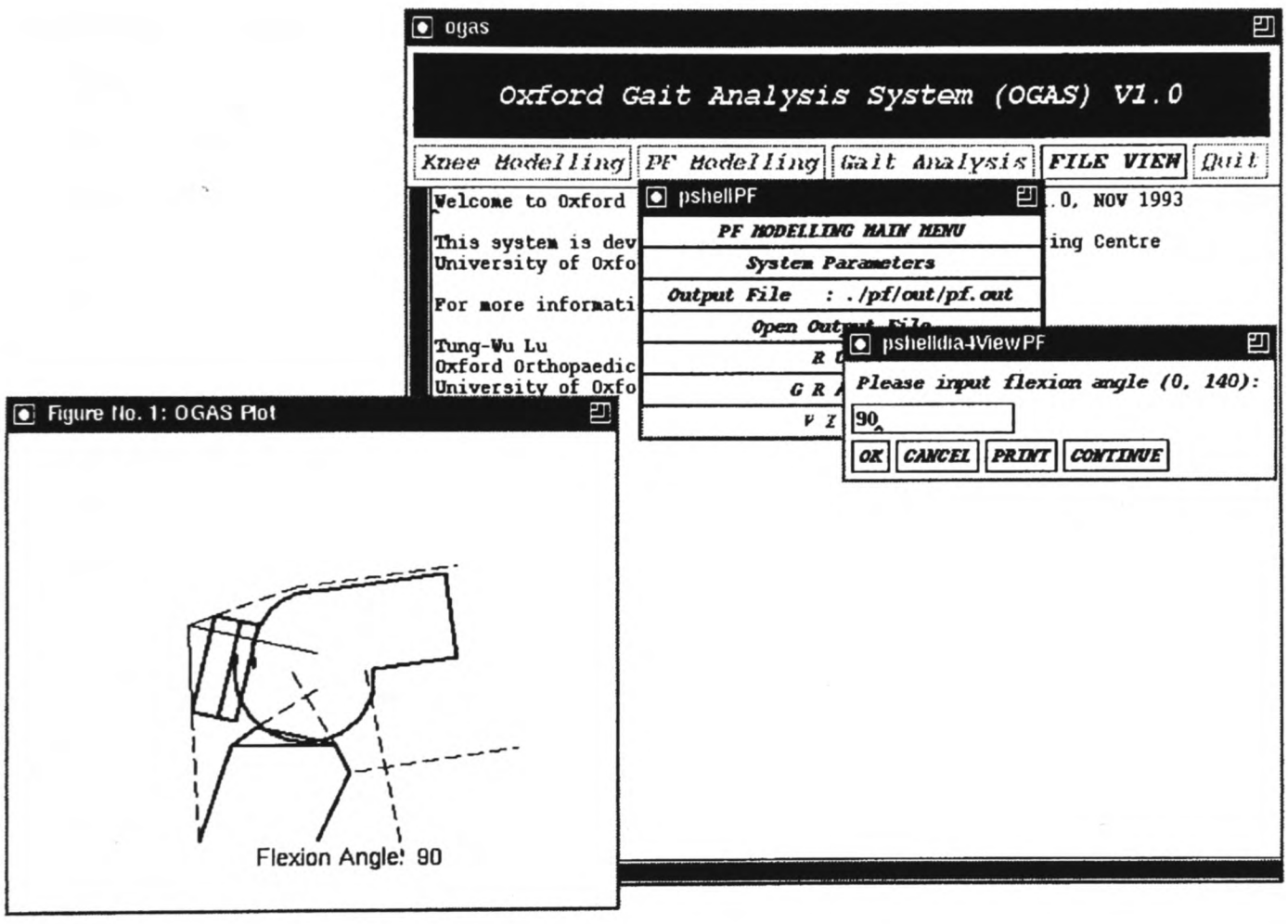



Figure 5.16: The interactive graphics-based window interface showing the animation of the passive motion of the knee joint

- Model parameters: Functions to set-up and change model parameters are facilitated in a 'list' window. Model parameters are displayed as a list of items. Each item triggers a dialogue box, where the user is allowed to supply the parameter value interactively. All changes should be confirmed or cancelled before leaving the 'list' window. With this facility, users are able to change parameter values at any stage of the modelling work so parameter sensitivity to the model can be examined easily. A potential use of this facility is to simulate surgery by changing model parameters.

- Graphs display: Numerical results of each module can be manipulated with the colour graphs display window. This window was designed with maximum flexibility to provide users with an interactive environment to create and print graphs according to their own preference. A set of model outputs is listed for selection. The graphs display is supported by MATLAB graphs library.

- Model animation: With calculated or measured data, models can be animated with coloured 2D stick figures. Different types of animation are also provided. Dialogue boxes are used for interactive control of animation when necessary. This feature allows the user to monitor the passive motion of joint models and to visualise the movement pattern of the model extremity animated by measured data.

- File editor: A file editing module is incorporated to control a simple text editor. With this module, users are allowed to change input files defining model parameters, an alternative to the model parameters window, and to examine numerical results, an alternative to the graphs display facility.

- Link with measured data: Measured data such as kinematic data, force plate data and EMG data are forwarded to the system as data files. Currently, data file formats are designed for Vicon system output. Slight changes are needed for reading output from different measuring systems.

- User preference: The appearance of the interface such as dimension, position, colour and text font, and its responses to user events are defined by a set of window 'resources'. By changing the resources in the resource file or using a command line parameter, users can customise the interface to their

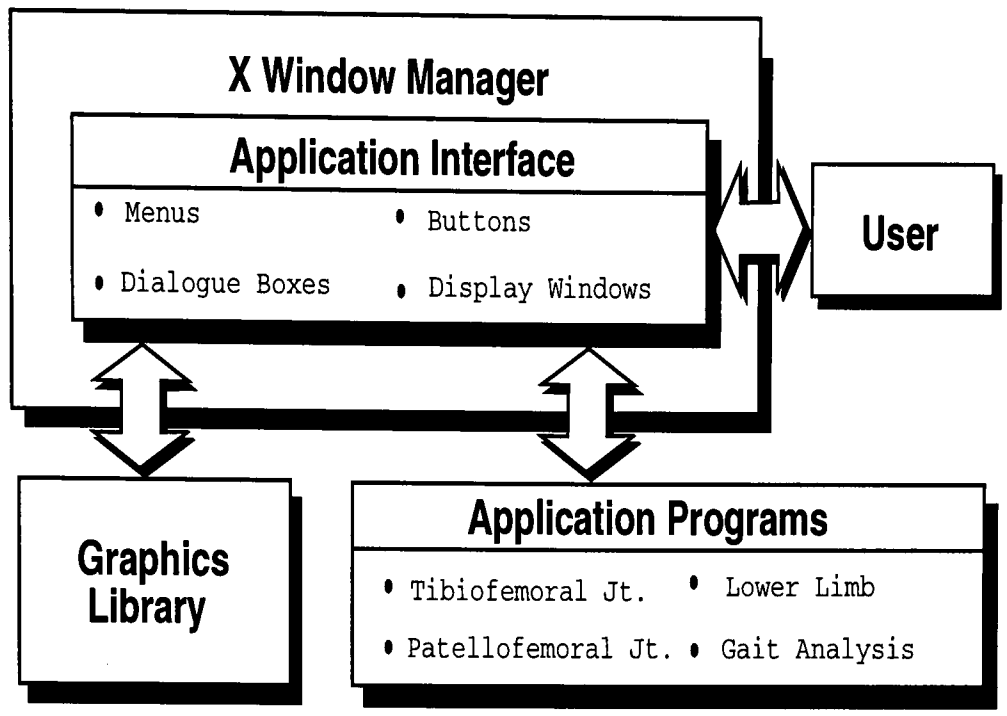



Figure 5.17: Schematic block diagram demonstrating the interaction between the user, X window manager, window interface and modelling modules

own preference. This feature demonstrates the user-friendly characteristic of the interface.

The block diagram shown in Figure 5.17 demonstrates the interaction between the user, X window manager, the window interface and modelling modules. Since all the models are unified by the window interface, which responds to user events interactively, users are free from memorising commands and can play with the interface. The modelling process can thus be done in 'trial and error' and 'look and feel' manner.

The system is presently dedicated to the study of kinematics and dynamics of human gait. With the aid of the graphical display, the lower limb model can be animated and the time-varying patterns of gait, components of ground reaction force and recruitment of muscles can be visualised. To further enhance the capability of the system, a structural analysis module for the determination of structural member forces should be incorporated and a realistic three-dimensional graphics-based model of the lower limb is needed.

Based on the experience in developing this prototype window interface, it is suggested that interactive graphics-based window interfaces are vital tools in filling gaps between clinical users and biomechanical workers.

## 5.5 Discussion

### 5.5.1 Effects of Ligament Elasticity

In the present studies, the knee ligaments were assumed to be inextensible. Further calculation to include ligament elasticity can be done with the following iterative procedure.

1. Take the EMG consistent DDOSC solution as a starting point.
2. Apply a small anterior (in the case of ACL) or posterior (in the case of PCL) displacement to the tibia with the femur fixed and calculate the new lines of action of the force-bearing structures, including the fibres recruited.
3. Calculate the resultant forces transmitted by the ligaments according to their mechanical properties.
4. With the current ligament forces, check equilibrium of the whole system and the one-sided constraints. If both conditions are satisfied, final solution is reached. Otherwise, increase the displacement and repeat steps 2-4.

It is noted that the unknown ligament force (either ACL or PCL) has been represented as a function of the unknown a/p displacement so the system remains statically determinate. Since MCL and LCL forces can also be related to the a/p displacement, further inclusion of these ligaments can be made without increasing the number of unknowns to the system. Therefore, force sharing between the ACL and MCL and between the PCL and LCL can be studied at this stage.

The effect of the assumption of inextensible ligaments on the model calculations, however, can be estimated before incorporating the elastic ligament models. As shown in Figure 5.18, anterior translations reduce the angles of the ACL and MCL relative to the tibial plateau whereas posterior translations reduce the angles of the PCL and LCL. These changes give the ligaments better orientations to resist the applied anterior or posterior shear forces. Therefore, for a given shear force the forces transmitted in the elastic ligaments will be smaller than those transmitted in the inextensible ligaments, which suggests that forces estimated based on inextensible ligaments always give upper bounds to the actual values. The same argument has been proposed by FitzPatrick and O'Connor [81] and Zavatsky and O'Connor [279]. So, the current force analysis can be considered as on the safe side.

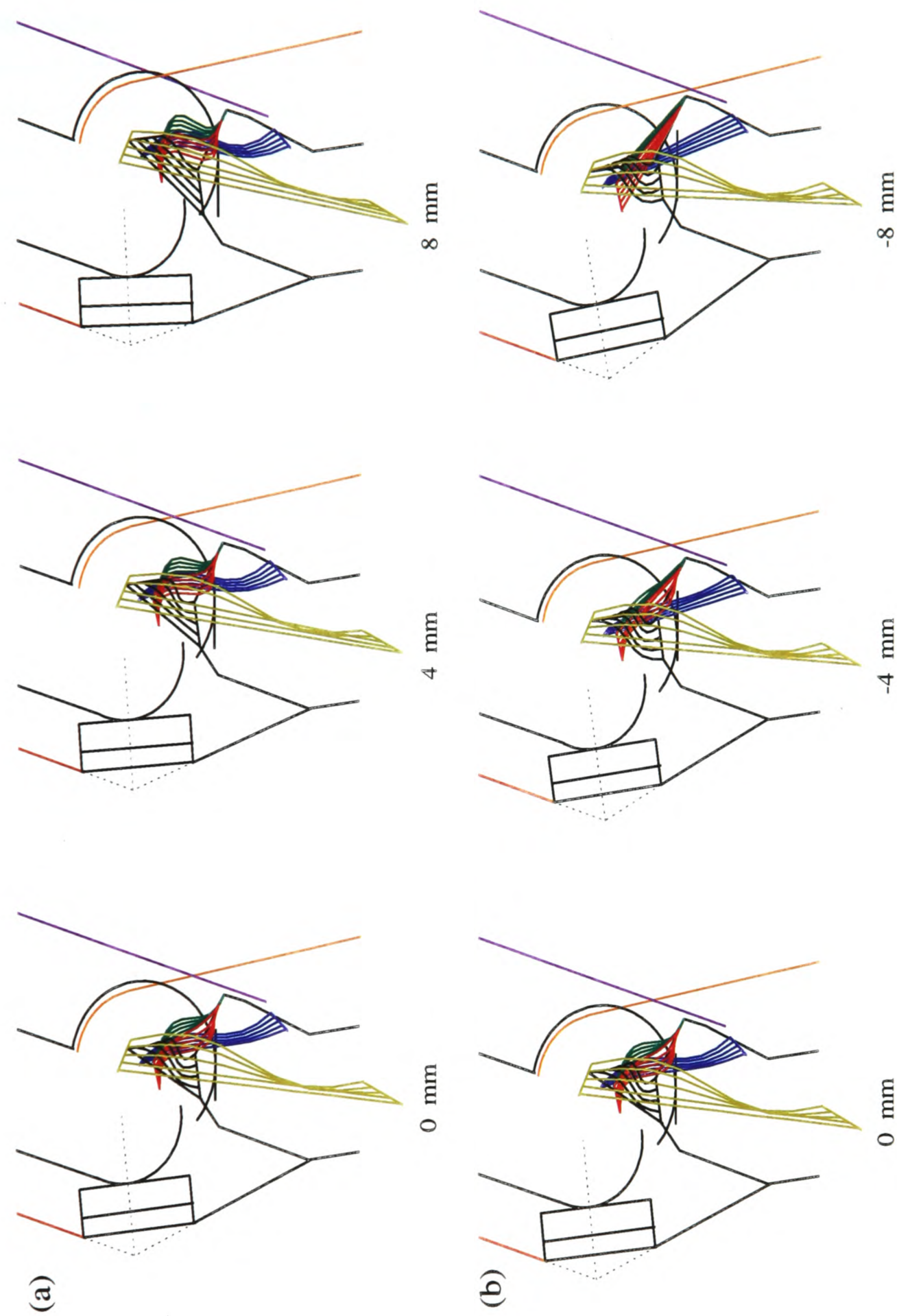



Figure 5.18: Geometry of the knee joints considering elastic ligaments with (a) anterior and (b) posterior translations of 4 and 8 mm at 25° of flexion.

Since the lengths of the ligaments are small, their lines of action are sensitive to the anterior/posterior translation which is determined by the muscle forces. However, for muscle forces, the effect of the assumption of inextensible ligaments are relatively less because a small amount of translation produces only a negligible change of orientation of the muscles. The change of the lines of action of the muscles due to a/p translation can hardly be seen in Figure 5.18. Therefore, ligament forces are sensitive to muscle forces while their effect on muscle forces are less. It is suggested that consideration of extensible ligament is important for the study of the stability of the joints but for the estimation of muscle forces the assumption of inextensible ligaments is appropriate. The latter has been supported by the good correspondence between the model calculations and the telemetered forces reported in the previous sections.

### 5.5.2 Ankle Modelling

After the present study was completed a four-bar linkage model for the ankle joint was developed jointly with Leardini and colleagues [146] so that the contribution of both the ligaments and articular surfaces in controlling the joint kinematics can be considered. A major improvement of incorporating the model into the lower limb model will be that the line of action of the contact force at the ankle is uniquely determined by the four-bar linkage and no prespecified ankle contact direction is needed. However, this will not affect the results of the present calculations because all the DDOSC solutions obtained involved directions of the contact forces at the ankle and hip as system unknowns. Therefore, it was decided to keep the ankle joint as a simple hinge as a starting point but suggested that further consideration of the ankle model as a four-bar linkage is necessary to study the forces transmitted in the ligaments during activity.

# Chapter 6

# Three-Dimensional Modelling of the Locomotor Apparatus [1]

The use of the two-dimensional model of the locomotor system to study the influence of the activity of the hip flexors and extensors on the forces in the femur has given results which were in good agreement with telemetered forces during isometric tests. During walking, the model underestimated the femoral forces because of inherent limitations of a 2D model. This encouraged further development of a three-dimensional model which accounted for effects of hip abductors and adductors as well as out-plane loadings and axial rotation. Such a model will be useful for the study of a wide range of activities. In this chapter, the development and implementation of a 3D geometric model of the locomotor apparatus is presented. It will begin with descriptions of models of the major joints, muscles and the complete lower limb. These will be followed by descriptions of three-dimensional computer graphics reconstruction and animation of the model. The use of the geometrical model in reducing stereophotogrammetric measurement errors, skin movement artefacts in particular, will also be presented. The comparison of the model predictions against the telemetered internal forces will be presented in Chapter 7.

[1] Part of the material in this chapter has been presented at the 3rd International Symposium on Computer Methods in Biomechanics and Biomedical Engineering, Barcelona, Spain, 1997 [156]. Co-authors: J.J. O'Connor, S.J.G. Taylor and P.S. Walker.

## 6.1 Knee Joint Model

In the sagittal plane, the four-bar linkage model presented in Chapter 4 successfully described the coupled rolling/sliding motion of the knee joint during flexion as observed in experiments [252] and is thus a good model for two-dimensional analysis. The motion of the knee joint in space, however, involves more than just flexion/extension. The so-called "*screw home*" mechanism, which refers to the external rotation of the tibia with respect to the femur during the later stages of extension of the knee, has long been noted [169] (cited in [122]) and generally described as an accessory degree of freedom of the joint [136, 257]. For a better description of the relative motion of the femur and tibia and the lines of action of the force-bearing structures at the joint, a three-dimensional model of the knee joint which accommodates the screw home mechanism is needed.

For the present studies, a three-dimensional model of the tibiofemoral joint developed by Wilson and O'Connor [259, 262] was adopted and incorporated into the model of the locomotor system. This involved the implementation of the model in the C programming language using the *Object-Oriented Programming (OOP)* approach. The model joint, like others which will be discussed in the following sections, was implemented as a reusable *object* to be used repeatedly in the programmes of the model of the locomotor system and the later computer graphics reconstruction and animation. A brief account of the formulation and solution of the model is given below. The discussion will be restricted to the features of the knee model which are directly relevant to the present studies. More detailed descriptions can be found in the above references.

### 6.1.1 General Description

The three-dimensional mathematical model of the knee was based on a parallel spatial mechanism comprising the two cruciate ligaments, the medial collateral ligament and the contact normals of the articular surfaces in the two condylar compartments [259]. It was developed from the assumption that, under unloaded conditions, the above five constraints control the movements of the femur on the tibia and reduce the number of degrees of unresisted freedom of the joint to unity. It can be regarded as a three-dimensional analogue of the four bar linkage model. The model not only predicted the coupled rolling and sliding movement of the femur on the tibia but also the coupled internal rotation of the femur during extension, the screw home mechanism. The predicted movement patterns

were in good agreement with those measured in *in vitro* experiments [259]. The model was purely kinematic [259] and was not applied to analyses of the forces transmitted by the structures of the joint. The process of the formulation and implementation of the model can be summarised as follows.

1. Based on experimental evidence, select links that constrain the motion of the joint to form an anatomical mechanism.

2. To facilitate a full description of the motion path, convert the anatomical mechanism to an equivalent multi-looped mechanical mechanism with lower pairs.

3. Perform mobility analysis on the mechanism to ascertain that the mechanism is equivalent to the natural knee which has been shown experimentally to possess an unresisted mobility of unity, Figure 4.1

4. Establish the initial configuration of the mechanism, chosen as the extended position, using parameters such as co-ordinates of the attachment points of the ligaments obtained from cadaveric studies.

5. Perform forward kinematic analysis to obtain a complete description of the kinematics of the mechanism during its full range of motion. The relative motion of the femur is then represented by the transformation from femur to tibia.

6. Compare the predicted motion paths with those obtained from experiment to establish the validity of the model.

## 6.1.2 Formulation of The Parallel Spatial Mechanism

### 6.1.2.1 Model Links

Several experimental studies [3, 215, 142, 210, 89, 226] have shown that under unloaded conditions there is a fibre in the ACL, PCL and MCL that remains isometric as the knee is flexed. Under the same condition, the LCL slackens during flexion so there is no isometric fibre in the LCL [251]. The isometric fibres in the ACL, PCL and MCL were chosen as links that contribute to the control of the motion of the joint and were modelled as inextensible links joining their femoral and tibial attachments. The tibia and the femur were assumed to

be rigid, with incompressible articular surfaces. As a first approximation the tibial condyles were modelled as planar surfaces and the femoral condyles as spheres. Contact was assumed to be frictionless [204] and to be maintained in both compartments through the range of movement of the joint. This provides further constraints to the motion of the joint, in addition to the ligament links. These links and constraints together control the passive motion of the joint and form an anatomical mechanism.

This formulation is based on the hypothesis that unresisted motion is possible because the selected ligament fibres can rotate about their origins and insertions without stretching or slackening and the articular surfaces can slide upon each other without tissue deformation. Unresisted motion is therefore appropriately modelled by a system with incompressible surfaces and inextensible ligaments. Tissue deformation need be considered only when the stability of the joint is under study.

#### 6.1.2.2 Equivalent Mechanism With Lower Pairs

In order to describe the passive motion of the joint under the control of the articular and ligamentous constraints, a full analysis of the above anatomical mechanism is necessary. This requires the conversion of the anatomical mechanism to an equivalent multi-looped mechanical mechanism with lower pairs which can then be solved using well established methods.

To form a mechanism with lower pairs, the isometric fibre in each ligament was first represented by a solid rod connecting a spherical pair (ball joint) at the insertion in the tibia to a spherical pair at the origin in the femur, Figure 6.1. This connection is kinematically equivalent to isometricity of the fibre because it constrains the femoral and tibial attachments not to separate through the range of motion, Figure 6.1. The spherical pairs were further replaced by a chain of three revolute pairs. For each ligament, this yields an equivalent connection with six revolute pairs with one redundant freedom. A ligament equivalent connection with appropriate freedom was obtained by removing one of the revolute pairs, as shown in Figure 6.1.

Contact between the femoral and tibial condyles was represented by a spherical pair at the centre of the femoral condyle connected by a solid rod to a planar pair on the tibial condyle, Figure 6.2. This connection allow rotation about the centre of the femoral condyle and sliding at the contact point. Kinematically,

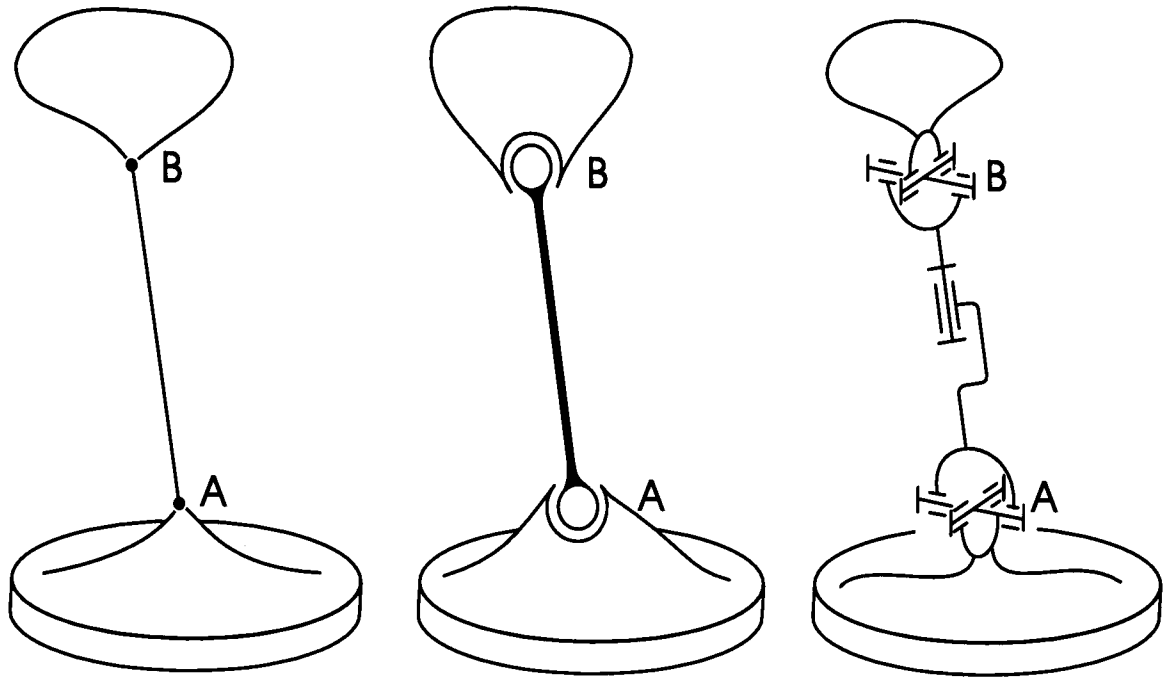



Figure 6.1: Equivalent configuration of a ligament (From Wilson [259])

it is equivalent to rolling and sliding of the spherical femur on the planar tibia. The spherical pairs were further replaced by a chain of three revolute pairs and the planar pair was replaced by a chain of two prismatic pairs. An articular equivalent connection, consisting of three revolute pairs and two prismatic pairs, is shown in Figure 6.2. The resulting geometric model is shown in Figure 6.3.

#### 6.1.2.3 Mobility Analysis

To check further the equivalence of the mechanism to the anatomical one, a mobility analysis was performed by Wilson [259]. According to the general mobility criterion [202], the mobility of a mechanism $m$ can be determined by the following.

$$m = 6(n-1) - \sum_{i=1}^{g}(6 - f_i) \tag{6.1}$$

or

$$m = 6(n-g-1) + \sum_{i=1}^{g} f_i \tag{6.2}$$

where $n$ and $g$ is the number of links and pairs, respectively. The freedom of each pair $i$ is given by $f_i$.

There are five anatomical connections (links), each with 5 one freedom pairs connected by 4 intermediate links, so together with the tibial link and the femoral link, give the mechanism a total of 22 links and 25 one freedom pairs. The mobility

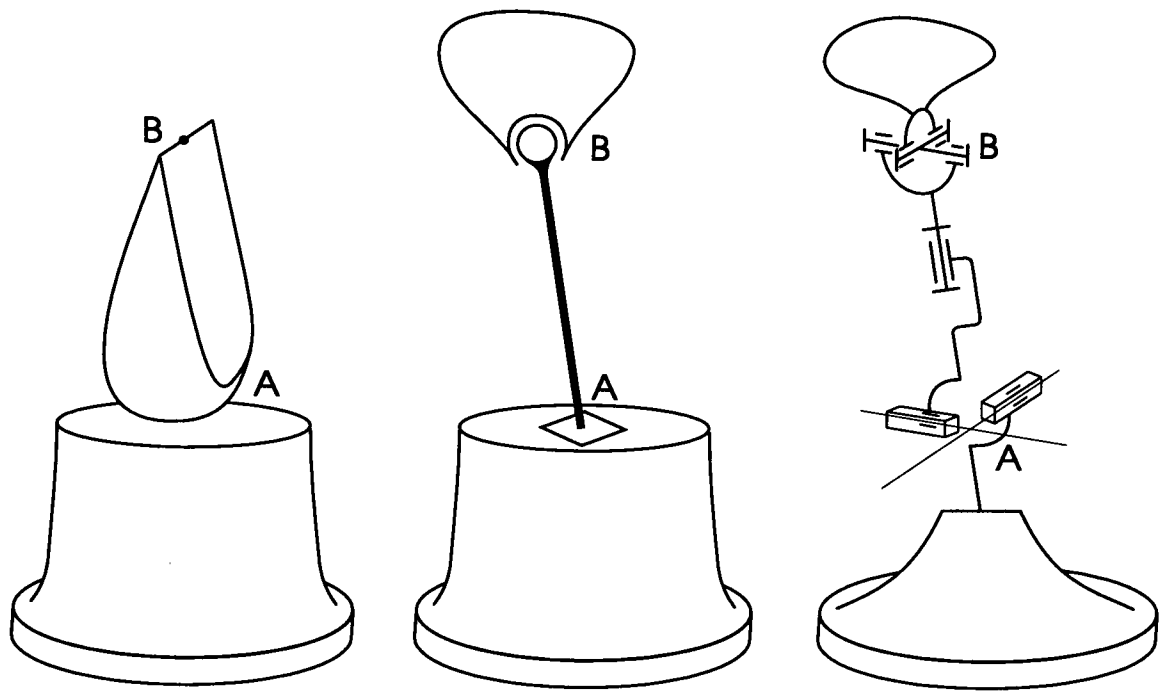



Figure 6.2: Equivalent configuration of a articular contact point (From Wilson [259])

of the mechanism is therefore

$$m = 6(22 - 25 - 1) + 25 = 1 \tag{6.3}$$

This shows that the mechanism indeed has a mobility of unity. In other words, the system has one degree of unresisted freedom [259]. Therefore, one input quantity is sufficient to specify the position of the femur relative to the tibia. Because of the parallel arrangement of the constraints, this mechanism is referred to as a *parallel spatial mechanism.*

#### 6.1.2.4 Forward Kinematic Analysis

The equivalent mechanism was divided into four independent closed loops; each consisted of two connections, one of which was the ACL. The four independent closed loops were: ACL-PCL, ACL-MCL, ACL-Medial Contact and ACL-Lateral Contact. Simultaneous closing of these loops enforces isometry of the ligaments and continuity of contact. The object of the calculation is to determine the motion path of the joint which satisfies the loop equations.

An iterative procedure developed by Uicker *et al.* [238] was used to perform the forward kinematic analysis of the multi-looped mechanism. This procedure uses a systematic convention for the definition of the geometry of the mechanism.

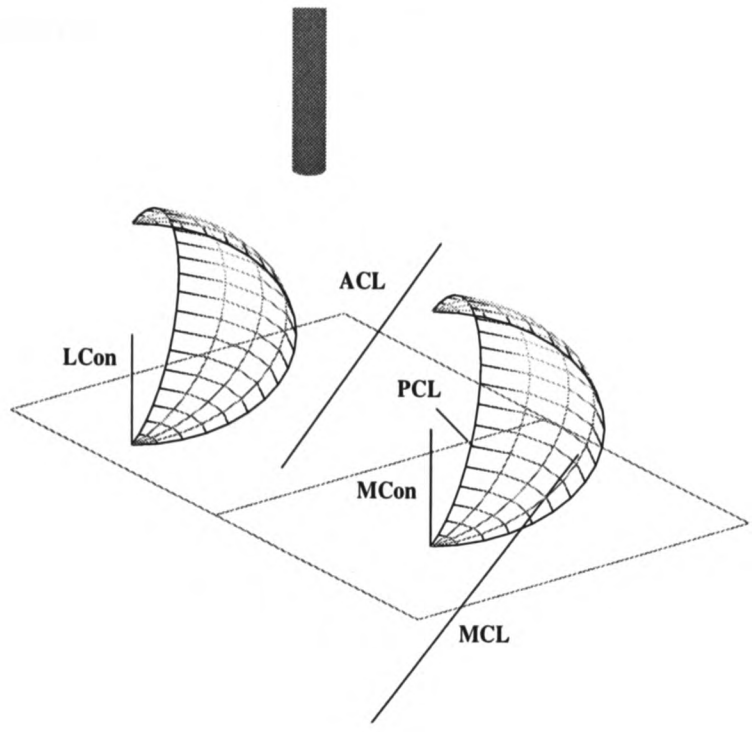



Figure 6.3: The parallel spatial mechanism model of the knee joint

For each loop, a loop equation with the following form is then written

$$A_1 A_2 A_3 ... A_k = I \tag{6.4}$$

where $k$ is the number of the pairs and $I$ is the $4 \times 4$ identity matrix. Matrix $A_i$ is the transformation from link $I+1$ to link $I$. Each loop equation is a set of non-linear equations in terms of the unknown pair variables. In the solution process, the pair defining the rotation of the ACL in the sagittal plane was chosen as the input pair. For a given value of the input pair variable, an iterative process using the first order information of the four loop equations is used to find the other unknown pair variables. By giving different values of the input pair variable, the complete range of motion of the mechanism can be fully described. More detailed description of the method of Uicker *et al.* can be found in the original reference [238] or in Wilson [259].

#### 6.1.2.5 Model Parameters

A parameter set from Wilson [259] was used in the present study. It was compiled from studies in the literature [24, 141] and thus taken as an average set. There is no doubt that parameters measured directly from a subject under test will give more specific features of that subject [78]. For the present study, however, the average set was used to provide a basis for customisation to individual subjects and to provide a more generalised picture of the knee joint. The choice of different

values of the parameters may affect the force sharing in the inextensible model ligaments [258] but the 2-D work of Chapter 5 suggests that the effects on the forces transmitted by the muscles will be small. A model parameter sensitivity analysis is beyond the scope of the present study but requires further investigation after a validated force distribution among the muscles has been established.

## 6.2 Hip Joint Model

### 6.2.1 General Description

The hip was modelled as a ball and socket (or spherical) joint with rigid, frictionless and congruent surfaces, allowing three degrees of rotational freedom. The head of the femur was modelled as a ball and the acetabulum was represented as a reciprocally shaped spherical cavity corresponding to the femoral head. The position of the hip joint centre (HJC) of rotation was taken to be the geometric centre of the femoral head. Given the co-ordinates of the HJC, parameters of the model, the relative motion of the pelvis and femur and thus the muscle attachments on the bones can then be described by the three rotational angles.

The estimation of the HJC has received much attention. This is because the accurate estimation of the HJC is essential for the calculation of the limb kinematics and the force analysis of the hip joint. However, since the HJC lies deep between the pelvis and the thigh, it is not palpable and also difficult to identify with palpable bony landmarks which are not close enough to ensure accuracy.

In the present studies, the HJCs of the instrumented subjects were obtained with sufficient accuracy from the positions of the two epicondyles and the "greater trochanter" using X ray. However, for the development of a general purpose model of the locomotor system, it was desirable to establish a reliable means of defining the HJC for future application in non-instrumented subjects.

As reviewed in Chapter 1, several methods have been proposed in the literature for the estimation of the HJC but generally they fall into three categories: *radiographic method*, *prediction approach* and *functional approach*. There are advantages and limitations associated with each method. The radiographic method is the most accurate method and has been used for studying hip joint mechanics [63, 133]. However, due to the risk of radiation overdose and high cost, it may not be preferred in routine gait analysis. Nonetheless, it provides a good reference

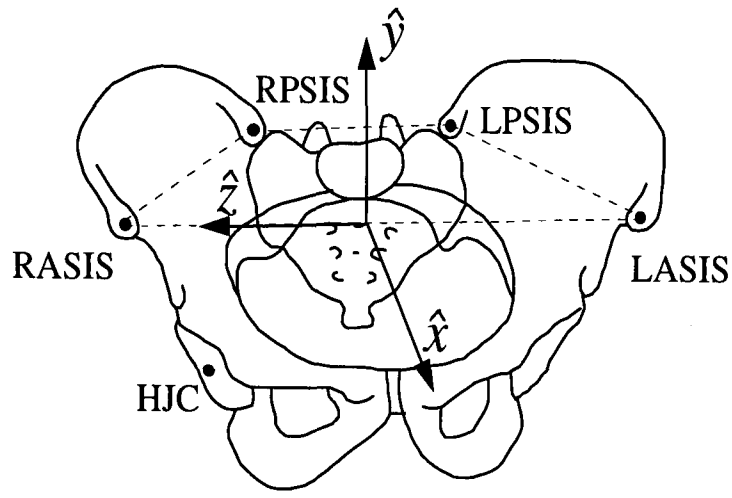



Figure 6.4: Co-ordinate system used for the evaluation of different methods for the estimation of the hip joint centre

for the evaluation of the other two methods [17, 40]. In the following sections, a preliminary evaluation of these two types of methods for the estimation of the HJC will be presented and the general direction of the selection of a method discussed.

### 6.2.2 Estimation of The Hip Joint Centre

One typical method from each of the prediction and functional approaches was tested: the prediction method proposed by Bell *et al.* [17] and the functional approach by Cappozzo [37]. A variation of the functional approach, here referred to as Revised Functional Approach (RFA), with further consideration of the rigid body assumption was also tested.

As shown in Figure 6.4, a co-ordinate system slightly different from the pelvic system $S_p$ defined in Chapter 2 was used for the present purpose. This new pelvic system was chosen to be consistent with those used in the literature so that a direct comparison of the results can be made. A co-ordinate transformation was needed to represent the estimated HJC in $S_p$.

#### 6.2.2.1 Prediction Approach (PA)

According to Bell *et al.* [17], the co-ordinates of the HJC can be expressed in terms of the pelvic width $D$, defined as the distance between the two $ASIS$s, by the following formula:

$$\vec{a}_{hip} = (-0.19D, -0.30D, i \cdot 0.36D) \tag{6.5}$$

where $i = 1$ for right hip and $i = -1$ for left.

#### 6.2.2.2 Functional Approach (FA)

The functional approach estimates the position of the HJC by assuming that the normal hip is a ball-and-socket joint and that every point on the femur remains an equal distance from the HJC during motion [37, 40]. By fitting the envelope of the motion of this point to a sphere, the HJC can be obtained as the centre of the sphere. The fitting process is usually done using a least squares approach.

#### 6.2.2.3 Revised Functional Approach (RFA)

It is noted that the current format of the functional approach uses only one marker to estimate the position of the HJC [40, 17]. However, since the estimated HJC will be indicated both at the pelvis and the femur for subsequent rigid body analysis, it is necessary to evaluate the differences between the one-marker estimation and the estimation considering rigid body motions of the femur and the pelvis. For this purpose, a revised functional approach (RFA) was formulated and is described below.

Basically, if the orientation of the pelvis and femur are known, the co-ordinates of the HJC in the laboratory system $S$ can be obtained either through the transformation from the pelvis co-ordinate system $S_p$, or through the thigh co-ordinate system $S_t$. The HJC position vector obtained through the pelvis can be calculated by the following transformation.

$$\vec{\beta} = \vec{v}_p + R_p \vec{\alpha}_p \tag{6.6}$$

where $\vec{\alpha}_p$ is the HJC relative to $S_p$ and $\vec{v}_p$ and $R_p$ are the translational and rotational transformations from $S_p$ to $S$. Similarly, the position vector through the femur is given as

$$\vec{\gamma} = \vec{v}_t + R_t \vec{\alpha}_t \tag{6.7}$$

where $\vec{\alpha}_t$ is the hip centre relative to $S_t$ and $\vec{v}_t$ and $R_t$ are the translational and rotational transformations from $S_t$ to $S$.

Theoretically, if the hip joint is a perfect ball and socket joint and the motion of the markers actually represent that of the underlying bone, then the above two equations should give the same value. However, due to skin movement artefacts, there will be discrepancies between the values calculated. For a data frame $i$, the difference can be expressed by an error term

$$E_i = \vec{\beta}_i - \vec{\gamma}_i \tag{6.8}$$

or

$$E_i = (\vec{v}_{pi} + R_{pi}\vec{\alpha}_p) - (\vec{v}_{ti} + R_{ti}\vec{\alpha}_t) \tag{6.9}$$

To find a solution closest to the actual value, the overall error over a series of $n$ data points should be minimised. In a least square sense, it is represented mathematically as follows.

$$\min \sum_{i=1}^{n} E_i^2(\vec{\alpha}_p, \vec{\alpha}_t) = \sum_{i=1}^{n} (\vec{v}_{pi} - \vec{v}_{ti} + R_{pi}\vec{\alpha}_p - R_{ti}\vec{\alpha}_t)^2 \tag{6.10}$$

The necessary condition for the above problem can be stated as follows

$$\begin{bmatrix} R_{pi} & -R_{ti} \end{bmatrix} \begin{bmatrix} \vec{\alpha}_p \\ \vec{\alpha}_t \end{bmatrix} = [-(\vec{v}_{pi} - \vec{v}_{ti})], \qquad i = 1, 2, ..., n. \tag{6.11}$$

Premultiplying both sides by $[R_{pi} - R_{ti}]^T$, the above equation becomes

$$\begin{bmatrix} \sum_{i=1}^{n} R_{pi}^T R_{pi} & -\sum_{i=1}^{n} R_{pi}^T R_{ti} \\ -\sum_{i=1}^{n} R_{ti}^T R_{pi} & \sum_{i=1}^{n} R_{ti}^T R_{ti} \end{bmatrix} \begin{bmatrix} \vec{\alpha}_p \\ \vec{\alpha}_t \end{bmatrix} = \begin{bmatrix} -\sum_{i=1}^{n} R_{pi}^T (\vec{v}_{pi} - \vec{v}_{ti}) \\ \sum_{i=1}^{n} R_{ti}^T (\vec{v}_{pi} - \vec{v}_{ti}) \end{bmatrix} \tag{6.12}$$

Since both the pelvis and thigh segments remain rigid, their rotational matrices are orthogonal. Therefore, the above equation becomes

$$\begin{bmatrix} I & -\sum_{i=1}^{n} R_{pi}^T R_{ti} \\ -\sum_{i=1}^{n} R_{ti}^T R_{pi} & I \end{bmatrix} \begin{bmatrix} \vec{\alpha}_p \\ \vec{\alpha}_t \end{bmatrix} = \begin{bmatrix} -\sum_{i=1}^{n} R_{pi}^T (\vec{v}_{pi} - \vec{v}_{ti}) \\ \sum_{i=1}^{n} R_{ti}^T (\vec{v}_{pi} - \vec{v}_{ti}) \end{bmatrix} \tag{6.13}$$

Solving the above equation gives the unknown position vectors of the HJC relative to $S_p$ and $S_t$. In the equation, the rotational matrices, $R_{pi}$ and $R_{ti}$, and translational vectors, $\vec{v}_{pi}$ and $\vec{v}_{pi}$ were obtained from segment level optimisation as described in Section 3.4.1.

#### 6.2.2.4 Data Collection and Analysis

A male subject (weight: 70 kg; height: 184 cm) who has received a Roentgen Stereophotogrammetric Analysis (RSA) to determine the co-ordinates of his right HJC [40] participated in the experiment. Data collection was performed

in the O.O.E.C. gait laboratory following the experimental protocol described in Chapter 3. Marker positions collected during subject calibration (standing in the anatomical position) were used to calculate the HJC using the formula provided by Bell *et al.* [17]. Two exercises were performed for the functional approach and the revised functional approach. The first involved a maximum hip flexion and abduction of the tested leg while standing on the other. During the exercise, the subject continuously flexed his hip, returned to the anatomical position and then abducted his hip joint before returning back to the anatomical position again. The second exercise was maximum hip circumduction. During both exercises, the subject was asked to keep his knee joint extended. Marker position data was collected for three cycles in each trial. For the functional approach, five markers, namely the greater trochanter (GT), mid-thigh (MT), lateral epicondyle (LE), head of fibula (FH) and lateral malleolus (LM), were used to calculate the HJC in order to study the effect of the choice of marker positions. The estimation error for each method was expressed by the distance ($\Delta$) between the estimated HJC and the true position measured with RSA.

#### 6.2.2.5 Results and Discussion

Since the above calculations were based on data measured from only one subject, a definite conclusion may not be appropriate. However, the results provided an opportunity for a closer examination of possible factors that can affect the outcome of the methods, which will give a guideline for the selection of a method suitable for a specific subject and purpose.

As shown in Table 6.1, the functional approach using FH position data from flexion-abduction exercise predicted the best result ($\Delta = 7$ mm). LM position data from maximum circumduction also predicted a result with the same error level. The biggest estimation error was from the revised functional approach, giving as much as 122 mm error during circumduction. The HJC obtained with prediction approach was 16 mm away from the true position, the second best among others, Table 6.1. Marker LE from maximum circumduction also yielded a result with an error level of 16 mm.

**Prediction Approach** Among the methods, the prediction approach was the easiest to implement. It was based on only one static measurement, standing position in the present study, so there was minimum soft tissue artefact involved. However, as discussed in Chapter 1, the current formula was derived from a

| *Flexion-Abduction* | | | | | | | |
|---|---|---|---|---|---|---|---|
| RMS | Prediction Approach | Functional Approach | | | | | Revised Functional Approach |
| | | GT | MT | LE | FH | LM | |
| $\Delta$x | -4 | 16 | 31 | 22 | 1 | 10 | 23 |
| $\Delta$y | 15 | 6 | -12 | -24 | 2 | -15 | -26 |
| $\Delta$z | 4 | 82 | 29 | 18 | 6 | 11 | 113 |
| $\Delta$ | 16 | 83 | 44 | 37 | 7 | 20 | 118 |
| *Circumduction* | | | | | | | |
| RMS | Prediction Approach | Functional Approach | | | | | Revised Functional Approach |
| | | GT | MT | LE | FH | LM | |
| $\Delta$x | -4 | 6 | -16 | -13 | 8 | -6 | 15 |
| $\Delta$y | 15 | 14 | 6 | 4 | -15 | -3 | -15 |
| $\Delta$z | 4 | 48 | -4 | -7 | 10 | 3 | 120 |
| $\Delta$ | 16 | 50 | 17 | 16 | 19 | 7 | 122 |

Table 6.1: Distance between the estimated and RSA determined HJCs in the pelvis co- ordinate system during flexion-abduction and circumduction exercises. The co-ordinates of the HJC measured with RSA is (-43, -90, 86). $\Delta$x, $\Delta$y and $\Delta$z are the three components of the distance, $\Delta$, along the three axes of the co-ordinate system. All the data are in millimetres. GT = greater trochanter; MT = mid thigh; LE = lateral epicondyle; FH = fibular head and LM = lateral malleolus.

limited number of cadavers so the accuracy of its application to subjects outside the data population is subject to doubt. For the present subject, the result was relatively accurate but for other subjects bigger errors may be expected [40]. Since the prediction approach provides a quick and easy means to estimate the HJC, it may be chosen if the subject under investigation is within the data population and if the application of the functional approach is prohibited due to restricted mobility of the subject's hip joint.

**Functional Approach** In contrast to the prediction approach, the functional approach works with a series of position data equi-distant from the HJC. However, because of the movement of the segment, skin movement artefact is a major factor affecting the outcome of the method. Theoretically, if a marker is far away from the HJC, the errors associated with marker movement will be very small. On the contrary, skin movement artefacts of a marker close to the HJC will have a significant effect on the estimation of the HJC. This effect was clearly seen in the

predictions from the GT, MT and LE. Given the same amount of skin movement, the LE marker (farthest) gave the best result whereas the GT (nearest) the worst. If the knee joint is perfectly fixed, the LM marker would have predicted the best result because it was the most distant marker on the leg. However, since the knee joint is not fixed, a small amount of flexion will give errors to the markers on the shank. For the markers on the shank, the more proximal the markers, the less the effect due to knee joint motion. During flexion-abduction exercise, since the movement happened in two very different directions, it was difficult to keep the knee joint extended. The effect was highlighted by the larger error with the LM marker. However, during circumduction the movement was continuous so the knee joint position was easier to maintain so the LM marker predicted the best result. From a practical point of view, since it is not certain that the subject will be able to keep the knee joint fixed, it is not recommended to use the FH or LM for the purpose of HJC estimation unless the relative movement between the femur and shank is properly prohibited. Based on the present study, it seems that the LE marker positions during circumduction give the best result when using the functional approach.

**Revised Functional Approach and Rigid Body Motion** Although both the prediction approach and the functional approach, with a proper choice of a reference marker (LE) and data collection exercise (circumduction), can predict the position of the HJC relative to the pelvis co-ordinate system with an accuracy of within 16 mm, the determination of the HJC position in the laboratory system and in the femoral system during motion represents another problem. Due to marker movement relative to the underlying bones, the femur and the pelvis do not move as two rigid bodies in the laboratory system about the HJC. Therefore, the global co-ordinates of the HJC calculated through the pelvis co-ordinate system will be different from that through the femoral co-ordinate system. To examine any possible discrepancies between the predicted HJC positions, the true HJC position was first assigned to the pelvis co-ordinate system and then represented in the femoral co-ordinate system in the subject calibration position. For the tested movements, the laboratory HJC co-ordinates were calculated both from the pelvis co-ordinate system and the femoral system. The discrepancies between the two were calculated. As shown in Figure 6.5, even though segment residual errors at both segments were relatively small, a big discrepancy in the HJC positions could exist. This explains why the revised functional approach,

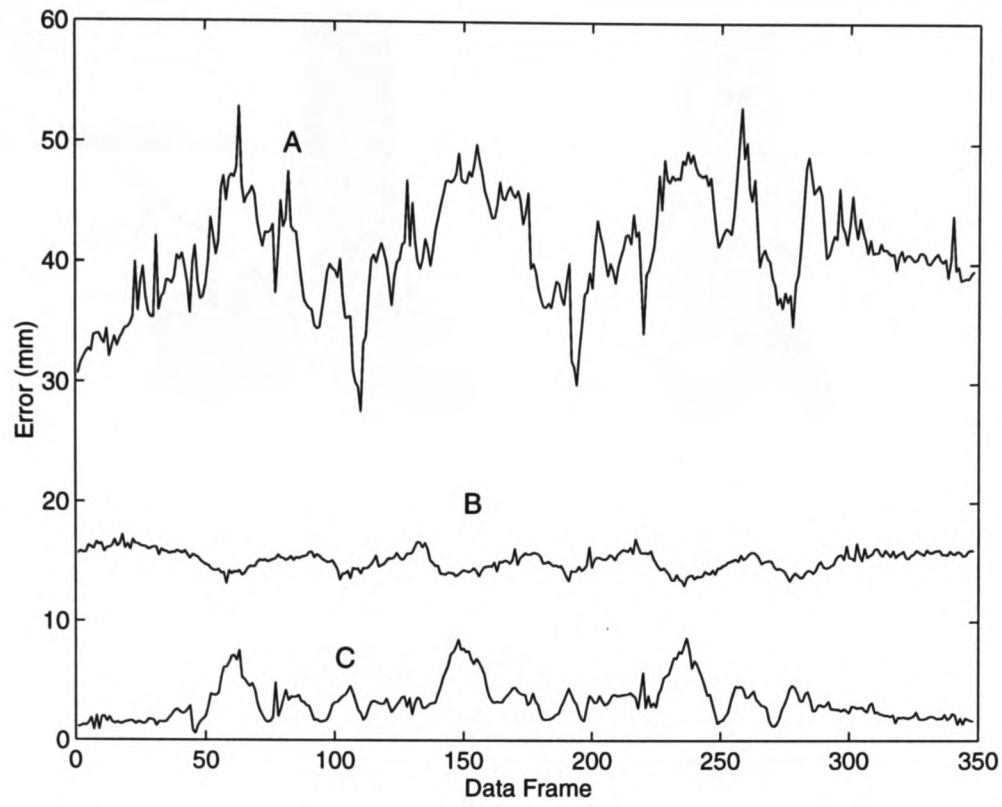



Figure 6.5: Errors associated with the rigid body assumption for the description of the motion of the pelvis-femur system. A: HJC errors; B: pelvis residual errors and C: femoral residual errors.

| | Pelvis | Femur | HJC |
|---|---|---|---|
| Flexion-Abduction | 15.2 (0.8) | 3.7 (2.2) | 44.7 (5.4) |
| Circumduction | 13.2 (1.8) | 4.4 (2.1) | 37.7 (2.5) |

Table 6.2: Time-averaged segmental residual errors and hip joint position errors during flexion-abduction and circumduction exercises. In parentheses are standard deviations.

which considers the rigid body assumption, predicted the worst result for the HJC. Skin movement artefacts were compensated when a single marker was used but when a rigid body assumption was considered all the errors associated with each marker were combined and magnified. It is noted that the HJC discrepancies were higher during flexion-abduction than circumduction, Table 6.2. This explains why results based on maximum circumduction were better than those predicted from the flexion-abduction exercise.

To accommodate properly the problem of apparent joint dislocations, a system level optimisation method for the determination of the orientation of a multijoint system was developed and will be described in the next chapter.

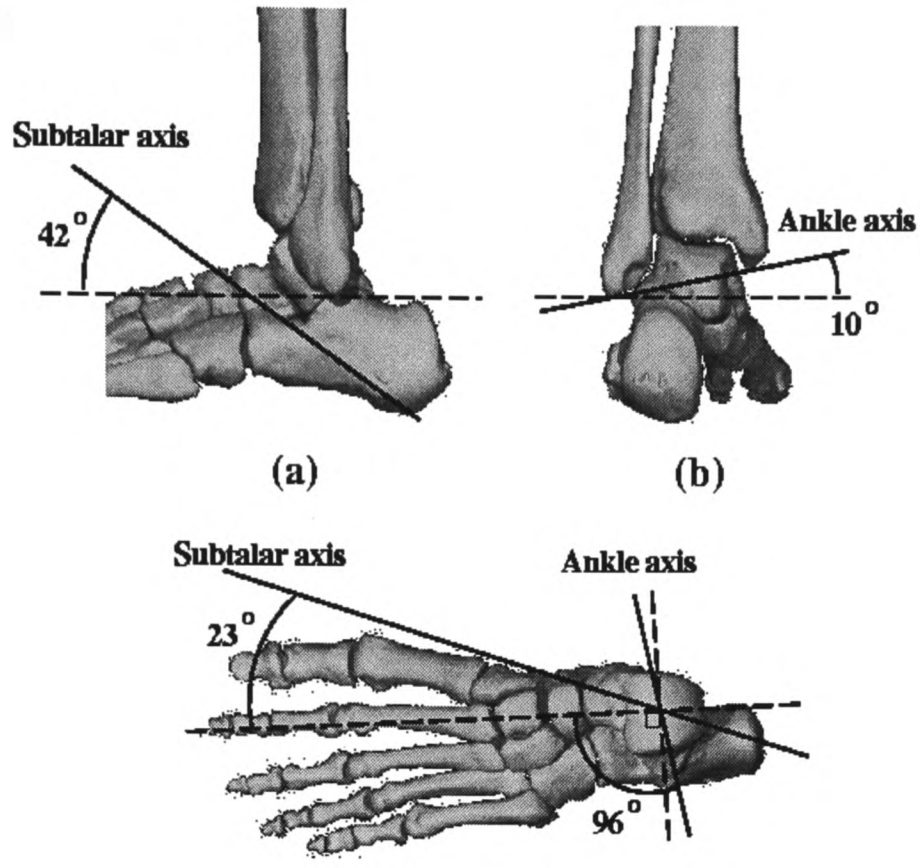



Figure 6.6: Axes of the ankle and subtalar joints: (a) sagittal view, (b) frontal view and (c) transverse view. Data compiled from Inman (1976)

## 6.3 Model of The Ankle Joint Complex

The human ankle joint complex, which connects the foot and the shank, can be functionally described as two separate sets of joints: the talocrural (or ankle) joint between shank and talus, and the talo-calcaneo-navicular (or subtalar) joints between talus and the foot [124]. In the present study, the ankle joint complex was modelled as a phenomenological joint with two hinges, one representing the ankle joint and the other the subtalar joint. The orientations of the two axes have been defined by the study of Inman [124] and were shown in Figure 6.6. According to Inman [124], the ankle joint axis was approximated by the line passing through the two malleoli which will make a 10° of tilt in the frontal plane and 6° inclination in the transverse plane. The axis of rotation of the subtalar joint was approximated by the line joining the navicular tuberosity and the lateral process of the calcaneus, making 42° inclination in the sagittal plane and 23° deviation in the transverse plane [124].

## 6.4 Force-Transmitting Structures

A geometric model serves as a preliminary to mechanical analysis. In order to obtain meaningful and useful information from the model, the force-transmitting structures of the locomotor system which need to be considered have to be included in the geometric model. However, the more numerous the structures included, the higher the degree of redundancy involved. Using the DDOSC method, this would mean an increase in the number of DD subproblems. Indeed, the selection of the force-bearing structures to be included will have a considerable influence upon the complexity of model that can be analysed and on the information that can be derived from the results of the analysis .

The muscles or muscle groups in the 3D lower limb model were selected with a view to reducing the unknown internal forces to a level at which the number of DD subproblems remains within a manageable limit without compromising the results that were meant to be given from the model, based on anatomical, physiological and mechanical considerations [171, 239, 257]. Muscles are neglected or grouped according the following criteria.

- Muscles with relatively small Physiological Cross-Sectional Areas (PCSAs) are neglected.
- Muscles with common functional activity are grouped together but with separate lines of action, based on EMG evidence.

In the subsequent mechanical analysis, the components of each group were assigned weighting factors corresponding to their PCSAs as a proportion of the whole area for the group. The assumption regarding PCSA as a weighting factor is made in the absence of any other factor that has been known to be a reliable predictor of load sharing between these synergistic muscles. The tension-bearing structures, namely the muscles or muscle groups and the ligaments, included in the present model are shown in Table 6.3. More detailed descriptions of the selection of these structures are given in the following sections according to the joint they span.

### 6.4.1 Knee Joint

In the sagittal plane model of the locomotor system described in Chapter 5, the cruciate ligaments were modelled as inextensible line elements so the four-bar

| *Muscle Groups and Ligaments* | | | |
|---|---|---|---|
| | Muscle Group | Muscle Unit | %PCSA |
| 1 | Iliopsoas | Iliacus | 48 |
| | | Psoas | 52 |
| 2 | Adductor Longus | Add longus | 100 |
| 3 | Adductor Brevis | Add brevis | 100 |
| 4 | Adductor Magnus | Add mag(m) | 50 |
| | | Add mag(p) | 50 |
| 5 | Glutial | Glut med(a) | 28 |
| | | Glut med(m) | 18 |
| | | Glut med(p) | 24 |
| | | Glut min(a) | 8 |
| | | Glut min(m) | 9 |
| | | Glut min(p) | 13 |
| 6 | Gluteus Max (f) | Glut max (f) | 100 |
| 7 | Gluteus Max (a) | Glut max (a) | 100 |
| 8 | Tensor Fasciae Latae | Ten fas lat | 100 |
| 9 | Rectus Femoris | Rectus fem | 100 |
| 10 | Med Hams | Semitendin | 33 |
| | | Semimembran | 67 |
| 11 | Lat Hams | Bic fem(l) | 77 |
| | | Bic fem(s) | 23 |
| 12 | Vasti | Vastus lat | 30 |
| | | Vastus int | 39 |
| | | Vastus med | 31 |
| 13 | ACL | | |
| 14 | PCL | | |
| 15 | MCL | | |
| 16 | Med Gas | Gastroc (m) | 100 |
| 17 | Lat Gas | Gastroc (l) | 100 |
| 18 | Soleus | Soleus | 100 |
| 19 | Ant tibial | Tibialis anterior | 55 |
| | | Ext dig long | 24 |
| | | Ext hal long | 21 |
| 20 | Peroneal | Peronius long | 56 |
| | | Peronius brev | 44 |
| 21 | Post tibial | Tibialis posterior | 51 |
| | | Flex dig long | 13 |
| | | Flex hal long | 36 |

Table 6.3: Muscle groups and ligaments considered in the three-dimensional lower limb model program. Also shown are the percentages of PCSAs of individual muscle units in their group.

linkage model could be used to determine their lines of action. The tibiofemoral contact forces in the two compartments were lumped and represented as a pure compressive force whose line of action was also determined by the four-bar linkage. Major knee muscles were grouped according to their function as extensors or flexors. In three-dimensions, however, a muscle may have a secondary and/or a tertiary function about the joint, apart from its primary function. For example, the semimembranosus is a primary flexor and a secondary adductor. Similarly, a ligament such as the ACL can transmit not only anterior but also medial shear forces due to its 3D orientation. Therefore, more detailed modelling of the 3D orientations of the muscles and ligaments are necessary for a better consideration of three-dimensional equilibrium.

Similar to the 2D model, the two cruciate ligaments and the medial collateral ligament were modelled in space as inextensible, straight-line elements attached to the bones at single points. These lines were taken to represent the lines of action of the resultant tensile forces transmitted by the ligaments. The directions of the lines of action of the ligaments changed relative to the tibia and femur continuously over the range of motion, as determined by the 3D knee model. The contact forces in the two compartments were modelled separately as pure compressive forces. Their lines of action were also defined by the 3D knee model.

As shown in Table 6.3, the musculature spanning the knee joint was reduced to eight groups: lateral gastrocnemius, medial gastrocnemius, lateral hamstrings, medial hamstrings, rectus femoris, vasti, tensor fasciae latae and gluteus maximus. Rectus femoris and vasti provided the extending moment at the knee through the patellar tendon whereas hamstrings and/or gastrocnemius were the main flexors. Knee abductors were the gluteus maximus and tensor fasciae latae, acting through the iliotibial tract. Medial hamstrings and medial gastrocnemius could also provide adducting moment at the knee. It is noted that all the muscles but the vasti were bi-articular muscles.

Sartorius, gracilis and popliteus were not considered explicitly in the model, because of their small PCSAs and/or small intrinsic lever arms [83, 173, 228, 256]. It was assumed that the moments exerted by these muscles at the knee were small compared to the other muscles.

### 6.4.2 Hip Joint

According to Crowninshield *et al.* [63], there are twenty-seven musculotendinous units at the hip which may be involved in force transmission. However, there are only six equipollence equations available at the joint. In order to facilitate later theoretical force analysis, the number of potential force-transmitting structures was reduced according to the principals set out above. The musculature controlling the movements at the hip was represented by eleven muscle or muscle groups: iliopsoas, adductor longus, adductor brevis, adductor magnus, glutei, mono-articular gluteus maximus, bi-articular gluteus maximus, tensor fasciae latae, rectus femoris, medial hamstrings and lateral hamstrings. Muscles excluded were sartorius, gracilis and small rotators of the hip. Rectus femoris and the iliopsoas were the main flexors whereas the mono-articular gluteus maximus, the medial and lateral hamstrings were the main extensors. The glutei included the gluteus minimus and medius, each represented by three parts: anterior, medial and posterior. Together with the tensor fasciae latae and bi-articular gluteus maximus, they provided the abducting moment at the hip. Adducting moments were mainly applied by the adductors, namely adductor longus, brevis and magnus. Here the adductor brevis and minimus were grouped together but with separate lines of action and force-sharing based on PCSAs.

The capsular ligaments of a normal hip (iliofemoral, ischiofemoral and pubofemoral) function primarily to constrain rotation and thus can only transmit load near the limits of the range of joint motion [64]. For example, extension is limited by tension in the iliofemoral ligament. Since the maximum angles of the hip motion encountered during the activities examined in this study take place within these limits, ligamentous constraints at the hip were not incorporated explicitly into the mathematical model.

The articular surfaces of the femoral head and the acetabulum were assumed to be frictionless and therefore the load transmitted between them was purely compressive. Thus, the line of action of the femoral-pelvic contact force lay along a common normal to the articular surfaces and passed through the HJC. Because the hip was modelled as a congruent articulation, the line of action of the resultant compressive force transmitted across the hip could lie anywhere along the surface of the femoral head as long as it remained within the embrace of the acetabulum.

### 6.4.3 Ankle Complex

There are twelve muscles and a complex arrangement of ligaments spanning the ankle joint complex. The musculature was represented by six muscles or muscle groups: medial gastrocnemius, lateral gastrocnemius, soleus, tibialis anterior group, peroneal group and tibialis posterior group. Gastrocnemius and soleus develop tension to provide plantar flexing moment at the ankle. Other plantar flexors also include peroneal group and tibialis posterior group. The peroneal group includes peroneus longus and brevis. Together they are also the main abductors of the ankle. The tibialis posterior group includes tibialis posterior, flexor digitorum longus and flexor hallicus longus. They are the main adductors. The tibialis anterior, extensor digitorum longus and extensor hallicus longus form the tibialis anterior group which is the main dorsiflexor. Plantaris was neglected in the present geometric model because of its small PSCA and small intrinsic lever arm about the ankle axis of rotation, compared to those of gastrocnemius and soleus [175].

The articular surfaces of the trochlea of the talus and the mortis formed by the tibia and fibula were assumed to be rigid and frictionless, transmitting pure compressive contact forces. The resultant talotibial contact force therefore passes through the axis of rotation of the ankle joint. Its line of action was characterised by three components along the three axes of the foot co-ordinate system and its point of application was described by the distance away from the centre of the joint which is taken as the mid point between the two malleoli. The ligamentous constraints of the ankle, namely the anterior and posterior talofibular, calcaneofibular and deltoid ligaments, were not included in the model [203].

## 6.5 Geometry of The Muscles and Their Tendons

Similar to the two-dimensional model described in Chapter 5, the origins and insertions of the muscles were approximated by single points. For muscles with broad attachments, further division into several units were used for better representation of the lines of action of the muscle. Each of these muscles or muscle units were then represented by a single line.

A set of muscle origin and insertion co-ordinates from White *et al.* [255] was used in the present study, Table 6.4.

| *Mean position (cm)* | | | | | | | | |
|---|---|---|---|---|---|---|---|---|
| | Origin | | | | Insertion | | | |
| *Muscle* | x | y | z | BCS | x | y | z | BCS |
| Iliopsoas | -3.1 | -4.5 | -3.8 | p | -2.3 | -3.4 | -7.2 | t |
| Add longus | -2.2 | -8.7 | -10.5 | p | -1.0 | -19.8 | -6.7 | t |
| Add brevis | -4.7 | -10.0 | -10.2 | p | -1.2 | -10.1 | -5.4 | t |
| Add min | -7.2 | -11.2 | -8.8 | p | -1.5 | -8.8 | -4.9 | t |
| Add mag(m) | -9.2 | -11.9 | -7.3 | p | -1.0 | -21.1 | -6.7 | t |
| Add mag(p) | -10.8 | -12.3 | -6.8 | p | -2.8 | -39.1 | -11.7 | t |
| Glut med(a) | -2.6 | 1.9 | 1.1 | p | -0.9 | 1.3 | -2.0 | t |
| Glut med(m) | -7.7 | 4.2 | -0.5 | p | -1.5 | 1.9 | -2.3 | t |
| Glut med(p) | -11.2 | 2.9 | -4.1 | p | -1.6 | 2.0 | -2.4 | t |
| Glut min(a) | -3.6 | 0.6 | -0.3 | p | -0.6 | 2.1 | -2.4 | t |
| Glut min(m) | -6.9 | 0.4 | -1.1 | p | 0.6 | 2.3 | -2.6 | t |
| Glut min(p) | -9.2 | -1.5 | -3.0 | p | 0.4 | 2.5 | -2.5 | t |
| Glut max | -15.1 | -1.4 | -6.8 | p | -1.5 | -7.5 | -4.2 | t |
| Ten fas lat | -1.1 | 0.7 | 1.0 | p | -1.9 | 3.1 | 2.3 | s |
| Rectus fem | -2.4 | -4.0 | -1.7 | p | 0.0 | 0.0 | 0.0 | s |
| Semitendin | -12.2 | -10.0 | -4.9 | p | -2.3 | -0.5 | -1.9 | s |
| Semimem | -11.0 | -9.9 | -4.4 | p | -4.6 | 1.4 | -1.5 | s |
| Bic fem(l) | -12.1 | -9.8 | -4.8 | p | -3.9 | 1.2 | 3.1 | s |
| Bic fem(s) | -0.4 | -18.6 | -4.1 | t | -3.9 | 1.2 | 3.1 | s |
| Vastus lat | -0.3 | -3.0 | -2.2 | t | 0.0 | 0.0 | 0.0 | s |
| Vastus int | 1.7 | -14.7 | -4.0 | t | 0.0 | 0.0 | 0.0 | s |
| Vastus med | -0.3 | -9.0 | -4.4 | t | 0.0 | 0.0 | 0.0 | s |
| Gastroc (m) | -2.0 | -38.0 | -7.9 | t | 0.5 | 0.0 | 0.2 | f |
| Gastroc (l) | -2.6 | -39.3 | -4.9 | t | 0.5 | 0.0 | 0.2 | f |
| Soleus | -4.2 | -3.2 | 0.1 | s | 1.0 | 0.0 | 0.2 | f |
| Tib ant | -1.6 | -9.1 | -0.3 | s | 14.1 | 0.5 | 0.3 | f |
| Ext dig long | -3.8 | -9.0 | 1.1 | s | 13.1 | -1.5 | 4.5 | f |
| Ext hal long | -4.2 | -19.0 | 0.0 | s | 22.7 | -2.6 | 3.0 | f |
| Peronius long | -4.6 | -5.5 | 2.0 | s | 13.4 | -0.8 | 2.4 | f |
| Peronius brev | -4.9 | -17.6 | 1.0 | s | 9.5 | -2.4 | 5.8 | f |
| Tib post | -4.4 | -13.6 | -0.7 | s | 11.1 | -0.2 | 0.2 | f |
| Flex dig long | -4.0 | -12.3 | -1.6 | s | 13.3 | -2.6 | 4.2 | f |
| Flex hal long | -5.4 | -19.7 | -0.4 | s | 22.6 | -3.8 | 2.8 | f |

Table 6.4: Mean position of muscle origin and insertion relative to body-embedded co-ordinate system (BCS) compiled from White *et al.* [255].

### 6.5.1 Wrapping Around Bones

As shown in Chapter 4, lever arms and lines of action of the muscles are affected by the representation of the muscle wrapping around bones. When a bone lies between the origin and insertion of the muscle, a simple straight line representation of its line of action would result in a nonanatomical situation where the muscle passes through the bone. While a detailed description of the path of a muscle wrapping around the underlying bone requires extensive knowledge of the three-dimensional geometry of the muscle and the bones, an approximation of the bony contours with simple cylinders and spheres can avoid the above non-anatomical situation and provide more accurate representation of the lines of action of the muscles. In the present model, the shafts of the femur and tibia were modelled as cylinders while the femoral head, greater trochanter and the two femoral condyles were modelled as spheres, Figure 6.7. The peroneal and tibialis posterior groups wrapped around the back of the two malleoli so they were modelled as wrapping around the cylinder defined by the two malleoli.

### 6.5.2 Lines of Action of the Muscle Tendons

For a muscle with origin $\vec{p}_{org}$ and insertion $\vec{p}_{ins}$ its line of action was defined by the unit vector pointing from its insertion to origin

$$\vec{l} = \frac{\vec{p}_{org} - \vec{p}_{ins}}{|\vec{p}_{org} - \vec{p}_{ins}|} \tag{6.14}$$

and the moment produced by a unit muscle force about a joint centre or a reference point $\vec{O}_j$ is calculated as the following

$$\vec{m} = (\vec{p}_{ins} - \vec{O}_j) \times \vec{l} \tag{6.15}$$

For the cases where the musculotendon wraps around the underlying bone, Equation 6.14 and 6.15 can be applied by appropriately substituting $\vec{p}_{org}$ and $\vec{p}_{ins}$ by wrapping points $\vec{p}_{wo}$ and $\vec{p}_{wi}$, Figure 6.7, calculated according to the wrapping models described in the previous section.

### 6.5.3 The Knee Extensor Mechanism

The knee extensor mechanism, formed by the patellar tendon, patella, patellofemora articular surfaces and quadriceps, provides an efficient means of transmitting the

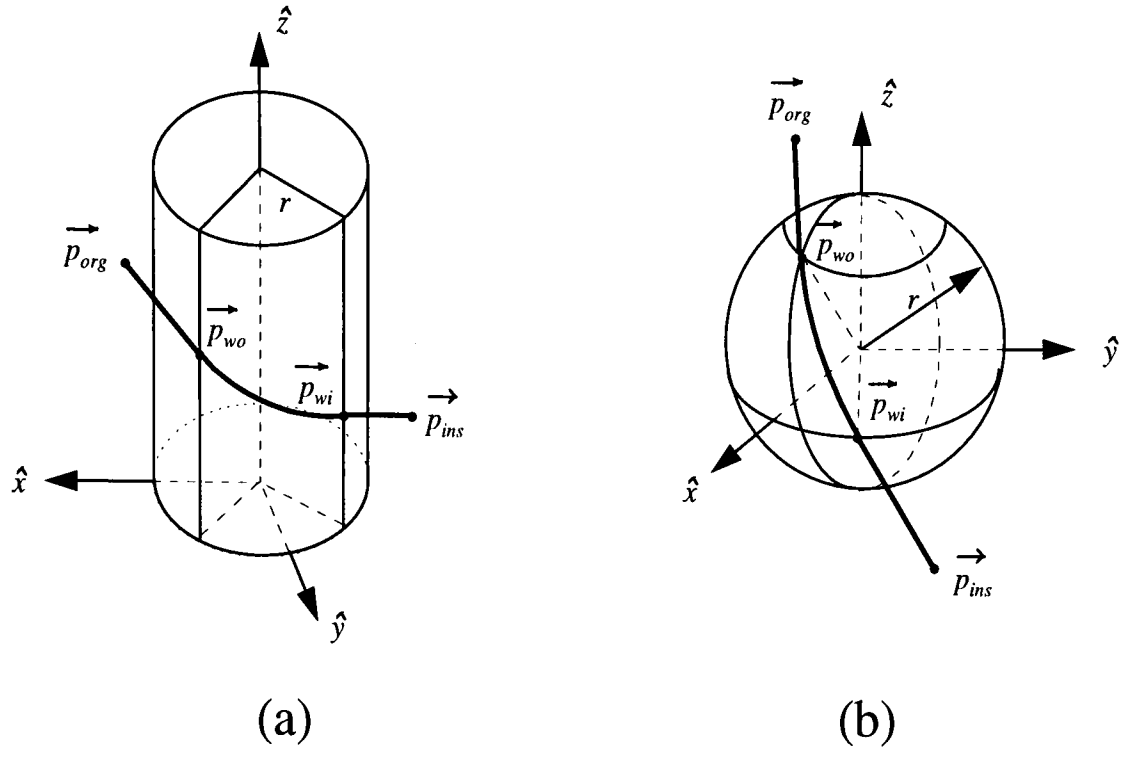



Figure 6.7: Two simple models for the description of muscles wrapping around the underlying bones: (a) a cylinder to simulate the shaft of a long bone such as the shaft of the femur and (b) a sphere to represent round bones such as the femoral head. $\vec{p}_{org}$ and $\vec{p}_{ins}$ are the position vecotrs of the origin and insertion of a muscle, respectively. The position vector of the wrapping point close to the origin of the muscle is represented by $\vec{p}_{wo}$ and the wrapping point close to the insertion of the muscle by $\vec{p}_{wi}$. The two wrapping points are determined by minimising the muscle length between the origin and insertion while subject to the constraint of the cylinder or the sphere.

quadriceps force to a powerful extending moment at the knee joint. A representation of the mechanism is required for a proper account of the forces and moments acting across the knee joint in the three dimensional model of the locomotor system.

The development of a full three-dimensional model of the patellofemoral joint to characterise the knee extensor mechanism is not straightforward. As discussed in Chapter 1, three-dimensional mechanical models such as those of Hirokawa [113] and Heegaard *et al.* [107] required detailed descriptions of the geometry of the articular surfaces and mechanical properties of the surrounding structures. The kinematics and mechanics of the joint had to be solved simultaneously under prespecified loading conditions. For the development of a geometric model, their approach was not preferred because loading conditions were usually not known as *a priori*. Moreover, incorporation of such a model would dramatically increase

the complexity of the entire locomotor system model and require much more computational effort. These will compromise the future applicability of the model in routine gait analysis.

A 3D analogy of the 2D anatomical model of the patellofemoral joint [93] described in Chapter 4 would be ideal but it would require simplification of the shape of the patella, the geometry of the articular surfaces and other geometrical constraints, based on experimental evidence. Such an attempt would cause an enormous increase of research effort and was beyond the present project limit. Therefore, it was decided to develop a phenomenological model of the patellofemoral joint as a first approximation. A 3D model analogous to the 2D model proposed by O'Connor *et al.* [183, 180] was developed. The 2D model was shown to predict satisfactory lines of action of the patellar tendon, quadriceps tendon and the patellofemoral contact force and was used for the estimation of the forces transmitted by these structures [183, 180].

The development of the 3D phenomenological model of the knee extensor mechanism is described in the following sections.

#### 6.5.3.1 Model Assumptions

Several simplifications and assumptions were made to facilitate the development of the 3D model:

- The patella was represented as a point, called the *patellar force centre.*
- The patellofemoral groove was approximated as a circular arc lying in the plane passing through the mid-point of and perpendicular to the transepicondylar axis [79]. Therefore, the patellar force centre moved in the same plane and at a constant distance about the patellofemoral groove axis which was parallel to the transepicondylar axis.
- Patellar tendon remained tight and isometric.
- The line of action of the rectus femoris was assumed to represent that of the quadriceps tendon.
- The three-dimensional motion of the tibiofemoral joint was controlled by the parallel spatial mechanism knee joint.

- The quadriceps force, patellar tendon force and the patellofemoral contact force should be concurrent and lying in the same plane to attain force equilibrium at the patellar force centre.

#### 6.5.3.2 Mathematical Description of The Model

With co-ordinates of the origin of the rectus femoris muscle ($RF$), insertion of the patellar tendon ($TT$), lateral epicondyle ($LE$) and medial epicondyle ($ME$) in the laboratory co-ordinate system $S$, the purpose of the patellofemoral joint model was to determine the patellar force centre, $PFC$, which defined the insertion of the quadriceps and the origin of the patellar tendon, and the line of action of the patellofemoral joint contact force.

Figure 6.8 shows a schematic representation of the geometry of the associated structures at the patellofemoral joint. For simplicity, a body-embedded co-ordinate system $S_{fem}$ was defined and fixed to the femur. $S_{fem}$ had an origin at $\vec{O}_{fem}$, which is the mid-point of the transepicondylar axis. The $z$ axis was along the transepicondylar axis and defined by

$$\hat{z}_{fem} = \frac{\hat{p}_{LE} - \vec{p}_{ME}}{|\hat{p}_{LE} - \vec{p}_{ME}|} \tag{6.16}$$

The $x$ axis was pointing anteriorly and perpendicular to both the $z$ axis and the long axis of the femoral shaft defined by a unit vector $\hat{n}_{FA}$, as follows.

$$\hat{x}_{fem} = \hat{n}_{FA} \times \hat{z}_{fem} \tag{6.17}$$

The $y$ axis was then defined by

$$\hat{y}_{fem} = \hat{z}_{fem} \times \hat{x}_{fem} \tag{6.18}$$

After defining $S_{fem}$, positions of $RF$ and $TT$ were transformed to $S_{fem}$ and the model was then described in the femoral co-ordinate system.

Define the patellofemoral groove axis $\hat{e}_{GR}$ which is parallel to $\hat{z}_{fem}$ and intersects with the $xy$ plane at the patellofemoral groove centre $GC$, the position of the patellar force centre can be calculated by considering the following geometric relations.

$$(\vec{a}_{TT} - \vec{a}_{PFC}) \cdot (\vec{a}_{TT} - \vec{a}_{PFC}) = L^2 \tag{6.19}$$

$$(\vec{a}_{PFC} - \vec{a}_{GC}) \cdot (\vec{a}_{PFC} - \vec{a}_{GC}) = R^2 \tag{6.20}$$

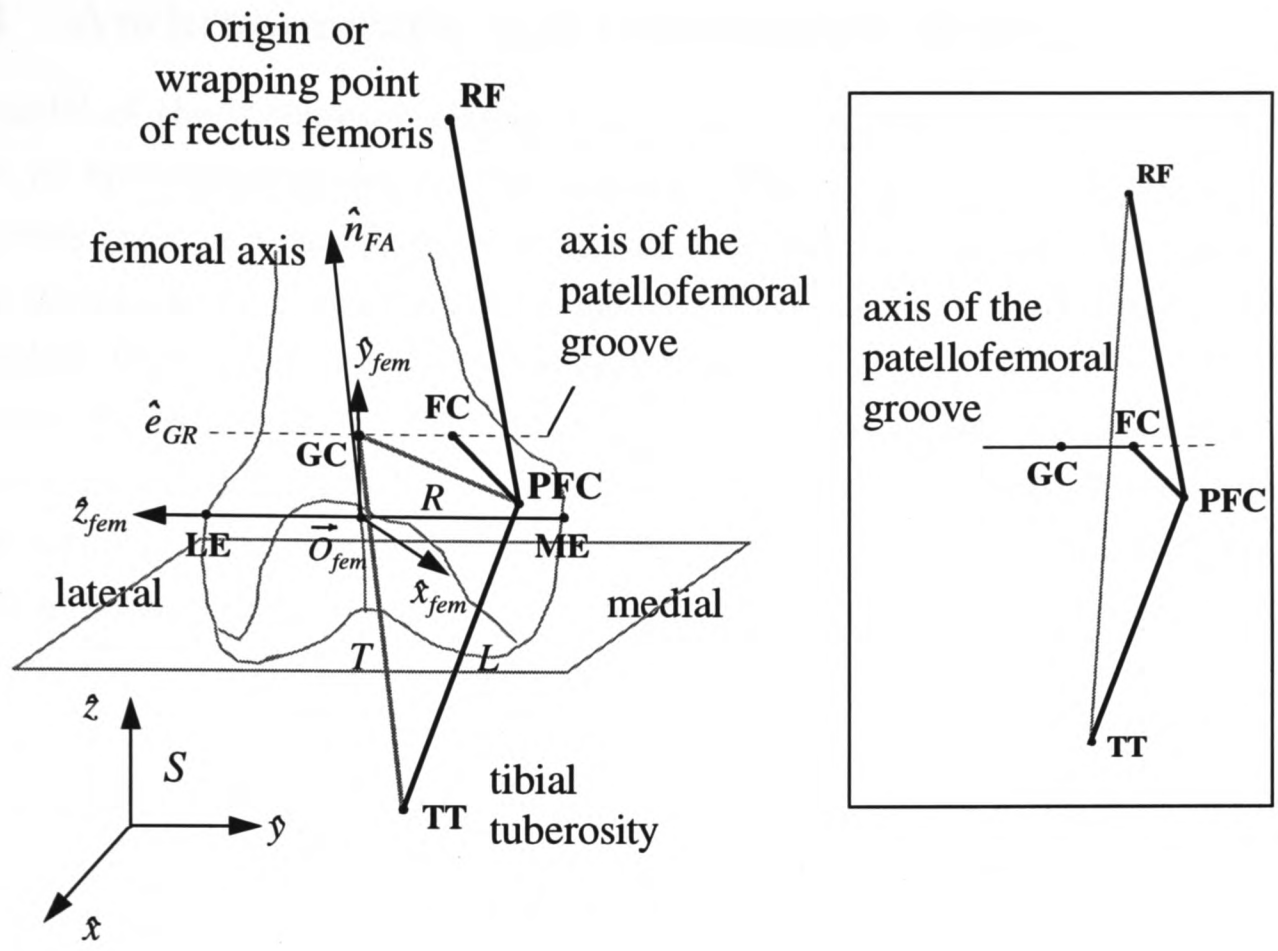



Figure 6.8: Schematic representation of the geometry of the structures at the patellofemoral joint. The inset figure shows the force equilibrium of the three forces at the patellar force centre.

$$\vec{a}_{PFC} \cdot \hat{z}_{fem} = 0 \tag{6.21}$$

where $\vec{a}_{TT}$, $\vec{a}_{PFC}$ and $\vec{a}_{GC}$ are position vectors of $TT$, $PFC$ and $GC$ in $S_{fem}$, respectively. $L$ is the length of the patellar tendon and $R$ is the distance between $PFC$ and $GC$. $L$, $R$ and $\vec{a}_{GC}$ are parameters of the model. Equations 6.19 and 6.20 require both $L$ and $R$ to be constant. Equation 6.21 ensures that the force centre remains in the same plane as the patellofemoral groove. Solving the above equations, the co-ordinates of the patellar force centre is obtained.

Since force equilibrium is required at the patella, the three forces acting at the patellar force centre, namely the quadriceps force, patellar tendon force and the patellofemoral contact force, should be concurrent and co-planar, Fig. 6.8. Since the patellofemoral contact force must also pass the patellofemoral groove axis, its line of action can be defined as the line joining $FC$ and $PFC$, Figure 6.8. $FC$ is the intersection of the patellofemoral groove axis and the plane formed by $TT$, $PFC$ and $RF$.

### 6.5.4 Anthropometric and Osteometric Scaling

The model of the locomotor system was scaled to individual subjects by a procedure of homogeneous osteometric scaling. This is based on the assumption that bones grow in a similar manner among individuals in an anthropometrically similar group. Several studies have suggested different schemes to scale database established from cadaveric measurements to living subjects for *in vivo* studies. According to Brand *et al.* [28] and White *et al.* [255], such a process can significantly reduce intersubject variability and therefore is a good starting point for the establishment of a customised model for future application to subjects in routine gait analysis. Scaling factors suggested by White *et al.* [255] and used in the present studies are shown in Table 6.5.

| Axis | Pelvis | Thigh | Shank | Foot |
|---|---|---|---|---|
| x | RASIS-RPSIS | - | - | HEE-FMET |
| y | - | GTRO-LEP | TT-LMA | - |
| z | RASIS-LASIS | LEP-MEP | LMA-MMA | - |

Table 6.5: Landmarks for homogeneous scaling

## 6.6 Three-Dimensional Computer Graphics Reconstruction and Animation

Computer graphics facilitate the visualisation of biomechanical models and their outputs in a very efficient way, as demonstrated by the two-dimensional modelling works described in Chapters 4 and 5. It brings the biomechanists and clinicians closer and makes biomechanical research results easier for clinical applications, which will eventually benefit the patients. Computer graphics visualisation and animation is particularly important and useful in three-dimensional modelling because, as described in Chapter 1, it would be extremely difficult for clinicians to reconstruct, from planar outputs, three-dimensional knowledge of the kinematics, kinetics and mechanics of the locomotor musculoskeletal system during a complex movement, without any technical assistance. Figure 6.9 shows the three-dimensional model of the locomotor system as stick figures in the sagittal plane during level walking. Pelvis-leg bones are represented by simply joining

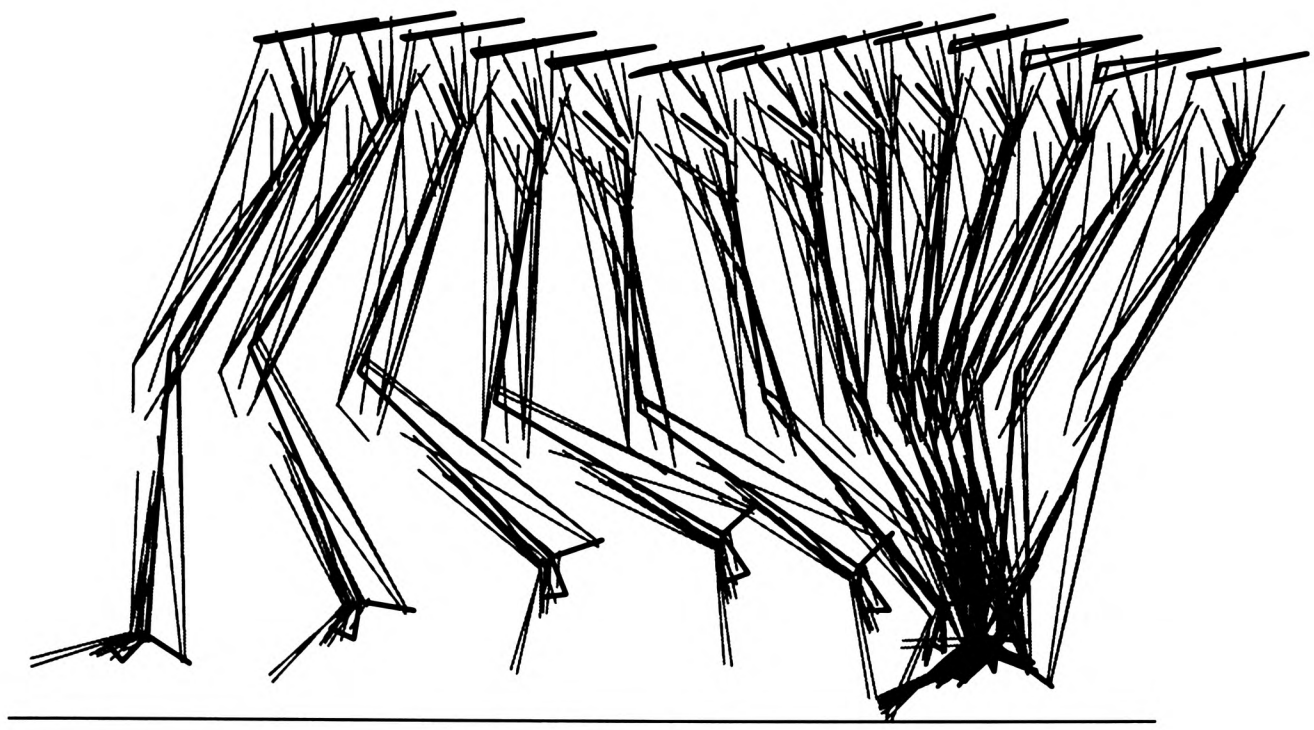


Figure 6.9: Stick figures of the three-dimensional model of the locomotor system during level walking in a series of positions.

lines between appropriate bony landmarks and muscles are also shown as single lines. All the lines are projected to the plane in which the image is to be displayed. From Figure 6.9 a general idea of the kinematic geometry of the system in the sagittal plane can be obtained but it is almost impossible to connect to a three-dimensional picture of the complex, time-varying geometry of the muscles and bones. A three-dimensional graphics display will help to create a more anatomical visualisation of the model. The three-dimensional reconstruction and animation of the present model using computer graphics techniques is described in this section.

### 6.6.1 Graphics Models

For visualisation of the whole model of the locomotor system, an important step was to describe mathematically or numerically the irregular shapes of the bones so that graphics models of each bone could be constructed. Muscles were represented as single lines or curves in the present studies so graphics models for the muscles were based on the paths calculated from the geometric model. Since bones are irregular in shapes, several methods have been used to obtain digitised data points on the bone surfaces [49, 68, 137]. The digitising process can be costly in effort and expense and usually involves extensive measurements and is also subject to the

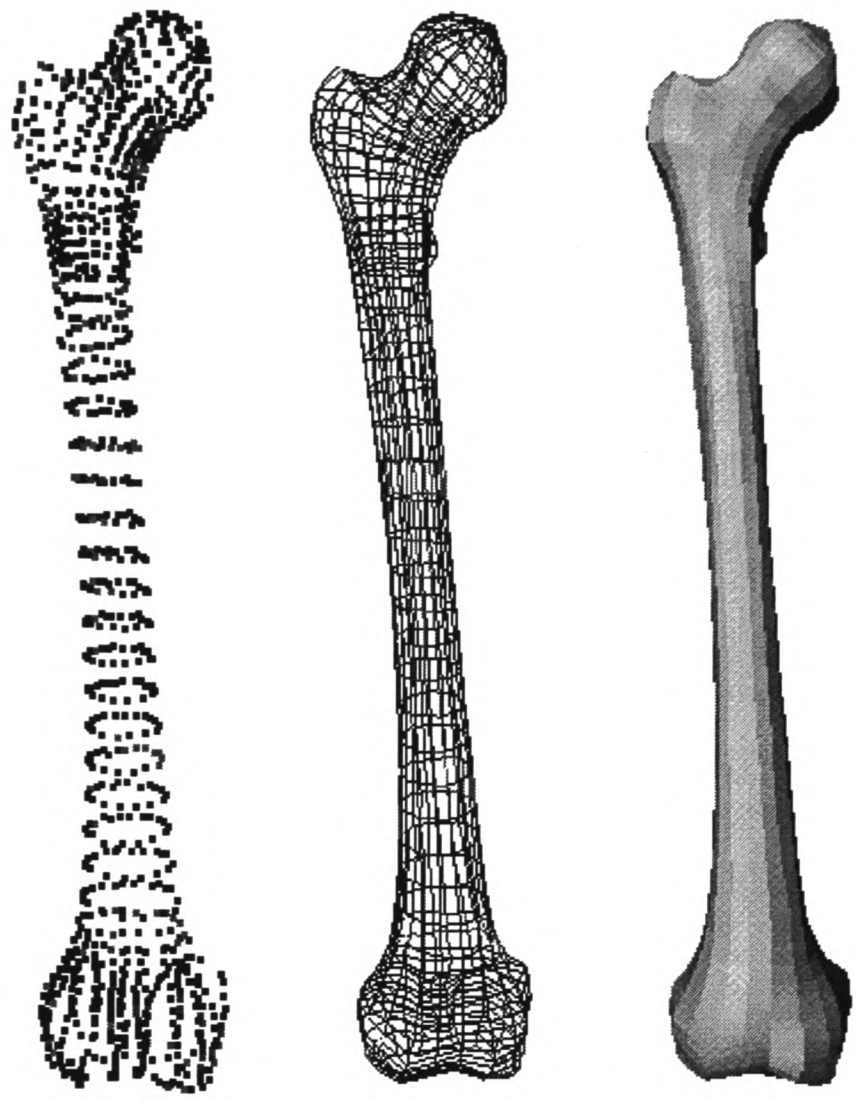



Figure 6.10: Three stages of reconstruction of a femur: (A) data points on the surface of the bone, (B) wire frame reconstruction and (C) rendering and lighting.

availability of the specimens. For the present study, a set of three-dimensional digitised data points defining the surfaces of the bones was obtained from the National Institutes of Health of the United States of America. These data were used to define a group of polygons (patches) which formed the wireframe models of the bones. In order to create realistic bone shapes and display onto the screen, these wireframe models were rendered under a single light source, simulating the shaded effects according to their normals in space. Reconstruction of a bone from surface data points, wireframe to the shaded solid model is shown in Figure 6.10 with the femur as an example.

Following the above procedure, generic graphics models of each bone were developed and implemented as reusable *objects*. Each object represents a type of data structure containing specific features which define the shape, size, rendering scheme (colour, texture and lighting), transformation information and muscle

attachment coordinates. Further features such as mechanical properties can be included. These objects can be duplicated and customised to a subject by feeding subject-specific parameters to the objects. Generic solid models for muscles and ligaments can be developed in the same manner once their volumetric information is available. However, since muscles and soft tissues change their shapes continuously during motion, a method which describes their deformation is needed before solid modelling can be attempted. For the present studies, muscles and ligaments were represented as either line objects or curve objects with the coordinates of a number of control points as main object features.

Using the *Object Oriented Programming* approach, an object can be replaced without affecting other objects or the entire model, which makes it easier for the future incorporation of new features and the establishment of databases of objects for different groups of subjects, normal or abnormal. This approach also enhances subsequent application to simulate surgical procedures.

All the graphics models were implemented on a Graphics Workstation (Silicon Graphics Indigo Extreme) using a graphical toolkit, Open Inventor, to take advantage of the powerful graphics hardware features and excellent software support.

### 6.6.2 The Computer Graphics-Based Animated Model

With graphics models as reusable objects, three-dimensional graphical reconstruction of the locomotor system model was made possible. For each subject, objects were created from the generic graphics models and customised to each subject by changing the features of the objects according to the 3D geometric model. The relative motion of these graphics models was also controlled by the locomotor system model. A graphics display window with four sub-windows was developed. Each sub-window provides a different view point. One of them provides a perspective view and the user is allowed to change his view point by moving the mouse pointer to choose an optimal display of the model. Details of the model can also be obtained by zooming into the area of interest. Animation of the model can be visualised in the graphics window, Figure 6.11. Ground reaction vector was incorporated into the display and further information such as EMG activity and joint force vectors can also be encapsulated into the graphical display. The advantage of 3D computer graphical display is clearly shown by comparing the anatomical graphics model in Figure 6.11 to the stick figure representation

in Figure 6.9 and to the primitive stick figure model from the Vicon system in Figure 3.9.

## 6.7 Kinematics of Multi-Joint Skeletal Systems From Co-ordinates of Markers

### 6.7.1 Introduction

As described in Chapter 3, several optimisation methods (least square methods) have been developed for the calculation of the kinematic variables of a rigid body from co-ordinates of markers considering possible measurement errors [45, 36, 223, 229, 249]. These variables, usually a rotation matrix and a translation vector, describe the motion from one reference position to another. Using these methods to study joint kinematics during activity involves the calculation of the kinematic variables on adjacent segments separately and then calculation of the joint orientation from the transformation matrix from one segment to the other. However, this approach can produce nonanatomical displacements at the joints [137] and thus lead to unreliable values of joint kinematics [90, 143] and uncertainties of joint kinetics. This is mainly due to measurement errors, especially skin or soft-tissue movement on the underlying bone. Although these optimization methods take account of these errors at the segmental level, joint constraints are not considered and joint dislocation can happen as the skin movement pattern at each segment may be quite different. Efforts have been put forward to the improvement of measurement techniques to minimise skin movement artefacts (e.g. Cappozzo *et al.* [39]) but these artefacts cannot be eliminated unless markers are applied directly or invasively through pins to the bone [143, 86].

While experimental and numerical techniques have both been proposed to take account of measurement errors, mathematical models of the musculoskeletal system which were developed to calculate kinematic and kinetic variables during activity did not consider the potential errors explicitly. In a study of the elbow joint, Chao and Morrey [50] calculated the rotation matrix $R$ from two vectors, pointing from one of the three segmental markers to the other two. The effects of the deformation of the array of the markers due to soft tissue movement were not taken into account. A similar approach has been used in most models for

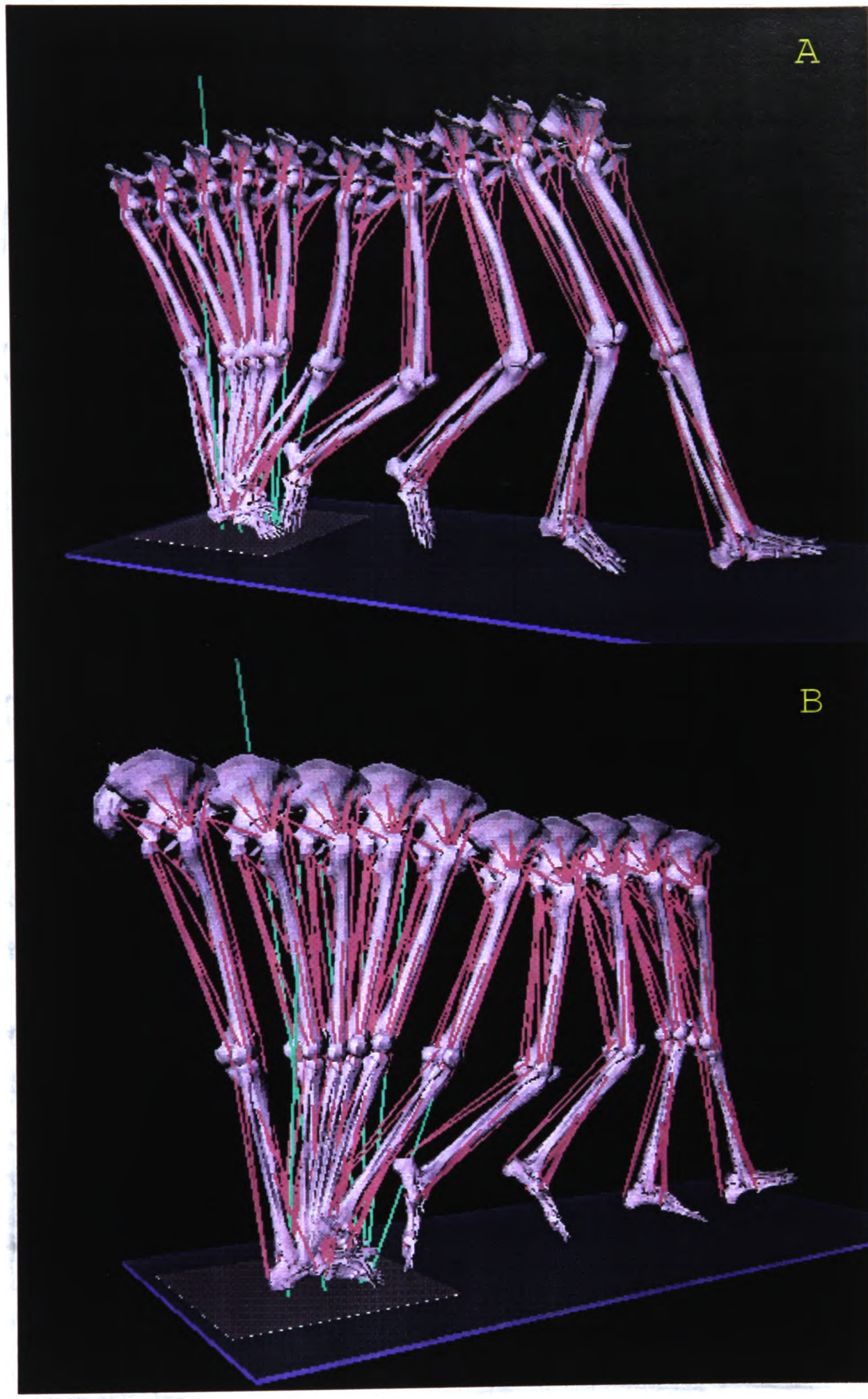



Figure 6.11: Animation of the 3D model of the locomotor system as a series images using data obtained from a normal subject: (A) anterolateral and (B) posterolateral view. Ground reaction forces are shown as green lines. The length of a GRF vector of one body weight was scaled to the height of the ASIS so that the dynamic effect of the motion can be viewed by the length of the GRF.

gait studies (e.g. [9, 134]). Further improvement of this approach was to consider segment level skin movement errors but joint centre positions calculated from each of the adjacent segments showed amplified errors [137]. The potential effects of these errors on the estimation of muscle lines of action and lever arms have not been studied but it is quite likely that uncertainties will arise in using marker position data to estimate forces transmitted in muscles and other structures.

Generally, simple joint models such as ball and socket joints or hinge joints were assumed in lower limb models for the study of the mechanics of joints or movement analysis [9, 63, 196, 222]. However, due to skin movements joint centre positions calculated from one segment will differ to a certain degree from the other depending on the level of errors involved, Figure 6.5. This will introduce errors to the mechanics of each segment and thus to the calculated values of the resultant forces and moments at joints, resulting in inaccuracies in the estimation of forces transmitted in the force-bearing structures. There is a need to take account of the measurement errors while using the marker position data to determine the kinematics and kinetics of the multi-joint systems considering the joint constraints. The purpose of this section was to propose a new method based on a least square approach to determine the spatial position of a multi-joint model of the locomotor system which may serve as a potential method for reducing measurement errors mathematically, including skin movement artefacts.

### 6.7.2 General Description of The Method

For a $n$-joint model, its position can be fully described by the three angles and three displacements of a reference link, $\vec{v}_0$ and $\vec{\theta}_0$, and joint variables ($\vec{v}_i$ and $\vec{\theta}_i$) of the $n$ joints. The basic concept of this new approach is to find the position of the multi-joint model such that the differences between measured marker co-ordinates and model-determined co-ordinates are minimised in a least square sense. Since the links of the model are rigid, the segment level rigid body assumption is automatically satisfied. The new approach can then be regarded as a global optimisation at the system level. The system level optimisation can be stated as follows:

Find design variables $\xi = [\vec{v}_0; \vec{\theta}_0; \vec{v}_1; \vec{\theta}_1; \vec{v}_2; \vec{\theta}_2 \cdots; \vec{v}_n; \vec{\theta}_n]$ to minimise the error function

$$f(\xi) = [P - P'(\xi)]^T W [P - P'(\xi)] \tag{6.22}$$

where $P$ and $P'(\xi)$ are the column vectors of the measured and model-calculated

co-ordinates of the markers, respectively and $W$ is a positive definite weighting matrix. For a given $\xi$, $P'(\xi)$ are calculated by transforming the co-ordinates of the markers in the subject calibration position to the current position. Therefore, geometrical relationship of the markers on each segment will remain unchanged because of rigidity. For simplicity, the number of markers on each segment $m$ is taken to be the same in the current formulation but different number of markers can be used. The weighting matrix $W$ is of the following form

$$W = \begin{bmatrix} W_0 & 0 & 0 & 0 \\ 0 & W_1 & 0 & 0 \\ 0 & 0 & \ddots & \\ 0 & 0 & 0 & W_n \end{bmatrix} \tag{6.23}$$

where $W_i$ is a $(3m \times 3m)$ weighting matrix assigned to the $ith$ segment. $W_i$ can be used to reflect the error distribution among the markers but for simplicity $W_i$ is chosen to give equal weighting for the markers on a segment. However, to reflect the amount of skin movement artefact on each segment, it is proposed here to use the residual square error of each segment as the corresponding weighting factor. For example, as shown by Cappozzo *et al.* [39], skin movements on the thigh are much bigger than on the pelvis and shank, with bigger residual square error; the weighting factor assigned to the thigh therefore must be less than those to the pelvis and shank. For each data frame, a segment level optimisation is performed on each segment to determine its transformation variables, as described in Section 3.5. The residual square error $e_i$ from reference geometry is also calculated to provide an index of the amount of marker frame deformation and serves to define the weighting matrix $W_i$,

$$W_i = \frac{1}{e_i} I \tag{6.24}$$

Since the resulting system level optimisation problem is a non-linear programming problem, it has to be evaluated numerically using iterative optimisation methods. Therefore, an initial guess for the design variables is needed. For this purpose, the transformation variables obtained during the segment level optimisation can be used as a very good initial guess.

In the present study, the new method was used to determine the position of the model of the locomotor system in space for further mechanical analysis.

## 6.7.3 Application to The Present Model

### 6.7.3.1 Model Variables

For the present model, the pelvis segment was chosen as the reference link. Its orientation, defined by the BCS $S_p$, was described by the transformation variables, $R_p$ and $\vec{v}_p$, relative to the LCS $S$. As described in Chapter 2, the $3 \times 3$ matrix $R_p$ can be further represented by three independent Cardan angles $(\phi_{px}, \phi_{py}, \phi_{pz})$. Therefore, a total of six variables were needed to describe the orientation of the pelvis link: $v_{px}, v_{py}, v_{pz}, \phi_{px}, \phi_{py}$ and $\phi_{pz}$. Any marker with a position vector $\vec{a}_p$ in the BCS can be transformed to the LCS once the six variables are given. This is given by

$$\vec{p}_p = R_p \vec{a}_p + \vec{v}_p \tag{6.25}$$

where $\vec{p}_p$ is the position vector in LCS.

Since the hip joint was modelled as a ball and socket joint, three joint angles were sufficient to describe the orientation of the thigh segment relative to the pelvis. With prescribed position vectors of the HJC $\vec{\alpha}_p$ and $\vec{\alpha}_t$ in $S_p$ and in the thigh BCS $S_t$, respectively, a marker with a position vector $\vec{a}_t$ in $S_t$ can be transformed to the LCS through $S_p$ as follows

$$\vec{p}_t = R_p(R_{t/p}(\vec{a}_t - \vec{\alpha}_t) + \vec{\alpha}_p) + \vec{v}_p \tag{6.26}$$

where $R_{t/p}$ is the rotation matrix from thigh to pelvis and is constructed by the three joint angles $(\phi_{hx}, \phi_{hy}, \phi_{hz})$.

The orientation of the shank segment relative to the thigh was controlled by the parallel spatial mechanism model of the knee with a mobility of unity. In other words, the joint angles and the displacements were all coupled so that only one variable was needed to define the joint position. In this case, the knee joint flexion angle $\phi_k$ was chosen as the joint variable and the transformation variables were all functions of it. Similar to thigh markers, a vector $\vec{a}_s$ in $S_s$ was transformed to the LCS by substituting $\vec{a}_t$ in Equation 6.26 by

$$R_{s/t}\vec{a}_s + \vec{v}_{s/t} \tag{6.27}$$

where $R_{s/t}$ and $\vec{v}_{s/t}$ were the rotational matrix and translational vector from shank to thigh, respectively, and were unique for a given $\phi_k$.

Between the foot and the shank, there were two revolute joints, each defined by a joint variable. For the ankle joint, the joint variable was the angle about the

axis of rotation designated by $\phi_u$. Similarly, the angle $\phi_l$ about the subtalar joint axis was taken as the second joint variable. A vector $\vec{a}_f$ in the foot system $S_f$ can be transformed to the shank system through the talus segment by the following transformation

$$R_{tal/s}(R_{f/tal}\vec{a}_f + \vec{v}_{f/tal}) + \vec{v}_{tal/s} \tag{6.28}$$

where $R_{f/tal}$ and $\vec{v}_{f/tal}$ are the transformation variables from foot to talus and The resulting vector can be further transformed to the LCS through the thigh and pelvis to get its laboratory coordinates.

Given the model parameters, the orientation of the model of the locomotor system was fully described by a set of the above described 12 model variables which was represented as a column vector

$$\xi = [v_{px}; v_{py}; v_{pz}; \phi_{px}; \phi_{py}; \phi_{pz}; \phi_{hx}; \phi_{hy}; \phi_{hz}; \phi_k; \phi_u; \phi_l) \tag{6.29}$$

#### 6.7.3.2 Solution Algorithm

The algorithm used to determine the orientation of the present model is summarised as follows. However, with proper selection of model variables, this algorithm can also be applied to other multi-joint models such as the upper limb.

1. Establish a fixed relationship between markers and the segment to which they are attached, from data obtained during subject calibration. The position vectors of these markers in the BCS will not change during motion because they represent the true motion of the bones.

2. For each data frame, perform segment level optimisation to determine transformation variables of each segment considering segmental marker movements. The residual square errors between the current marker configuration and the rigid frame are used as the weighting factors for each segment. From these transformation variables, a first estimation of the design (model) variables can be made and will serve as the initial guess for the subsequent iterative procedure of the system level optimisation.

3. Use a nonlinear optimisation method to solve the above optimisation problem.

The above solution algorithm was incorporated into the present locomotor system model for the determination of the optimal orientation of multi-joint system. Unweighted system residual errors were used to provide a measure of the

quality of the measured marker co-ordinates. The application of this measure for the selection of proper experimental trials for further mechanical analysis will be discussed in the next chapter.

### 6.7.4 Discussion

Segment level optimisation has provided a good basis for the study of the motion of a single segment with consideration of errors introduced by the assumption of rigidity. However, as far as the multi-joint system is concerned, least square fit at segment level does not necessarily guarantee a system level optimum. The differences between the end points (joint centres) calculated from each segment have been used as a measure of measurement error [137]. However, the problem of the determination of the position of a multi-joint system model considering both joint constraints and skin movement artefacts are more important for the study of joint kinematics and multi-joint movements. A reliable procedure for the calculation of the position of the multi-joint model from spatial markers is essential. The residual unweighted square error provides a measure of both the rigid body assumption and the assumptions associated with the joint models. The selection of the weighting factors according to the amount of the measurement errors allows the compensation of errors of a segment from other segments with more accurate measurements. With relatively accurate modelling of the joints, for example accurate knowledge of the HJC, the proposed approach may be used to reduce the effects of measurement errors on the calculation of the kinematics and kinetics of the multi-joint system.

It should be noted that the proposed method was formulated assuming that each joint of the system is properly modelled. Its application to patients should take account of the specific motion characteristics of the affected joints.

# Chapter 7

# Three-Dimensional Analysis of Forces in The Locomotor System: Evaluation and Validation [1]

The three-dimensional geometric model of the locomotor system described in the previous chapter provides a necessary basis for a full analysis of the forces transmitted by the force-bearing structures of the locomotor system. It can be applied to the study of a wide range of activities such as standing and walking, to which 2-D models can make limited contribution due to the 3-D nature of these activities. However, although a 3-D model is able to overcome some of the limitations of a 2-D model, the inclusion of one more dimension inevitably increases the complexity of the model and the uncertainty of the model predictions. Therefore, before it can be applied to a larger population of subjects, comparison is necessary with measurements from the patients described in Chapter 3.

In this chapter, the use of the 3-D geometric model for the analysis of the forces transmitted in the locomotor system during the isometric tests, single and double leg stance and level walking is presented. The DDOSC method was used to resolve the redundancy problem. The results obtained from the model were compared to the telemetered internal forces, which represented a quantitative evaluation and validation of the model. The evaluation is useful for the determination of aspects of the model which require further development. On the other hand, once validated, insight into some important yet controversial biomechanical

[1] Part of the material in this chapter has been presented at the 3rd International Symposium on Computer Methods in Biomechanics and Biomedical Engineering, Barcelona, Spain, 1997 [156]. Co-authors: J.J. O'Connor, S.J.G. Taylor and P.S. Walker

issues could be gained and suggestions could be made from the validated model calculations.

## 7.1 Experimental Data and Tests

### 7.1.1 Model Examination of the Quality of Kinematic Data

Since the kinematic (geometric), kinetic and structural analyses of the locomotor system were dealt with separately and sequentially in the present studies, kinematic data obtained from the two instrumented subjects could be examined using the geometric model before further mechanical analysis. This was to ensure a reasonable level of quality of the kinematic data because the orientation of the multi-joint model and thus the lines of action of all the force-bearing structures relied very much on the marker positions. It was hoped to limit the variability of the likely errors introduced by kinematic data so that a more reliable evaluation of the model could be performed.

Kinematic data from each trial was first used to calculate the orientation of each segment using segment level optimisation. Since some markers might be obscured in the course of data collection, spline fitting techniques, Section 3.5.1, were used to interpolate the positions of the missing markers. Three-dimensional computer graphics models were then used to reconstruct the locomotor musculoskeletal system. This allowed the visual inspection of the quality of the kinematic data. If there was only reasonably small joint dislocations, it was assumed that the kinematic data was suitable for further mechanical analysis with system level optimisation corrections. Otherwise, the data should be discarded.

During the examination process, it was found that the RASIS marker of subject DG was obscured during most of the trials and broken trajectories were also found for the MTHI marker due to the interference from the energiser coil and wiring of the prosthesis applied at the mid-thigh. After applying spline fitting to fill the gaps in these broken trajectories, unsatisfactory hip joint dislocations were still present in the three-dimensional graphics reconstruction. Since these obscured markers were not required in the 2-D calculations, their effects were not significant. However, in three-dimensions one obscured marker would cause difficulties in the calculation of segment orientations if less than three were left on each segment. Data interpolation was useful for a small number of affected

frames but was not as effective if the marker trajectory was broken for a long period of time, which unfortunately was true in the case of DG . Attempt was made to repeat experiments on DG during a second visit to the O.O.E.C. but permanent damage to the internal prosthesis coil was found before starting data collection so the experiment had to be abandoned.

The quality of IM's kinematic data was proved to be good and less variable following the same checking process. The unweighted system residual errors calculated with system level optimisation were less than 1 cm during static tests and 1.5 cm during level walking. For the purposes of model evaluation and validation, a better data set was necessary to provide a good reference for the theoretical calculations. Therefore, the evaluation and validation of the present 3D model had to be limited to the data from IM.

### 7.1.2 Tests

The full set of tests described in Chapter 3 were considered in the present study: isometric tests of hip muscles, single and double leg stance and level walking.

### 7.1.3 Isometric Tests

Isometric tests were designed to maximise the lever arms available to the external forces so that limb moments at joints and at the level of prosthesis transducers were maximum. This provided a clear and direct situation in which the percentage of the total limb moment transmitted by the bones could be examined. Also since external moments were balanced mainly by appropriate agonist muscles, the influence of muscle activity on the forces and moments in the bones was easier to identify. Isometric tests on the hip flexors, extensors, abductors and adductors were each analysed using the 3D model.

### 7.1.4 Stance Postures

Double and single leg stance were of fundamental importance because double leg stance (DLS) is a frequent posture in daily life and also a preliminary to walking while single leg stance (SLS) resembles the single stance phase of slow walking. They also represent two extremes of daily weight bearing. Values obtained from these tests should provide a range of forces transmitted in the locomotor system during daily living. As indicated in Chapter 3, the tensor fasciae latae (TFL)

was almost silent during DLS but as soon as the subject shifted his weight to his instrumented leg, a significant increase of EMG activity in the TFL was seen, indicating force build-up in the IT. The EMG envelope reaches its maximum when the subject was finally standing with single leg. The measured axial forces were less than one body weight during DLS and reached 3.1 times body weight during SLS, Section 3.6.2. Since the 2D model in Chapter 5 would underestimate the axial forces in the bones during the standing postures as it did for walking, it was hoped the 3D model would provide a complete picture of the force transmission between the two postures.

### 7.1.5 Level Walking

Level walking is a complex activity and represents a great challenge to a theoretical model. The 2D model underestimated the axial forces in the femur during level walking. With the inclusion of adductors and abductors and consideration of three-dimensional loading, it would be interesting to see if the 3D model would predict forces that matched the telemetered internal forces.

## 7.2 Mechanical Analysis

Complete three-dimensional inverse dynamics analyses were performed to calculate resultant intersegmental forces and moments and those at the level of the prosthesis transducers during each test, Chapter 2. Associate force distribution problems were then formulated to determine the force sharing among the force-bearing structures involved. The indeterminate force distribution problem was resolved using the DDOSC method.

Based on the 3D geometric model, there were 32 system unknowns to be determined from the 18 equipollence equations at the hip, knee and ankle. With the DDOSC method, there were a total of $4.7 \times 10^8$ DD subproblems to be considered. Since each DD subproblem represented a determinate system, a partial set of the equations could be used to give solutions to some of the system unknowns which would remain unchanged even when further equations were considered. In other words, if a DD subproblem involved only six structures at the knee, consideration of the six equations at the joint would be sufficient to determine the force transmission at the joint. However, since there were several bi-articular muscles crossing the knee joint, this condition might not happen very often. Mechanical

analyses performed only at the knee joint [58, 131, 132, 172, 217] may not represent the actual force distribution. In order to compare with telemetered femoral axial forces, a full knowledge of the forces transmitted by all the muscles crossing the femur was needed. Since all bi-articular muscles except the two heads of the gastrocnemius spanned the knee and hip joints, for the determination of the force distribution in the femur, the equipollence at the hip and knee were considered to be sufficient.

## 7.2.1 Problem Formulations

### 7.2.1.1 Number of Model Unknowns

Since lines of action of muscles, ligaments and the tibiofemoral contact forces were determined from the geometric model, only force magnitudes were considered as system unknowns except for the hip where the total joint contact force was defined by three orthogonal force components. Therefore, there were twenty-two unknowns to be determined for the twenty structural members. Symbols used to represent these system unknowns are shown in Table 7.1. It is noted that since the gluteus minimus and medius were sutured to the fasciae latae during surgery, it was modelled as a bi-articular muscle group that could affect the forces transmitted both at the hip and knee joints, as well forces in the femur.

### 7.2.1.2 Equations for Structural Analysis

Since the intersegmental forces and moments calculated must be provided by the corresponding force-bearing structures, they represent a force/moment system that is dynamically equivalent to (or equipollent with) the system formed by the actual force-bearing structures, such as muscles, ligaments and bones. At the knee, the two vector equipollence equations at the knee force centre, defined by the mid-point of the transepicondylar axis, can be expressed in the following form

$$\sum_{i=1}^{n_k} F_i \vec{l_i} = \vec{R}_k \tag{7.1}$$

$$\sum_{i=1}^{n_k} \vec{d_i} \times (F_i \vec{l_i}) = \vec{M}_k \tag{7.2}$$

where $F_i, \vec{l_i}$ and $\vec{d_i}$ are the force magnitude, unit vector of the line of action and lever vector of the *ith* structure, respectively; $\vec{R}_k$ is the resultant force; $\vec{M}_k$ is the resultant moment; and $n_k$ is the number of unknowns.

| **System Unknowns** |
|---|
| **Force-Bearing Structures at the Knee** |
| mK = Magnitude of the Medial Knee Contact Force,<br>lK = Magnitude of the Lateral Knee Contact Force,<br>A = Anterior Cruciate Ligament, P = Posterior Cruciate Ligament,<br>M = Medial Collateral Ligament, V = Vasti<br>lG = Lateral Gastrocnemius, mG = Medial Gastrocnemius |
| **Force-Bearing Structures at the Knee and Hip** |
| R = Rectus Femoris, T = Tensor Fasciae Latae, Ab = Abductors,<br>L2 = Bi-Articular Gluteus Maximus,<br>mH = Medial Hamstrings, lH = Lateral Hamstrings |
| **Force-Bearing Structures at the Hip** |
| I =Iliopsoas, L1 = Mono-Articular Gluteus Maximus,<br>AdB = Adductor Brevis, AdL = Adductor Longus,<br>AdM = Adductor Magnus,<br>Hx = X component of the Hip Contact Force,<br>Hy = Y component of the Hip Contact Force,<br>Hz = Z component of the Hip Contact Force |

Table 7.1: System unknowns considered in the present study.

Similarly, at the hip we have

$$\sum_{i=1}^{n_h} F_i \vec{l_i} = \vec{R}_h \tag{7.3}$$

$$\sum_{i=1}^{n_h} \vec{d_i} \times (F_i \vec{l_i}) = \vec{M}_h \tag{7.4}$$

where symbols are defined as were in Equations 7.1 and 7.2 except the subscript $h$ is used to indicate the hip.

Therefore, a total of 12 equipollence equations were formed and resulted in about 150,000 DD subproblems for each data frame.

### 7.2.2 Calculation of Forces and Moments in Bones

Once an EMG consistent DDOSC solution was obtained, the forces and moments transmitted by the bone, Figure 7.1, at any cross-section $T$ were calculated by considering the force and moment equipollence at the centroid of the cross-section $\vec{O}_T$.

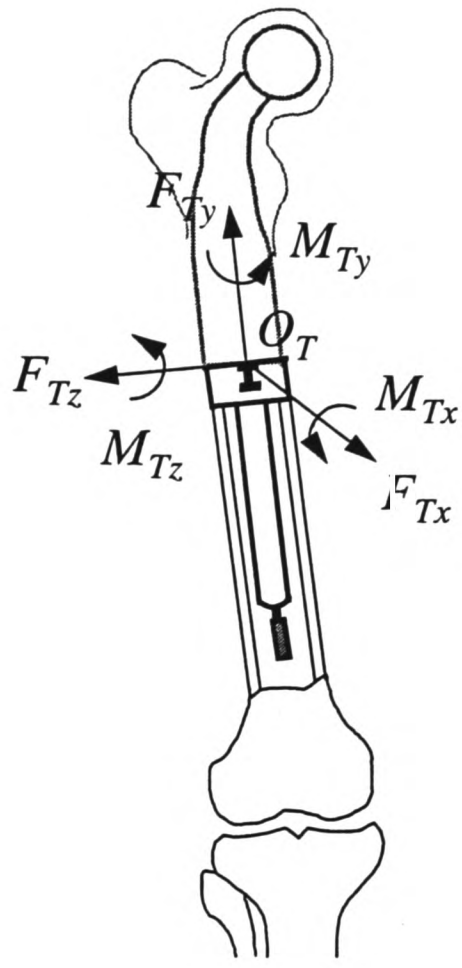



Figure 7.1: Co-ordinate system at the level of prosthesis transducers used to represent the forces and moments transmitted by the prosthesis shaft.

$$\sum_{i=1}^{n} L_i \vec{F}_i + \vec{F}_B = \vec{R}_T \tag{7.5}$$

$$\sum_{i=1}^{n} \vec{d}_i \times (L_i \vec{F}_i) + \vec{M}_B = \vec{M}_T \tag{7.6}$$

where $\vec{R}_T$ and $\vec{M}_T$ are the resultant limb force and moment vectors obtained from inverse dynamics analysis; $\vec{F}_i$ is the force developed in the *ith* muscle and $\vec{d}_i$ is the corresponding lever vector about $\vec{O}_T$. The forces and moments transmitted by the bone are represented by $\vec{F}_B$ and $\vec{M}_B$, respectively. Only those muscles that span the cross-section will affect the force transmission so the influence factor $L_i$ for the *ith* muscle was used to take this into account. The influence factor was defined as follows

$$L_i = \begin{cases} 1 & \text{if the } ith \text{ muscle span across } \vec{O}_T \\ 0 & \text{otherwise} \end{cases} \tag{7.7}$$

Therefore, $\vec{F}_B$ and $\vec{M}_B$ were calculated as the following

$$\vec{F}_B = \vec{R}_T - \sum_{i=1}^{n} L_i \vec{F}_i \tag{7.8}$$

$$\vec{M}_B = \vec{M}_T - \sum_{i=1}^{n} \vec{d}_i \times (L_i \vec{F}_i) \tag{7.9}$$

For the present study, the cross section was selected as the level of the prosthesis transducers. The muscles that span this level in the case of IM were rectus femoris, semitendinosus, semimembranosus, long head of the biceps, adductor magnus, adductor longus, bi-articular gluteus maximus and tensor fasciae latae. Since the gluteus medius and minimus were sutured to the fasciae latae, forces generated by these muscles were transmitted to the tibia through the iliotibial tract together with bi-articular gluteus maximus and tensor fasciae latae and therefore had influence on the femur.

Since moments are vectors in three-dimensions, the relationship between the Pauwels couple $M_{pauwels}$, bone moment $M_{bone}$ and limb moment $M_{limb}$ defined in Equation 5.4 should be revised into vector forms as follows.

$$\vec{M}_{limb} = \vec{M}_{pauwels} + \vec{M}_{bone} \tag{7.10}$$

The ratio between the Pauwels couple and limb moment, $M_{pauwels}/M_{limb}$ could only be calculated for each moment component. In the present study, the component in which the major limb moment occurred was taken and the $M_{pauwels}/M_{limb}$ ratio calculated.

## 7.3 Results

Time-averaged values of the model calculated femoral axial forces and the corresponding telemetered forces together with their mean differences during static exercises were summarised in Table 7.2. More detailed information about the predicted solutions are described in the following sections.

### 7.3.1 Isometric Tests

#### 7.3.1.1 Isometric Hip Flexion

For the hip flexion exercises, the model predicted over the data frames an average of 82 (S.D. = 7) DDOSC solutions out of about 150,000 DD subproblems. Recalling that the iliopsoas and mono-articular gluteus maximus in the

| Exercise | Experiment | Theory | Mean Error |
|---|---|---|---|
| Flexion | 2050 | 2280 | 298 |
| Extension | 2007 | 2282 | 239 |
| Adduction | 2405 | 2228 | 234 |
| Abduction | 1639 | 1540 | 88 |
| DLS | 866 | 947 | 63 |
| SLS | 2715 | 2834 | 160 |
| Gait | - | - | 270 |

Table 7.2: Comparison of the time-averaged femoral axial forces: theory versus experiment. Forces are in Newtons.

subject were either removed or immobilised during surgery, about 80% of these DDOSC solutions, which involved the two muscles, were rejected. Further consideration of EMG activity reduced the remaining DDOSC solutions to four, namely mK-lK-A-P-mG-R-T-L2-AdB-Hx-Hy-Hz, mK-lK-A-P-lG-R-T-L2-AdB-Hx-Hy-Hz, mK-lK-A-M-mG-R-T-L2-AdB-Hx-Hy-Hz and mK-lK-A-M-lG-R-T-L2-AdB-Hx-Hy-Hz. Since these solutions differed only at the knee joint, they predicted the same values of femoral axial forces. From the fibre recruitment theory described in Chapter 4, it was unlikely that the ACL and PCL would be recruited simultaneously. The two solutions involving lG predicted a very high force in the muscle and contact forces of more than ten times body weight at the knee. Since the plantar flexion moment required at the ankle was less than 1 Nm, it was unlikely that a big gastrocnemius force would be required. Based on these considerations, a single solution mK-lK-A-M-mG-R-T-L2-AdB-Hx-Hy-Hz was selected. The axial forces calculated in this combination together with the telemetered forces and the external forces are shown in Figure 7.2. The calculated axial forces had an average of 298 N higher than the measured forces, Table 7.2.

Among the 150 data frames, those within 100 N difference from the measured forces were used to calculate the major $M_{pauwels}/M_{limb}$ ratios at the level of the prosthesis transducers. During the hip flexion exercises, the major limb moment was about the $z$ (medio-lateral) axis. The average $M_{pauwels}/M_{limb}$ ratio at the level of the prosthesis transducers about this axis was 0.66. $M_{pauwels}$ was mainly provided by the agonist rectus femoris.

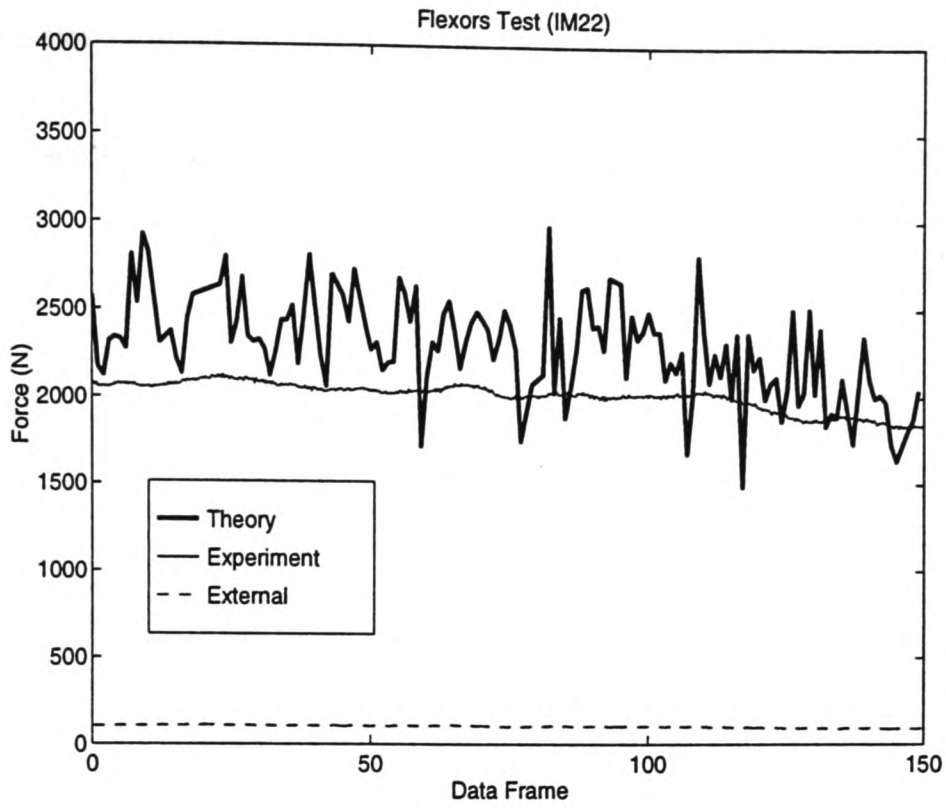



Figure 7.2: Femoral axial forces during flexors test: theory (thick lines) and experiment (thin lines).

#### 7.3.1.2 Isometric Hip Extension

Analysis of the hip extension exercises using the 3D model yielded an average of 40 (S.D. = 4) DDOSC solutions over the data frames. After considering muscular pathology and EMG activity, one DDOSC solution mK-lK-M-lG-V-mH-lH-L2-Ab-Hx-Hy-Hz was selected. Axial forces calculated in this combination, telemetered forces and the external forces are shown in Figure 7.3. The calculated axial forces were higher than the measured forces, with an average difference of 239 N, Table 7.2.

Among the 150 data frames, those within 100 N difference from the measured forces were used to calculate the major $M_{pauwels}/M_{limb}$ ratios at the level of the prosthesis transducers. During the hip extension exercises, the major limb moment was about the $z$ (medio-lateral) axis. The average $M_{pauwels}/M_{limb}$ ratio at the level of the prosthesis transducers about this axis was 0.75. The hamstrings were the main agonists that were recruited to balance the major limb moments.

#### 7.3.1.3 Isometric Hip Adduction

An average of 217 (S.D. = 21) DDOSC solutions over the data frames was predicted by the model during isometric hip adduction exercises. Since the iliopsoas

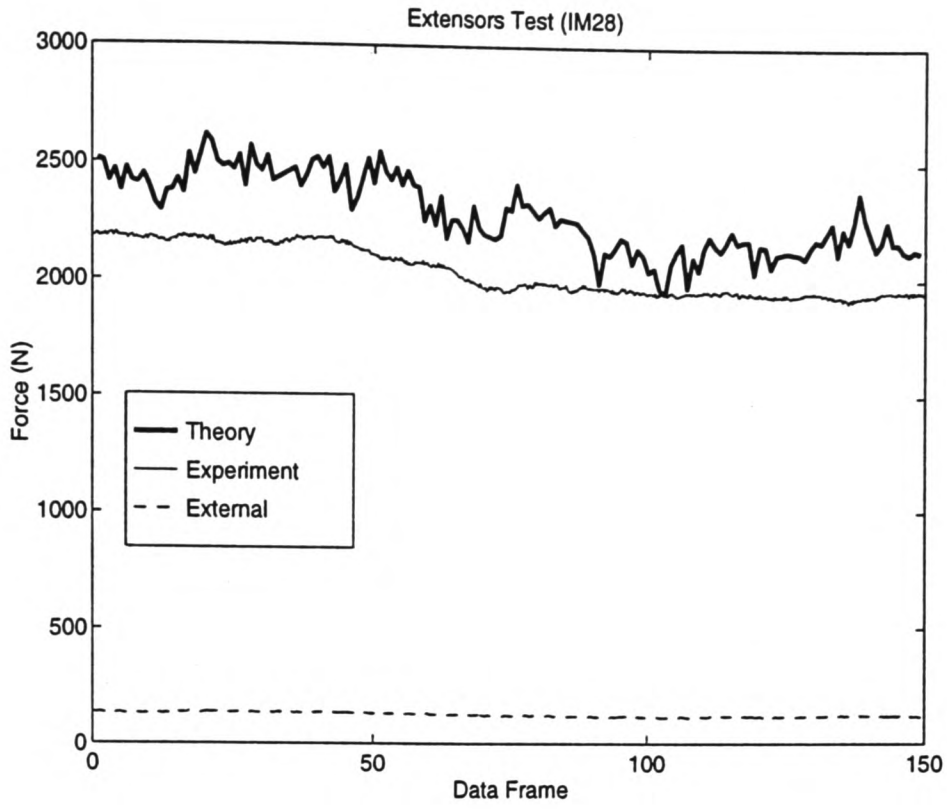



Figure 7.3: Femoral axial forces during extensors test: theory (thick lines) and experiment (thin lines).

and the mono-articular gluteus maximus have adduction function at the hip, about 70% of the predicted DDOSC solutions involved these two muscles. After rejecting these solutions, about 65 DDOSC solutions remained. Compared with the EMG activity, one DDOSC solution mK-lK-A-M-mG-V-R-L2-AdM-Hx-Hy-Hz was selected. Axial forces calculated in this combination, telemetered forces and the external forces are shown in Figure 7.4. The calculated forces followed well the trend of the measured forces, slightly lower in the first half of the data frames but much higher in the other half. The overall predictions were close to the measured force levels, with an average difference of about 230 N, Table 7.2.

The major $M_{pauwels}/M_{limb}$ ratios at the level of the prosthesis transducers were calculated about the $x$ (antero-posterior) axis. The average $M_{pauwels}/M_{limb}$ ratio at the level was 0.4. The adductor magnus was the main agonist to balance the major limb moments.

From the calculations, the medial compartment of the knee joint was found to transmit an average of 54% of the total contact forces, under an abducting moment of 38 Nm applied at the knee joint.

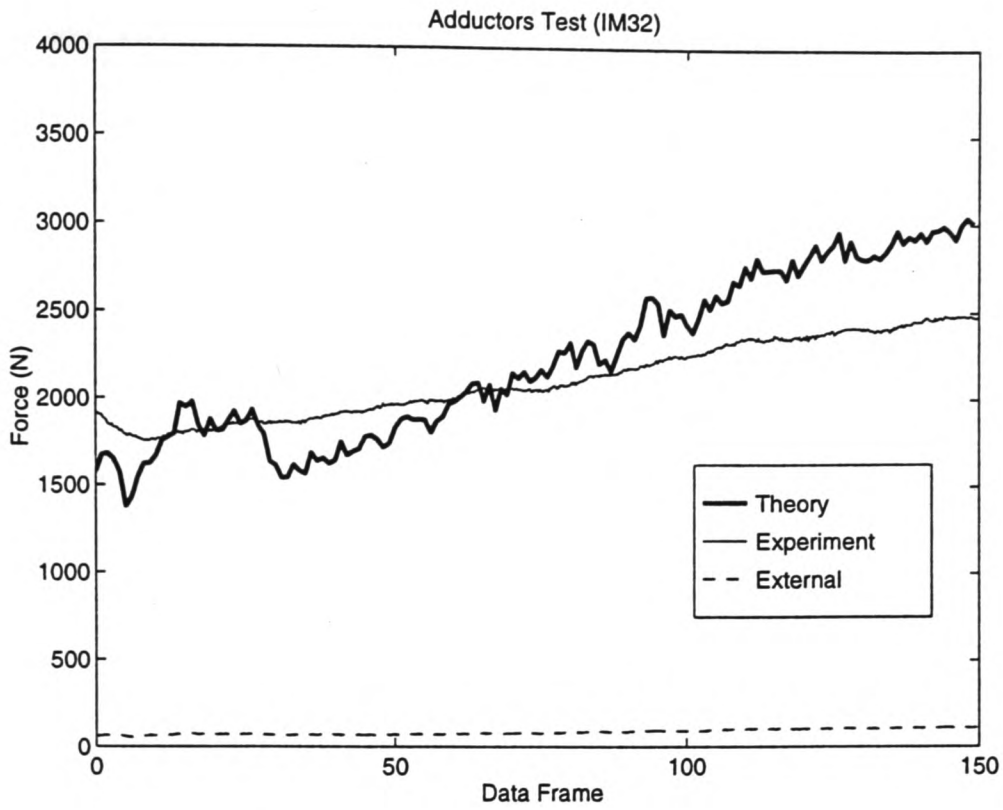



Figure 7.4: Femoral axial forces during adductors test: theory (thick lines) and experiment (thin lines).

#### 7.3.1.4 Isometric Hip Abduction

During the hip abduction exercises, the model predicted over the data frames an average of 56 (S.D. = 8) DDOSC solutions. Considering the actual musculature conditions, about 65% of these DDOSC solutions, which involved the mono-articular gluteus maximus and iliopsoas, were rejected. Further consideration of the EMG activity reduced the remaining DDOSC solutions to four, namely mK-lK-A-P-mG-V-lH-T-Ab-Hx-Hy-Hz, mK-lK-A-P-lG-V-lH-T-Ab-Hx-Hy-Hz, mK-lK-A-M-mG-V-lH-T-Ab-Hx-Hy-Hz and mK-lK-A-M-lG-V-lH-T-Ab-Hx-Hy-Hz. Since these solutions differed only at the knee joint, they predicted the same values of femoral axial forces. Following the same argument for the hip flexion exercises, solutions with simultaneous ACL and PCL were rejected. The two solutions involving mG predicted a very high force in the muscle and contact forces of more than ten times body weight at the knee. Since the plantar flexion moment required at the ankle was less than 0.5 Nm, it was unlikely that a big gastrocnemius force would be required. Based on these considerations, a single solution mK-lK-A-M-lG-V-lH-T-Ab-Hx-Hy-Hz was selected. The axial forces calculated in this combination together with the telemetered forces and the external forces are shown in Figure 7.5. The calculated axial forces were very close to the measured forces, with an average difference of 88 N, Table 7.2.

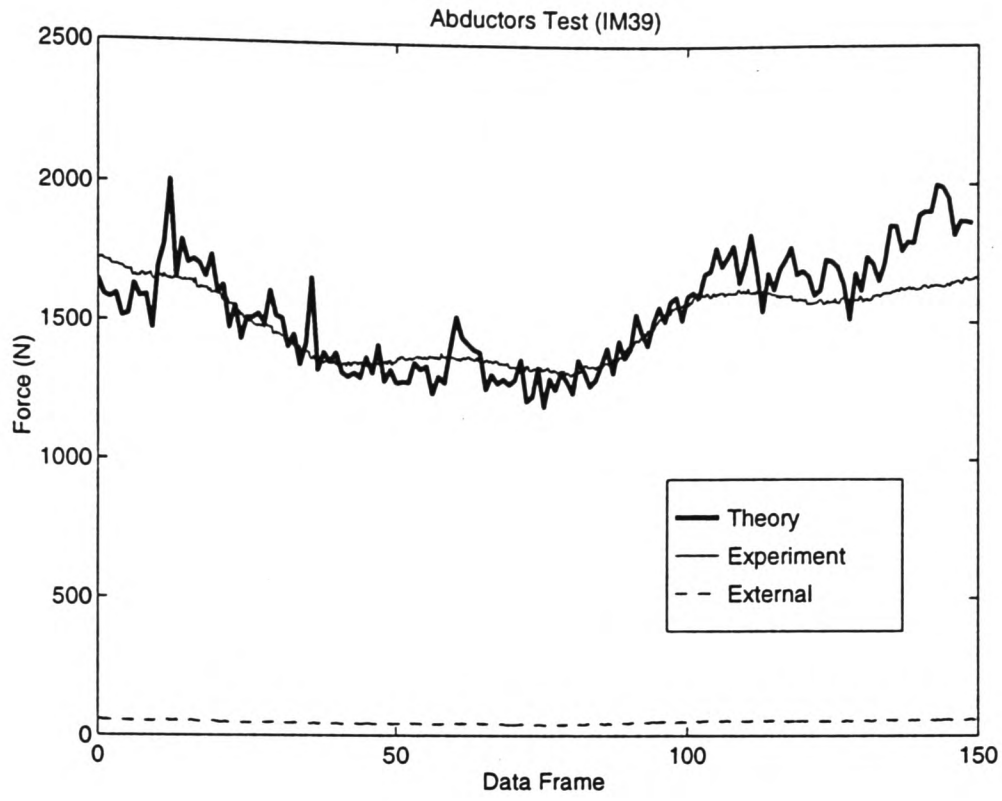



Figure 7.5: Femoral axial forces during abductors test: theory (thick lines) and experiment (thin lines).

The major $M_{pauwels}/M_{limb}$ ratios at the level of the prosthesis transducers about the $x$ (antero-posterior) axis were calculated. The average $M_{pauwels}/M_{limb}$ ratio at the level of the prosthesis transducers about this axis was 0.45. $M_{pauwels}$ was mainly provided by the agonist forces in the iliotibial tract, including TFL and the abductors sutured to the fasciae latae.

An average of 39% of the total knee contact forces were found to be transmitted by the medial compartment, under an adducting moment of 26 Nm applied at the knee joint.

### 7.3.2 Standing Postures

The calculated versus telemetered femoral axial forces during double leg stance (DLS) and single leg stance (SLS) are shown in Figure 7.6. Time-averaged forces transmitted in the force-bearing structures as calculated by the model are summarised in Table 7.3.

#### 7.3.2.1 Double Leg Stance (DLS)

The model predicted an average of 154 (S.D. = 9) DDOSC solutions during DLS over the data frames. After rejecting those with dissected or inactive muscles, an

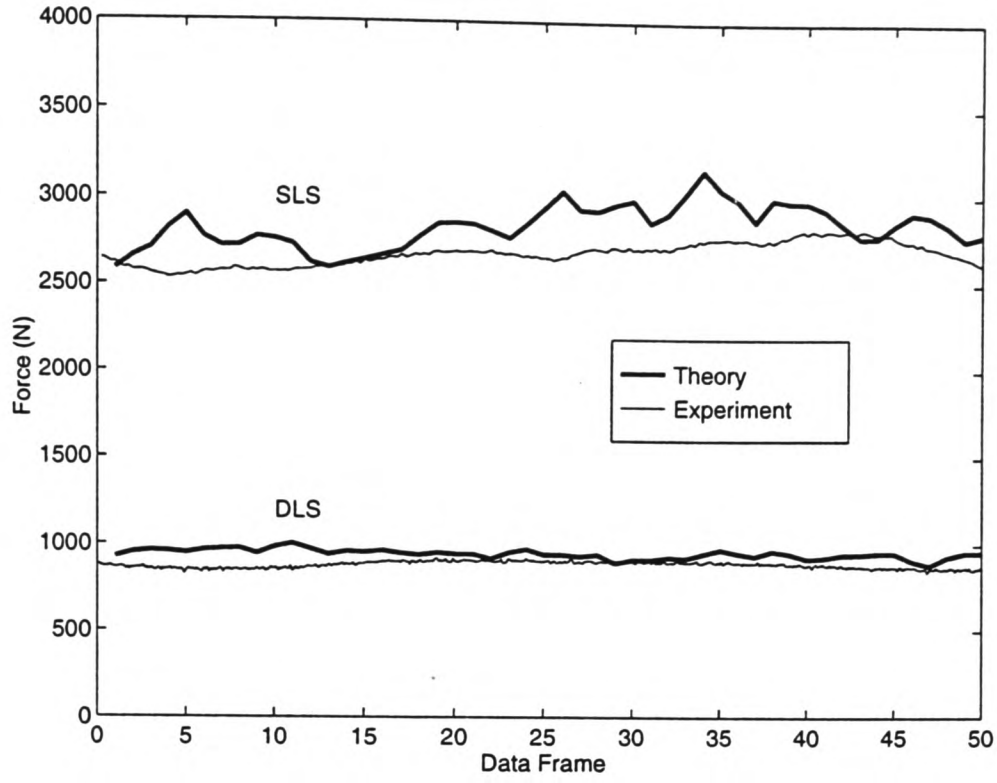



Figure 7.6: Comparison of femoral axial forces during SLS and DLS: theory (thick lines) and experiment (thin lines).

EMG consistent solution, mK-lK-A-M-mG-V-R-mH-L2-Hx-Hy-Hz, was obtained. There was a good match between the calculated axial forces and the measured forces, with an average difference of 63 N, Table 7.2.

During DLS, the ground reaction force passed near the centroid of the prosthesis so the limb moments were all very small, $\vec{M}_{limb} = (-3.7, -1.7, -0.01)$ Nm. The calculated bone moments were about the same order of the limb moments, $\vec{M}_{bone} = (-3.8, 7, 2.9)$ Nm. Since muscles were less active during DLS, the effect of the Pauwels couple was not significant during this posture.

At the knee joint, an average of 57% of the total knee contact forces were found to be transmitted by the medial compartment, with an absolute value of 1218 N, Table 7.3. Compared to the muscle force levels, relatively high forces were transmitted by the ACL and the MCL, Table 7.3.

#### 7.3.2.2 Single Leg Stance (SLS)

During SLS, there were an average of 37 (S.D. = 10) DDOSC solutions predicted by the model. Only one DDOSC solution, namely mK-lK-A-M-lG-V-mH-T-L2-Hx-Hy-Hz, satisfied both the musculature condition of the subject and the EMG activity. The calculated axial forces were generally close to but slightly higher than the measured forces, with an average difference of 160 N, Table 7.2.

| *Structure* | *Forces (N)* | | | |
|---|---|---|---|---|
| | SLS | | DLS | |
| | Mean | S.D. | Mean | S.D. |
| Gluteus maximus | 1639 | 105 | 23 | 2 |
| Tensor fasciae latae | 791 | 62 | - | - |
| Iliotibial tract | 1325 | 87 | 23 | 2 |
| Rectus femoris | - | - | 224 | 11 |
| Semitendinosus | 393 | 15 | 133 | 4 |
| Semimembranosus | 798 | 31 | 270 | 9 |
| Vasti | 1367 | 209 | 292 | 41 |
| Patellar tendon | 1052 | 160 | 397 | 34 |
| Medial Gastrocnemius | - | - | 326 | 32 |
| Lateral Gastrocnemius | 607 | 248 | - | - |
| ACL | 402 | 111 | 567 | 45 |
| MCL | 602 | 52 | 379 | 19 |
| Medial Knee Contact | 2640 | 217 | 1218 | 72 |
| Lateral Knee Contact | 2713 | 311 | 921 | 31 |
| Total Hip Contact | 3861 | 183 | 964 | 23 |

Table 7.3: Time-averaged forces transmitted in the force-bearing structures calculated by the model during DLS and SLS.

Transferring from DLS to SLS caused the ground reaction force to be directed medialy to the femur and passed medial to the hip joint, resulting in a major adducting limb moment of 37 Nm at the level of the prosthesis transducers. Due to the action of the limb abductors, the corresponding bone moment was only 2 Nm. The average $M_{pauwels}/M_{limb}$ ratio at the level was thus 0.95.

At the knee joint, an average of 49% of the total knee contact forces were transmitted by the medial compartment, with an absolute value of 2640 N, more than twice as much as in DLS, Table 7.3. The total contact forces were also two times higher than those in DLS but the ACL and MCL forces had similar levels in both postures, Table 7.3, indicating that a major part of the total contact forces came from muscle action.

### 7.3.3 Level Walking

The DDOSC solutions predicted by the model during the stance phase of gait ranged from 56 to 130 with a mean of 89. During swing phase, more DDOSC

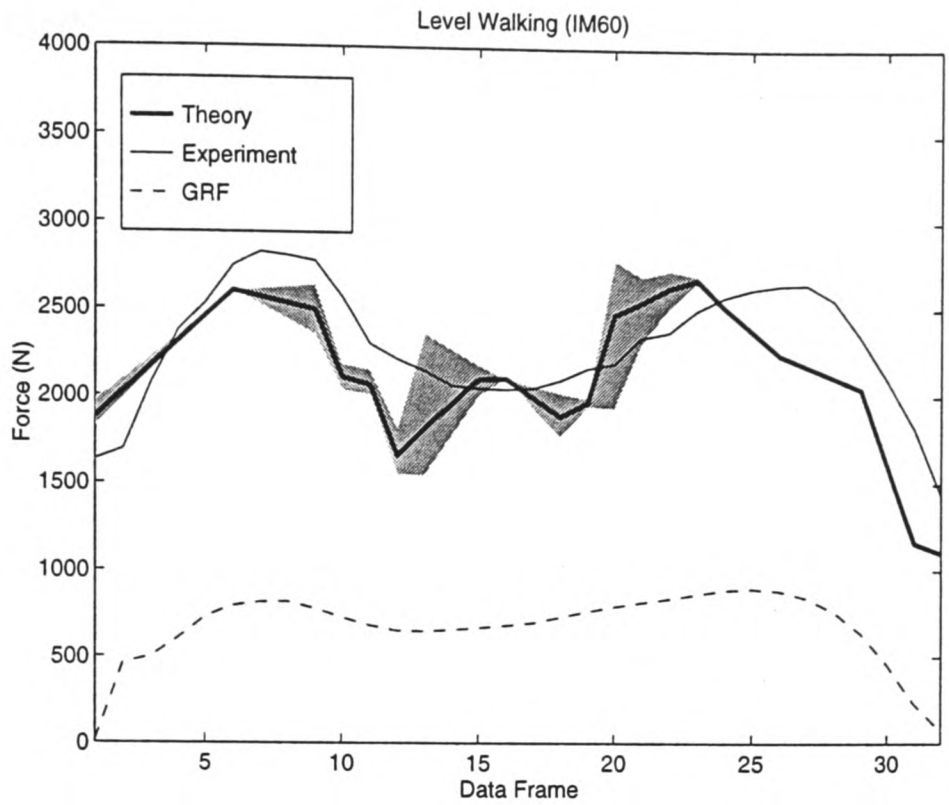



Figure 7.7: Femoral axial forces during stance phase of gait: theory (thick lines) and experiment (thin lines).

solutions were predicted (minimum: 123; maximum: 237; mean: 160). Since complete weight-bearing occurred during stance phase, information about the force transmission during this period was of more interest for clinical applications. The comparison between the model calculations and measurements was thus performed during this phase. Using EMG information and the anatomical condition of the subject, the multiplicity of the DDOSC solutions was reduced or removed. The maximum number of DDOSC solutions left was 8 in a few frames during mid-stance phase. During early stance phase, there were three DDOSC solutions left. Unique solutions were found during the late stance phase. The calculated femoral axial forces were plotted with the telemetered forces in Figure 7.7, together with the measured ground reaction forces. For those frames with more than one DDOSC solutions, the average values were calculated and the upper and lower bounds were indicated with a shaded area, Figure 7.7. Although an average difference of 270 N and at certain frames a maximum of 605 N difference were present, the model predictions gave a rather good fit to the telemetered axial forces.

## 7.4 Discussion

### 7.4.1 Validation of the Model

By comparing the calculated and telemetered femoral axial forces, the performance of the 3D model in the analysis of forces transmitted in the locomotor system was evaluated. In general, the model predicted results that were in good agreement with the telemetered force values, as shown in Table 7.2 and Figures 7.2 to 7.7. The biggest average difference was found in isometric hip flexion where the model predictions were about 15% higher than the measured forces. Big fluctuation was also present in this exercise. But for other activities, the model calculations were all within a range of 10% of the telemetered forces and the time-varying patterns of the measured forces were well followed.

It is acknowledged that the three-dimensional model was built upon a number of simplifications of the real system, which would inevitably contribute to the errors in the predictions. Removal of these simplifications, however, would result in an extremely complex system which is almost impossible to solve. The consistent performance of the model in the different activities considered in the present study suggests that the level of simplification and assumptions made were reasonable in terms of the ability to reproduce the major features of the locomotor system. These results not only provided a validation of the geometric model but also the mechanical solution procedure. Although these results were obtained from a single subject, from the experience of the 2D studies it would be expected that the 3D model would predict reasonable results for other subjects in similar activities provided that proper procedures for data collection and subject scaling were applied. Within an acceptable tolerance, it can also be used to estimate mechanical responses of the musculoskeletal structures in the locomotor system during other activities. For these further applications, factors that might affect the model estimations should be noticed and steps taken to control or minimise these factors. In this context, possible source of errors and parameter sensitivity are discussed in the following section.

### 7.4.2 Possible Source of Errors and Parameter Sensitivity

As discussed in the previous section, the 3D model represented an ensemble of a number of different types of information, including model parameters and input data. Several sources can therefore introduce errors into the 3-D model and

the resulting predictions. Since the general features of the model and solution procedures and methods would be the same for different activities and subjects, it is then reasonable to believe that model parameters and measured input data are the two major factors that can affect the outcome of the model. Anatomical variations that are beyond the assumptions of the model such as patients with deformed hip joints or other joint prostheses should be dealt with separately and are beyond this discussion. Proper modification of the model joints would be necessary for these cases.

Since model parameters were fixed in IM, the fluctuation of the predicted femoral axial forces seen in Figure 7.2 can be attributed partly to the noise embedded in the measured kinematic data, coupled with the jerky movement of the lower extremity and the markers on the restraining wire. Nonsmooth results have been recognised in all inverse dynamics models [51] because calculations are performed on a frame by frame basis. Various smoothing techniques can be used to remove some of this noise but there is always a risk of loosing important information. For example, over-smoothing may filter out the jerky motion of the lower limb which is in fact part of the signal, indicating how the subject was trying to pull the wire as much as he could. In the present study, the data inspection process with three-dimensional graphics and system level optimisation has been used to monitor the quality of the input data. It has helped to pick up the unacceptable kinematic data of DG. It is felt that as long as major features of the system, such as the proper articulation of the joints, are maintained, the level of smoothness of the data and the results are subject to further study. It is suggested that proper data inspection using computer graphics and system level optimisation is necessary for further application of the model to other subjects and activities. Further improvement is also needed in the accuracy of all the relevant measurements.

Another major factor that will affect the application of the model would be the selection of model parameters. It is noted that there are more than one hundred parameters required for the definition of the three-dimensional model of the locomotor system. A full parameter sensitivity analysis for the present subject requires a huge amount of computation and was not considered in the present study. However, for the estimation of the forces transmitted by the force-bearing structures, it is not surprising that the parameters defining the origins and insertions of the muscles are of great importance among others. The present model utilised

the average set of muscle origins and insertions from the literature. A homogeneous scaling scheme was applied to the subject under investigation. Although the calculated results suggested that the customisation process worked well for the present subject who was anthropometrically within the data population, its application to subjects outside the population may be erroneous. Residual differences that can not be accommodated by the homogeneous scaling process would affect the predicted results. A subject-specific parameter set can be obtained through CT or MRI scan and would be helpful for more accurate results but this would result in difficulties in subjects in whom such screening could not be justified merely for the determination of the model parameters.

From the point of view of the present project, an average set of model parameters as a basis for customisation to individual subjects was sufficient because it is almost impossible to collect subject-specific model parameters for each subject under investigation. But it is suggested that different databases for different subject groups are needed for future applications, such as the study of children with cerebral palsy. A better scaling scheme may also help to reduce anatomical variations.

### 7.4.3 The DDOSC method

The application of the DDOSC method in three dimensions involved a big number of possible DD subproblems, 150,000 in the present study, each subproblem required the solution of a $12 \times 12$ matrix. With modern advances in computer technology, these subproblems were solved within 3 minutes per data frame, much less than the solution of a small 2-D finite element analysis problem. Therefore, there is no technical difficulty in the implementation of this method. After calculation, it was found that a majority of the DD solutions were inconsistent with the one-sided constraints, leaving less than 200 DDOSC solutions in most of the activities tested. Taking account of the anatomical condition of the subject, more than half of these solutions were rejected. This was because iliopsoas and gluteus maximus were main hip flexors and extensors, respectively. They could have contributed to most of the activities considered in the present studies. With comparison with EMG, a single solution (in the cases of static tests) or a small number of solutions (during walking) could be selected. As discussed in Chapter 5, the nature of multiple DDOSC solutions indicates that there are several redundant muscle recruitment strategies that can serve to achieve the desired motion. They

provide a compensatory mechanism for the locomotor system, which was shown in the two subjects. In the present study, although the dissection of the iliopsoas and mono-articular gluteus maximus took away more than half of the recruitment strategies, there were still several different possibilities that could be chosen by the locomotor system to perform activity. The remaining redundancy was further reduced or removed by reference to EMG activity. Based on the present studies, it seems that the locomotor musculoskeletal system is not redundant in a way that all the force-bearing structures have to be used to perform activity but is redundant in terms of the possible recruitment strategies to achieve movement. In this regard, the inability of the DDOSC method to yield a unique solution directly may not be a major drawback but, compared with other methods, is in fact an advantage. Using the DDOSC method, all the possible solutions are generated and the redundancy of strategies can be reduced or removed, depending on the available EMG information. On the other hand, with a pre-specified criterion, optimisation procedures can be used to remove the redundancy and find a unique solution but as described in Chapters 1 and 5, before a true or near-true criterion is established, it is inappropriate to discard the other possibilities.

In terms of application to other subjects or activities, the limitation of the current form of the DDOSC method should be recognised. Although the redundancy of the locomotor system was not as high as it appeared to be (200 DDOSC solutions out of 150,000 DD subproblems) in the activities tested in the present studies, application to other activities may increase the number of the DDOSC solutions. This has been proved to be true in the application by other students of the 2D model to normal subjects in activities such as rising up from a chair in which a maximum of about 60 DDOSC solutions were found, compared with only 7 in isometric hip flexion and 24 during walking, Chapter 5. The increase of the number of DDOSC solutions will increase the difficulty in the identification of a final solution. This can be predicted from the present studies. For example, since the iliopsoas muscle is a deep muscle, it is almost impossible to collect its activity using surface EMG. If the iliopsoas muscle had not been dissected during surgery, more than four DDOSC solutions would remain and the choice of a single solution may be difficult. In other words, if the EMG or other forms of physiological information are available, the selection process can be automated by the implementation of a simple pattern match algorithm; otherwise, more than one DDOSC solution will remain. The present approach for this situation was taking the mean values of the predicted forces, as it was during gait, Figure 7.7.

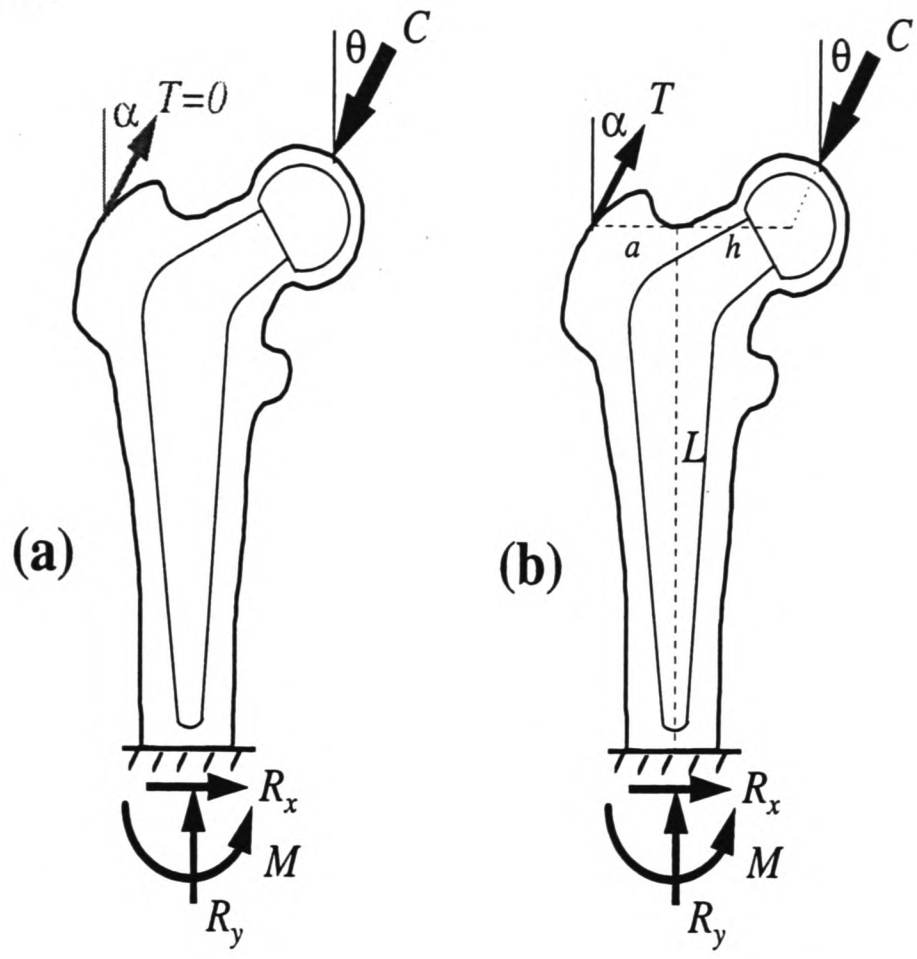



Figure 7.8: Schematic representations of two typical proximal femoral models with the mid-shaft fixed and (a) subjected to a concentric force at the head of the femur or (b) additionally with simulated abductor muscle force.

As discussed in Section 5.3.4, the final solution is a linear combination of the DDOSC solutions. Taking the mean value of the DDOSC solution was based on the assumption that all the DDOSC solutions had equal weightings. However, this may not be valid for all sorts of activities. Further studies will be needed to systematically adapt the weightings, according to the physiological information available, to reach a best-compromised solution.

## 7.5 Clinical Relevance

In the light of the validated model calculations, clinical implications for hip and knee replacement are discussed in this section.

### 7.5.1 Implication for Hip Replacement

In order to obtain a better understanding of the failure of hip prosthetic stems and the improvement of the long-term fixation of implants, *in vitro* studies using strain gauges placed on cadaveric femurs with or without prostheses and theoretical studies using finite element methods have been conducted. The loading conditions of the human hip joint and femur, however, were greatly simplified. To study the strain/stress distributions, many authors applied a simple concentrated load to the head of the femur or prosthesis with the femur fixed at mid-shaft and transmitting all the bending moment [118, 165, 170, 191, 253], Figure 7.8(a). Others had used a similar model but with the addition of hip abductor muscle forces applied through the greater trochanter [62, 80, 120, 207, 208, 218, 254], Figure 7.8(b). A similar approach has also been adopted by Carter *et al.* [42, 44, 43] in their studies of bone remodelling, Figure 7.8(b). In these studies, devoted to the strain/stress distribution in the proximal femur, fixed end boundary conditions were imposed at mid-shaft and bi-articular muscle activities were thus excluded. This approach does not account for the action of the flexor or extensor muscles or of the bi-articular muscles (such as rectus femoris, hamstrings and the muscles inserting into the ilio-tibial tract) although kinetic analyses [63, 135] have shown that peak segmental flexion/extension moments at the hip joint, which should be balanced by extensors and flexors, mono- or bi-articular, are generally higher than peak abduction/adduction moments during gait.

From the validated calculations, it is noted that muscle activity reduced the principle limb moments significantly. In most of the tests, the $M_{pauwels}/M_{limb}$ ratios were much higher than 0.4. In all the tests, the bone moments were less than 30 Nm. During single leg stance whose loading has been used for the analysis of hip replacements, the $M_{pauwels}/M_{limb}$ ratio for the adducting moments reached as high as 0.95, indicating that the major limb moments were mostly transmitted by $M_{pauwels}$. To compare the present results and those loading conditions usually used in the literature, the resultant forces and moments transmitted by the femoral shaft at the same level of the prosthesis transducers were calculated and summarised in Table 7.4. It is noted that under loading cases 2 and 3, small contact forces at the hip and tensile forces in the abductors produced huge bending moments at the shaft, compared with only 1.99 Nm during SLS and the maximum of 30 Nm in most of the tests, calculated from the 3D model which considered muscle activity. Loading case 1 gave reasonable bending moment but the axial

| Parameters & Reactions | Loading Cases | | | | | | |
|---|---|---|---|---|---|---|---|
| | 1 | 2 | 3 | 4 | SLS | Gait 1 | Gait 2 |
| $C$ (N) | 2317 | 1158 | 1548 | 3000 | 2800 | 3670 | 3820 |
| $\theta$ (deg) | 24 | -15 | 56 | 24 | - | - | - |
| $T$ (N) | 702 | 351 | 468 | 0 | - | - | - |
| $\alpha$ (deg) | 28 | -8 | 35 | 0 | - | - | - |
| $M$ (Nm) | -5.7 | 96.7 | -132.6 | -93.24 | 1.99 | 26.7 | 30.5 |
| $R_x$ (N) | 612.8 | -250.86 | 1014.9 | 1220.2 | 120.5 | -51 | -181 |
| $R_y$ (N) | 1496.9 | 770.96 | 482.3 | 2740.6 | 2834 | 2353 | 2522 |

Table 7.4: Resultant forces and moments transmitted at the mid shaft of the femur in the coronal plane under different loading conditions. Loading cases 1 to 3 were used by Carter *et al.* [43]. Loading condition 4 was from Huiskes [119]. Forces and moments calculated from the present model during SLS and gait are also listed for comparison. Two extreme loading conditions during walking were selected: Gait 1 corresponds to the first peak and Gait 2 the second, Figure 7.7. Conventions are according to Figure 7.8. For the present subject, $a$ = 15 mm, $h$ = 43 mm, and $L$ = 173 mm.

force along the shaft was only half of the forces in SLS which may not represent an physiological loading in extreme conditions.

From the present calculations, it is suggested that future studies of stress distributions in the proximal femur should account for the action of the flexors and extensors and for the bi-articular action of the leg abductors.

### 7.5.2 Force Sharing Between the Knee Compartments

Loading sharing between the compartments of the knee joint has important implication to the gonarthritis (OA), knee replacements and post-operative rehabilitation. While the level of the forces transmitted at the hip have been revealed using instrumented prostheses, such as Rydell [214], English and Kilvington [76], Davy *et al.* [67] and Bergmann *et al.* [19, 20, 21], only theoretical studies have been reported at the knee. Most of them were devoted to the estimation of the total knee joint contact force (e.g. Seireg and Arvikar [222], Collins and O'Connor [58] and other 2D studies). Only a few of them tried to study the force sharing between the medial and lateral compartments [117, 131, 132, 172, 217]. The general result is that the knee joint contact force passes predominately through the medial compartment and directly associated with the adducting moment at the knee. It

is noted that these studies were done without considering any contribution from the limb abductors and only the equipollence at the knee was considered. Since direct measurement of the contact forces in the knee joint has not been reported, the question of validation of the theoretical calculations remains open. However, the validated results from the 3D model of the locomotor system provided a good opportunity to re-examine the force sharing between the two compartments of the knee joint.

The interest of studying the force distribution between the compartments of the knee joint arises mainly from the attempt to understand the development of osteoarthritis as well as the design of the surgical procedures for the correction of the resulting pathomechanics of the joint, such as high tibial osteotomy or total knee arthroplasty. Previous theoretical studies in the literature have suggested that axial alignment is an important factor in the force distribution at the knee and thus plays a major role in the formation of OA and needs to be accurately restored in knee osteotomy. It would be useful to see if other factors such as the activity of muscles, especially the limb abductors, would affect the force distribution at the knee.

The effect of muscle activity on the force sharing between the two compartments of the knee joint can be studied by examining results calculated by different DDOSC solutions. The EMG consistent DDOSC solution in most of the tests predicted a rather even distribution between the two compartments. However, although not reported in the present thesis, it is noted that with different muscle action (different DDOSC solutions), the distribution of the contact forces transmitted by the two compartments of the knee changed significantly; forces in one compartment can be several times higher than the other. In other words, if different recruitment strategies were adopted, the force sharing would be different.

In the study of the force sharing during gait, Schipplein and Andriacchi [217] related knee joint adducting moment to the amount of the force shared by the medial compartment of the knee joint. However, as indicated in the abductors test where the adducting moment was maximised, only about 40% of the total contact force was transmitted by the medial compartment. According to their arguments, it would be straightforward to relate abducting moment to the forces transmitted by the lateral compartment. However, on the contrary, in the adductors tests, the medial compartment rather than the lateral compartment transmitted more than half of the total contact force. The difference between the present results and others can be explained by the simplification of their model

calculations. They first considered the flexion moment at the knee and determine the forces transmitted by either the extensors or flexors, depending on the direction of the external moment. Since the extensors or flexors also contributed to the equilibrium of the abduction/adduction of the knee, they attributed the unbalanced adducting/abducting moments to the two contact forces and the soft tissues or passive forces on the medial or lateral side of the joint. In other words, only two moment equilibrium equations at the knee joint were considered. These forces, although balanced the knee joint in the two directions, can not balance the moment equilibrium at the hip. In reality, the requirement of a big abducting moment at the hip required the recruitment of the hip abductors. These active abductor forces, through the iliotibial tract contribute to the direct modulation of the forces between the two compartments. This was clearly shown in the results from the DLS and SLS, Table 7.3.

From the present results, it seems that the force sharing of the two compartments of the knee joint depends on the use of the muscles in response to the applied external forces. If, for example, the abductors for the hip and the knee do not function properly, a case similar to the assumptions embedded in the calculation process of other works [117, 131, 132, 172, 217], the medial compartment will transmit more forces than the lateral compartments under an adducting moment. Therefore, without proper muscle activity, normal force sharing between the compartments can not be achieved. This suggests that proper restoration of muscle strength and activity is more important in modulating the force sharing between the two compartments of the knee joint after prosthetic replacement. Appropriate simulation of muscle forces is critical in *in vitro* experiments and in theoretical studies of force transmission at joints and bones, as well as prosthesis design and testing.

# Chapter 8

# Conclusions, Suggestions and General Summary

Studies of the locomotor system reported in the literature were reviewed in Chapter 1 of this thesis. It was found that combined theoretical and experimental approaches were, in general, necessary because internal forces in the locomotor musculoskeletal system can not be measured without using invasive methods. It was also found that these studies were limited due to the difficulties and/or inability in describing the kinematic geometry of the multi-joint system and due to uncertainties of the methods used to estimate the forces transmitted by the muscles and other force-bearing structures. Validation of these studies were also restricted to a qualitative basis. It was thus proposed that models of the locomotor system based on a proper consideration of the motion of the joints and with a quantitative validation would provide a very useful tool with which one could obtain a more in-depth knowledge of the force transmission in the locomotor system.

The primary goal of this thesis was to develop and implement mathematical models of the musculoskeletal system of the locomotor apparatus as an integrated tool for the study of the interactions between muscles, bones and ligaments in response to external loading. Telemetered internal axial forces transmitted in the instrumented proximal femoral prostheses from two patients were used for the quantitative evaluation and validation of the models. The work was carried out in the following stages:

- The experimental studies on patients with instrumented massive proximal femoral prostheses.

- Two-dimensional geometric modelling and validation of the knee joint and its surrounding force-bearing structures.
- Two-dimensional modelling and validation of the locomotor system and the development of a prototype computer windows system, which allows a unified approach to the geometric and mechanical modelling of the locomotor system with graphical animation and display.
- Three dimensional modelling of the pelvis-leg apparatus and the use of 3D computer graphics techniques to reconstruct the musculoskeletal system of the locomotor system animated by movement data measured from the gait laboratory.
- Validation of the 3D model of the locomotor system by comparing results with telemetered force data from the instrumented patients.

In this chapter, the main conclusions that can be drawn from the present studies are summarised. Recommendations for further studies into the development of the models of the locomotor system and the applications of the models to clinical problems are given. A general summary concludes the thesis.

## 8.1 Conclusions

### 8.1.1 Experimental Studies of The Instrumented Patients

Simultaneous *in vivo* measurements of external loads and the telemetered axial compressive forces along the instrumented prostheses of the subjects provided an opportunity to examine the effects of muscle activity on the forces in the femur. By selecting tests with different lever arms available to the external forces, these effects were systematically studied. The following conclusions were drawn from the experimental studies:

1. Flexors/extensors contribute a significant part of the forces in the femur;
2. Bi-articular muscles may have a major role in modulating forces in the bones; and
3. Muscles transmit external bending moments by applying axial compressive forces along the bones and thus increase the axial compressive force in the bone shaft.

4. Quantitative analysis of these activities were needed to estimate the forces transmitted within the musculoskeletal system.

5. Modelling work was required to enhance further applications to daily clinical practice.

The experimental study also formed a strong basis for the subsequent development and validation of the models of the locomotor system.

### 8.1.2 Two-Dimensional Modelling of the Knee Joint

The computer graphics-based model of knee ligaments at the architectural level, described in Chapter 4, provided a good tool for the study of the shape changes and fibre recruitment of the ligaments during knee movement, under unloaded and loaded conditions. It was concluded that computer graphics-based models provide a more direct and efficient way to visualise the results of the simulation. The knee ligament model may help to provide insight into the possible mechanism of ligament injuries, to improve replacement design and to assist clinical diagnosis.

In the second part of Chapter 4, the validation of the 2D knee model in terms of the model-predicted lines of action and moment arms of the surrounding force-bearing structures was performed by comparing with experiments reported in the literature. With relatively simple and less extensive measurements, the anatomy-based mathematical model predicted results that are comparable to those experimentally measured. It was suggested that, in order to take account of anatomical variations, efforts should be concentrated on the measurement of subject-specific model parameters. Further, since moment arms represent the ability of a load-bearing structure to generate or resist angulation of the joint about its flexion axis, it seems appropriate to express the moment arms in relation to the moving flexion axis.

### 8.1.3 Two-Dimensional Modelling of the Locomotor System

The development of the model of the locomotor system in the sagittal plane was described in the first part of Chapter 5. It was used as a basis for the comparative study of the DDOSC method and the optimisation methods with various criteria during normal walking. The following conclusions were drawn from the study:

- Optimisation methods with a single criterion are not able to predict results that reflect the real situation in the locomotor system.
- The final learned gait pattern may be the result of a compromise of multiple objectives.
- Before a full understanding of the compromise between possible objectives is established, it is inadequate to approach the force distribution problem using a single-objective optimisation method.
- For the purpose of clinical applications, however, the DDOSC method represents a more reasonable and flexible way to examine the force interactions between structural members of the human locomotor system.

In the second part of Chapter 5, the 2D model of the locomotor system was validated by comparing the model predictions to the telemetered internal forces from the two instrumented subjects. The validated results were then used to study the influence of activity of hip flexors and extensors on the forces in the femur during isometric hip flexion/extension exercises and level walking. The study represented a first attempt at quantitative validation of a theoretical multi-joint model of the human lower limb. Axial forces calculated by the model during isometric exercises were in good agreement with telemetered forces. During gait, the model underestimated the axial forces but suggested that about 70% of the maximum axial force in the femur was a result of action of the flexors or extensors. It was shown that bi-articular muscles are major force modulators for the bones. It was suggested that appropriate simulation of muscle force is necessary in *in vitro* laboratory experiments and in theoretical studies of stress distributions in bone.

The development of the prototype windows system, described in the final part of Chapter 5, suggests that interactive graphics-based window interfaces are vital tools in bridging the gap between clinical users and biomechanical workers.

### 8.1.4 Three-Dimensional Modelling of the Locomotor System

The development and validation of the computer graphics-based animated model of the locomotor system, described in Chapters 6 and 7, was a major extension of the 2D models. By comparing the calculated and telemetered femoral axial

forces, the performance of the 3D model in the analysis of forces transmitted in the locomotor system was evaluated. In general, the model predicted results that were in good agreement with the telemetered force values. For most of the activities tested, the model calculations were all within a range of 10% of the telemetered forces and the time-varying patterns of the measured forces were well followed. These results not only provided a validation of the geometric model but also the mechanical solution procedure.

The geometric modelling and validated calculations supported the following general conclusions:

- As with the 2D studies, computer graphics-based modelling and animation are vital tools in bridging the gap between clinical users and biomechanists.
- System level optimisation is needed for multijoint models so as to take account of marker position errors, including skin movement artefacts.
- The 3D model would predict reasonable results for other subjects in the activities tested provided that proper procedures for data collection and subject scaling were applied.
- Within an acceptable tolerance, the 3D model can also be used in other activities.
- An average set of model parameters as a basis for customisation to individual subjects with homogeneous scaling techniques is adequate.
- Different databases for different subject groups are needed for future applications, such as the study of children with cerebral palsy.
- A significant part of the bending moments along limbs are transmitted by a combination of tensile forces in muscles and compressive forces in bones so moments transmitted by the bones are much less than the limb moments.
- Appropriate simulation of muscle forces is critical in *in vitro* experiments and in theoretical studies of force transmission at joints and bones, as well as prosthesis design and testing.
- Proper restoration of muscle strength and activity is important in modulating the force sharing between the two compartments of the knee joint after prosthetic replacement.

- Future studies of stress distributions in the proximal femur should account for the action of the flexors and extensors and for the bi-articular action of the leg abductors.

## 8.2 Suggestions for Further Studies

Several suggestions for extending some of the ideas, concepts and models presented in this report are summarised as follows:

### 8.2.1 Model Development

In the present studies, the geometric and mechanical modelling and analysis of the locomotor system were approached separately and sequentially. Since geometric modelling provides a necessary basis for any subsequent mechanical analysis, special emphasis was placed on the modelling of the major joints. The hip and the tibiofemoral joints were modelled by considering the kinematic effects of their anatomical structures. This allowed a more accurate description of the relative motion of the associated segments and thus of the lines of action of the surrounding structures, including muscles, ligaments and articular surfaces.

The four-bar linkage model and the parallel spatial mechanism model of the knee joint provided a good modelling approach to the consideration of ligamentous and articular contributions to the control of the motion of the joint. A further development of the present locomotor system model would be to extend the current bi-axial phenomenological ankle model to an anatomical one, along the line of the 3D knee model. Preliminary experimental studies [145] have led to the development of a four-bar linkage model of the ankle joint [146]. A three-dimensional analogue of this model would contribute to a more accurate modelling of the ankle complex and a detailed mechanical analysis of the ankle ligaments during activity could then be attempted.

Another possible improvement to the present locomotor system model would be to refine the patellofemoral joint model so as to include more anatomical representation of the patella and the articular surfaces. This would provide a better description of the geometry of the extensor mechanism and could serve as a preliminary to the stress/strain analysis of the patella.

In the present 3D model, the knee ligaments were modelled as inextensible line elements. As shown in the 2D modelling studies, with further consideration of

ligament elasticity, compatibility equations could be used to reduce system redundancy and allow better estimation of force-sharing between ligaments. Modelling of the ligaments as arrays of fibres will be useful for the study of ligament shape changes and fibre recruitment patterns in three-dimensions.

In terms of the method for the solution of the force distribution problems, the DDOSC method worked very well in the tests considered in the present studies. However, application to other activities may increase the number of the DDOSC solutions. The increase of the number of DDOSC solutions will increase the difficulty in identifying a final solution. As discussed in Section 5.3.4, the final solution is a linear combination of the DDOSC solutions. Further studies will be needed to systematically adapt the weightings, according to the physiological information available, to reach a best-compromised solution.

### 8.2.2 Application of Computer Graphics-Based Models

The three-dimensional computer graphics-based model described in this thesis was developed to contribute to computer-aided motion analysis. With the present graphics-based model, the difficulties in relation to the presentation and interpretation of the data collected using modern motion analysis systems could be reduced. The model could be used to confirm the correct placement of markers during subject calibration as well as to allow visual inspection of the quality of the measured kinematic data during motion.

By altering the features (bone shapes, muscle origins and insertions, etc.) of the graphics models (objects), the model could be used to simulate surgical procedures. The computer graphics representation of each patient's anatomy could be reconstructed from MRI or computer tomography scans. The mechanical consequences of each change could provide a theoretical set of optimal geometric and coordinate parameters or several alternative ways of treating the patient. With further development of user friendly interfaces, the model could eventually become an important tool for the orthopaedic surgeon. Such software could allow the clinician to compare and explore several options and forms of treatment before committing the patient to a specific and often irreversible operation. The application of the software in the planning and evaluation of rehabilitation programmes is also expected.

## 8.3 General Summary

This research has been concerned with the construction and validation of mathematical models of the human locomotor system and the computer graphics reconstruction, visualisation and animation of the system.

The modelling and analysis of the locomotor system were approached by considering two aspects: geometric and mechanical. They were dealt with separately and sequentially using fundamental principles of geometry and mechanics as well as a minimum number of anatomical measurements. Modern computer graphics techniques were used to assist the interpretation, presentation and application of the modelling results by creating graphics models of the locomotor system. The inverse dynamics approach was used to analyse the tested activities. The redundancy of the musculoskeletal system was resolved using the DDOSC method. Models of the locomotor system were developed both in the sagittal plane and in three-dimensions.

Experiments were performed on two patients with custom-made instrumented massive proximal femoral prostheses implanted after tumour resection. Telemetered axial forces transmitted along the prostheses, together with kinematic, force plate and electromyographic data, were recorded synchronously during level walking, single and double leg stance, and isometric tests of the hip muscles. Both the 2D and 3D models of the locomotor system were evaluated and validated quantitatively with the telemetered femoral axial forces.

It is concluded that (a) a major part of the bending moments along limbs are transmitted by a combination of tensile forces in muscles and compressive forces in bones so moments transmitted by the bones are much less than the limb moments, (b) bi-articular muscles play a major role in modulating forces in bones, (c) appropriate simulation of muscle forces is important in experimental or theoretical studies of load transmission along bones, (d) computer graphics-based modelling and animation are vital tools in bridging the gap between clinical users and biomechanists.

# Appendix A

# Anatomical Terminology

In presenting the present studies, it was assumed that the reader was familiar with anatomical terminology. However, for those unfamiliar with the terminology, the more important anatomical terms, describing reference planes and motion, are included here for easy reference.

Terminology used to describe the body structures and functions is defined in relation to the standard *anatomical position*, in which the body is in an upright attitude with the arms at the sides and palms facing forward. Three reference planes are then defined as follows (Figure A.1):

- *Median or Mid-Sagittal Plane* - A vertical plane that divides the body into equal right and left sides. Any plane parallel to the median plane is referred to as a sagittal plane.
- *Frontal or Coronal Plane* - A plane that runs vertically and divides the body into *anterior* and *posterior* portions.
- *Transverse Plane* - A horizontal plane, perpendicular to the median and frontal planes, which divides the body into *superior* and *inferior* sections.

Terms used to describe the locations of various anatomical structures:

- *Anterior* - describing or relating to the front portion of the body or limbs.
- *Posterior* - situated near the back of the body or limbs.
- *Superior* - situated uppermost in the body in relation to another structure or surface.

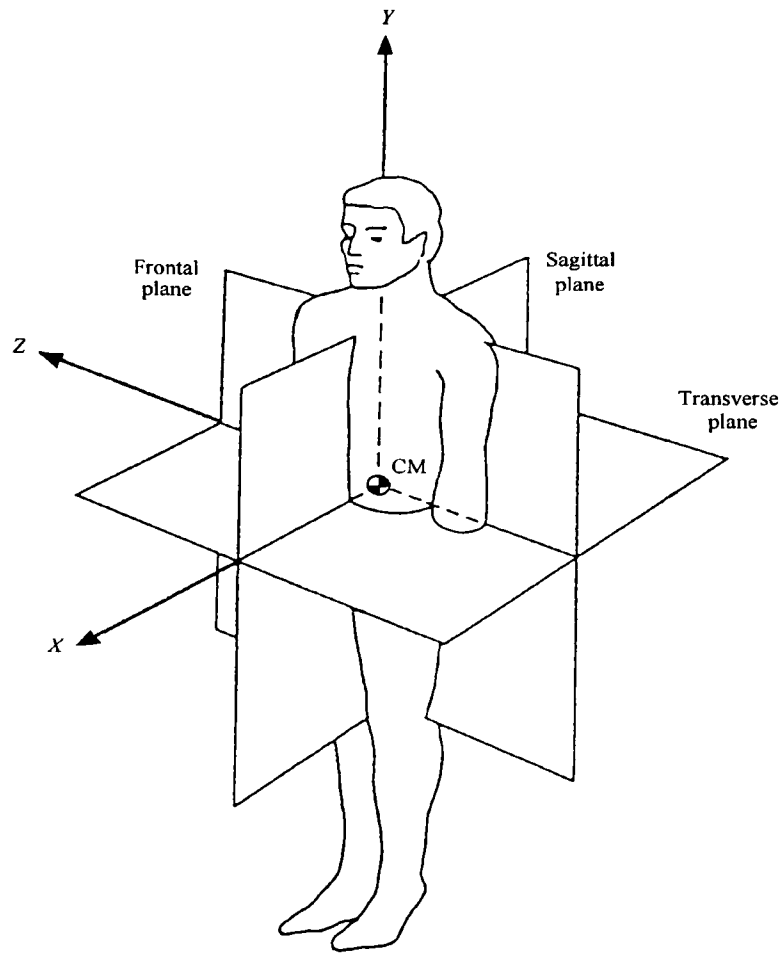



Figure A.1: The three reference body planes with a representative body in the standard anatomical position.

- *Inferior* - lower in the body in relation to another structure or surface.
- *Lateral* - situated away from the *median plane* of the body.
- *Medial* - situated toward the *median plane* of the body.
- *Distal* - situated away from the origin or point of attachment or away from the *median plane* of the body.
- *Proximal* - situated close to the origin or point of attachment or close to the median plane of the body.

Terms which are used to indicate movements (Figure A.2):

- *Flexion* - The bending of a joint such that the bones forming it are brought toward each other. At the ankle joint, flexion of the foot is called *dorsiflexion.*

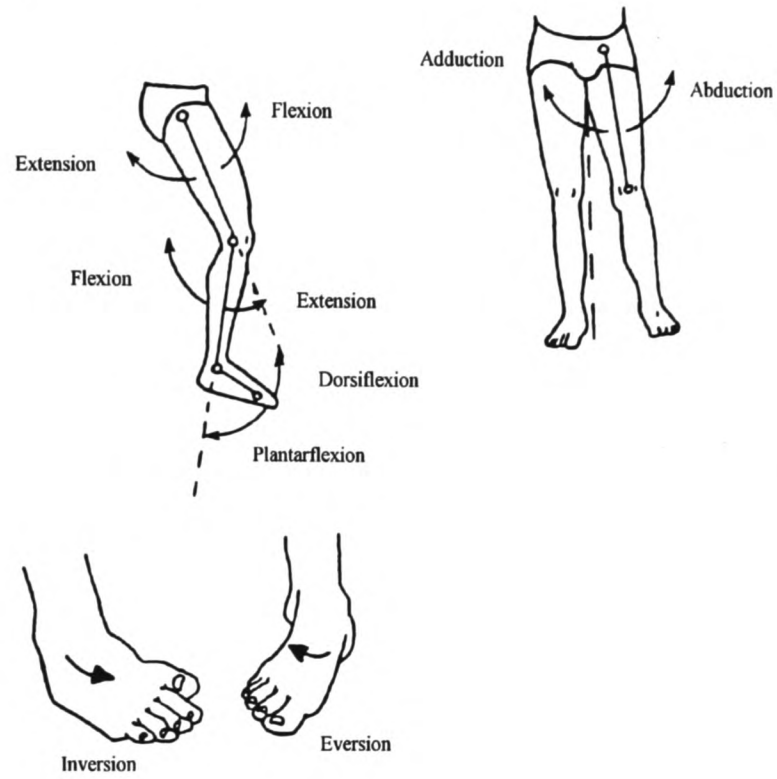



Figure A.2: System for naming joint angles.

- *Extension* - The straightening of a joint such that the bones forming it are moved away from each other. At the ankle joint, extension is referred to as *plantarflexion.*
- *Adduction* - Movement of a limb or any other part toward the median plane of the body
- *Abduction* - Movement of a limb or any other part away from the median plane of the body
- *Internal Rotation* - The rotation of a body segment along its long axis and toward the median plane of the body
- *External Rotation* - The rotation of a body segment along its long axis and away from the median plane of the body
- *Inversion* - Movement of the whole foot to bring the sole to face medially.
- *Eversion* - Movement of the whole foot to bring the sole to face laterally.

# Appendix B

# Abbreviations

The abbreviations used in the thesis are listed below.

| ABBREVIATIONS | DESCRIPTION |
|---|---|
| ACL | anterior cruciate ligament |
| ASIS | anterior superior iliac spines |
| BCS | body-embedded coordinate system |
| CT | computerised tomography |
| DD | dynamically determinate |
| DDOSC | dynamically determinate one-sided constrained |
| DG | subject DG |
| DLS | double leg stance |
| DLT | direct linear transformation |
| EMG | electromyography, electromyogram |
| FA | functional approach |
| FMET | fifth metatarsal |
| FMR | force magnification ratio |
| GRF | ground reaction force |
| GTRO | greater trochanter |
| HEEL | posterior projection of the calcaneus |
| HJC | hip joint centre |
| HF | head of fibula |
| IM | subject IM |
| IT | iliotibial tract |
| JCS | joint coordinate system |
| LASIS | left anterior superior iliac spine |

| | |
|---|---|
| LCL | lateral collateral ligament |
| LCS | laboratory coordinate system |
| LEP | lateral femoral epicondyle |
| LMA | lateral malleolus |
| MCL | medial collateral ligament |
| MEP | medial femoral epicondyle |
| MMA | medial malleolus |
| MRI | magnetic resonance imaging |
| NT | navicular tubercle |
| OA | osteoarthritis |
| OOP | object-oriented programming |
| PA | prediction approach |
| PCL | posterior cruciate ligament |
| PCSA | physiological cross-sectional area |
| PSIS | posterior superior iliac spines |
| RASIS | right anterior superior iliac spine |
| RFA | revised functional approach |
| RPSIS | right posterior superior iliac spine |
| SLS | single leg stance |
| SQP | sequential quadratic programming |
| SVD | singular variable decomposition |
| TCS | technical coordinate system |
| TFL | tensor fasciae latae |
| TT | tibial tuberosity |

# Appendix C

# Computer Programs

During the course of development of the models described in this thesis, several computer programs were written. The main C and C++ programs are listed below:

1. 2dm: C computer programs of the two-dimensional models.

2. ogas: C computer programs of the graphics-based window interface for the 2D models.

3. 3dm: C computer programs of the three-dimensional models.

4. 3dmview: C++ computer programmes of the three-dimensional graphics-based models and graphics display windows.

The source codes for the main programs listed above are contained on the CD stored in the envelope on the inside back cover of this thesis.

# Bibliography


[1] A. M. Ahmed, D. L. Burke, and A. Hyder. Force analysis of the patellar mechanism. *J Orthop Res*, 5(1):69–85, 1987.

[2] A.A. Amis and G.P.C. Dawkins. Functional anatomy of the anterior cruciate ligament: fibre bundle actions related to ligament replacements and injuries. *J Bone Jt Surg [Br]*, 73-B:260–267, 1991.

[3] A.A. Amis and T.D. Zavras. Isometricity and graft placement during anterior cruciate ligament reconstruction. *The Knee*, 2:5–17, 1995.

[4] K.N. An, L. Berglund, W.P. Cooney, E.Y. Chao, and N. Kovacevic. Direct *in vivo* tendon force measurement system. *J Biomech*, 23:1269–1271, 1990.

[5] K.N. An, B.M. Kwak, E.Y. Chao, and B.F. Morrey. Determination of muscle and joint forces: a new technique to solve the indeterminate problem. *Trans ASME - J Biomech Engng*, 106:364–367, 1984.

[6] K.N. An, K. Takahashi, T.P. Harrigan, and E.Y. Chao. Determination of muscle orientations and moment arms. *Trans ASME - J Biomech Engng*, 106:280–282, 1984.

[7] T.P. Andriacchi, G.B.J. Andersson, R.W. Fermier, D. Stern, and J.O. Galante. A study of lower-limb mechanics during stair-climbing. *J Bone Jt Surg [Am]*, 62A:749–757, 1980.

[8] T.P. Andriacchi, J.O. Galante, and R.W. Fermier. The influence of total knee-replacement design on walking and stair-climbing. *J Bone Jt Surg [Am]*, 64A:1328–1335, 1982.

[9] J. Apkarian, S. Nauman, and B. Cairns. A three-dimensional kinematic and dynamic model of the lower limb. *J Biomech*, 22:143–155, 1989.

[10] J.S. Arora. *Introduction to Optimum Design.* McGraw-Hill, New York, 1989.

[11] M.L. Audu and D.T. Davy. The influence of muscle model complexity in musculoskeletal motion modelling. *Trans ASME - J Biomech Engng*, 107:147–157, 1985.

[12] G.R.G. Barnes and D.N. Pinder. *In vivo* tendon tension and bone strain measurement and correlation. *J Biomech*, 7:35–42, 1974.

[13] C.H. Barnett, D.V. Davies, and M.A. Mac Conaill. *Synovial Joints. Their Structure and Mechanics.* Thomas, IL: Springfield, 1961.

[14] R.L. Barrack and H.B. Skinner. The sensory function of knee ligaments. In D.M. Daniel, W.H. Akeson, and J.J. O'Connor, editors, *Knee Ligaments - Structure, Function, Injury, and Repair*, pages 95–114. Raven Press, 1990.

[15] J.V. Basmajian and C.J. De Luca. *Muscles Alive.* Williams and Wilkins, Baltimore, fifth edition, 1985.

[16] R. Beckett and K. Chang. An evaluation of the kinematics of gait by minimum energy. *J Biomech*, 1:147–159, 1968.

[17] A.L. Bell, D.R. Pedersen, and R.A. Brand. A comparison of the accuracy of several hip center location prediction methods. *J Biomech*, 23:617–621, 1990.

[18] M.G. Benedetti, F. Catani, A. Leardini, and A. Cappozzo. Anatomical landmark definition and identification. In *Measurement and data processing methodology in clinical movement analysis*, March 1994. CEC Programme AIM, Project A-2002 CAMARC II, Deliverable 15.

[19] G. Bergmann, F. Graichen, and A. Rohlmann. Hip joint loading during walking and running, measured in two patients. *J Biomech*, 26:969–990, 1993.

[20] G. Bergmann, F. Graichen, and A. Rohlmann. Is staircase walking a risk for the fixation of hip implants? *J Biomech*, 28:535–553, 1995.

[21] G. Bergmann, H. Kniggendorf, F. Graichen, and A. Rohlmann. Influence of shoes and heel strike on the loading of the hip joint. *J Biomech*, 28(7):817–827, 1995.

[22] R.E.D. Bishop and R.A. Denham. A note on the ratio between tensions in the quadriceps tendon and infra-patellar ligament. *Engng Med*, 6:53–4, 1977.

[23] L. Blankevoort, R. Huiskes, and A. de Lange. The envelope of passive knee joint motion. *J Biomech*, 21(9):705–720, 1988.

[24] L. Blankevoort, R. Huiskes, and A. de Lange. Recruitment of knee joint ligaments. *Trans ASME - J Biomech Engng*, 113:94–103, 1991.

[25] L. Blankevoort, J.H. Kuiper, R. Huiskes, and H.J. Grootenboer. Articular contact in a three-dimensional model of the knee. *J Biomech*, 24:1019–1031, 1991.

[26] M.F. Bobbert and H.C. Schamhardt. Accuracy of determining the point of force application with piezoelectric force plates. *J Biomech*, 23(7):705–710, July 1990.

[27] J. P. Boysen, P. R. Francis, and R. T. Thomas. Interactive computer graphics in the study of human body planar motion under free fall conditions. *J Biomech*, 10:783–787, 1977.

[28] R. A. Brand, R. D. Crowninshield, C.E. Wittstock, D. R. Pedersen, C. R. Clark, and F. M. van Krieken. A model of lower extremity muscular anatomy. *Trans ASME - J Biomech Engng*, 104:304–310, November 1982.

[29] R.A. Brand. Knee ligaments: a new view. *Trans ASME - J Biomech Engng*, 108:106–110, May 1986.

[30] R.A. Brand, D.R. Pedersen, D.T. Davy, G.M. Kotzar, K.G. Heiple, and V.M. Goldberg. Comparison of hip force calculations and measurements in the same patient. *J Arthroplasty*, 9:45–51, 1994.

[31] O.C. Brantigan and A.F. Voshell. The mechanics of the ligaments and menisci of the knee joint. *J Bone Jt Surg [Am]*, 23-A:44–66, 1941.

[32] W. Braune and O. Fischer. Uber die lage des schwerpunkt des menschlichen korpers. *Abh Math Phys Klasse d.Kgl Saschen, Ges d. Wiss*, 15, 1889.

[33] B. Bresler and J.P. Frankel. The forces and moments in the leg during level walking. *Trans. ASME*, 72:27–35, 1950.

[34] R.H. Brown, A.H. Burstein, and V.H. Frankel. Telemetering *in vivo* loads from nail plate implants. *J Biomech*, 15:815–823, 1982.

[35] W.E. Caler, D.R. Carter, and W.H. Harris. Techniques for implanting an *in vivo* strain gage system. *J Biomech*, 14:503–507, 1981.

[36] A. Cappello, P. Francesco, L. Palombara, and A. Leardini. Optimization and smoothing techniques in movement analysis. *Int J Biomed Comp*, 41:137–151, 1996.

[37] A. Cappozzo. Gait analysis methodology. *Human Mvmt Sci.*, 3:27–50, 1984.

[38] A. Cappozzo, F. Catani, U. Della Croce, and A. Leardini. Position and orientation in space of bones during movement: anatomical frame definition and determination. *Clin. Biomech.*, 10:171–178, 1995.

[39] A. Cappozzo, F. Catani, A. Leardini, M.G. Benedetti, and U. Della Croce. Position and orientation in space of bones during movement: experimental artefacts. *Clin. Biomech.*, 11:90–100, 1996.

[40] A. Cappozzo, A. Leardini, S.T. Larsen, F. Catani, and M.G. Benedetti. A comparison of the accuracy of several hip centre location methods by using RSA techinque. In *Proceedings XVth Congress of the International Society of Biomechanics*, pages 152–153, Jyvaskyla, July 1995. International Society of Biomechanics.

[41] A. Cappozzo, T. Leo, and A. Pedotti. A general computing method for the analysis of human locomotion. *J Biomech*, 8:307–320, 1975.

[42] D.R. Carter, D.P. Fyhrie, and R.T. Whalen. Trabecular bone density and loading history: regulation of connective tissue biology by mechanical energy. *J Biomech*, 20:785–794, 1987.

[43] D.R. Carter, T.E. Orr, and D.P. Fyhrie. Relationships between loading history and femoral cancellous bone architecture. *J Biomech*, 22:231–244, 1989.

[44] D.R. Carter, T.E. Orr, D.P. Fyhrie, and D.J. Schurman. Influences of mechanical stress on prenatal and postnatal skeletal development. *Clin Orthop Rel Res*, 219:237–250, 1987.

[45] J.H. Challis. A procedure for determining rigid body transformation parameters. *J Biomech*, 28:733–737, 1995.

[46] J.H. Challis and D.G. Kerwin. An analytical examination of muscle force estimations using optimization techniques. *Proc Inst Mech Eng Part H, J Engng Med*, 207:139–148, 1993.

[47] E.Y. Chao, R.K. Laughman, E. Schneider, and R.N. Stauffer. Normative data of knee joint motion and ground reaction forces in adult level walking. *J Biomech*, 16(3):219–233, 1983.

[48] E.Y. Chao, R.K. Laughman, and R.N. Stauffer. Biomechanical gait evaluation of pre and postoperative total knee replacement patients. *Arch Orthop Troumat Surg*, 97:309–317, 1980.

[49] E.Y. Chao, J.D. Lynch, and M.J. Vanderploeg. Simulation and animation of musculoskeletal joint system. *Trans ASME - J Biomech Engng*, 115:562–568, 1993.

[50] E.Y. Chao and B.F. Morrey. Three-dimensional rotation of the elbow. *J Biomech*, 11:57–73, 1978.

[51] E.Y. Chao and K. Rim. Application of optimization principles in determining the applied moments in the human leg joints during gait. *J Biomech*, 6:497–510, 1973.

[52] L. Cheze, B.J. Fregly, and J. Dimnet. A solidification procedure to facilitate kinematic analysis based on video system data. *J Biomech*, 28:879–884, 1995.

[53] L.S. Chou, S.M. Song, and L.F. Draganich. Predicting the kinematics and kinetics of gait based on the optimum trajectory of the swing limb. *J Biomech*, 28:377–385, 1995.

[54] C.K. Chow and D.H. Jacobson. Studies of human locomotion via optimal programming. *Math Biosci*, 10:239–306, 1971.

[55] G.K. Cole, B.M. Nigg, J.L. Ronsky, and M.R. Yeadon. Application of the joint coordinate system to three-dimensional joint attitude and movement representation: a standardization proposal. *Trans ASME - J Biomech Engng*, 115:344–349, 1993.

[56] J.J. Collins. *Joint Mechanics - Modelling of the Lower Limb.* PhD thesis, University of Oxford, 1990.

[57] J.J. Collins. The redundant nature of locomotor optimization laws. *J Biomech*, 28:251–267, 1995.

[58] J.J. Collins and J.J. O'Connor. Muscle-ligament interactions at the knee during walking. *Proc Inst Mech Eng Part H, J Engng Med*, 205:11–18, 1991.

[59] R. Contini and R. Drillis. Biomechanics. *Applied Mechanics Reviews*, 7:49–52, 1954.

[60] R.D. Crowninshield. Use of optimization techniques to predict muscle forces. *Trans ASME - J Biomech Engng*, 100:88–92, 1978.

[61] R.D. Crowninshield and R.A. Brand. A physiologically based criterion of muscle force prediction in locomotion. *J Biomech*, 14:793–801, 1981.

[62] R.D. Crowninshield, R.A. Brand, R.C. Johnson, and J.C. Milroy. An analysis of femoral component stem design in total hip arthroplasty. *J Bone Jt Surg [Am]*, 62-A:68–78, 1980.

[63] R.D. Crowninshield, R.C. Johnston, J.G. Andrews, and R.A. Brand. A biomechanical investigation of the human hip. *J Biomech*, 11:75–85, 1978.

[64] R.D. Crowninshield, R.C. Johnston, R.A. Brand, and D.R. Pederson. Pathological ligamentous constraints of the hip. *Clin Orthop Rel Res*, 181:291–297, 1983.

[65] R.B. Davis, S. Ounpuu, D. Tyburski, and J.R. Gage. A gait analysis data collection and reduction technique. *Hum Mvmt Sci*, 10:575–587, 1991.

[66] D.T. Davy and M.L. Audu. A dynamic optimization technique for predicting muscle forces in the swing phase of gait. *J Biomech*, 20:187–201, 1987.

[67] D.T. Davy, G.M. Kotzar, R.H. Brown, K.G. Sr Heiple, V.M. Goldberg, K.G. Jr Heiple, J. Berilla, and A.H. Burstein. Telemetric force measurements across the hip after total arthroplasty. *J Bone Jt Surg [Am]*, 70A:45–50, 1988.

[68] S.L. Delp, J.P. Loan, M.G. Hoy, F.E. Zajac, E.L. Topp, and J.M. Rosen. An interactive graphics-based model of the lower extremity to study orthopaedic surgical procedures. *IEEE Trans Biomed Eng*, 37(8):757–767, August 1990.

[69] C.A.M. Doorenbosch, J. Harlaar, M.E. Roebroeck, and G.J. Lankhorst. Two strategies of transferring from sit-to-stand; the activation of monoarticular and biarticular muscles. *J Biomech*, 27(11):1299–1307, 1994.

[70] W.F. Dostal and J.G. Andrews. A three-dimensional biomechanical model of hip musculature. *J Biomech*, 14:803–812, 1981.

[71] J. Dul and G.E. Johnson. A kinematic model of the human ankle. *J Biomed Eng*, 7:137–143, 1985.

[72] J. Dul, G.E. Johnson, R. Shiavi, and M.A. Townsend. Muscular synergism-II. a minimum-fatigue criterion for load sharing between synergistic muscles. *J Biomech*, 17:675–684, 1984.

[73] J. Dul, M.A. Townsend, R. Shiavi, and G.E. Johnson. Muscular synergism-I. on criteria for load sharing between synergistic muscles. *J Biomech*, 17:663–673, 1984.

[74] H. Elftman. Forces and energy changes in the leg during walking. *Am J Physiol*, 125:339–356, 1939.

[75] M.I. Ellis, B.B. Seedhom, A.A. Amis, Dowson. D., and V. Wright. Forces in the knee joint whilst rising from normal and motorized chairs. *Engng in Med*, 8:33–40, 1979.

[76] T. A. English and M. Kilvington. *In vivo* records of hip loads using a femoral implant with telemetric output. *J Biomed. Engng*, 1:111–115, 1979.

[77] J.R. Essinger, P.F. Leyvraz, J.H. Heegard, and D.D. Robertson. A mathematical model for the evaluation of the behaviour during flexion of condylar-type knee prostheses. *J Biomech*, 22:1229–1241, 1989.

[78] J.D. Feikes, D.R. Wilson, and J.J. O'Connor. Knee replacements and mathematical models. In *Proc. of the British Orthopaedic Research Society Meeting*, page 8, Sheffield, U.K., 1997. British Orthopaedic Research Society.

[79] W.K. Feinstein, P.C. Noble, and E. Kamarice. The anatomic alignment of the patellar bearing surface of the femur. In *Transactions of the 42nd Annual Meeting of the Orthopaedic Research Society*, page 719, Atlanta, Georgia, Februrary 1996. Orthopaedic Research Society.

[80] R.E. Field and N. Rushton. Proximal femoral surface strain gauge analysis of a new epiphyseal prosthesis. *J. Biomed. Eng.*, 11:123–129, 1989.

[81] D.P. FitzPatrick and J.J. O'Connor. Theoretical modelling of the knee applied to the anterior drawer test. In *Proc Inst Mech Eng - Changing Role of Engineeering in Orthopaedics*, pages 79–83, 1989.

[82] A. Fitzsimmons, A.C. Nicol, and I.G. Kelly. Hip joint forces during activities of daily living. In *Proceedings of the 10th Conference of The European Society of Biomechanics*, page 267, Leuven, Belgium, 1996. The European Society of Biomechanics.

[83] J.A. Friederich and R.A. Brand. Muscle fiber architecture in the human lower limb. *J Biomech*, 23(1):91–95, Jan 1990.

[84] N.F. Friederich, W. Muller, and W.R. O'Brien. Klinische anwendung biomechanischer und funktionell anatomischer daten am kniegelenk. *Orthopade*, 21:41–50, 1992.

[85] J.P. Fulkerson and D.S. Hungerford. *Disorders of the patellofemoral joint.* Williams and Wilkins, London, England, second edition, 1990.

[86] J. Fuller, L.J. Liu, and M.C. Murphy. A comparison of lower-extremity skeletal kinematics measured using skin- and pin-mounted markers. In *Proceedings of the Fourth International Symposium on 3-D Analysis of Human Movement*, Grenoble, France, 1996. International Society of Biomechanics.

[87] Y.C. Fung. *Biomechanics.* Springer-Verlag, New York, 1981.

[88] F.K. Fuss. Anatomy of the cruciate ligaments and their function in extension and flexion of the human knee joint. *Am J Anat*, 184:165–76, 1989.

[89] F.K. Fuss. Anatomy of the cruciate ligaments and their function in extension and flexion of the human knee joint. *Am J Anat*, 184:165–176, 1989.

[90] P. Genoud. Some considerations on joint kinematics during gait. In *Proceedings of the Fourth International Symposium on 3-D Analysis of Human Movement*, Grenoble, France, 1996. International Society of Biomechanics.

[91] J.M. Gere and S.P. Timoshenko. *Mechanics of Materials.* Van Nostrand Reinhold, London, 2nd si edition edition, 1987.

[92] H.S. Gill and J.J. O'Connor. Sagittal plane mechanics of the extensor apparatus: a computer model of the human patellofemoral joint. OUEL report, University of Oxford, Wellington Square, Oxford, England, June 1994.

[93] H.S. Gill and J.J. O'Connor. Biarticulating two-dimensional computer model of the human patellofemoral joint. *Clin. Biomech.*, 11:81–89, 1996.

[94] H.S. Gill and J.J. O'Connor. A new testing rig for force platform calibration and accuracy tests. *Gait Post*, in press, 1997.

[95] F.G. Girgis, J.L. Marshall, and A.R.S. Al Monajem. The cruciate ligaments of the knee joint - anatomical, functional, and experimental analysis. *Clin Orthop*, 106:216–231, 1975.

[96] J.W. Goodfellow, D. Hungerford, and M. Zindel. Patello-femoral joint mechanics and pathology: I. functional anatomy. *J Bone Jt Surg [Br]*, 58B:283–287, 1976.

[97] J.W. Goodfellow and J.J. O'Connor. The mechanics of the knee and prosthesis design. *J Bone Jt Surg [Br]*, 60:358–369, 1978.

[98] D.T. Greenwood. *Principles of Dynamics.* Prentice Hall, New Jersey, second edition, 1988.

[99] E.S. Grood and W.J. Suntay. A joint coordinate system for the clinical description of three-dimensional motions: application to the knee. *Trans ASME - J Biomech Engng*, 105:136–144, 1983.

[100] D.E. Hardt. Determining muscle forces in the leg during normal human walking - an application and evaluation of optimization methods. *Trans ASME - J Biomech Engng*, 100:72–78, 1978.

[101] H. Hatze. A new method for the simultaneous measurement of the moment of inertia, the damping coefficient and the location of the centre of mass of a body segment *in situ*. *Europ J Appl Physiol*, 34:217–226, 1975.

[102] H. Hatze. The complete optimization of a human motion. *Math. Biosci.*, 28:99–135, 1976.

[103] H. Hatze. A complete set of control equations for the human musclo-skeletal system. *J Biomech*, 10:799–805, 1977.

[104] H. Hatze. A comprehensive model for human motion simulation and its application to the take-off phase of the long jump. *J Biomech*, 14(3):135–142, March 1981.

[105] E.J. Haug and J.S. Arora. *Applied Optimal Design.* John Wiley and Sons, New York, 1979.

[106] W.C. Hayes, J.D. Gran, M.L. Nagurka, J.M. Feldman, and C. Oatis. Leg motion analysis during gait by multiaxial accelerometry: theoretical foundations and preliminary validations. *Trans ASME - J Biomech Engng*, 105:283–289, 1983.

[107] J. Heegaard, P.F. Leyvraz, A. Curnier, L. Rakotomanana, and R. Huiskes. The biomechanics of the human patella during passive knee flexion. *J Biomech*, 28(11):1265–1279, 1995.

[108] M.S. Hefzy and E.S. Grood. Review of knee models. *Appl Mech Rev*, 41(1):1–13, 1988.

[109] W. Herzog and T.R. Leonard. Validation of optimization models that estimate the forces exerted by synergistic muscles. *J Biomech*, 24(Suppl. 1):31–39, 1991.

[110] W. Herzog, T.R. Leonard, and A.C.S. Guimaraes. Forces in gastrocnemius, soleus, and plantaris tendons of the freely moving cat. *J Biomech*, 26:945–953, 1993.

[111] W. Herzog and L. Read. Lines of action and moment arms of the major force-carring structures crossing the human knee joint. *J Anat*, 182:213–230, 1993.

[112] R.N. Hinrichs. Regression equations to predict segamental moments of inertia from anthropometric measurements: an extension of the data of Chandler *et al.* (1975). *J Biomech*, 18(8):621–624, 1985.

[113] S. Hirokawa. Three-dimensional mathematical model analysis of the patellofemoral joint. *J Biomech*, 24(8):659–671, 1991.

[114] H.P. Hirshman, D.M. Daniel, and K. Miyasaka. The fate of unoperated knee ligament injuries. In D.M. Daniel, W.H. Akeson, and J.J. O'Connor, editors, *Knee Ligaments - Structure, Function, Injury, and Repair*, pages 481–504. Raven Press, 1990.

[115] A.L. Hof and J. van den Berg. Linearity between the weighted sum of the EMGs of the human triceps surae and the total torque. *J Biomech*, 10, 1977.

[116] J.M. Hollis, S. Takai, D. J. Adams, S. Horibe, and S. L-Y. Woo. The effects of knee motion and external loading on the length of the anterior cruciate ligament (ACL): a kinematic study. *Trans ASME - J Biomech Engng*, 113:208–214, 1991.

[117] R.W.W. Hsu, S. Himeno, M.B. Coventry, and E.Y.S. Chao. Normal axial alignment of the lower extremity and load-bearing distribution at the knee. *Clin Orthop Rel Res*, 255:215–227, 1990.

[118] J. Hua and P.S. Walker. Closeness of fit of uncemented stems improves the strain distribution in the femur. *J Orthop Res*, 13:339–346, 1995.

[119] R. Huiskes. The various stress patterns of press-fit, ingrown, and cemented femoral stems. *Clin Orthop Rel Res*, 261:27–38, 1990.

[120] R. Huiskes, H. Weinans, H.J. Grootenboer, M. Dalstra, B. Fudala, and T.J. Slooff. Adaptive bone-remodelling theory applied to prosthetic-design analysis. *J Biomech*, 20(11/12):1135–1150, 1987.

[121] A. Huson. Biomechanische probleme des kniegelenks. *Orthopade*, 3, 1974.

[122] A. Huson, C.W. Spoor, and A.J. Verbout. A model of the human knee, derived from kinematic principles, and its relevance for endoprosthesis design. *Acta Morphol Neerl-Scand*, 27:45–62, 1989.

[123] V. T. Inman, H. J. Ralston, and F. Todd. *Human Walking.* Williams and Wilkins, Baltimore, 1981.

[124] V.T. Inman. *The Joints of the Ankle.* Williams and Wilkins, Baltimore, 1976.

[125] R.E. Isman and V.T. Inman. Anthropometric studies of the human foot and ankle. *Bulletin of Prosthetics Research*, 10:97–129, 1969.

[126] R.J. Jaeger and P. Vanitchatchavan. Ground reaction forces during termination of human gait. *J Biomech*, 25(10):1233–1236, 1992.

[127] R.H. Jensen and D.T. Davy. An investigation of muscle lines of action about the hip: a centroid line approach vs the straight line approach. *J Biomech*, 8:103–110, 1975.

[128] R.H. Jensen and W.K. Metcalf. A systematic approach to the quantitative description of musculoskeletal geometry. *J Anat*, 119:209–221, 1975.

[129] H. Johansson. Role of knee ligaments in proprioception and regulation of muscle stiffness. *J Elect Kinesiol*, 1:158–179, 1991.

[130] H. Johansson, P. Sjolander, and P. Sojka. A sensory role for the cruciate ligaments. *Clin Orthop Rel Res*, 268:161–178, 1991.

[131] F. Johnson, S. Leitl, and W. Waugh. The distribution of load across the knee. *J Bone Jt Surg [Br]*, 62-B:346–349, 1980.

[132] F. Johnson, P. Scarrow, and W. Waugh. Assessments of loads in the knee joint. *Med Biol Eng Comput*, 19:237–243, 1981.

[133] R.C. Johnston, R.A. Brand, and R.D. Crowninshield. Reconstruction of the hip. *J Bone Jt Surg [Am]*, 61-A:639–652, 1979.

[134] M.P. Kadaba, H.K. Ramakrishnan, and M.E. Wootten. Measurement of lower extremity kinematics during level walking. *J Orthop Res*, 8(3):383–392, 1990.

[135] M.P. Kadaba, H.K. Ramakrishnan, M.E. Wootten, J. Gainey, G. Gorton, and G.V.B. Cochran. Repeatability of kinematic, kinetic, and electromyographic data in normal adult gait. *J Orthop Res*, 7(6):849–860, 1989.

[136] I.A. Kapandji. *The Physiology of the Joints. Volume 2 The Lower Limb.* Churchill Livingstone, Edinburgh, 1987.

[137] T.M. Kepple, A.S. Arnold, S.J. Stanhope, and K.L. Siegel. Assessment of a method to estimate muscle attachments from surface landmarks: a 3d computer graphics approach. *J Biomech*, 27:365–371, 1994.

[138] P.V. Komi. Relevance of *in vivo* force measurements to human biomechanics. *J Biomech*, 23(Suppl 1):23–34, 1990.

[139] B. Koopman, H.J. Grootenboer, and H.J. de Jongh. An inverse dynamics model for the analysis, reconstruction and prediction of bipedal walking. *J Biomech*, 28(11):1369–1376, 1995.

[140] G.M. Kotzar, D.T. Davy, V.M. Goldberg, K.G. Heiple, J. Berilla, K.G. Heiple, Jr., R.H. Brown, and A.H. Burstein. Telemeterized *in vivo* hip joint force data: a report on two patients after total hip surgery. *J Orthop Res*, 9(5):621–633, 1991.

[141] H. Kurosawa, P.S. Walker, S. Abe, A. Garg, and T. Hunter. Geometry and motion of the knee for implant and orthotic design. *J Biomech*, 18(7):487–499, 1985.

[142] H. Kurosawa, K-I. Yamakoshi, K. Yasuda, and T. Sasaki. Simultaneous measurement of changes in length of the cruciate ligaments during knee motion. *Clin Orthop Rel Res*, 265:233–40, 1991.

[143] M.A. Lafortune, P.R. Cavanagh, H.J. Sommer III, and A. Kalenak. Three-dimensional kinematics of the human knee during walking. *J Biomech*, 25:347–357, 1992.

[144] J.H. Lawrence and C.J. De Luca. Myoelectric signal vs. force relationship in different human muscles. *J Applied Physiol*, 54:1653–1659, 1983.

[145] A. Leardini, F. Catani, and J.J. O'Connor. The one degree of freedom nature of the human ankle/subtalar complex. In *Proc. of the British Orthopaedic Research Society Meeting*, page 41, Brighton, U.K., 1996. British Orthopaedic Research Society.

[146] A. Leardini, T.-W. Lu, F. Catani, and J.J. O'Connor. A four bar linkage model for the human ankle joint. In *Proc. of the British Orthopaedic Research Society Meeting*, page 16, Brighton, U.K., 1996. British Orthopaedic Research Society.

[147] M. Lengsfeld, U. Stammberger, and S. Reeh. Spatial measurement and transformation of muscular attachments at the lower extremity. *Trans ASME - J Biomech Engng*, 16:518–525, 1994.

[148] B.F. LeVeau. Biomechanics. a summary of perspectives. *Phys Ther*, 64(12):1812, 1984.

[149] W.D. Lew and J.L. Lewis. An anthropometric scaling method with application to the knee joint. *J Biomech*, 10:171–181, 1977.

[150] J.L. Lewis, W.D. Lew, and J. Schmidt. A note on the application and evaluation of the buckle transducer for knee ligament force measurement. *J Biomed Engng*, 104:125–128, 1982.

[151] J.L. Lewis, W.D. Lew, and J.R. Zimmerman. A nonhomogeneous anthropometric scaling method based on finite element principles. *J Biomech*, 13:815–824, 1980.

[152] O.C.J. Lippold. The relationship between integrated action potentials in a human muscle and its isometric tension. *J Physiol*, 117:492–499, 1952.

[153] T.-W. Lu, H.S. Gill, and J.J. O'Connor. An interactive graphics-based window interface for geometric and mechanical modelling of the lower limb. In J. Middleton, M.L. Jones, and G.N. Pande, editors, *Computer Methods for Biomechanics and Biomedical Engineering*, pages 497–506. Gordon and Breach, 1996.

[154] T.-W. Lu and J.J. O'Connor. Fibre recruitment and shape changes of knee ligaments during motion: as revealed by a computer graphics-based model. *Proc Inst Mech Eng Part H, J Engng Med*, 210:71–79, 1996.

[155] T.-W. Lu and J.J. O'Connor. Lines of action and moment arms of the major force-bearing structures crossing the human knee joint: comparison between theory and experiment. *J Anatomy*, 189:575–585, 1996.

[156] T.-W. Lu, J.J. O'Connor, S.J.G. Taylor, and P.S. Walker. Comparison of femoral forces during double and single stance: theory and experiment. In *3rd International Symposium on Computer Methods in Biomechanics and Biomedical Engineering*, Barcelona, 1997. Gordon and Breach.

[157] T.-W. Lu, J.J. O'Connor, S.J.G. Taylor, and P.S. Walker. Validation of a lower limb model with *in vivo* femoral forces telemetered from two subjects. *J Biomech*, in press, 1997.

[158] T.-W. Lu, S. Taylor, H.S. Gill, P.S. Walker, R.S.M. Ling, and J.J. O'Connor. Gait analysis of patients with instrumented massive proximal femoral prostheses. *J Bone Jt Surg [Br]*, 77B, Suppl:321, 1996.

[159] T.-W. Lu, S.J.G. Taylor, J.J. O'Connor, and P.S. Walker. Influence of muscle activity on the forces in the femur: an *in vivo* study. *J Biomech*, in press, 1997.

[160] P.G.J. Maquet. *Biomechanics of the Knee.* Springer-Verlag, Berlin, 1976.

[161] E.J. Marey. *Movement.* Appleton Co., New York, 1895.

[162] K.L. Markolf, J.S. Mensch, and H.C. Amstutz. Stiffness and laxity of the knee - the contributions of the supporting structures. a quantitative *in-vitro* study. *J Bone Jt Surg [Am]*, 58-A:583–593, 1979.

[163] G.T. Marzan and H.M. Karara. A computer program for direct linear transformation solution of the colinearity condition, and some applications of it. In *Proc of the Symposium on Close-Range Photogrammetric Systems*, pages 420–476. American Society of Photogrammetry, 1975.

[164] S.T. McCaw and P. DeVita. Errors in alignment of center of pressure and foot coordinates affect predicted lower extremity torques. *J Biomech*, 28:985–988, 1995.

[165] H. McKellop, E. Ebramzadeh, P.G. Niederer, and A. Sarmiento. Comparison of the stability of press-fit hip prosthesis femoral stems using a synthetic model femur. *J Orthop Res*, 9:297–305, 1991.

[166] T.M. McLaughlin, T.J. Lardner, and C.J. Dillman. A kinematic model of the performance in the parallel squat by champion powerlifters. *Medicine and Science in Sports*, 9:128–133, 1977.

[167] T.A. McMahon. *Muscles, Reflexes, and Locomotion.* Princeton University Press, Princeton, New Jersey, 1984.

[168] A. Menschik. Mechanik des kniegelenkes - teil 1. *Z Orthop*, 112:481–95, 1974.

[169] H. Meyer. Die mechanick des kniegelinks. *Archiv fur Anatomie und Physiologie*, pages 497–547, 1853.

[170] A.W. Miles, D.M. Dall, and M. Rivarola. A study of antero-posterior load transfer in total hip replacement using a modelling technique. *Engng in Med*, 12:113–115, 1983.

[171] D. B. Moffat and R. F. Mottram. *Anatomy and Physiology for Physiotherapists.* Blackwell Scientific Pulications, Osney Mead, Oxford, England, 1979.

[172] J.B. Morrison. Bioengineering analysis of force actions transmitted by the knee joint. *Bio-med Engng*, 3:164–170, 1968.

[173] J.B. Morrison. The mechanics of muscle function in locomotion. *J Biomech*, 3:431–451, 1970.

[174] J.B. Morrison. The mechanics of the knee joint in relation to normal walking. *J Biomech*, 3:51–61, 1970.

[175] M.P. Murray, G.N. Guten, J.M. Baldwin, and G.M. Gardner. A comparison of plantar flexion torque with and without the triceps surae. *Acta Orthop Scand*, 47:122–124, 1976.

[176] E. Muybridge. *The human figure in motion.* Chapman and Hall, London, 1901. Reprinted in 1955 by Dover Publications Inc., New York.

[177] R. Nisell, G. Nemeth, and H. Ohlsen. Joint forces in extension of the knee. *Acta Orthopaedica Scandinavica*, 57:41–46, 1986.

[178] J. O'Connor, E. Biden, J. Bradley, D. FitzPatrick, S. Young, C. Kershaw, and J. Daniel, D. Goodfellow. The muscle-stabilized knee. In D.M. Daniel, W.H. Akeson, and J.J. O'Connor, editors, *Knee Ligaments - Structure, Function, Injury, and Repair*, pages 239–278. Raven Press, 1990.

[179] J. O'Connor, T. Shercliff, D. FitzPatrick, E. Biden, and J. Goodfellow. Mechanics of the knee. In D.M. Daniel, W.H. Akeson, and J.J. O'Connor, editors, *Knee Ligaments - Structure, Function, Injury, and Repair*, pages 201–238. Raven Press, 1990.

[180] J. O'Connor, T. Shercliff, D. FitzPatrick, J. Bradley, D. Daniel, and J. Biden, E. Goodfellow. Geometry of the knee. In D.M. Daniel, W.H. Akeson, and J.J. O'Connor, editors, *Knee Ligaments - Structure, Function, Injury, Repair*, pages 163–200. Raven Press, 1990.

[181] J.J. O'Connor. Can muscle co-contraction protect knee ligaments after injury or repair. *J Bone Jt Surg [Br]*, 75-B(1):41–8, January 1993.

[182] J.J. O'Connor, J. Goodfellow, and E. Biden. Designing the human knee. In I.A.F. Stokes, editor, *Mechanical Factors and the Skeleton*, pages 52–64. John Libbey, London, 1981.

[183] J.J. O'Connor, T. Shercliff, and J. Goodfellow. The mechanics of the knee in the sagittal plane. In W. Muller and W. Hackenbruck, editors, *Proceedings of the Second Congress of the European Society for Surgery and Arthroscopy of the Knee*, pages 12–30, Berlin, 1988. European Society for Surgery and Arthroscopy of the Knee.

[184] J.J. O'Connor, T.L. Shercliff, E. Biden, and J.W. Goodfellow. The geometry of the knee in the sagittal plane. *Proc Inst Mech Eng Part H, J Engng Med*, 203:223–233, 1989.

[185] S.J. Olney and D.A. Winter. Predictions of knee and ankle moments of force in walking from EMG and kinematic data. *J Biomech*, 18:9–20, 1985.

[186] S. Onyshko and D.A. Winter. A mathematical model for the dynamics of the human locomotion. *J Biomech*, 13:361–368, 1980.

[187] L.R. Osternig, J. Hamill, D. M. Corcos, and J. Lander. Electromyographic patterns accompanying isokinetic exercise under varying speed and sequencing conditions. *Am J Phys Med*, 63:289–3297, 1984.

[188] M.G. Pandy, F.C. Anderson, and D.G. Hull. A parameter optimization approach for the optimal control of large-scale musculoskeletal systems. *Trans ASME - J Biomech Engng*, 114:450–460, 1992.

[189] M.G. Pandy and F.E. Zajac. Optimal muscular coordination strategies for jumping. *Trans ASME - J Biomech Engng*, 24:1–10, 1991.

[190] M.G. Pandy, F.E. Zajac, E. Sim, and W.S. Levine. An optimal control model for maximum-height human jumping. *J Biomech*, 23(12):1185–1198, 1990.

[191] M.M. Panjabi, T. Trumble, J.E. Hult, and W. Southwick. Effect of femoral stem length on stress rasiers associated with revision hip arthroplasty. *J Orthop Res*, 3:447–445, 1985.

[192] A.G. Patriarco, R.W. Mann, S.R. Simon, and J.M. Mansour. An evaluation of the approaches of optimization models in the prediction of muscle forces during human gait. *J Biomech*, 14:513–25, 1981.

[193] J.P. Paul. Bio-engineering studies of the forces transmitted by joints: II. Engineering analysis. In R.M. Kenedi, editor, *Biomechanics and Related Bio-Engineering Topics*, pages 369–380. Pergamon Press, 1965.

[194] J.P. Paul. Forces transmitted by the joints in the human body. *Proc Instn Mech Engrs*, 181:8–15, 1966-67.

[195] F. Pauwels. Principles of construction of the lower extremity. their significance for the stressing of the skeleton of the leg. *Z. Anat. Entwickl. Gesch.*, 114:525–538, 1950.

[196] D.R. Pedersen, R.A. Brand, Cheng C., and J.S. Arora. Direct comparison of muscle force predictions using linear and nonlinear programming. *Trans ASME - J Biomech Engng*, 109:192–199, 1987.

[197] A. Pedotti. A study of motor coordination and neuromuscular activities in human locomotion. *Biol Cybern*, 26:53–62, 1977.

[198] A. Pedotti, V.V. Krishnan, and L. Stark. Optimization of muscle force sequencing in human locomotion. *Math Biosci*, 38:57–76, 1978.

[199] J. Perry. *Gait Analysis: Normal and Pathological Function.* SLACK, 1992.

[200] J. Perry and G.A. Bekey. EMG-force relationships in skeletal muscle. *CRC Critical Review in Biomedical Engineering*, December:1–22, 1981.

[201] J.C. Pezzack, R.W. Norman, and D.A. Winter. An assessment of derivative determining techniques used for motion analysis. *J Biomech*, 10:377–382, 1977.

[202] J. Phillips. *Freedom in Machinery.* Cambridge University Press, Cambridge, 1984.

[203] P. Procter and J.P. Paul. Ankle joint biomechanics. *J Biomech*, 15:627–634, 1982.

[204] E.L. Radin and I.L. Paul. Response of joints to impact loading: I. *in vitro* wear. *Arth. Rheum.*, 14:356–362, 1971.

[205] M.R. Ramey and A.T. Yang. A simulation procedure for human motion studies. *J Biomech*, 14(4):203–213, 1981.

[206] N.S. Richard, E.Y. Chao, and A.N. Gyory. Biomechanical gait analysis of the diseased knee joint. *Clin Orthop Rel Res*, 126:246–255, 1977.

[207] A. Rohlmann, U. Mossner, and G. Bergmann. Finite-element-analysis and experimental investigation in a femur with hip endoprosthesis. *J Biomech*, 16(9):727–742, 1983.

[208] A. Rohlmann, U. Mossner, G. Bergmann, G. Hees, and R. Kolbel. Effects of stem design and material properties on stresses in hip endoprostheses. *J. Biomed. Eng.*, 9:77–83, 1987.

[209] H. Rohrle, C. Sigolotto, and W. Sollbach. Joint forces in the human pelvis-leg skeleton during walking. *J Biomech*, 17(6):409–424, 1984.

[210] J.S. Rovick, J.D. Reuben, R.J. Schrager, and P.S. Walker. Relation between knee motion and ligament length patterns. *Clin Biomech*, 6:213–20, 1991.

[211] R.H. Rozendal. Bi-articular muscles: an anatomical comment. In *VIII Meeting of the European Society of Biomechanics*, page 243, Rome, June 1992. European Society of Biomechanics.

[212] S.G. Rugg, R.J. Gregor, B.R. Mandelbaum, and L. Chiu. *In vivo* moment arm calculations at the ankle using magnetic resonance imaging (MRI). *J Biomech*, 23(5):495–501, 1990.

[213] C.F. Runge, F.E. Zajac, J.H.J. Allum, D.W. Risher, A.E. Jr Bryson, and F. Honegger. Estimating net joint torques from kinesiological data using optimal linear system theory. *IEEE Trans Biomed Eng*, 42(12):1158–1164, 1995.

[214] N.W. Rydell. Forces acting on the femoral head prosthesis. *Acta Orthop. Scand.*, 88 (Suppl.):37, 1966.

[215] A.A. Sapega, R.A. Moyer, C. Schneck, and N. Komalahiranya. Testing for isometry during reconstruction of the anterior cruciate ligament. *J Bone Jt Surg [Am]*, 72-A:259–267, 1990.

[216] S. Sathasivam and P.S. Walker. Optimization of the bearing surface geometry of total knees. *J Biomech*, 27:255–264, 1994.

[217] O.D. Schipplein and T.P. Andriacchi. Interaction between active and passive knee stabilizers during level walking. *J Orthop Res*, 9:113–9, 1991.

[218] H. Schmotzer, G. Tchejeyan, and J. Song. A comparison of various loading configurations of the proximal femur for the evaluation of reconstructive surgical procedures. *Proc Inst Mech Eng Part H, J Engng Med*, 206:29–36, 1992.

[219] E. Schneider, M. C. Michel, M. Genge, and S. M. Perren. Loads acting on an intramedullary femoral nail. In G. Bergmann, F. Graichen, and A. Rohlmann, editors, *Proc. of a Workshop on Implantable Telemetry in Orthopaedics*, pages 93–102. Freie Universitat, 1990.

[220] S.H. Scott and D.A. Winter. Talocrural and talocalcaneal joint kinematics and kinetics during the stance phase of walking. *J Biomech*, 24:743–752, 1991.

[221] A. Seireg and R.J. Arvikar. A mathematical model for evaluation of forces in lower extremeties of the musculo-skeletal system. *J Biomech*, 6:313–326, 1973.

[222] A. Seireg and R.J. Arvikar. The prediction of muscular load sharing and joint forces in the lower extremeties during walking. *J Biomech*, 8:89–102, 1975.

[223] G. Selvik. *A roentgen stereophotogrammetric method for the study of the kinematics of the skeletal system.* PhD thesis, University of Lund, Sweden, 1974.

[224] M.H. Sherif, R.J. Gregor, L.M. Liu, R.R. Roy, and C.L. Hager. Correlation of myoelectric activity and muscle force during selected cat treadmill locomotion. *J Biomech*, 16:691–701, 1983.

[225] R. Shiavi, T. Limbird, M. Frazer, K. Stivers, A. Strauss, and J. Abramovitz. Helical motion analyis of the knee - II. kinematics of uninjured and injured knee during walking and pivoting. *J Biomech*, 20:653–665, 1987.

[226] J.A. Sidles, R.V. Larson, J.L. Garbini, D.J. Downey, and F.A. Matsen. Ligament length relationships in the moving knee. *J Orthop Res*, 6:593–610, 1988.

[227] S. Siegler, J. Chen, and C.D. Schneck. The three-dimensional kinematics and flexibility characteristics of the human ankle and subtalar joint - Part I: kinematics. *Trans ASME - J Biomech Engng*, 110:364–373, 1988.

[228] C.W. Spoor and J.L. van Leeuwen. Knee muscle moment arms from MRI and from tendon travel. *J Biomech*, 25:201–206, 1992.

[229] C.W. Spoor and F.E. Veldpaus. Rigid body motion calculated from spatial co-ordinates of markers. *J Biomech*, 13:391–393, 1980.

[230] H. Strasser. *Lehrbuch der Muskel- und Gelenkmechanik.* Springer, Berlin, 1917.

[231] S. Takai, S.L-Y. Woo, G.A. Livesay, D.J. Adams, and F.H. Fu. Determination of the *in situ* loads on the human anterior cruciate ligament. *J Orthop Res*, 11:686–695, 1993.

[232] S. J. Taylor and N. Donaldson. Instrumenting stanmore prostheses for long-term strain measurement *in vivo*. In G. Bergmann, F. Graichen, and A. Rohlmann, editors, *Proceedings of a Workshop on Implantable Telemetry in Orthopaedics*, pages 93–102. Freie Universitat Berlin, 1990.

[233] S. J. Taylor, N. Donaldson, J. M. Meswania, and J. S. Perry. A telemetry system for *in vivo* strain measurement in orthopaedic endoprostheses. In

E. Little, editor, *Experimental Mechanics: Technology Transfer between High Tech Engineering and Biomechanics*, pages 365–376. 1992.

[234] S. J. G. Taylor, J. S. Perry, J. M. Meswania, N. Donaldson, P. S. Walker, and S. R. Cannon. Telemetry of forces from proximal femoral replacements and relevance to fixation. *J Biomech*, 30:225–234, 1997.

[235] M.A. Townsend, M. Izak, and R.W. Jackson. Total motion knee goniometry. *J Biomech*, 10:183–193, 1977.

[236] C.S. Tsai and J.M. Mansour. Swing phase simulation and design of above knee prostheses. *Trans ASME - J Biomech Engng*, 108:65–72, 1986.

[237] C.M. Tylkowski, S.R. Simon, and J.M. Mansour. Internal rotation gait in spastic cerebral palsy in the hip. In J.P. Nelson, editor, *Proceedings of the 10th Open Scientific Meeting of the Hip Society*, pages 89–125. Mosby, St. Louis, 1982.

[238] J.J. Uicker, J. Denavit, and R.S. Hartenberg. An iterative method for the displacement analysis of spatial mechanisms. *Trans ASME - J Applied Mechanics*, pages 309–314, 1964.

[239] Advisory Committe on Artificial Limbs University of California. The pattern of muscular activity in the lower extremity during walking. Prosthetic devices research project institute of engineering research, University of California, Berkeley, Series 2, Issue 25 1953.

[240] A.J. van den Bogert, G.D. Smith, and B.M. Nigg. *In vivo* determination of the anatomical axes of the ankle joint complex: an optimization approach. *J Biomech*, 27:1477–1488, 1994.

[241] R. van Dijk. *The behaviour of the cruciate ligaments of the knee.* PhD thesis, Catholic University, Nijmegen, The Netherlands, 1983.

[242] R. van Dijk, R. Huiskes, and G. Selvik. Roentgen stereophotogrammetric methods for the evaluation of the three dimensional kinematic behavior and cruciate ligament length patterns of the human knee joint. *J Biomech*, 12:727–731, 1979.

[243] T.M.G.J. van Eijden, E. Eouwenhoven, J. Verburg, and W.A. Weijs. A mathematical model of the patellofemoral joint. *J Biomechanics*, 19(3):219–229, 1986.

[244] G.J. van Ingen Schenau. Proposed actions of bi-articular muscles. An overview. In *VIII Meeting of the European Society of Biomechanics*, page 240, Rome, June 1992. European Society of Biomechanics.

[245] J.L. van Leeuwen and C.W. Spoor. On the role of biarticular muscles in human jumping. *J Biomech*, 25(2):207–209, 1992.

[246] L.J. van Ruijven and W.A. Weijs. A new model for calculating muscle forces from electromyograms. *Eur J Appl Physiol*, 61:479–485, 1990.

[247] A.J. van Soest, A.L. Schwab, M.F. Bobbert, and G.J. van Ingen Schenau. The influence of the biarticularity of the gastrocnemius muscle on vertical-jumping achievement. *J Biomech*, 26(1):1–8, 1993.

[248] C.L. Vaughan. Smoothing and differentiation of time-displacement data: an application of splines and digital filtering. *Int J Bio-Medical Computing*, 13:375–386, 1982.

[249] F.E. Veldpaus, H.J. Woltring, and L.J.M.G. Dortmans. A least-squares algorithm for the equiform transformation from spatial marker co-ordinates. *J Biomech*, 21:45–54, 1988.

[250] P.S. Walker. Principles of hip replacement: design of total hip replacement. *Current Orthopaedics*, 6:146–153, 1992.

[251] C-J. Wang, P.S. Walker, and B. Wolf. The effects of flexion and rotation on the length patterns of the ligaments of the knee. *J Biomech*, 6:587–596, 1973.

[252] W.E. Weber and E.F.W. Weber. *Mechanik der menschlichen Gehwerkzeuge.* der Dietrichschen Buchhandlung, Gottingen, 1836.

[253] H. Weinans, R. Huiskes, and H.J. Grootenboer. Trends of mechanical consequences and modeling of a fibrous membrane around femoral hip prostheses. *J Biomech*, 23:991–1000, 1990.

[254] H. Weinans, R. Huiskes, and H.J. Grootenboer. The behavior of adaptive bone-remodeling simulations models. *J Biomech*, 25:1425–1441, 1992.

[255] S. C. White, H. J. Yack, and D. A. Winter. A three-dimensional musculoskeletal model for gait analysis. anatomical variability estimates. *J Biomech*, 22(8/9):885–893, 1989.

[256] T.L. Wickiewicz, R.R. Roy, P.L. Powell, and V.R. Edgerton. Muscle architecture of the human lower limb. *Clin Orthop Rel Res*, 179:275–283, 1983.

[257] P.L. Williams, R. Warwick, M. Dyson, and L.H. Bannister. *Gray's anatomy.* Churchill Livingstone, Berlin, 37nd edition, 1989.

[258] D. R. Wilson, A. B. Zavatsky, and J. J. O'Connor. Cruciate ligament forces at the knee in gait: parameter sensitivity and effects of ligament elasticity. In *International Society of Biomechanics, 1993 Abstracts*, pages 1466–1467, July 1993.

[259] D.R. Wilson. *Three-Dimensional Kinematics of The Knee.* PhD thesis, University of Oxford, 1996.

[260] D.R. Wilson, J.D. Feikes, A.B. Zavatsky, F. Bayona, and J.J. O'Connor. The one degree-of-freedom nature of the human knee joint - basis for a kinematic model. In *Proceedings of the Fourth International Symposium on 3-D Analysis of Human Movement*, Grenoble, France, 1996. International Society of Biomechanics.

[261] D.R. Wilson and J.J. O'Connor. A three-dimensional geometric model of the knee joint. In *Canadian Society of Biomechanics Conference 1994.* Canadian Society of Biomechanics, 1994.

[262] D.R. Wilson and J.J. O'Connor. A three-dimensional geometric model of the knee joint for the study of joint forces in gait. *Gait and Posture*, 5:108–115, 1997.

[263] D.A. Winter. *Biomechanics and Motor Control of Human Movement.* John Wiley and Sons, New York, 2nd edition, 1990.

[264] D.A. Winter, H.G. Sidwall, and D.A. Hobson. Measurement and reduction of noise in kinematics of locomotion. *J Biomech*, 7:157–159, 1974.

[265] D.A. Winter and H.J. Yack. EMG profiles during normal human walking: stride-to-stride and inter-subject variability. *Electroencephalography and Clinical Neurophysiology*, 67:402–411, 1987.

[266] J. Wismans, F. Veldpaus, J. Janssen, A. Huson, and P. Struben. A three-dimensional mathematical model of the knee-joint. *J Biomech*, 13:677–685, 1980.

[267] J.L. Wolff. *The Law of Bone Remodelling.* Springer, Berlin, 2nd edition, 1986.

[268] H.J. Woltring. A Fortran package for generalized, cross-validatory spline smoothing and differentiation. *Adv Eng Software*, 8:104–107, 1986.

[269] H.J. Woltring. Representation and calculation of 3-D joint movement. *Human Movement Science*, 10:603–616, 1991.

[270] G.A. Wood and L.S. Jennings. On the use of spline functions for data smoothing. *J Biomech*, 12:477–479, 1979.

[271] G. Wu and P.R. Cavanagh. ISB recommendations for standardization in the reporting of kinematic data. *J Biomech*, 28(10):1257–1261, 1995.

[272] G.T. Yamaguchi and F.E. Zajac. A planar model of the knee joint to characterize the knee extensor mechanism. *J Biomech*, 22(1):1–10, 1989.

[273] S. Yamamoto, Y. Suto, H. Kawamura, T. Hashizume, and S. Kakurai. Quantitative gait evaluation of hip diseases using principle component analysis. *J Biomech*, 16(9):717–726, 1983.

[274] M.R. Yeadon and M. Morlock. The appropriate use of regression equations for the estimation of segmental inertia parameters. *J Biomech*, 22(6/7):683–689, 1989.

[275] F.E. Zajac. Do biarticular muscles fine-tune muscle coordination? In *VIII Meeting of the European Society of Biomechanics*, page 242, Rome, June 1992. European Society of Biomechanics.

[276] A.B. Zavatsky, D.J. Beard, and J.J. O'Connor. Cruciate ligament loading during isometric muscle contractions: a theoretical basis for rehabilitation. *Am J Sports Med*, 22(3):418–423, 1994.

[277] A.B. Zavatsky and J.J. O'Connor. A model of human ligaments in the sagittal plane. Part 1: Response to passive flexion. *Proc Inst Mech Eng Part H, J Engng Med*, 206:125–134, 1992.

[278] A.B. Zavatsky and J.J. O'Connor. A model of human ligaments in the sagittal plane. Part 2: Fibre recruitment under load. *Proc Inst Mech Eng Part H, J Engng Med*, 206:135–145, 1992.

[279] A.B. Zavatsky and J.J. O'Connor. Ligament forces at the knee during isometric quadriceps contractions. *Proc Inst Mech Eng Part H, J Engng Med*, 206:7–18, 1993.

[280] A.B. Zavatsky and J.J. O'Connor. Three-dimensional geometrical models of human knee ligaments. *Proc Inst Mech Eng Part H, J Engng Med*, 208:229–240, 1994.

[281] E.N. Zuniga and D.G. Simon. Non-linear relationship between averaged electromyogram potential and muscle tension in normal subjects. *Arch Phys Med*, 50:613–620, 1969.